THE UNIVERSITY *of* EDINBURGH

Quantifying and Reducing Uncertainty in Tidal Energy Yield Assessments

Robert Clayton

2020

This thesis is submitted in partial fulfilment of the requirements for the award of an Engineering Doctorate, jointly awarded by the University of Edinburgh, the University of Exeter, and the University of Strathclyde. The work presented has been conducted under the industrial supervision of Wood Clean Energy, previously SgurrEnergy, as a project within the Industrial Doctoral Centre for Offshore Renewable Energy (IDCORE).

Declaration

I declare that this thesis has been composed solely by myself and that it has not been submitted, either in whole or in part, in any previous application for a degree. Except where otherwise by reference or acknowledgment, the work presented is entirely my own.

Robert Clayton

May 2020

"If a man will begin with certainties, he shall end in doubts; but if he will be content to begin with doubts, he shall end in certainties."

Francis Bacon

"*Every line is the perfect length, if you don't measure it"*

Marty Rubin

Abstract

Tidal stream energy has the potential to contribute to a diverse future energy mix. As the industry moves towards commercialisation and array scale deployment, there is an opportunity to better understand the uncertainties around energy yield assessments. Energy yield assessments are used widely in the wind industry to evaluate the potential energy production from a prospective project. One of the key challenges is to quantify and reduce uncertainty in energy yield assessment. This thesis investigates ways to achieve this through utilising lessons learnt from the established wind industry. An evaluation of both the wind and tidal energy yield assessment process is conducted, highlighting where synergies can be used to increase understanding of uncertainty for the nascent tidal industry.

The processes are comparable starting with a campaign to collect site data to characterise the resource at the measurement location. The next stage is to evaluate the long term variations, however this is where the two methods differ. Analysis of long term wind effects requires correlations to be made between short term site data and long term reference data from alternative sources. An assessment of tidal variations over longer periods utilises harmonic analysis, which is capable of deconstructing the individual astronomical variations of the tide and reconstructing them to predict future variations.

Despite harmonic analysis being able to determine the astronomical effects of the tide, there are uncertainties in the measurements of tidal flow which are associated with non-astronomical effects. Effects such as turbulence introduce uncertainty when evaluating measured tidal data. This is one area which is investigated further in the thesis. Methods to evaluate the turbulence intensity from real ADCP data are investigated.

The next stages require creating a numerical model of the site to extrapolate the data spatially to other areas of interest (such as a turbine location). Energy yield predictions for both wind and tidal are made by combining a power curve with the long term resource. The energy yield outputs are then adjusted to account for energy losses and uncertainties are applied to produce final energy yield values with the attributed probability values associated.

Statistical methods are applied to harmonic analysis to assess the level of uncertainty in long term predictions of tidal variations. A method using spectral analysis is applied to evaluate the residuals between measured and modelled data and proves to be accurate at determining missing tidal constituents from the analysis. A method for evaluating the turbulence intensity of the flow is shown, to better understand the stochastic nature of the tidal signal. An investigation is conducted to assess the propagation of bed friction uncertainty, in hydrodynamic modelling, and the resulting

impact on the predicted power output from a theoretical fence of tidal turbines spanning a tidal channel. The methodology is based on first conducting sensitivity studies by varying a parameter in the model and calculating the power. Then using a mean and standard deviation for the input parameter, the impact of the uncertainty can be transferred to the estimate of power. The results show that a larger uncertainty associated with the bed roughness tends to over predict the estimation of power.

This work aims to inform the standardisation of practices and guidelines in tidal resource assessment and to support developers, consultants and financiers in future tidal energy yield assessments. The final chapter includes procedural recommendations for future tidal energy projects, summarising methods to calculate uncertainty and recommendations to reduce them.

Acknowledgements

This EngD thesis would not be possible without the support and help of many key people.

Firsty, I would like to thank my academic supervisors Dr. Helen Smith and Prof. Alistair Borthwick, who without their advice and encouragement I would not have succeeded. Thank you for your time and energy in guiding the thesis and for all your input into the research. I would also like to thank my industrial supervisors at Wood, who have been involved in this project; James Stewart, Richard Boddington, Roisín Fahey and Alan Mortimer. It was a pleasure to work with SgurrEnergy and be a part of the transition process to Wood Group Clean Energy and then, most recently, Wood. I am also grateful that I was given the opportunity to continue working with such a great team of colleagues on such interesting projects. I want to thank all my other colleagues at Wood, who have always offered words of encouragement and seemed to show genuine interest in my work.

I would like to thank my family and friends who have patiently supported me through the journey of completing this thesis. To many of them I have become a bit of a recluse and I am looking forward to reconnecting with them all, now that the project is finished. I would also like to thank my dog Dougal for always sitting by my side as I worked at my desk.

I would like to thank IDCORE for giving me the opportunity to complete an EngD and conduct this research. The knowledge and skills I have gained through the process will stay with me forever. I would like to also thank my IDCORE peers, who have all become long lasting friends. I thoroughly enjoyed studying together in Edinburgh and will always look back fondly at the four years of IDCORE we shared together.

I would like to thank my wife, Abi, who I want to dedicate this thesis to. She was the person who first encouraged me to apply to IDCORE and then, faithfully, moved up to Scotland to be with me. She has supported me through the whole process and given me the encouragement I needed when I lacked the determination to keep going. She has put up with a lot of lonely evenings and weekends, while I worked away on the thesis has sacrificed a great deal. I will forever be grateful to her for her love, patience and support. Thank you Abi!

Finally, I would like to thank God, who has been with me through it all. Especially in the quiet, solitary times, He lifted my soul and kept me going on the journey.

Contents

List of Figures

List of Tables

Abbreviations

ADCP	Acoustic Doppler Current Profiler
ADV	Acoustic Doppler Velocimeter
AEP	Annual Energy Production
CDF	Cumulative Density Function
CFD	Computational Fluid Dynamics
CFL	Courant Friedrichs Lewy
CLT	Central Limit Theorem
DSCR	Debt Service Coverage Ratio
EMEC	European Marine Energy Centre
EWEA	European Wind Energy Association
FFT	Fast Fourier Transform
GUI	Graphical User Interface
IEC	International Electrotechnical Commission
JCGM	Joint Committee for Guides in Metrology
LIDAR	Light Detection and Ranging
LMADT	Linear Momentum Actuator Disc Theory
MAE	Mean absolute error
MAPE	Mean absolute percentage error
MCP	Measure Correlate Predict
MET	Meteorological
MW	Megawatt
OAT	One at a time
OREC	Offshore Renewable Energy Catapult
PDF	Probability Density Function
PE	Percentage energy
RMS	Root mean square
RMSE	Root Mean Squared Error
SNR	Signal to noise ratio
SODAR	Sonic Detection and Ranging
UTide	Unified Tide
WAsP	Wind Atlas Analysis and Application Program

Nomenclature

$\overline{x_i}$	mean value
h_m	hydraulic mean depth
A_n	amplitude of tide
C_P	coefficient of power
C_T	turbine roughness
C_d	bed roughness/shear stress value
K_1	lunar diurnal harmonic constituent
K_s	effective sand roughness height
L_q^{smaj}	semi major axis length
L_q^{smin}	semi minor axis length
M_2	principal lunar semidiurnal harmonic constituent
N_i	number of samples
O_1	lunar diurnal harmonic constituent
$\bar{P}$	maximum average power
P_r	Probability
P_w	wetted perimeter
Q_{max}	maximum flow rate
R_h	hydraulic radius
S_2	principal solar semidiurnal harmonic constituent
S_h	source or sink of fluid
S_i	standard uncertainty
$\overline{U}$	depth averaged speed
U_h	horizontal component of tidal flow
U_i	uncertainty contributor
U_r	velocity along central axis of turbine
U_v	vertical component of tidal flow
V_z	average wind speed
a_i	uncertainty bound
k_o	natural bed roughness
k_t	additional friction due to presence of tidal turbine
u_i	relative standard uncertainty
$\bar{v}$	mean long term flow speed
x_i	a random integer
z_0	surface roughness
ξ_i	incident wave
σ^2	Variance
τ_b	bed-shear stress

ω_n	tidal frequency
ϕ_n	phase lag
A	cross sectional area
a	tide amplitude
F	node factor
Fr	Froude number
G	acceleration due to gravity
h	mean water depth
i	bin integer
k_{tide}	Epoch
k	expansion or coverage factor
K	von Karman's constant
m	mass (kg)
n	Manning coefficient
Pr	fluid pressure
P	Power
p	probability value (%)
r	ADCP range
R	correlation coefficient
R^2	coefficient of determination
R_T	radius of tidal turbine swept area
U	Accuracy
v	mean flow velocity (m/s)
X	mean of distribution
z	height above seabed
CI	confidence interval
$E[P]$	expected power
F	gravitational force
G	gravitational constant
S	slope/gradient of channel
Z	free surface elevation
$f(x)$	Function
t	Time
w	Width
x, y, z	Cartesian coordinate system in a three-dimensional space
α	wind shear component
β	Constant
δ	interannual variation
ζ	slope of surface elevation
θ	angle/direction
λ	number of years of long-term reference data

μ	Mean
π	Pi
ρ	water density
σ	standard deviation

Chapter 1

Introduction & Background

1.1 Background Overview

There is a global need to reduce dependency on fossil fuels for the supply of energy. Many countries are aware of this and have begun decarbonising their energy systems (Troup, 2016; Zhu *et al.*, 2019). The motivations stem from three main areas: the finite supply of fossil fuels; concerns regarding energy security; and the increasing rate of climate change (MacKay, 2008). As a result, there is high demand for electricity, not just for the raw supply of electricity, but also for transport and heating systems, which are transitioning to electrification to reduce carbon use (Costello, 2018; Ruhnau *et al.*, 2019). Sourcing low carbon alternatives for energy and electricity is a key aspect of governmental strategies to limit global warming to no more than 1.5°C, as set by the global Paris climate change agreement in 2015 (United Nations, 2015).

The effects of burning coal, oil & gas are of major concern not only because of the harmful gases produced, which contribute to global warming, but also because these fuels are in finite supply. Countries unable to meet their own demand for electricity have become increasingly dependent on other countries for their supply (Högselius and Kaijser, 2019). In recent history, Russia has threatened to disrupt Europe's gas supplies, which could have led to potential fuel shortages across the whole of Europe (Withnall, 2015). Countries have become highly exposed to the risk of supply disruption from imports, which could have far reaching geopolitical consequences (Marshall, 2015; Noguera-Santaella, 2016).

Renewable energy is a multi-faceted solution to many of the world's problems. Reducing the amount of carbon dioxide we emit from burning fossil fuels will reduce the negative impacts of climate change (Hay *et al.*, 2016; Bhattacharya, 2019). Even though generating electricity from renewable sources is not a new concept, the world is still active in searching for new technology concepts to contribute to a cleaner, renewable electricity supply. Governments are increasingly aware of the benefits that electricity generation from renewable sources can have and many countries are active in deploying renewable technologies (Yuan *et al.*, 2018). Renewable energy allows countries to harness their own natural resources and hence reduce their reliance on supply from other countries.

Renewable energy has received financial backing from the UK Government, enabling technology such as wind, both onshore and more recently offshore, and solar to become cost competitive with fossil fuel generation (IRENA, 2018). Wind and solar have seen huge increases in installed capacity, as shown in Figure 1.1. This is primarily due to the technology becoming commercially viable, through lower cost accompanied by improvements in technology reliability, availability and performance. However, this was not always the case. In its early phase of development, the wind industry was plagued with technology failures and slow growth (Gipe, 1995). Initial investment came from government organisations through incentives and grants. Wind and solar benefitted from lessons learnt at small scale and improvements in technology. It was only after a return to small-scale turbines, with incremental development and a significant level of deployment (approximately 5GW globally), that the sector was able to deliver what it had initially thought possible: large rotors and multi-megawatt turbines (MacGillivray, 2016).

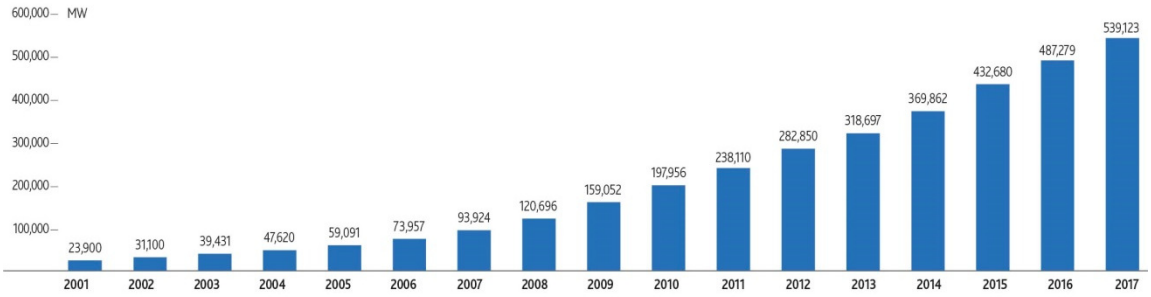

Figure 1.1: Global cumulative installed wind capacity 2001-2017 (Global Wind Energy Council, 2017)

Nowadays, the wind energy industry is booming, with thousands of turbines deployed and the focus shifting offshore, to take advantage of higher wind speeds, and less competition for space compared to onshore wind farms. There has been, and continues to be, a wind energy revolution. A similar path is also possible for the nascent tidal stream industry, which has the opportunity to benefit from the experience gained by the wind industry and to develop a more effective route to commercialisation. Prospective tidal energy sites require very strong tidal currents, which are often limited to straits between islands and around headlands. As an island nation, with approximately 17,850 km of coastline, the UK waters provide a great natural resource which could be harnessed to secure additional electricity supply. Tidal stream energy is close to commercialisation, but there are significant challenges to overcome, and many investors and decision makers lack confidence in the sector (Lamy and Azevedo, 2018).

1.2 Tidal Stream Energy – State of the Art

Tidal stream energy has potential to contribute to a diverse energy mix across the globe. Across the world, there are many regions where the bathymetry and coastline work together to provide

ideal locations in which to deploy tidal stream turbines. The scientific theory behind the tides is discussed further in Chapter 4. Tidal stream energy benefits from being highly predictable and much less intermittent than wind or solar energy. These characteristics are highly favourable to developers and investors seeking projects with minimised risk. However, one of the main challenges is to prove that the technology can work and survive in the harsh environments. Section 1.2 therefore provides background information on the current state of the art of tidal stream technology and highlights some of the flagship projects in recent years.

In recent history, various conceptual designs have been investigated to harness the movement of water from the tides. Over 110 tidal energy device developers have been identified by EMEC (EMEC, 2018); many of these developers are at the prototype stage, and very few have achieved physical deployment of technology. Tidal stream energy technology developers are pioneering the development of devices to harness the kinetic energy of the ocean tides, with the industry largely focussed on horizontal axis turbines. Much like a wind turbine, the kinetic energy of the fluid is captured as it flows across several rotating blades. These in turn drive an electrical generator. A small number of these technologies are in the early stages of project demonstration, having successfully developed and deployed prototypes and progressed on to multiple unit arrays (Vögler *et al.*, 2017). Tidal energy convertors are not yet cost competitive with more mature renewable energy technologies, such as onshore wind; however, demonstrable progress is being made in achieving cost reductions, with further reduction expected in the short term (MacGillivray, 2016).

The turn of the 21st century saw a resurgence in the level of international interest for wave and tidal electricity generation at academic, industrial, and political levels – both in national (UK) and internationally (EU and global) environments (Ocean Energy Europe, 2017). A report published in 2018, by the Offshore Renewable Energy Catapult (OREC), states that there is currently 10 MW of operational tidal stream energy capacity and it is expected that the levelised cost of energy (LCOE) will reduce from the current estimate of £300 per MWh to £150 per MWh, after 100 MW of installed capacity has been achieved (OREC, 2018). The report continues by predicting a further reduction to £90 per MWh could be achieved, once 1 GW of tidal stream technology has been deployed. These reductions will be driven initially by economies of scale and volume enhanced by specific innovations and learning by doing.

A pivotal development for the marine energy sectors was the establishment of the European Marine Energy Centre (EMEC) in 2003. Set up by a grouping of public sector organisations following a recommendation by the House of Commons Science and Technology Committee (2001), EMEC has received approximately £34 million of public funding investment by a range of organisations including both the Scottish and UK Governments. EMEC is the first major open

water test facility for marine energy technologies, offering grid connections to sites suitable for demonstration and full-scale devices.

Technology to harness electricity from tidal stream energy was first demonstrated in 2003 with the deployment of SeaFlow, a 300kW 2-bladed tidal turbine, off the coast of Lynmouth in Devon. The turbine was developed by Marine Current Turbines (MCT), who then went on to develop the world's first commercial scale tidal turbine, deployed in Strangford Lough in Northern Ireland. The SeaGen turbine had a rated capacity of 1.2MW and began generating in 2008 (Westwood, 2008). This flagship tidal device was decommissioned in 2017 after generating approximately 10 GWh of electricity (reNEWS, 2016).

One of the main challenges for the sector is access to funding. However, the UK Government has offered financial support to help the development of marine energy devices. One example includes the Saltire prize, which was announced in 2008. The challenge awarded £10 million to the first company to produce 100 GWh of electricity, over a continuous two-year period using only the power of the sea. However, the path to commercialisation took longer than expected and there was a lack of dedicated market support mechanisms for commercial scale projects. As a result, no company achieved the goal and the competition was closed in 2017 (Bennett, 2018). However, the challenge has recently been reopened with the £10 million fund specifically targeting tidal stream energy generation (Scottish Government, 2019).

A number of programs initiated by the Carbon Trust, such as the Marine Renewables Proving Fund (MRPF) and the Marine Renewables Commercialisation Fund (MRCF), have provided sizeable financial investment. The £22.5 million MRPF supported technologies including, Atlantis Resources, Aquamarine, Pelamis, Marine Current Turbines (MCT), Hammerfest Strom and Voith Hydro in proving device concepts at full-scale and in real sea conditions (Carbon Trust, 2011). However, the funds were focused on megawatt (MW) class technologies, which encouraged developers to scale up quickly. The expectation of the sector was inflated, leading to a number of investments from large companies. However, the challenges of commercialisation were greater than expected and many began selling their stakes in tidal companies. In 2015, Siemens sold MCT, once seen as the leading tidal turbine in the industry (Shankleman, 2015).

The remaining companies supported by the MRPF, Atlantis Resources Ltd (now SIMEC Atlantis Energy) and Hammerfest Strom UK (now Andritz Hydro Hammerfest), joined forces to develop the world first commercial scale tidal array: MeyGen, which has deployed four 1.5 MW tidal turbines in the Pentland Firth in the north of Scotland. The first turbine in the array, developed by Andritz Hydro Hammerfest (AHH), was installed and connected to the grid in 2016, with the full array installed and generating electricity in 2018 (Marine Energy, 2018). The Phase 1A array consists of three turbines developed by AHH and one by SIMEC Atlantis Energy. In 2010, the

Crown Estate granted the option to develop a tidal stream project at the MeyGen site of up to 398 MW and the aim is to achieve this in various stages of development (SIMEC Atlantis Energy, 2019).

A recent debate in the tidal industry addresses the issue of scale; specifically, whether it is more efficient, at this stage in the industry's development, to construct tidal devices with smaller (< 1 MW) or larger (> 1 MW) capacity. Most devices that are being deployed are of the MW scale. For example, Nova Innovation is a tidal turbine developer which has opted to focus on smaller scale devices. The main benefits include much lower cost, which enables multiple iterations by which turbines can be designed, built and tested. This leads to much lower financial risk for projects and enables the resource interactions to be fully understood. Once characterised, the turbine performance can be improved, and the design can be scaled up. Nova has received significant grant funding from the European Commission; most notably, Nova was awarded €2.3 million for the Enabling Future Arrays in Tidal (EnFAiT) Project in 2016 (Reid, 2016). The project demonstrates cross-border collaboration to support the development of a six 100 kW tidal turbine array in Bluemull Sound in Shetland (EnFAiT, 2017).

Orbital Power (previously ScotRenewables) is another leading tidal turbine developer, which is operating at larger scale. The company has developed a tidal energy device with the greatest combined capacity of any tidal energy device to date. The 2 MW floating platform comprises of two 1 MW tidal turbines connected together. This enables the device to be accessed and maintained more easily, as well as utilising the faster tidal flows near the top of the water column. Last year, the company announced that its SR2000 tidal device installed at EMEC had generated 3 GWh of electricity over a 12 month period, which equates to 25% of Orkney's power demand (reNEWS, 2018).

This section has provided an overview of the tidal energy sector, identified some of the key industrial stakeholders, and considered certain projects currently under development. However there remain several challenges facing the tidal industry, particularly regarding proving the technology and improving performance efficiency (Khare *et al.*, 2019). Away from the technical challenges, there is also the problem of acquiring funding and increasing investor confidence (Segura *et al.*, 2017). Most tidal stream projects would not be possible without the significant public funding it has received in recent history (MacGillivray, 2016). However, this funding may not be available in the future, and so the industry needs to be able to acquire funds through other means. In order to guide the tidal industry in the future, it is reasonable to look to the wind industry for inspiration and understand how it achieved its successful development and vibrant market place.

1.3 History of the Wind Energy Industry

Over the last three decades, the wind industry has seen rapid increases in the size and scale of individual turbines and of the largest wind farm projects. In addition to onshore wind development, offshore wind turbines are now opening up even larger unit sizes and rotor diameters. In the early stages of wind turbine generator development, small turbines were built and prototyped by experimenters, but government funded research projects in the UK, Denmark, Germany and the USA focused on multi-megawatt wind turbine generators with large diameter rotors. Whilst these large industrial machines were designed with correct assumptions in mind, noting that economies of scale favoured larger wind turbine generators for lower overall levelised cost of energy (LCOE), there was no ability to iterate cost effectively, or adapt designs to respond to early component or system failures (MacGillivray, 2016).

Conversely, the commercial wind turbines became established through development at small scale (tens of kW) and increased slowly, through better understanding of the resource and incremental improvements in design. Since 1980, the maximum rotor diameter of the largest wind turbine generators has doubled with each passing decade (Bergek and Jacobsson, 2003). Wind turbine generator tower and hub heights have also increased correspondingly. At various stages of the industry's development, each generation of wind turbine generators was believed by many to be at the limit of physical scalability. However advances in design, analysis, material properties, testing and demonstration enabled wind turbine generators to keep evolving and surpassing previous unit benchmarks. The growth in rotor diameter and tower height has allowed wind turbine generators to capture the stronger winds accessible at higher elevations and has allowed an improvement in unit performance to be demonstrated (Olivecrona, 1995; Smith, 2011).

The commercial wind industry, an industry that is now prevalent across the globe, has grown from a small beginning. After the 'oil crisis' in 1973, interest grew in wind turbine technology, and countries such as Denmark encouraged small industrial companies to begin to manufacture wind turbines. As a result of USA government incentives, the period between 1981 and 1990 saw over 16,000 machines installed, ranging from 20 to 350kW (a total of 1.7GW), in California. Initially the wind industry was fashioned for the domestic Danish market, but it soon began supplying a new, expanding Californian market. The companies involved included Vestas, Bonus, Nordtank and Micon, all of which are still active today in various guises (Bonus became Siemens Wind Power, now Siemens Gamesa Renewable Energy (SGRE), and Nordtank and Micon combined to form NEG Micon, which was later acquired by Vestas). The vibrant Californian market encouraged these small Danish companies to enter into an export market long before such activity would traditionally have been advisable. American suppliers also emerged, most notably, US

Windpower which subsequently became Kenetech and, after a long journey through Enron Wind, became part of General Electric (GE).

The developing wind industry benefited from the availability of small-scale experimental projects (Garrad, 2012). Lessons could be learnt from testing technologies at a unit size where the costs and risks could be minimised. Failures are to be expected as part of the natural development of a new technology, and it is vital to learn from these mistakes and make necessary improvements, as the design iterates through each development phase. Failures occurred frequently in the early wind industry, with the most common components of failure being the blades and gearboxes (Garrad, 2012). As wind turbine generators increased in size and capacity, the industry required coordination and convergence to ensure the devices were designed and constructed safely and reliably. Common standards and certification procedures were developed, such as ISO/IEC 17025 for testing and calibration laboratories (ISO, 2005), which has since been revised in 2017. In the early days, the certification process was fairly straightforward, however the requirement for standards and certification laid the foundations for important regulation and improvement to technology quality.

The role of classification and certification bodies, in particular GL in Germany and DNV in Denmark (now part of the same global company, DNV-GL) has been crucial in the provision of sets of rules and design appraisals for the wind industry. In parallel to the development of certification rules, comprehensive standards have been developed under the aegis of the International Electrotechnical Committee (IEC). There is now a series of standards, known as IEC 61400, that cover many aspects of wind turbine design, safety and measurement. This collection of international standards is the cornerstone of the wind energy industry and has taken several decades of development to become the comprehensive resource it is now. The wind industry has set a precedent for the nascent marine energy sector to follow. This process is already underway, with the creation of the IEC Technical Committee 114, which is tasked with the preparation of international standards for marine energy.

Device developers active in the tidal energy sector need to establish a reputation as commercially viable technology providers, with demonstrable technology performance, reliability, availability, and economic attractiveness if the sector is to grow into its potential as a valuable contribution to the global energy mix. Certain of the key challenges and lessons learned from the development of the wind industry are discussed in a paper by Garrad (2012), including the following:

- Survivability is essential, ensuring that tidal turbines can withstand the extreme environment in which they are deployed.

- The industry must expect failures and be prepared to learn from them. For wind, the most common failures, especially in the early years, were of blades and gearboxes.
- The tidal industry should focus on deploying technology in the water and learning from operating in the environment.
- Deploying the maximum number of sensors is key to measuring the dynamic response of the turbine and is useful to validate numerical models.
- The main cost reductions will come primarily from the volume of deployments.
- Certification and standards are vital in ensuring a balance between reassurance and constraint and help owners and lenders gain confidence in turbine designs.

1.4 Research Motivation

The wind industry has matured into a fully commercial industry, in which investors and financers are comfortable with risk and uncertainty in energy yield estimates. This allows project developers to acquire funding from debt and other lenders, through an evaluation of the potential energy yield production of a project. This is typically achieved through a detailed energy yield assessment by a third-party independent consultant. The assessment will quantify the average energy yield production, estimated over the lifetime of the project. Significant emphasis is put on the quantification of uncertainty associated with the assessment, which is of particular interest to financers and developers, as this directly relates to the amount of funding available for the project.

The tidal industry has the opportunity to learn from the wind industry and understand where uncertainties arise and what methods to use to reduce the level of overall uncertainty. Despite many present tidal projects depending on grant and other public funding, there is an opportunity to prepare for future debt financing options as the industry moves towards commercialisation. A better understanding of uncertainty, at this stage, will better prepare developers, consultants and financers to quantify uncertainty and enable future project finance to be acquired. The primary motivation behind this work is to increase investor confidence in the industry by increasing understanding of uncertainty in energy yield predictions.

1.5 Knowledge Gaps

The tidal industry is heading towards commercialisation. However, uncertainty is not always included in project planning, despite being an important aspect which impacts heavily on the amount of finance available for a prospective project. Some of the more technical challenges for tidal turbines, such as turbine blade and gearbox design are being investigated through other work (Li *et al.*, 2016; Elasha *et al.*, 2017; Touimi, Benbouzid and Tavner, 2018). Research into energy yield uncertainty has led to its categorisation and a definition of the sources of uncertainty.

However a detailed investigation into the quantification and reduction of uncertainties has not yet been conducted (ORE Catapult, 2015a, 2015b). As tidal energy standards are currently being developed, decisions are being made about how to guide current and future developers on a procedure for conducting energy yield uncertainty assessment.

The IEC TS 62600-201:2015 technical specification for tidal energy resource assessment is currently undergoing revision (IEC, 2015). This enables experience from the developed wind industry to be understood and transferred to inform the tidal industry. Uncertainty is often merely treated as an afterthought, and so the tidal industry does not yet fully understand how to address uncertainty. Key gaps in the current research and understanding of uncertainty for the tidal industry include:

- A thorough understanding of energy yield uncertainty and where it arises within the resource assessment process.
- An evaluation of methods to reduce the most significant factors contributing to overall uncertainty
- An overview of how uncertainty quantification is achieved in the wind industry and where knowledge can be transferred to the tidal industry.
- Advice for technology and project developers on how to quantify and reduce uncertainty in future tidal energy yield assessments.

1.6 Research Aims and Objectives

The aim of this thesis is to increase the understanding of uncertainty in tidal energy yield assessment procedures and develop methods to quantify and reduce specific sources of uncertainty. To achieve this aim, four specific objectives are pursued:

1. To assess current methodologies for quantifying uncertainty in tidal energy yield and identify synergies between established uncertainty procedures used in wind energy yield assessments. (Chapter 3)
2. To evaluate uncertainty in the long-term prediction of tidal variations, through the statistical analysis of measured site data. (Chapter 4)
3. To evaluate uncertainty propagation within hydrodynamic modelling, through an investigation of the impact of a key model parameter on the predicted power. (Chapter 5)
4. To provide tools to enhance incorporation of uncertainty quantification in tidal energy resource assessment at Wood. (Appendix A-E)

1.7 Thesis Structure

The thesis is structured into the following chapters:

Chapter 2 outlines the foundation knowledge behind uncertainty assessment and introduces terms and concepts which are used in the thesis. The chapter provides an overview of the statistical and mathematical processes behind the quantification of uncertainty as well as theory behind harmonic analysis and hydrodynamic modelling.

Chapter 3 compares the processes used to conduct tidal energy and wind energy yield assessments. Specific consideration is given to areas where experience from the wind industry may carry over to tidal yield assessment. Based on this comparative investigation, two key topics are identified as requiring further evaluation of uncertainty, the intention being to improve the methodology approaches used by industry.

The first topic is examined in Chapter 4, which focusses on harmonic analysis methods, unique to understanding tidal variations. An assessment using measured tidal flow data from an ADCP is evaluated to improve understanding of where uncertainty in harmonic analysis arises and how it can be reduced. An evaluation of the stochastic nature of the tide at the site is carried out through an assessment of the turbulence intensity and some of the non-harmonic tidal influences, including wave height, wind speed and atmospheric pressure.

The second topic is hydrodynamic modelling, which contributes the most to overall uncertainty in tidal resource assessment (ORE Catapult, 2015b). A study is conducted in Chapter 5, using Telemac-2D, to determine how bed friction uncertainty affects the expected power and its variance for a fence of tidal turbines in a strait. This methodology could be applied to a range of modelling inputs to help quantify and reduce the uncertainty.

Chapter 6 discussed the key contributions to knowledge arising from this thesis, and its potential commercial impact. The chapter lists the overall conclusions and limitations of the research, and provides recommendations for future work.

Chapter 2

Uncertainty Theory and Methods

2.1 Statistical Uncertainty Theory

Error analysis is the study of uncertainties and aims to quantify the level of doubt around measurements. It allows scientists to estimate the size of the uncertainties and to reduce them where necessary. All measurements, however careful and scientific, are subject to uncertainty. Uncertainties arise wherever there is a margin of doubt around a value. Whenever there is an attempt to quantify a measurement, the value should ideally be supported with an associated uncertainty value, in order to give an indication of the measurement's quality. This provides confidence in the accuracy of the measurement.

Measurement uncertainty assigns a value to the doubt that exists about the result of a measurement. For example, if a distance was measured with a ruler, the uncertainty around that value is based on a number of factors such as the resolution and calibration of the ruler and the skill of the user. The analysis of uncertainties is a vital part of any scientific experiment, because real measurements can never be 100% accurate. Bell (1999) states that errors and uncertainties may arise from any of the following reasons:

- The measurement instrument – instruments can suffer from errors including bias, changes due to ageing, wear, slow change in response (known as drift), poor readability, noise (for electrical instruments).
- The parameter being measured – which may be unstable and change rapidly over time.
- The measurement process – the measurements themselves may be difficult to make, for example; measuring the weight of an animal that is particularly energetic.
- "Imported" uncertainties – calibration of the instrument has an uncertainty which is then built into the uncertainty of the measurements taken.
- Operator skill – some measurements depend on the skill and judgement of the operator.
- Sampling issues – the measurements must be properly representative of the process being assessed. For example, to monitor the ambient temperature in a room, it would not be representative to take measurements from a thermometer placed near a radiator.

- The environment – temperature, air pressure, humidity, and other conditions that differ from those when the instrument was calibrated, can affect the instrument or the parameter being measured.

In many instances, multiple errors will be present in a measurement prediction. Cumulative errors account for errors whose magnitude does not approach zero as the number of observations increase. In other words, errors associated with a series of measurements or connected calculations that gradually increase as they are combined (Joint Committee For Guides In Metrology, 2008).

The effects that give rise to uncertainty in measurement can either be random or systematic. For random effects, the best way to assess the reliability is to repeat the measurement several times and examine the different values obtained. In practice this is not always feasible, as repeating measurements can be costly and time consuming. Systematic effects cannot be assessed by statistical analysis based on repeated measurements and other methods are required to estimate the uncertainties. For this reason, uncertainties are classified into two groups: the random uncertainties (Category A), which can be treated statistically, and the systematic uncertainties (Category B), which cannot. This is discussed in greater detail in Section 2.1.1.

This chapter introduces some of the theory of uncertainties and outlines concepts used in this thesis. The chapter places a particular focus on the statistics and mathematical processes behind the quantification of uncertainty. Section 2.1.1 aims to defines key uncertainty terms, differentiating between commonly misused terms. Section 2.1.1.1 introduces probability distributions and outlines the most commonly used. The theory behind combining uncertainties and how uncertainties propagate through calculations is outlined in Section 2.1.2. Finally, methods of assessing uncertainty used in this thesis are introduced in Section 2.1.3.

2.1.1 Term definition

It is important from the outset to clearly define the uncertainty terminology that is used. The following definitions are often used when discussing uncertainties and are defined here, for clarity in subsequent chapters. More information on defining uncertainty terms can be found in the document “Evaluation of Measurement Data – Guide to the Expression of Uncertainty in Measurement” (Joint Committee For Guides In Metrology, 2008).

Mean

The mean is the most common statistic used to define the average of a numerical dataset. It is calculated by summing all the numbers in a dataset and dividing the value by the number of points in the sample. The mean can be significantly influenced by outliers and hence may not be an

appropriate representation of the data. It is therefore common to calculate and present the standard deviation with the mean value.

Standard Deviation

The standard deviation accounts for the amount of variability or spread in the values of a dataset. In its simplest terms, it is the average distance from a point to the mean value. The smaller the standard deviation, the closer or more concentrated the data are around the mean. The equation for calculating the standard deviation, σ, is defined in Equation 2.1, where n equals the number of values in the dataset, each x represents a number in the dataset, and $\bar{x}$ is the mean value of all the data:

$$\sigma = \sqrt{\sum_{i=1}^{n} \frac{(x_i - \overline{x_i})^2}{n-1}} \tag{2.1}$$

The standard deviation is also used to describe where most of the data should fall, in a relative sense, compared to the average. The result is called the empirical rule (Rumsey, 2011) where, providing the data is normally distributed, approximately:

- 68.0% of a sample will fall within one standard deviation (σ) of the mean ($\overline{x_i}$),
- 95.0% will fall within two standard deviations of the mean, and
- 99.7% will fall within three standard deviations of the mean.

See Section 2.1.1.1 for more information on the normal distribution.

Error

The term ‘error’ is often confused with ‘uncertainty’. Error is the difference between the measured value and the ‘true value’ of the parameter being measured.

Uncertainty

Uncertainty is a quantification of doubt about a measurement result. Whenever possible it is important to correct any known errors: for example, by applying corrections to data based on calibration certificates. However, any error whose values are unknown is a source of uncertainty (Bell, 1999). In order to quantify an uncertainty, two numbers are required. The first is the width of the margin, or interval, and the other is a confidence level that the ‘true value’ lies within a given margin.

Standard uncertainty is the uncertainty of the result of a measurement, expressed as a standard deviation. Uncertainties are typically assessed using either statistical analysis of series of

observations (Category A) or by other means, not using statistical analysis (Category B) (Zio and Pedroni, 2013).

Category A – Random Uncertainty

Category A uncertainties are those evaluated by repeated measurements, which give a random variation in the result. Also known as random uncertainties, they can be described through probabilistic modelling. Within these types of measurements, the higher the number of repeated measurements made, the better the estimate that can be expected. Type A data are typically collected from experimental studies, where repeatability, reproducibility and stability testing are important.

Category A uncertainties are based on the standard deviation of the scatter in each bin. Statistical theory requires that the standard uncertainty also reflects the number of points in the bin. The equation to calculate the standard uncertainty, S_i, is:

$$S_i = \frac{\sigma_i}{\sqrt{N_i}} \tag{2.2}$$

where N_i is the number of samples and σ_i is the standard deviation of measurements for the ith bin.

Category B – Systematic Uncertainty

Category B uncertainties (known as systematic uncertainties) cannot be assessed in the same way as Category A. In this case, nothing is gained by repeating measurements. The uncertainties are associated with the lack of knowledge about the properties and conditions of the phenomena underlying the behaviours of the systems. In this case the same influence affects the result for each of the repeated measurements and this is usually hard to identify. Other methods are needed to estimate uncertainties due to systematic effects, e.g. calibration certification, manufacturer specifications, published information, and user experience.

Category B uncertainties must be estimated from knowledge of the instrument. If, for example, a sensor has an accuracy of $\pm U$, it is reasonable to assume that the real value is likely to fall within this interval.

In both cases, the standard uncertainty is obtained from a distribution of possible values of the input quantity. This probability distribution may be frequency based (i.e. based on repeating readings – Category A) or it may be a theoretical or best estimate distribution (i.e. assumed based on information available – Category B). It is important to note than in both cases, the distributions

are models that are used to represent the level of knowledge. The different distributions commonly used in uncertainty analysis are described further in Section 2.1.1.1.

Bias

Bias is defined as systematic error and in some cases, can be alleviated if fully understood. It refers to the tendency of a measurement process to over- or under- estimate the value of a parameter. Bias, or systematic error, differs from random error as illustrated in Figure 2.1.

The target in the top-left has large random error, as the points are scattered widely, but with small systematic error as they are not systematically off-centre. The target in the bottom-left has large random and systematic errors compared to the target in the bottom-right where the random errors are small, but the systematic errors are much larger. The target in the top-right shows a low level of systematic and random error, as all of the points are close to one another and the distribution of shots is centred on the middle of the target.

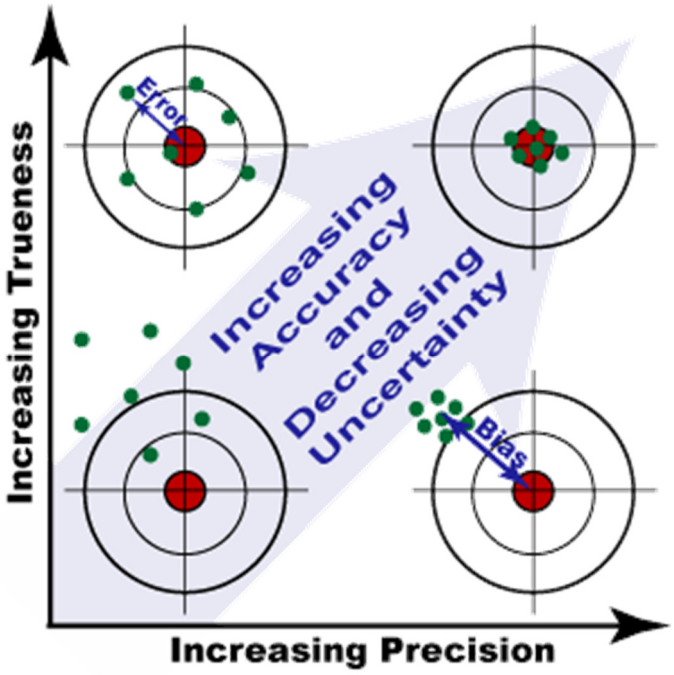

Figure 2.1: Comparison of random and systematic error, through the analogy of varying shots at a target (Iowa State University, 2012)

Figure 2.2 shows a probability distribution of a measured or predicted value. The graph shows a typical Gaussian, or normal, distribution, where the frequencies of the values are concentrated around the mean. With every estimated value there is a level of uncertainty introduced. This is defined as how much the distribution is skewed/stretched from the mean value. Bias is introduced

when the true value is known and therefore the mean value is shifted by a specific known value. A correction can then be applied to calculate the true value.

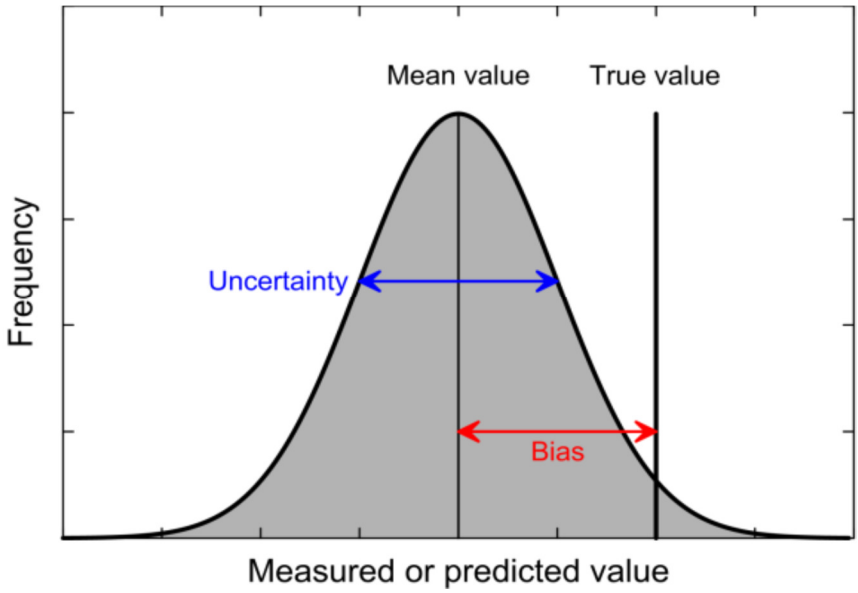

Figure 2.2: Typical normal distribution curve to show the difference between uncertainty and bias (Lyndon Department of Atmospheric Sciences, 2000)

2.1.1.1 Probability Distributions

Probability distributions show the relationship between the outcome of an event and its frequency of occurrence. They are useful because they are used as a graphical representation of measurement functions and show probability characteristics. When predicting future events, it is common to state the likelihood of the event occurring. When evaluating extreme weather events, such as the 1 in 50 year storm, wave, or earthquake, the value will be calculated from probabilistic statistics. The same is true when the energy yield of a renewable energy project is predicted. It is necessary to calculate the probability distribution around the long term energy production estimate over the project's lifetime.

Within statistics, there are a wide range of different distributions for categorical and numerical data. The more commonly used distributions for estimating measurement uncertainty are:

- Normal (Gaussian) distribution
- Rectangular distribution

The following sections provide an overview of each of the distributions, including a discussion of their primary application.

The Normal Distribution

One of the most frequently used distributions is the normal distribution, also known as the Gaussian distribution, shown in Figure 2.3. It is typically used for evaluating Type A data (see Section 2.1.1) The mean is directly in the centre of the normal distribution due to symmetry and the standard deviation is measured by the distance from the mean to the inflection point (where the curvature of the bell-shape changes from concave up to concave down). It is a function that represents the distribution of many random variables as a symmetrical bell-shaped graph, where the peak is centred about the mean and is symmetrically distributed in accordance with the standard deviation. Values near the centre are most likely to occur. Around 68% of the data are within one standard deviation (σ) of the mean, and as the distance from the mean increases, the frequency of values decreases either side of the mean.

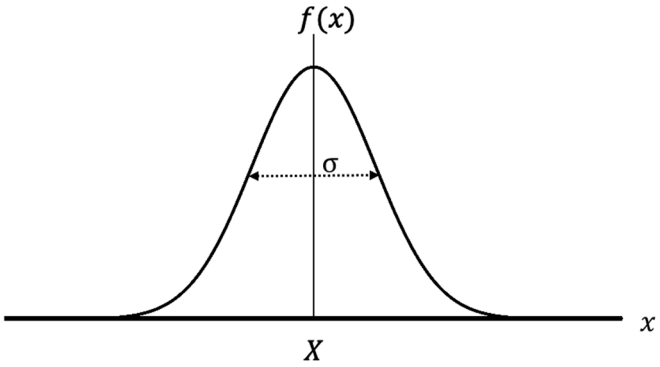

Figure 2.3 - Normal Distribution Curve

Equation 2.3 gives the equation for the normal distribution curve, where *X* is the centre value and σ is the width of the distribution or the standard deviation.

$$f(x) = \frac{1}{\sigma\sqrt{2\pi}} e^{-\frac{(x-X)^2}{2\sigma^2}} \tag{2.3}$$

To calculate the relative standard uncertainty, u_i, given a normally distributed data, Equation 2.4 can be used. This allows uncertainties from various sources, with different distributions to be evaluated and compared. The variable *U* is the value of the uncertainty contributor, and *k* is the value of the expansion or coverage factor as detailed in Table 2.1.

$$u_i = \frac{U_i}{k} \tag{2.4}$$

A probability value is a level of belief that an event will occur. A confidence interval is a range of values that is likely to contain an unknown parameter. Confidence intervals differ from the probability level as they give an indication of how many of the observations fall within a given range. If a high number of random samples are collected, then a certain percentage of the population will fall within defined confidence intervals. The confidence level is not the probability that a specific confidence interval contains the population parameter (Joint Committee For Guides In Metrology, 2008).

Confidence intervals can be applied to many different statistical distributions but are understood simplest when considering the normal distribution. The confidence intervals for the normal distribution are linked to the mean (X) and standard deviation (σ) of the sample, in the following way:

- Approximately 50% of all observations fall in the interval $X \pm (2/3)\sigma$
- Approximately 68% of all observations fall in the interval $X \pm \sigma$
- Approximately 95% of all observations fall in the interval $X \pm 2\sigma$
- Approximately 99% of all observations fall in the interval $X \pm 3\sigma$

This can also be defined as a coverage factor, k, linked to the level of confidence as shown in Table 2.1. Figure 2.4 shows the relationship between the probability and the standard deviations graphically.

Table 2.1- Value of the coverage factor *(k)* that produces an interval having a probability value *(p)* assuming a normal distribution (Rumsey, 2011)

Probability value, p (%)	Coverage factor, k
50.00	0.675
68.27	1.000
90.00	1.645
95.00	1.960
95.45	2.000
99.00	2.576
99.73	3.000

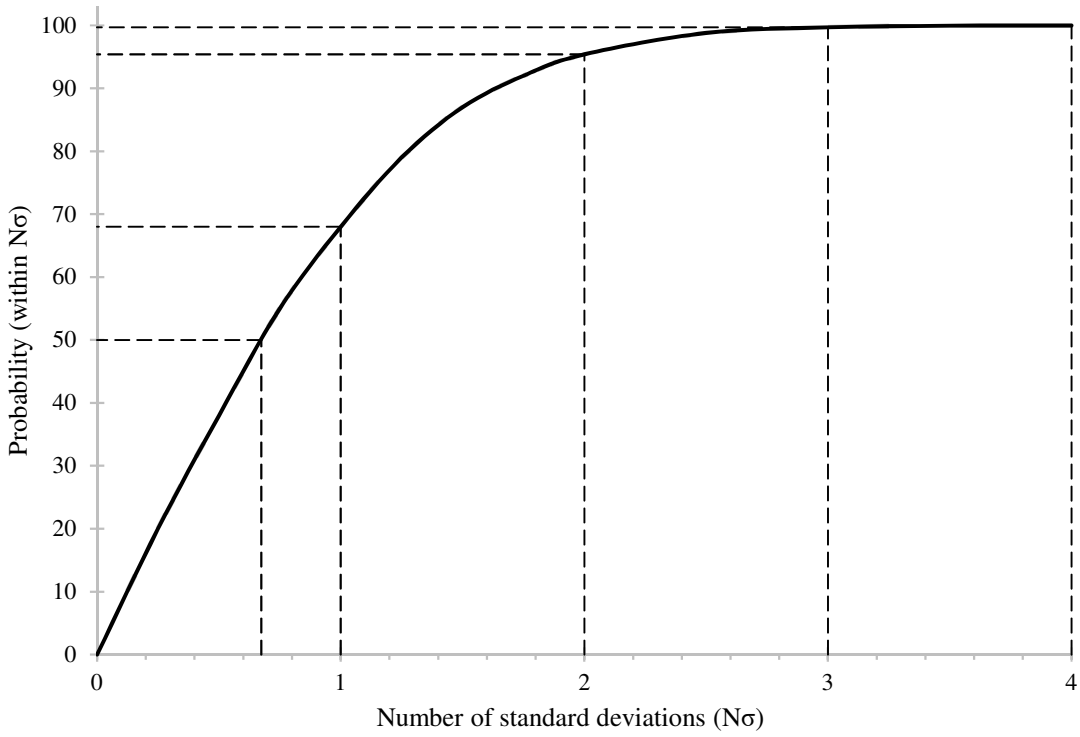

Figure 2.4 - Relationship between standard deviation and the probability, assuming a normal distribution

The normal distribution relies on one key assumption, known as the central limit theorem. The central limit theorem states that if a value has a non-normal distribution, or if the distribution is unknown, the shape of the sampling distribution is approximately normal as long as the sample size, n, is large enough. In other words, an approximate normal distribution can be assumed for the means of large samples, even if the distribution of the original values is not normal. Most statisticians agree that if n is at least 30, the approximation will be reasonably close in most cases (Rumsey, 2011). The larger the sample size, the closer the distribution of the sample means will be to a normal distribution. This is one of the main assumptions for assuming a normal distribution and is widely used in calculating energy yield uncertainty.

The Rectangular Distribution

The rectangular distribution is a function that represents a continuous uniform distribution and constant probability. In this case, all the outcomes are equally likely to occur. This distribution is most commonly used in uncertainty analysis when the exact distribution is unknown but it can be estimated to be between two values, as illustrated in Figure 2.5. For example, if the accuracy of a measurement is said to be ±1 mm, then it is unknown where the true value lies, but it can be said it lies between the two values. During laboratory testing, the environmental conditions are usually provided with an associated uncertainty. For example, the air temperature during a test may be

given in the following format 24.9°C ± 0.2°C. This could be an example of a rectangular distribution, where the upper and lower bounds are provided with the mean value. This states that the value may lie anywhere within the two limits, without actually specifying a level of confidence around the mean value.

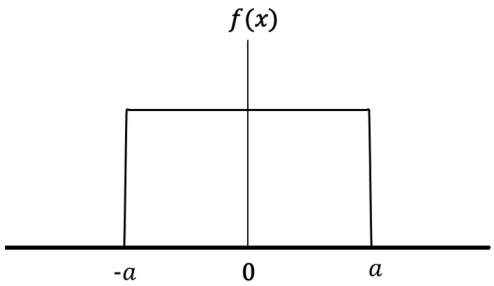

Figure 2.5 – A rectangular distribution

If the distribution is not known, it is best to evaluate it conservatively. In this case, the rectangular distribution is a good default option. To calculate the equivalent standard uncertainty, u_i, from a rectangular distributed uncertainty, Equation 2.5 can be used, where a_i is the value of the known uncertainty bounds.

$$u_i = \frac{a_i}{\sqrt{3}} \tag{2.5}$$

Skewness – measure of asymmetry (n=3)

In probability theory and statistics, skewness is a measure of the asymmetry of the probability distribution of a variable around its mean. The skewness value can be positive or negative, with the normal distribution having a skewness of 0 (i.e. perfectly symmetrical).

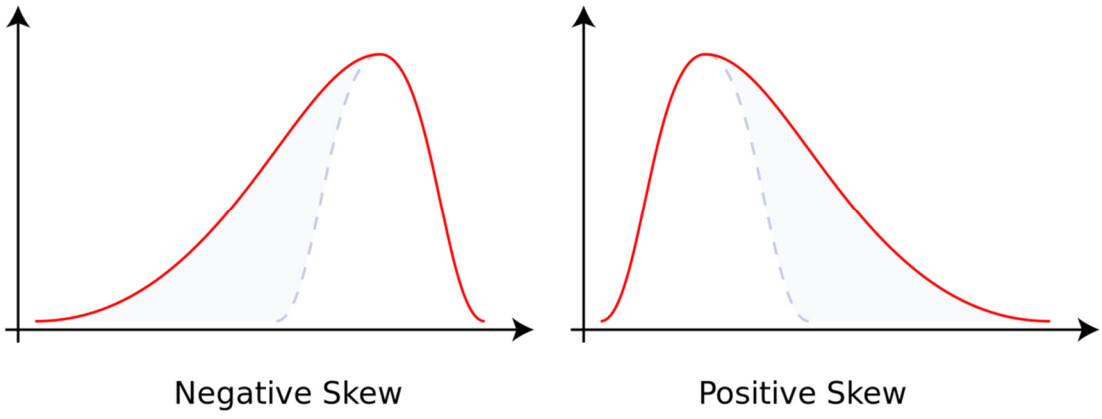

Figure 2.6: Comparison of positive and negative skew within a normal distribution curve

Figure 2.6 shows the difference between a distribution with a positive and negative skew. A negatively skewed distribution has a longer left tail, which indicates that the mass of the distribution is concentrated to the right and the mean has been skewed to the left of a typical centre of the data. A positively skewed distribution has a longer right tail, which indicates that the mass of the distribution is concentrated to the left and the mean has been skewed to the right of a typical centre of the data.

Kurtosis – measure of peakedness or tailedness (n=4)

Like skewness, kurtosis is a statistical measure used to describe a distribution. Kurtosis is a measure of the peakedness or flatness of the distribution, with a normal distribution having a kurtosis of 3. Distributions with kurtosis values greater than 3 exhibit tail data exceeding the tails of the normal distribution, whereas distributions with kurtosis lower than 3 show that the tail data is generally narrower that the normal distribution.

2.1.2 Propagation of uncertainty

When a measurement involves a process with more than one step, the estimation of uncertainties also requires many steps. It is important to fully understand how to combine uncertainties associated with different steps in the measurement process. Therefore, it is necessary to estimate the uncertainty in the initial measurement and then determine how these uncertainties 'propagate' through the calculations to produce an overall uncertainty (Taylor, 1997). The following subsections outline a number of methods to combine uncertainties depending on how they are related. Section 2.1.2.4 outlines the difference between dependent and independent uncertainties and the different methods to evaluate them.

2.1.2.1 Uncertainty in sums and differences

If several quantities x, y, z are measured with uncertainty $\delta x, \delta y, \delta z$ and the measured values used to compute,

$$q = x + y - z \tag{2.6}$$

then the uncertainty in the computed value of q, is the sum,

$$\delta q \approx \delta x + \delta y + \delta z \tag{2.7}$$

This demonstrates that the method of calculating uncertainty associated with summing or subtracting parameters, is to add the uncertainty in those quantities together.

2.1.2.2 Uncertainty in products and quotients

If several quantities *x*, *y*, *z* are measured with uncertainty $\delta x, \delta y, \delta z$ and the measured values used to compute

$$q = \frac{xy}{z} \tag{2.8}$$

then the fractional uncertainty in the computed value of q is the sum,

$$\frac{\delta q}{|q|} \approx \frac{\delta x}{|x|} + \frac{\delta y}{|y|} + \frac{\delta z}{|z|} \tag{2.9}$$

I.e., when quantities are multiplied or divided the fractional uncertainty adds.

2.1.2.3 Special cases

Two special cases are highlighted as important rules when combining uncertainty. The first is concerned with measuring a quantity *x* and then using the measured value to calculate the product $q = Bx$, where the number B has no uncertainty. In this case, the uncertainty in q is just $|B|$times that in *x*.

$$\delta q = |B|\delta x \tag{2.10}$$

The second special case concerns the evaluation of a power of a measured quantity. For example, to measure the speed (v) of an object and then, to find its kinetic energy, $\frac{1}{2}mv^2$, the square of v must be calculated. At first glance, it might seem proper to square the uncertainty. However, v^2 is just $v \times v$ and therefore the fractional uncertainty in v^2 is twice the fractional uncertainty in v. More generally, if the quantity *x* is measured with uncertainty δx and the measured value is used to compute the power $q = x^n$, then the fractional uncertainty in q is n times that in *x*,

$$\frac{\delta q}{|q|} = n\frac{\delta x}{|x|} \tag{2.11}$$

Assessing the propagation of uncertainty not only allows the quantification of the size of the combined uncertainty, but also illustrates the best ways to reduce the uncertainty. Evaluating the individual uncertainties that combine to produce an overall uncertainty, helps to identify the largest contributors, and thereby the ones to focus on reducing.

2.1.2.4 Independent vs. Dependent Uncertainty

Two random variables are statistically independent if their joint probability distribution is the product of their individual probability distributions. If the original uncertainties are independent

and random, a more realistic (and smaller) estimate of the final uncertainty is given by similar rules in which the uncertainties (or fractional uncertainties) are added in quadrature.

To illustrate this, consider computing the sum, $q = x + y$, of two values *x* and *y* that have been measured in the standard form, therefore giving the uncertainty $\delta q \approx \delta x + \delta y$. To see why this formula is likely to overestimate δq, consider how the actual value of q could equal the highest extreme. This will occur if the value of x is underestimated by the full amount δx and y by the full δy. This is a fairly unlikely event; if *x* and *y* are measured independently and the errors are random in nature, there will be a 50% chance that an underestimate of *x* is accompanied by an overestimate of *y*, or vice versa. Clearly then, the probability of underestimating both x and y by the full amounts δq and δq is fairly small. Therefore, the value $\delta q \approx \delta x + \delta y$ exaggerates the most probable error.

If the measurements of *x* and *y* are made independently and are both governed by the normal distribution, then the uncertainty in $q = x + y$ is given by Equation 2.12, known as the root-mean-square (RMS) technique. To best explain this methodology, it is helpful to consider each uncertainty contributor as a vector with independent quantities of displacement and magnitude. Therefore to calculate the net displacement and magnitude, each vector is summed up in quadrature. This is the common method of combining independent uncertainties (Joint Committee For Guides In Metrology, 2008), where

$$\delta q = \sqrt{(\delta x)^2 + (\delta y)^2} \tag{2.12}$$

The wind industry has become comfortable with the RMS approach for combining independent uncertainties. The ORE Catapult (2015) states that this assumption may not be valid for tidal energy yield assessments. If the overall uncertainty is dominated by one or two contributors which are not normally distributed, then the end results will not be normally distributed. If the overall uncertainty is higher than wind energy, the validity of the central limit theorem may reduce.

In principle, Monte-Carlo simulation has the potential to overcome these problems, as discussed in Section 2.1.3.3. However, this is more complex and time-consuming than the RMS method and the results are less intuitive to interpret. When uncertainties are considered to be dependent, i.e. calculating one value has a direct effect on another value, then the uncertainties are combined in a different manner. The standard RMS method cannot be used if the values are not independent.

2.1.3 Methods of Analysing Uncertainty

There a number of ways to analyse uncertainty. The simplest method is to evaluate the standard deviation value, as outlined in Section 2.1.1.1. However, there are times when the standard deviation is not available and therefore other methods are required to quantify uncertainty. This

section outlines four further methods of analysing uncertainties that are used in energy yield uncertainty calculation. These are also used in subsequent chapters of this thesis.

2.1.3.1 Jack-Knife Method

The jackknife, or "leave one out", procedure is a cross validation technique developed to estimate the bias of an estimator. It was later expanded to include variance estimation and adopted the name of jack-knife because - like a pocket knife akin to a Swiss army knife - this technique can be used as a "quick and easy" replacement tool for a lot of more sophisticated and specific tools found in the literature (Miller, 1974; Bissell and Ferguson, 1975; Abdi and Williams, 2010).

The jack-knife method is an iterative process. First, the output of a process is estimated using the whole sample. Then a different subsection of the data is, in turn, dropped from the sample and the output is estimated from this smaller sample. This estimation is called a partial estimate (or a jack-knife replication). A pseudo-value is then computed as the difference between the whole sample estimate and the partial estimate.

In the wind industry, the jack-knife method can be used to estimate the uncertainty of an analysis process by taking a whole data set and splitting it into subsections as illustrated in Figure 2.7 & Figure 2.8. Time series data, from beginning to end, are represented as a bar indicating that all of the data are used in the analysis.

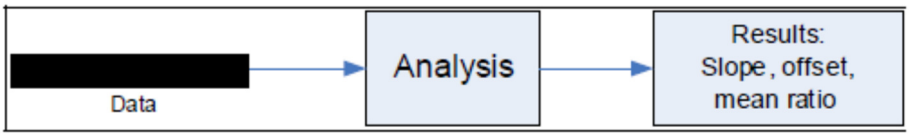

Figure 2.7 - Illustration of standard analysis process

The jack-knife estimate of variance calculates the uncertainty of the results of an analysis by considering the variability of results when subsequent subsets of the data are removed from the analysis as illustrated in Figure 2.8. In this case, six results are calculated each using a different 5/6 of the whole data set. The white sections represent where a subsection of the data has been removed from the whole sample. The uncertainty of the results is then determined from the difference between the results.

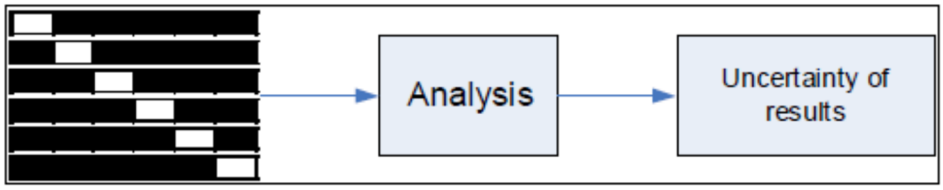

Figure 2.8 - Illustration of jack-knife method for determining uncertainty

Within wind energy yield analysis, the jack-knife method can be used to calculate the uncertainty in the long term prediction by assessing the correlation between short term site data and long-term reference data through the Measure – Correlate – Predict (MCP) process. The MCP is used to calculate the long term mean wind speed for various subsets of data and the variance in the output results is used to calculate the uncertainty. Detail of the jack-knife method used in wind energy for MCP uncertainty analysis is outlined in the literature (Mortimer, 1994; Rogers, Rogers and Manwell, 2005b, 2005a) and discussed further in Chapter 4.

The variance can be determined by calculating the difference between the known mean wind speed and the estimated speeds from the jack-knife subset. The total jack-knife variance (σ_{jk}) is calculated as:

$$\sigma_{jk} = \frac{N-1}{N}\sum_{n=1}^{n}(\overline{v} - \overline{x}_n)^2 \tag{2.13}$$

Where N is the total number of jack-knife sub-sets, $\overline{v}$ is the mean long term flow speed using the whole data set, $\overline{x}$ is the mean long term flow speed using the jack-knife subset n of the full data set.

The uncertainty (u_{jk}) is calculated using the total variance in the following equation:

$$u_{jk} = \frac{\sqrt{\sigma_{jk}}}{\overline{v}} \tag{2.14}$$

2.1.3.2 Sensitivity Studies

Sensitivity studies are a widely used method to assess how uncertainty in the output of a numerical process can be assigned to different sources of uncertainty in its inputs. A numerical process or mathematical model can be highly complex, and as a result, the relationships between inputs and outputs may be poorly understood. In these cases, a model can be regarded as a black box (i.e. the output is an 'opaque' function of its inputs).

Uncertainties calculated using sensitivity studies only apply if the model is well validated. It is important to recognise that the sensitivity of the parameter in the equation is what is being determined, not the sensitivity of the parameter in nature. If the model is wrong or if it is a poor representation of reality, determining the sensitivity of an individual parameter in the model is a meaningless pursuit (Pilkey and Pilkey-Javis, 2007). This highlights the need to produce accurate models that represent reality as truthfully as possible. Models should not be used in an isolated manner but should be validated with measured data.

In many cases, model inputs are subject to sources of uncertainty, including errors or measurement, missing information and poor understanding of the driving forces. This uncertainty imposes a limit on the confidence in the response of the model. In models developed using input variables, sensitivity analysis is an essential part of analysing uncertainty in a model. The choice of method of sensitivity analysis is typically dictated by a number of problem constraints or settings (Saltelli, 2002). Some of the most common are:

- Computational expense – if a single run of the model takes a significant amount of time, or the model has a large number of uncertain inputs.
- Correlated inputs – most common sensitivity analysis methods assume independence between model inputs, but sometimes inputs can be strongly correlated.
- Nonlinearity – linear regression approaches can't accurately measure sensitivity when the model response is nonlinear, with respect to its inputs. In such cases, variance-based measures are more appropriate.
- Model interactions – interactions may occur within a model when two or more inputs cause variation in the output greater than the variation in each of the individual inputs.
- Multiple outputs – most sensitivity analysis methods only consider a single variable output, despite many models output a large number of possible data varying in space or time. For each variable of interest, a different sensitivity analysis may be performed. However, it may be difficult to interpret the results from a single variable, if the outputs are correlated.
- Data from an unknown source – in some cases, the sensitivity analysis is performed with data gathered from an external source, where the values of the model inputs for each run cannot be chosen by the analyst.

There are multiple approaches to performing a sensitivity analysis, many of which have been developed to address one or more of the constraints above. A typical sensitivity study follows this general outline:

1. Identify the model outputs to be analysed

2. Run the model several times, varying the input parameters for each iteration and using the chosen method, dependent on the input uncertainty
3. Using the resulting model outputs, calculate the sensitivity measures of interest.
4. Quantify the uncertainty

One approach to sensitivity studies is local sensitivity analysis, which is derivative based. This is a one-at-a-time (OAT) technique which analyses the effect of one parameter, keeping the other parameters fixed. This type of assessment only addresses the point estimates chosen and not the entire parameter distribution (Hamby, 1994). Sensitivity analysis usually proceeds by changing one variable or assumption at a time, but it can also be done by varying a combination of variables simultaneously to determine the robustness of the results to widespread changes (Saltelli and Annoni, 2010). A more intensive approach to evaluating sensitivities is implemented using Monte Carlo techniques as outlines in Section 2.1.3.3.

2.1.3.3 Monte Carlo Analysis

Monte Carlo analysis (also known as the Monte Carlo Method) is used in a wide range of industries such as finance, project management, energy, manufacturing, research and development, insurance, transportation, and the environment. It seeks to solve complex problems using random and probabilistic methods. It relies on the generation of a large number of random samples in which the variables interact with the structure of the simulation to provide a probability of possible outcomes. The idea is to isolate a number of key variables that control and describe the outcome of the experiment and assign a probability distribution after a large number (potentially thousands or tens of thousands) of random iterations are performed. In effect, it repeats the deterministic calculation over many iterations, however the input variables are defined using stochastic methods. As the number of iterations increases, the resulting distribution converges towards an analytical solution (Palisade Corporation, 2015).

Provided that the application of Monte Carlo analysis is practical for a given application, the main benefit of the process is that it propagates the distributions through the functional relationship rather than the standard uncertainties. Monte Carlo methods overcome many of the drawbacks of other deterministic methods, such as those discussed in ISO-GUM guidelines (Joint Committee For Guides In Metrology, 2008), as they do not require assumptions regarding the shape and correlation of the distributions. Shah (2018) discusses a Monte Carlo analysis framework for tidal energy annual yield uncertainty analysis and compares it to the currently recommended ISO-GUM method. On the other hand, one drawback of Monte Carlo analysis, apart from the extensive amounts of time it can take to conduct, is that it provides only statistical estimates and not exact results, so it is only as good as the model of the data and their interactions.

Ensemble modelling is another form of Monte Carlo analysis, typically used in forecasts of the weather and climate predictions (Murphy *et al.*, 2004). The idea being that, instead of relying on a single weather model, a set (or ensemble) of predictions are made. The ensemble results give a indication of the range of potential future outcomes of the atmosphere. The benefit of using multiple simulations, is to reduce uncertainty in:

- Errors introduced by the use of imperfect initial conditions, amplified by the chaotic nature of the atmosphere (Russell *et al.*, 2017);
- Errors introduced due to imperfections in the model formulation, such as the mathematical methods used to solve the equations (Miftakhova *et al.*, 2019).

Ideally, the verified future atmospheric conditions should fall within the predicted ensemble spread, and the amount of spread should be related to the uncertainty of the forecast. In general, this approach can be used to make probabilistic forecasts of any dynamical system, and not just for weather predictions (Nourani, Gökçekuş and Umar, 2019; Rao, Vaishnavi and Pais, 2019).

2.1.3.4 Analysis of residuals

Another method to assess uncertainties involves calculating the error between predicted values (f_i) and measured values (y_i) of a variable, known as the residuals. There are a few standard error measures used in statistics that can be applied to indicate the level of uncertainty (Willmott and Matsuura, 2006; Hyndman and Athanasopoulos, 2013). These include:

- Mean absolute error (MAE) is used to measure how close predictions are to actual measured data. This is achieved by calculating the residuals between the measured and modelled data. The average of the absolute errors, or residuals, is then calculated using Equation 2.15, where n is the number of data points and f_i and y_i are the same as above:

$$MAE = \frac{1}{n}\sum_{n-1}^{n}|f_i - y_i| \tag{2.15}$$

- Mean absolute percentage error (MAPE) is a measure of prediction accuracy of a forecasting method in statistics. It expresses accuracy as a percentage, and is defined by formula 2.16:

$$MAPE = \frac{1}{n}\sum_{n-1}^{n}\left|\frac{y_i - f_i}{y_i}\right| * 100 \tag{2.16}$$

- Root mean squared error (RMSE) is used to measure the difference between predicted values and the actual observed values. It represents the sample standard deviation of the residuals and can be calculated using Equation 2.17:

$$RMSE = \sqrt{\frac{\sum_{t=1}^{n}(f_i - y_i)^2}{n}} \tag{2.17}$$

- The coefficient of determination (R^2) is a value that indicates how well data fits a statistical model. An R^2 of 1 indicates that the regression line perfectly fits the data, while an R^2 of 0 indicated that the line does not fit the data at all. Equation 2.18 shows how to calculate R^2, where $\overline{y}$ is the mean of the observed data:

$$R^2 = 1 - \frac{\sum_i (y_i - f_i)^2}{\sum_i (y_i - \overline{y})^2} \tag{2.18}$$

2.2 Tide Analysis Theory

Tides are highly predictable due to the gravitational forces between the Earth, Moon and Sun and are governed by the interactions between their orbits and mutual forces of gravitational attraction. The rise and fall of the tides are well understood, enabling tide tables to be produced with high accuracy far into the future. However, when it comes to predicting future tidal flow velocities, factors other than astronomical forcing makes predictions more difficult. This has the potential to influence the expected power production from tidal turbine arrays.

One of the main differences between the nature of the wind and the tide, is that wind variations are stochastic, whereas tidal variations are deterministic. What this means in practice is that the wind has a random probability distribution and aperiodic fluctuations, that can be analysed statistically, but not predicted precisely. Wind forces are driven by stochastic atmospheric forces and pressure differences caused by convection currents from the sun. The direction and speed of these are difficult to predict further than a few days into the future. Tides, in contrast, can be explained by the relative astronomical movements of the Earth, Moon and Sun in their various orbits, rotations, and axis tilts. The tidal forcing can be attributed to different tidal frequencies that are resolved using the mathematical method known as harmonic analysis. There are also non-astronomical effects that contribute to variations in the tides; caused mainly by wind, atmospheric pressure, waves, and turbulence.

Harmonic analysis has been used for almost 150 years as an effective way to predict the long-term variations of tidal flow, by deconstructing the tide into individual harmonic constituents (Thomson, 1881). However, the earliest tide tables were invented a long time before that, as early as 1056, in China (Zuosheng, Emery and Yiu, 1989). For a complete historical background on tidal analysis prediction see Cartwright (1999). The study of tides, using harmonic analysis, was first defined by Laplace, William Thomson (Lord Kelvin) and George Darwin, while A.T. Doodson

extended their work, introducing the Doodson Number notation to organise the hundreds of resulting terms.

Despite harmonic analysis being used for a long time, there are still uncertainties within tidal predictions. This chapter researches new methods and practices for predicting long-term variations in tidal energy flow and assesses statistical methods to quantify uncertainty in harmonic analysis procedures. The following sections discuss the theory of the tides and provides detail of harmonic analysis techniques used in the literature.

2.2.1 Harmonic Analysis

Harmonic analysis aims to characterise the tide by splitting a signal into individual astronomical factors. The Moon's orbit around the earth is closer to an ellipse than a circle. However, the orientation (as well as the shape) of this orbit is not fixed. Due to the nearly circular orbital paths of astronomical bodies, sinusoidal variations are suitable for defining tidal motion. One of the main assumptions is that tidal variations can be represented by a finite number of harmonic terms or constituents, that are calculated from astronomic influences on the Earth. Each individual constituent, h, can be expressed as a cosine wave and the variation over time can be calculated using Equation 2.19.

$$h(t) = A_n \cos(\omega_n t - \phi_n) \tag{2.19}$$

where A_n is the amplitude of the wave, ω_n is the angular speed and φ_n is the phase lag on the equilibrium tide (also known as the epoch). Harmonic analysis involves decomposing the tidal signal into individual cosine waves, that represent energy at specific astronomical frequencies. The frequencies are associated with celestial relative motions, therefore the accuracy of the harmonic analysis methods dependent on the ocean's response to celestial (gravitational) forcing at these same frequencies.

The notation typically used to represent harmonic constituent is using a letter followed by a subscript number. The number indicates the approximate number of cycles per day of that constituent. For example, the M_2 tidal constituent is due to the influence of the Moon on the Earth's tides and there are commonly two cycles of the M_2 constituent per day. Table 2.2 outlines some of the principal tidal constituents. There are also a number of constituents named with Greek letters (e.g. μ_2, ν_2, λ_2, and ρ_1) as well as others that are known as compound tides, whose names have more than one capital letter (e.g. $2MN_2$, $2MS_2$, MK_3, MN_4, etc.). The first letter indicates the primary constituent from which the compound constituent was nonlinearly generated by shallow water. There are also long-period tides which are commonly represented with a capital letter and one or more lower case letter (e.g. Mn, Mf, Sa, Ssa, etc.).

Table 2.2 – Principal harmonic constituents of the tides (NOAA, 2001)

Harmonic Constituent	Symbol	Period (hr)	Speed rate(°/hr)	Relative Size
Semi-diurnal				
Principal lunar	M2	12.421	28.984	100
Principal solar	S2	12.000	30.000	47
Larger lunar elliptic	N2	12.658	28.440	19
Luni-solar	K2	11.97	30.075	13
Diurnal				
Luni-solar	K1	23.934	15.041	58
Principle lunar	O1	25.819	13.943	42
Principle solar	P1	24.07	17.956	19
Larger lunar elliptic	Q1	26.87	13.398	8
Long period				
Lunar fortnightly	Mf	327.9	1.0978	17
Lunar monthly	Mm	661.3	0.544	9
Solar semi-annual	Saa	4383	0.082	8
Solar annual	Sa	8766	0.041	1

The total number of tidal constituents is a contentious one as there are only a small number of constituents that dominate a signal. Many of the other constituents have minor impacts on the overall variations. One source lists over 150 constituents which all correspond to individual astronomical factors that influence the tide (Parker, 2007). Another source lists a total of 175 constituents (Zervas, 1999). The principle harmonic constituents of the tide are illustrated in Table 2.2. A study indicated that over 91% of the flow characteristics at a site can be predicted using only the dominant constituents M2, S2, K1, and O1(Lu and Lueck, 1999). However, the type and size of the constituents varies depending on the location of the site. Each constituent represents a periodic change of relative position of the Earth, Sun and Moon.

The 'relative size' value, in the final column of Table 2.2, represent values from equilibrium theory presented originally by Schumerman (Schureman, 1941). Equilibrium theory assumes that the earth is totally covered by water and does not consider frictional effects on tidal water motions. It is a simplified method to describe most tidal characteristics. The values are expressed as a

percentage of the M_2 tidal constituent, to indicate the level of influence that the constituent has on the overall tidal variation.

The Moon orbits around the Earth in the same approximate direction as the rotation of the Earth, so that one lunar day (i.e. one complete rotation of the Earth, with respect to the Moon) is longer that the 24-hour solar day, approximately 24.812 hours. The Moon takes approximately 28 days to rotate around the earth. This means that during a 24-hour period, i.e. a single Earth rotation, the Moon has only revolved a small distance.

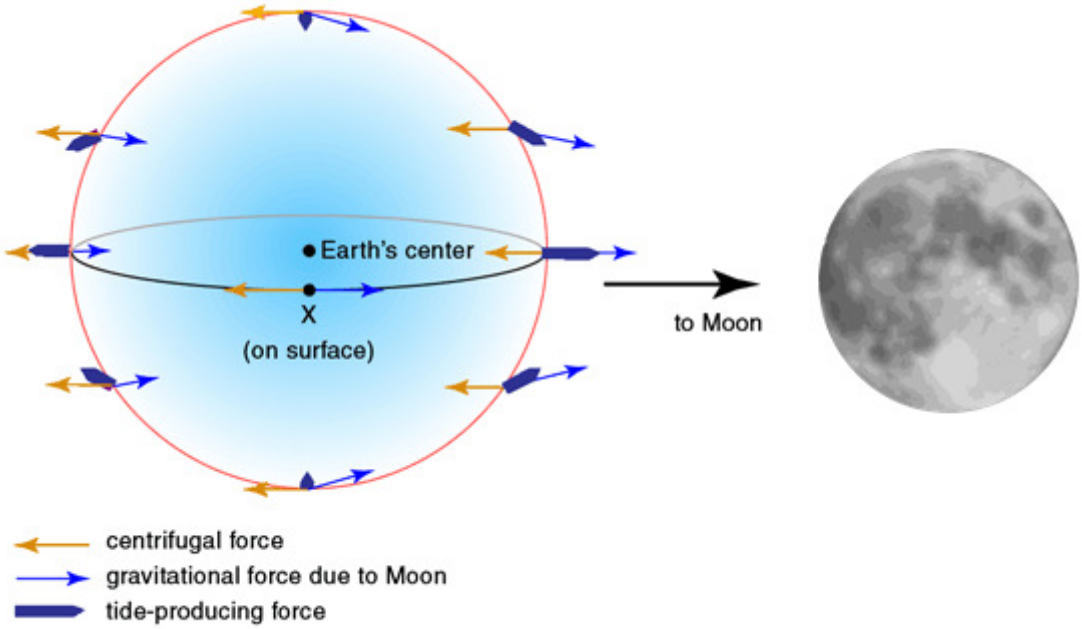

Figure 2.9 - Astronomical forcing on the Earth from the Moon and the resulting effect on the tidal forces (Department of Oceanography, 2018)

At any one time, there are two tidal "bulges" on the Earth, as seen in Figure 2.9. The first tide producing force, closest to the Moon, is due to the gravitational pull of the Moon on the Earth. The second tide producing force, acting away from the Moon, is due to the centrifugal force of the Earth-Moon system (Open University, 1989). This explains why the largest semidiurnal lunar harmonic constituent, M_2, is half a lunar day, or 12.4206 hours. The resulting frequency frequency is 1/12.4206 hours, which is calculated to be 1.9323 cycles per (solar) day.

The Earth rotates relative to the Sun exactly once every solar day, which is represented by the solar semidiurnal tidal constituent, S_2, with a period of 12.00 hours. Even though the Sun is approximately 27 million times larger than the Moon, it is approximately 339 times further from the Earth. As a result, the S_2 constituent is typically much smaller in size than the M_2 constituent.

This is due to the tidal force being inversely proportional to the cube of the distance. The magnitude of the gravitational force, F, between two objects with masses of m_1 and m_2, can be calculated as

$$F = G\frac{m_1 M_2}{r^2} \tag{2.20}$$

where G is the gravitational constant (6.67 x10^{-11} m^3 kg^{-1} s^{-2}) and r is the distance between the two celestial bodies.

- The mass of the Earth is approximately 5.972 x 10^{24} kg
- The mass of the Moon is approximately 7.348 x 10^{22} kg
- The mass of the Sun is approximately 1.989 x 10^{30} kg
- The distance between the Earth and Moon is approximately 384.4 x 10^6 m
- The distance between the Earth and Sun is approximately 149.6 x 10^9 m

To calculate and compare the force of the tide from the Moon and the Sun, it is necessary to calculate the change in gravitational force over the distance between the celestial bodies. Therefore, through differentiation of Equation 2.20, it is possible to calculate the magnitude of the force as

$$\frac{\delta F}{\delta R} = -\frac{2Gm_1 M_2}{r^3} \tag{2.21}$$

Substituting in the values above, the tidal force exerted on the Earth from the Moon is calculated as

$$\frac{\delta F}{\delta R_M} = -\frac{2 \times (6.67 \times 10^{-11}) \times (7.348 \times 10^{22}) \times (5.972 \times 10^{24})}{(384.4 \times 10^6)^3} \tag{2.22}$$

$$\frac{\delta F}{\delta R_M} = -1.03 \times 10^{12} N/m \tag{2.23}$$

The tidal force exerted on the Earth from the Sun is calculated as

$$\frac{\delta F}{\delta R_S} = -\frac{2 \times (6.67 \times 10^{-11}) \times (1.989 \times 10^{30}) \times (5.972 \times 10^{24})}{(149.6 \times 10^9)^3} \tag{2.24}$$

$$\frac{\delta F}{\delta R_S} = -4.73 \times 10^{11} N/m \tag{2.25}$$

Therefore, the gravitational force of the Moon on the Earth's tide is approximately 2.2 times greater than the force of the Sun. This calculation, even though it is simple in nature, has been included for completeness.

When the Moon and the Sun are in alignment, at the new and full Moons, their combined tidal forces result in increased tide ranges, called spring tides. Conversely, when the Moon and the Sun are at first and third quarters, their gravitational forces are out of phase with each other and produce smaller tidal ranges, called neap tides, as depicted in Figure 2.10.

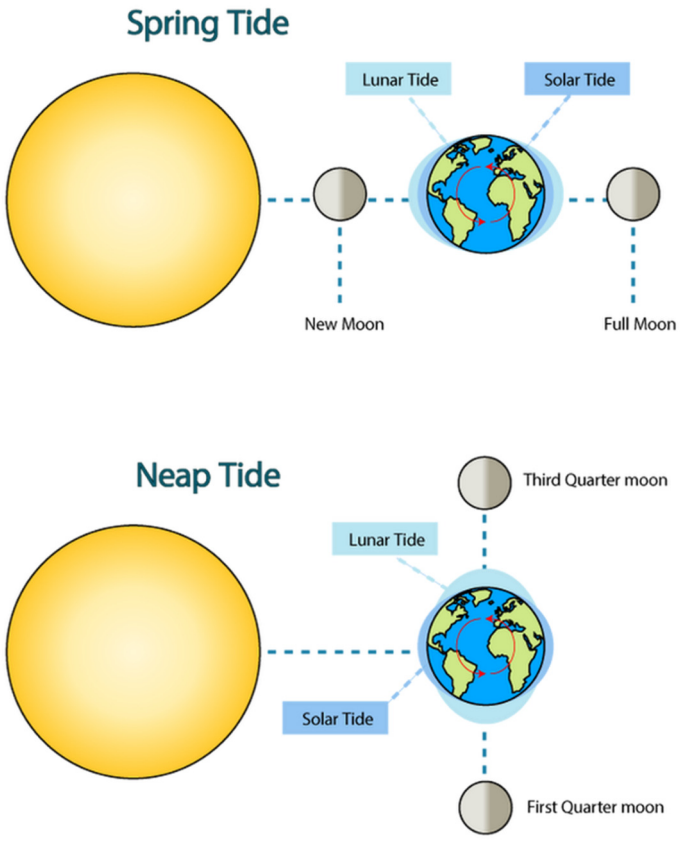

Figure 2.10 - Image showing the combined effects of gravitational forces from the Moon and sun on the tides (Clark, 2016)

There are three basic types of tides: semi-diurnal (semi-daily), diurnal (daily) and mixed as shown in Figure 2.11. Semi-diurnal tides typically have two high tides and two low tides each tidal day. A tidal day is the time taken for the Earth to rotate to the same position on the Moon, which has a mean value equal to 24.84 hours. Diurnal tides have one high tide and one low tide each tidal day. The third classification, mixed tides, are generally a combination of semi-diurnal and diurnal and typically have two high tides and two low tides, which have recognisable differences in their amplitudes.

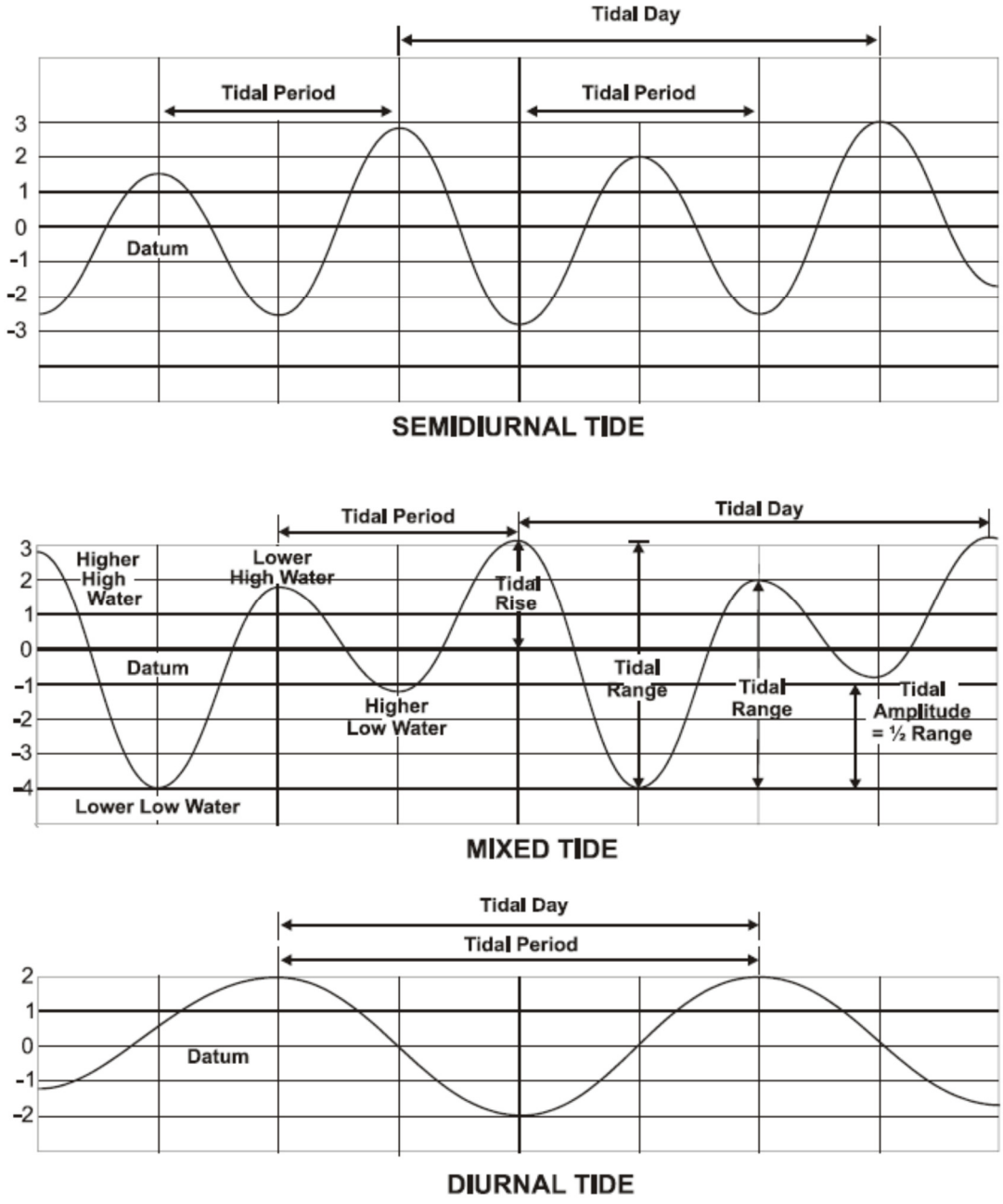

Figure 2.11 - Graphical representation of semi-diurnal, mixed and diurnal tides (Parker, 2007)

An important longer period modulation in the amplitude of the tide, due to orbital paths of the earth and Moon, is the nodal cycle. The apparent path of the Earth around the Sun, as seen from the Sun, is called the ecliptic. This path may be represented on a globe of the Earth by drawing a circle around the Earth which makes an angle of 23° 27' relative to the Earth's equator. Likewise, the apparent path of the Moon around the Sun may be referenced to the ecliptic, such that the Moon's path around the Sun makes an angle of 5° with respect to the ecliptic. When the Moon's ascending node corresponds to the vernal (i.e. spring) equinox (the equinoxes occur twice a year, March 21 and September 23, when the sun crosses the earth's equator, and day and night have the

same length), the angle of the path of the Moon around the Sun is about 28.5° (Schureman, 1941). When the Moon's descending node corresponds to the vernal equinox, the angle of the Moon's path about the sun is about 18.5°. This variation in the path of the Moon around the Sun has a period of about 18.6 years and is called the regression of the Moon's nodes. Schureman presents information on the effect of the longitude of the Moon's node. His work showed that each of the above coefficients are gradually modulated over an 18.6-year cycle and that a coefficient can be used to account for the regression of the Moon's nodes. The regression of the nodes explains a key variation in the amplitude of the annual mean range of the tide, as may be seen in Figure 2.12. The dark black curve is the annual mean range, or the difference in height between the mean high water and mean low water level. The time elapsed between trough to trough, or peak to peak, is the period of oscillation of the regression, and is approximately 18.6 years.

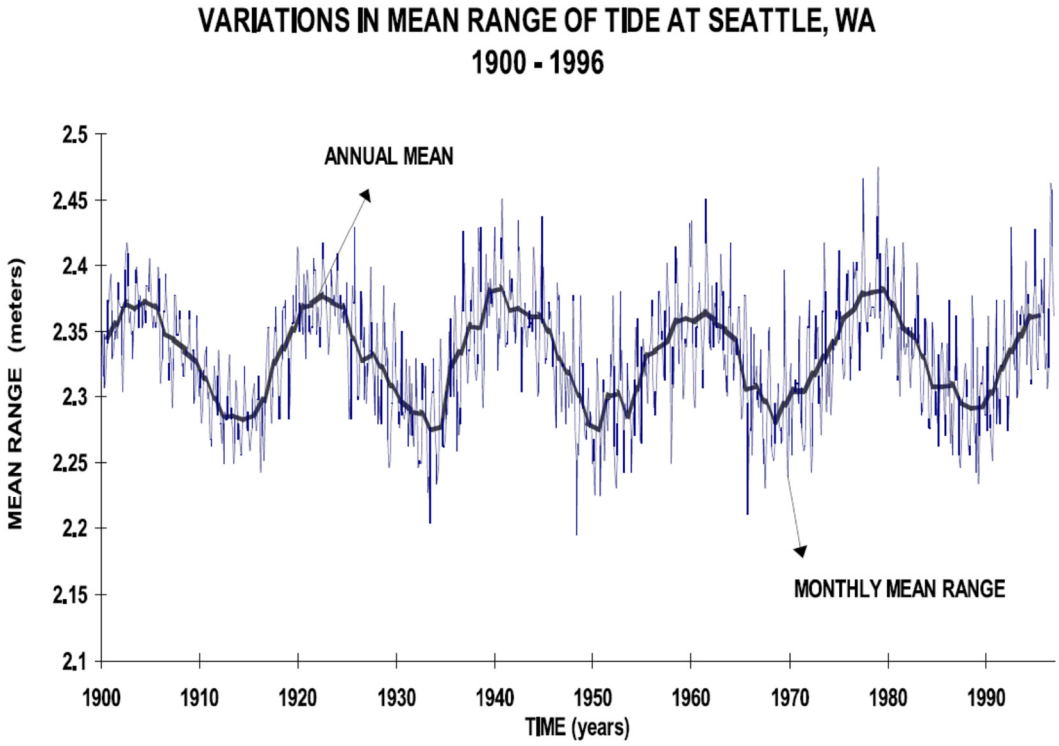

Figure 2.12 - An illustration of the effect of the 18.6-year regression of the Moon's nodes on the water levels at Seattle, USA (Parker, 2007)**.**

The orbit of the Moon lies in a plane that is inclined about 5.14° with respect to the ecliptic plane. The line of intersection of these planes passes through the two points at which the Moon's orbit cross the ecliptic plane: the ascending node, where the Moon enters the Northern Celestial Hemisphere, and the descending node, where the Moon moves into the Southern Celestial Hemisphere. The draconic, or nodical, month is the average interval between two successive transits of the Moon through the same node. The torque exerted by the Sun's gravity on the angular

momentum of the Earth-Moon system results in, the plane of the Moon's orbit gradually rotating westward, which means the nodes gradually rotate around the Earth. The nodes of the Moon's orbit precess or rotate 360° in approximately 6,798 days (18.6 years).

Another major variation to the orbit of the Moon around the Earth is known as the apsidal precession. This is the gradual rotation of the line joining the apsides of the orbit, which are the points of closest (perigee) and furthest (apogee) approach. The time taken for the one apsidal rotation is approximately 3,233 days (8.85 years).

The nodal cycle and apsidal precession are two important astronomical factors that influence the longer-term variation of the tide and should be considered through the harmonic analysis. This is discussed further in Section 4.4.6.

Harmonic analysis is a method of predicting tide variations by summing up the oscillating contributions of a number of tidal constituents. The formula to represent a single tidal constituent, h_1, at a point in time, can be written as:

$$h_1 = fH\,cos(V_o + u - k) \tag{2.26}$$

which is represented graphically in Figure 2.13. The amplitude, h_1, of the tide is calculated by multiplying the height of the tide, *H*, by a node factor, *f*, to account for the modulation effect of the 18.6 year lunar cycle. The phase is made up of three parts: the first, V_o, changes with time and is determined by the frequency; the second, *u*, is a phase relationship for the idealised equilibrium tide, based on astronomical variations; and the third, *k*, a phase lag relative to the equilibrium tide, usually called the epoch. In order to make a tide prediction, it is the amplitude, *H*, and epoch, *k,* that are required. Similarly, it is the *H* and *k* value, for each constituent, that are calculated from harmonic analysis.

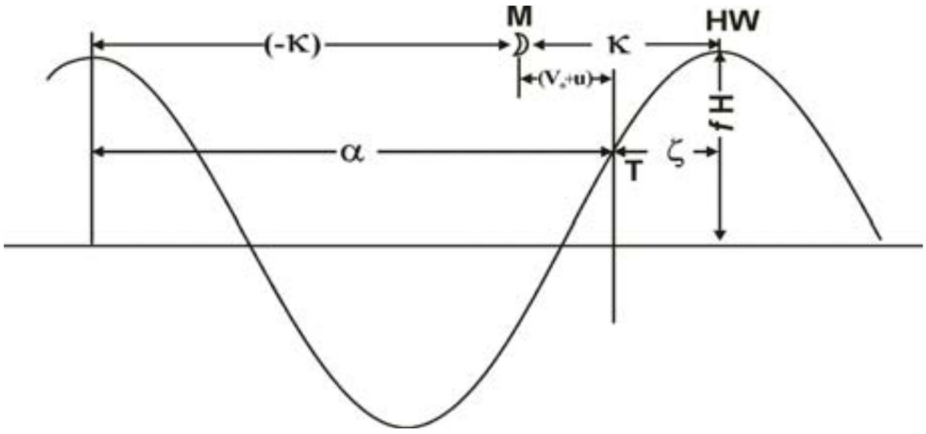

Figure 2.13 – A graphical representation of the amplitude and epoch (phase lag) of a single tidal constituent and its time relationship to the Moon's transit (Schureman, 1941)**.**

The overall accuracy of deriving individual constants is intrinsically linked to the length of the observation period. By increasing the observation period, it is possible to predict more constituents, therefore, reducing the inherent error in the derived values. For a period of 30 days, it has been shown that a minimum of 23 constituents can be resolved (EMEC, 2009). The IEC technical specification for tidal resource assessment states that at least 20 constituents should be derived to accurately understand the flow variations, and that the minimum required data length to achieve this is 35 days of measured data (IEC, 2015). Once the individual harmonic constituents have been derived, the resolved values can be used to reconstruct the tidal flow over any desired long term period.

Harmonic analysis can be used to determine harmonic constituents using either tidal height or tidal flow speed data. Analysis of tidal current data differs from tidal height data because there's a requirement to analyse two data time series, instead of one. This isn't a problem, however it requires additional work to process the input data and apply additional understanding to interpret the results. Harmonic constants are presented as a major and minor axis pair, which require combining to characterise the tidal current ellipse.

This can be achieved through the use of harmonic analysis software, as discussed in Section 2.2.4. When presenting the results of derived constituents, one source suggests that the precision of the calculated values should be restricted to reflect the length of observation (UK Hydrographic Office, 2006). The report states that the calculated values should be presented with a specific precision to ensure that results are not misinterpreted to be of higher quality. Table 2.3 outlines the recommended number of decimal places for the results of amplitude and phase of tidal constituents.

Table 2.3 - Suggested precision of calculated values of tidal constituents, depending on length of measurement period (UK Hydrographic Office, 2006)

Measurement period (t)	Recommended Number of Decimal Places of Results	
	Amplitude	Phase Angle
t < 90 days	2	0
90 days ≤ t < 1 year	3	1
t ≥ 1 year	3	1

2.2.2 Stochastic Variability in Tidal Signals

The variations in the tidal signal can also be affected by non-linear effects typically cause by varying weather conditions, bathymetry induced turbulence and meteorological conditions, which cannot be explained by harmonic analysis. Waves created by the wind, interact with the tidal current and can have a significant effect on the flow characteristics. This is usually confined to the top layer of the water column, near the surface. Therefore, it is a particularly important factor when considering floating tidal devices. Wave-current interactions are difficult to quantify, however, the impacts have been considered in the literature (Soulsby *et al.*, 1993; Wolf and Prandle, 1999; Saruwatari, Ingram and Cradden, 2013; Hashemi *et al.*, 2015). Harmonic analysis has been used widely in the assessment of tidal resource as is discussed in Section 2.2.5.

2.2.3 Tidal Current Ellipses

To fully understand the analysis of tidal data through harmonic analysis, it is important to understand tidal current ellipses. A tidal current can be represented by a vector tracing out an ellipse or circle with time. This is often seen on tidal charts, where the tide at a location is represented as an arrow pointing in the direction of the primary flood tide. The flood tide is the incoming phase of the tide, when water rises and the ebb tide is the outgoing phase, when the tide level reduces. It is then possible to define a tidal vector, as two orthogonal speed components, such as the north and east components. This is also applied to harmonic constituents, whereby the magnitude and direction of each constituent is represented by the major and minor component. The major axis being the direction of maximum flood and the minor axis perpendicular to the major axis. The relationship between the tidal current vector and the major and minor components is depicted in Figure 2.14.

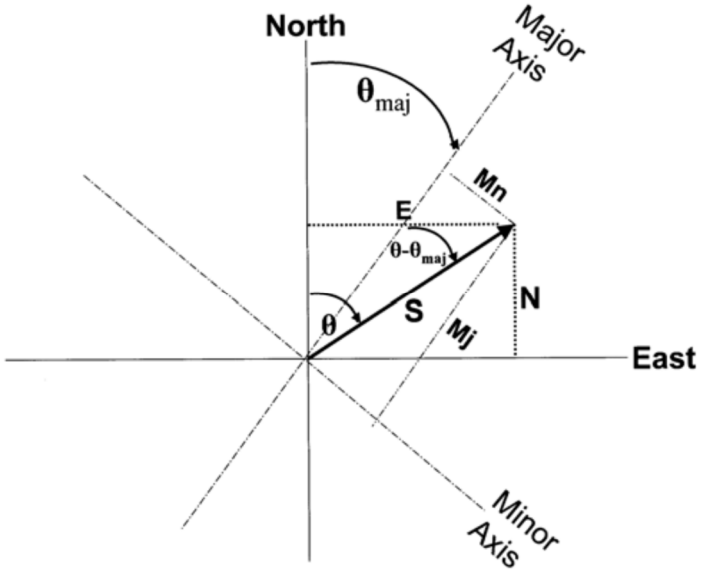

Figure 2.14 – Definition of tidal ellipse for harmonic analysis. A current vector, S, and direction, θ, split into north, N, and east, E, components and into major, Mj, and minor, Mn, components (Parker, 2007)**.**

The tidal current ellipse is dependent on many factors, including influences of the earth's rotation (Coriolis effect), centrifugal forces, friction and inertial effects. They combine to gradually change the current's directions with time, between flood and ebb. For such rotary currents, the shape of the curve traced out by the tip of the current vector over a tidal cycle can be elliptical or even circular as shown in Figure 2.15. For many sites, the current vector maps out a quasi-elliptical path during each tidal cycle.

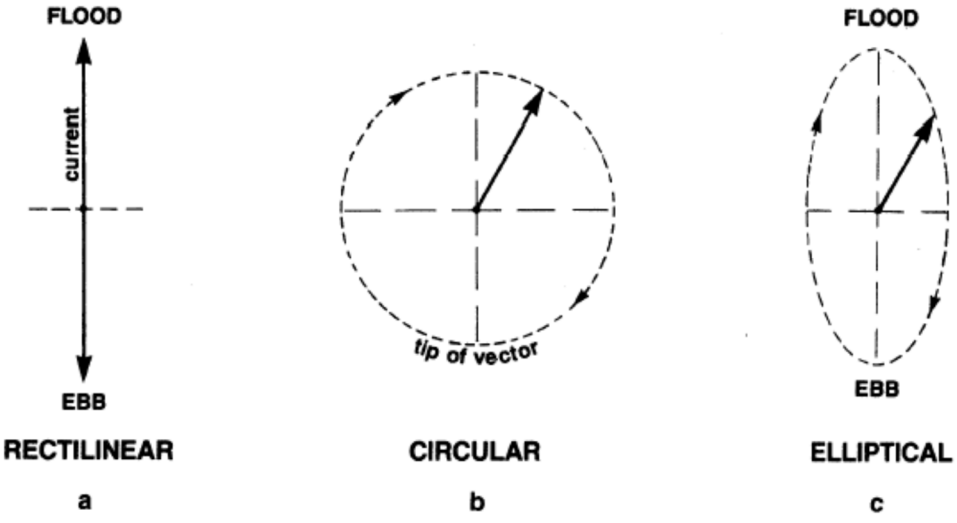

Figure 2.15 – Different types of current streams: a) rectilinear, b) circular; and c) elliptical (Cornett, 2008)

2.2.4 Harmonic Analysis Software Tools

The process of conducting harmonic analysis is made easier though the use of numerical tools and specialised software. These have been developed by a number of individuals and organisations from across the world. Most of them are open source codes developed for research purposes, however there are also commercial codes developed by organisations specialising in oceanographic processes. Table 2.4 lists some of the most common harmonic analysis tools used across the industry.

Table 2.4 - Details of the main tools used for harmonic analysis

Harmonic Analysis Tool	Developed By	Availability	Software Platform
T_Tide	Rich Pawlowicz - University of British Columbia	Open source	Matlab
UTide	Dan Codiga - University of Rhode Island	Open source	Matlab/Python
TASK	National Oceanography Centre	Commercial	Proprietary software
POLTIPS 3	National Oceanography Centre	Commercial	Proprietary software
Tide Predictions	National Oceanic and Atmospheric Administration	Open source	Proprietary software
WorldTides 2009	John Boon – Virginia School of Marine Science	Open source	Matlab

The harmonic analysis work conducted in this chapter uses the UTide code, created by Dan Codiga, through the numerical simulation software Matlab (MathWorks, 2018). The UTide harmonic analysis codes were originally adapted from the T_tide codes.

The T_Tide harmonic analysis tool, developed in 2001, was a modification of a set of Fortran programs developed by Mike Foreman in 1977 (Foreman M.G.G, 1996). Considered outdated by some, it was Steve Lentz, Bob Beadsley and Rich Pawlowicz who converted the codes into Matlab, incorporating many useful extra functions, including calculating confidence intervals (Pawlowicz, Beardsley and Lentz, 2002). Then in 2011, Dan Codiga built on the work conducted at the University of British Columbia and developed the UTide Matlab functions which have even more functionality. One of the main advances of the UTide code is its ability to specifically handle record times that are irregularly distributed and/or include gaps (Codiga, 2011). This is currently

the most widely used tidal prediction tool and is cited in the most recent IEC technical specification for tidal resource assessment (IEC, 2015) as the recommended method for analysing long-term variations in tides. UTide has replaced Fourier analysis solution techniques with a least-squares solution (LSS) technique; the latter based on minimising the squared differences between tidal data and computed tidal predictions (Codiga, 2011).

2.2.5 Developments in Harmonic Analysis

Since harmonic analysis was first developed, by William Thomson in 1881, there have been a number of developments to assess and improve its accuracy. This section provides a summary of harmonic analysis in recent published literature and the techniques used to assess its accuracy and evaluate uncertainties.

It was Doodson who expanded Darwin's work on tides and suggested that the astronomical forcing on the tides can be written as a combination of sinusoidal terms, having distinct amplitude, phase and temporal frequency. This was the first work that expressed each sinusoidal response as a tidal constituent. It was also Doodson who distinguished 388 tidal frequencies, by applying the lunar theory of E. W. Brown, developing the tide-generating potential in harmonic form (Doodson, 1921). Doodson discovered that all of the tidal frequencies linear combinations of the rate of change of six astronomical variables, that uniquely define the position of the Sun and Moon (with approximate period):

- τ – the mean lunar time (24.84 hours)
- s – the mean longitude of the Moon (27 days)
- h - the mean longitude of the sun (1 year)
- p - the mean longitude of the lunar perigee (8.8 years)
- n' - the negative of the longitude of the moon's ascending node (18.6 years)
- p' - the mean longitude of the solar perigee (21,000 years)

The integer coefficient of these 6 harmonics are called the Doodson numbers and are still used today (Foreman and Henry, 1989).

Due to the sheer number of individual tidal constituents, it was decided that it was neither practical nor mathematically feasible to include all constituents in every analysis. It was Godin (1972) who resolved the dilemma by defining constituent clusters and applied the Rayleigh separation equation (Equation 2.27) to restrict the inclusion of constituent clusters in the analysis.

Inference is another important correction applied aiming to include constituents previously excluded due to the Rayleigh criterion and the small length of measurement period. Inference can

reduce the residual error in the least square solution as well as eliminating a periodic behaviour in the estimation of amplitude and phases of the reference constituents (Epler, 2010).

The length of data needed to accurately distinguish the amplitudes and phases of two constituents is called the synodic period. The synodic period requires each constituent to be separated by at least one complete period from their neighbouring constituent (Pugh, 1996), i.e. it is the length of time in which the higher frequency constituent completes exactly one more cycle than the lower frequency. The Rayleigh Criterion determines which constituents can be evaluated in the harmonic analysis. The minimum period, *N* (in days), required to separate two constituents can be approximately calculated from

$$\frac{1}{\sigma_2 - \sigma_1} \approx N\ days \tag{2.27}$$

where σ_2 and σ_1 are the frequency (cycles per day) of the two constituents. For example, to resolve the M_2 and N_2 constituents, the approximate number of days of data required is calculated to be

$$\frac{1}{1.932 - 1.896} \approx 28\ days \tag{2.28}$$

The measured currents can be divided into 3 main components: the deterministic currents, defined by harmonic constituents; meteorological currents, induced by wave and wind interactions; and turbulent currents, which include eddies of all magnitude and isotropic turbulence (Polagye and Thomson, 2013). These can all be combined to produce a tidal current sample. Therefore, to fully understand the characteristics of measured tide data, it is necessary to attempt to deconstruct the signal into these components. This process has been shown in Cornett et al. (2015) and Stock-Williams et al. (2013).

An example of a study to assess the accuracy of harmonic analysis predictions was shown in Serhadlioğlu et al. (2013). The M2 and S2 components of the tide in the Anglesey Skerries in Wales were evaluated and the predictions of the tidal amplitude shown to be within 5% of observed data from the Admiralty Tide Tables. The model validation showed variations between the Irish and Welsh-English coasts which was attributed to the Coriolis force, which deflects the propagating wave towards the eastern Irish Sea.

A methodology for estimating and validating tidal current time series was introduced through the use of 'tidal diamonds', available from Admiralty chart data. The TotalTide software package (UK Hydrographic Office, 2018) was used to interrogate the tidal data. However, 'pseudo diamonds' were created based on interpolation from surrounding tidal diamonds as the spatial resolution was poor. A limitation of the TotalTide software package is that it only encapsulated the variability for the M2 and S2 tidal harmonic constituents. The predicted velocity was compared to measured

ADCP data at an EMEC site in Orkney and was shown to have a quality of correlation of 0.94 (Iyer *et al.*, 2013).

A study was carried out by Waldman *et al.*, (2017) to evaluate harmonic predictions within hydrodynamic modelling. The methodology used the T_Tide harmonic analysis software and compared outputs from two hydrodynamic models, created in MIKE-3 and Delft3D. Harmonic analysis of ADCP data was conducted in T_Tide and input to the hydrodynamic models. The resulting amplitudes and phases of the M2 and S2 constituents were compared to measured ADCP data. The data for the study was collected from the Inner Sound of the Pentland Firth in Scotland, the body of water that separated the north Scottish mainland from Stroma Island. The analysis using the Delft3D model predicted the amplitude and phase of the two constituents to within 3.1% and 15.2% respectively, compared to the observed values averaged across 3 depths (Waldman *et al.*, 2017). The MIKE3 model gave a 22.5% variation in the amplitude prediction and a 2% variation in the phase prediction. This study showed that the Delft3D model predicted the amplitude of the tide more accurately than the MIKE-3 model. However, the MIKE-3 model predicted the phase more accurately than the Delft3D model (Waldman *et al.*, 2017). This is one example which highlights the variation between tidal hydrodynamic modelling results.

Various methods to derive tidal constituent from a water level or current time series were outlined in (Zervas, 1999). A common method is the least squares method, which involves creating a matrix of covariance between each individual constituent time series and the observed time series. The matrix is inverted to solve for the amplitudes and phases of the harmonic constituents.

Another analysis software, the Tidal Analysis Software Kit (TASK) produced by Proudman Oceanographic Laboratory, was used to analyse tidal elevations records from one year of tide gauge data, at three locations, on the south coast of the UK (Blunden and Bahaj, 2006). A hydrodynamic model of the area was created using TELEMAC-2D and the tidal predictions compared to the harmonic analysis using the TASK code. The results showed a good agreement between the modelled and predicted sea-level elevations over the period. However, The RMS error was shown to be 10.0 cm, which represents 9.6% error relative to the spring tidal amplitude of 1.04 m. It is important to note that the majority of the error was produced in the first 12 hours of the model run, as the tide was initialised in the model.

2.3 Hydrodynamic Modelling

In science, a model is a representation of an idea, an object or a process, which is often used to describe phenomena that cannot be experienced directly. Models typically take two main forms; physical and numerical. Physical models are those commonly using scaled down versions of the real-life environment. Numerical models may refer to computer codes using numerical software

which solve mathematical equations that describe the system of interest. Models are very widely applied, for example: in architecture, where scaled down representations of buildings are built to communicate design ideas (Liebowitz, Criminisi and Zisserman, 1999); finance, where mathematical models represent the performance of a financial asset, business, or investment (Campbell, Lo and MacKinlay, 1997); and in automotive engineering where computer aided design is used to improve the performance of a car without the timely and costly construction of the actual car (Tovey, 1989).

The offshore marine industry utilises models, both physical and numerical, to help develop concepts and ideas. Physical model tests play a major part in the development of an energy device concept, providing a controlled environment to test design and functionality (McCombes *et al.*, 2010). For marine energy technologies, such tests are usually undertaken in a water tank, where the wave and flow characteristics are controlled to fit the user's requirements. Numerical models are routinely used in the marine industry to design turbines and calculate expected loads on a structure. Hydrodynamic models are used for predicting the available marine renewable energy resource at a site (see Pérez-Ortiz et al. 2013) for an example relating to tidal stream power assessment.

For exploitation of marine energy, a suitable site must have significant resource and thereby the potential to harness the maximum amount of energy. The UK is a prime location for deploying marine energy devices, and a number of sites have already been identified (ABPmer, The Met Office and Proudman Oceanograhic Laboratory, 2008). The tidal stream resource across the UK is highly dependent on the shape of the coastline (e.g. Draper 2011). The strongest tidal stream resource is through channels, around headlands and bays, where the tide is forced through constricted regions as it moves from the Atlantic Ocean towards the North Sea. As the tide travels onto the continental shelf, it propagates around the UK coastline. It is in coastal basins that tidal stream energy has the greatest potential to be captured by a tidal energy device. The potential extractable tidal stream resource from European waters is predicted to be 48 TWh/yr (World Energy Council, 2016) and 20 TWh/yr of the total could be harnessed from the seas around the UK (Offshore Renewable Energy Catapult, 2014).

Chapter 5 investigates the propagation of uncertainty in a hydrodynamic model for tidal stream resource assessment, through an investigation using Telemac-2D, a widely used open source software (Moulinec *et al.*, 2011; EDF R&D *et al.*, 2014). A step by step description is given, in Appendix E:, of the methodology required to build the Telemac model. However, there are limits to how far models can be used to replicate real environments, as errors and uncertainties are introduced (Adcock *et al.*, 2013).

A discussion is included of several common issues that may be encountered when developing a model. Chapter 5 concludes with an application of a numerical methodology for estimating the effect of bed friction uncertainty on tidal power statistics using a procedure proposed by Kreitmair (2018). The chapter presents an introduction to tidal stream power assessment, a description and review of hydrodynamic models, an outline of Telemac and how it is applied to a strait between the ocean, and results from a parameter study examining how bed friction uncertainties affects the expected power and its variance for a fence of tidal turbines in a strait. This the first time that the methodology is applied to estimate the uncertainty in power of a tidal stream turbine using a model developed in Telemac. The methodology presented here could be adapted and applied to consider uncertainty arising from other model inputs, such as eddy viscosity, turbine drag and turbulence.

Section 2.3.1 provides background information relating to the bed friction parameter used in a hydrodynamic model. Section 2.3.2 introduces hydrodynamic models and provides detail of commonly used software, describing the theoretical governing equations applied. Section 2.3.3 describes the main literature for hydrodynamic modelling of tidal stream turbines.

2.3.1 Background Theory

Prior to deploying a renewable energy device, it is necessary to determine the likely amount of energy it will capture. This directly impacts the financial viability of the project, as discussed in Chapter 3. Resource assessment aims to predict accurately the available energy at a potential site. Through carrying out a detailed study using a numerical model, the characteristics and behaviour of the resource can be quantified over time and space. In order to understand the characteristics of the tides at a prospective tidal energy site, it is important to know the likely flow speed. For early arrays, with less than 10 MW of installed capacity, it may be possible to deploy an ADCP at each turbine location (IEC, 2015). However, for larger arrays with more turbines, it becomes less economical to use this approach, and it may be necessary to extrapolate the site measurements across the site to the turbine locations. This is where hydrodynamic modelling comes in.

Several factors influence the available power at a tidal site. Bed roughness has been investigated in previous studies (You, 2006; Lewis *et al.*, 2017a), but is often used as a "tuning" parameter, to fit modelled flow speeds to measured values (e.g. Adcock et al. 2013). Within the wind industry it is common to specify the roughness of the land based on the land usage. Areas of water and open land are typically given low roughness values, whereas areas of forestry and built up urban areas are attributed high roughness values. For tidal sites it is much more difficult to specify a roughness value, although it is possible to attribute particular bed roughness values to specific seabed material (see e.g. Soulsby 1997). Table 2.5 shows the Manning coefficient, n, for various channel bed

characteristics. It should be noted that at many tidal sites, the flow has sufficiently high velocity to have washed away sediment particles, exposing the bed rock.

Table 2.5: Values of Manning Coefficient, *n* (Manning, 1895)

Wetted Perimeter	Manning Coefficient, n ($s.m^{-1/3}$)
Natural channels	
Clean and straight	0.030
Sluggish with deep pools	0.040
Major rivers	0.035
Excavated earth channels	
Clean	0.022
Gravelly	0.025
Woody	0.030
Stony, cobbles	0.035

Water movements through channels, estuaries, around headlands and along rivers are driven primarily by gravity. For prospective tidal stream energy sites, this is a result of a water-level gradient induced by the tides. Momentum is dissipated along the course of the flow due to friction of the water against the bed and the banks, irregularities of the bed (called "bedforms"), channel bends, turbulence, density currents, sediment transport, friction at the free surface, waves, and irregularities in the cross section. Not all of these phenomena are accounted for individually and explicitly in operational models.

Bed roughness is a variable that plays an important role in hydrodynamic modelling. The parameter is used to define the friction caused by the seabed as water flows over it. The bed roughness value will impact the velocity of the flow near to the seabed but it will also have implications across the water column and it therefore will greatly impact on the results of a hydrodynamic model (van Rijn, 2005).

Nikuradse (1933) introduced the concept of an equivalent or effective sand roughness height, K_s, to simulate the roughness of arbitrary roughness elements of the bottom boundary. In the case of sediments that are transported along the seabed, the effective bed roughness is generated by skin friction and form drag. The bed-shear stress (τ_b) can then be defined (Soulsby, 1997) and the bed roughness value, C_d, estimated as

$$C_d = 2\left[\log_{10}\left(\frac{K_s}{12h}\right)\right]^{-2} \quad (2.29)$$

where h is the mean water depth (Committee on Hydromechanics of the Hydraulics Division - ASCE, 1963). The effective bed roughness for a given bed material size is not constant, but is dependent on the flow conditions. For example, analysis from Mississippi River data (Leopold, 1953) shows that K_s strongly decreases from about 0.5 m at low flow velocity (0.5 m/s) to about 0.001 m at high flow velocity (2.0 m/s). This is due to the bed forms becoming more rounded and being transported away at higher velocities. The fundamental problem of bed roughness prediction is that the bed characteristics and hence the bed roughness depend on the main flow variables (depth, velocity) and sediment transport rate (sediment size). These hydraulic variables are, however, in turn strongly dependent on the bed configuration and its roughness.

Clastic sediments (material eroded from land) can be classified according to grain size as shown in Table 2.6. Grain sizes are indicative of the state of advancement of the weathering process. The oceanic and coastal seabeds are mainly formed by the settling of sediment particles out of suspension, which is mainly determined by the particle fall velocity (which in turn depends on size and density). Because the density of different types of sediments is similar, the grain size is determinant. The larger the grain size, the higher the fall velocity. The sediment in suspension is held there by a balance between fall velocity and upward turbulent flux. At very high concentrations, the fall velocity decreases, because particles increasingly interfere with each other, a phenomenon that is called hindered settling. Detailed reviews of coastal sediment transport are given by van Rijn (2005), Soulsby (1997) and Sumer & Fredsoe (2002).

Using the characteristics of the sediment found in a channel, forming the bed surface, may be used to define the bed roughness, in the same way that the wind industry defines the roughness of the land, as discussed in Chapter 3.

Table 2.6: Sedimentary particles and the corresponding grain size, adapted from (Huggett, 2007), the equivalent Chézy roughness values were adapted from the Manning roughness values in (Arcement and Schneider, 1989) and the bed roughness values were calculated from Equation 6.1 (Appendix E:).

Particle Type	Particle Name	Grain size [mm]	Chézy value	Bed roughness value, C_d
Gravel	Boulders	> 256	45 - 26	0.0048 – 0.0148
	Cobbles	64 – 256	60 - 36	0.0027 – 0.0075
	Pebbles	4 – 64	62 - 52	0.0025 – 0.0037

Particle Type	Particle Name	Grain size [mm]	Chézy value	Bed roughness value, C_d
	Granules	2 – 4	64 - 62	0.0024 – 0.0025
Sand	Very course	1 – 2	70 - 51	0.0020 – 0.0037
	Coarse	0.5 – 1	82 - 69	0.0015 – 0.002
	Medium	0.25 – 0.5	150 - 80	0.0004 – 0.0015
	Fine	0.125 – 0.25	-	-
	Very fine	0.0625 – 0.125	-	-
Silt		0.002 – 0.0625	-	-
Clay		< 0.002	-	-

2.3.2 Hydrodynamic Models

Hydrodynamics is the study of motion of liquids, in particular water. A hydrodynamic model is a tool able to describe or represent the motion of water. Nowadays, modelling hydrodynamics is conducted numerically using computational models, which are able to run a wide range of simulations quicker and cheaper than physical models.

With the scientific development of numerical models along with advances in computer technology, hydrodynamic modelling has become part of a larger field of computational fluid dynamics (CFD). Hydrodynamic modelling differs from other CFD specialisations through its focus on the movement of water (which is often assumed to be incompressible). The common basis for modelling hydrodynamic phenomena is the numerical solution of the governing equations of conservation of momentum and mass in a fluid.

The basis of computational hydrodynamic models is the set of equations that describe the motion of fluids: the continuity equations, and Navier-Stokes momentum equations in conservative form are:

$$\frac{\partial u}{\partial x}+\frac{\partial v}{\partial y}+\frac{\partial w}{\partial z}=0 \tag{2.30}$$

$$\frac{\partial u}{\partial t}+\frac{\partial u^2}{\partial x}+\frac{\partial uv}{\partial y}+\frac{\partial uw}{\partial z}=X-\frac{1}{\rho}\frac{\partial P}{\partial x}+v\left[\frac{\partial^2 u}{\partial x^2}+\frac{\partial^2 v}{\partial y^2}+\frac{\partial^2 w}{\partial z^2}\right] \tag{2.31}$$

$$\frac{\partial v}{\partial t}+\frac{\partial uv}{\partial x}+\frac{\partial v^2}{\partial y}+\frac{\partial vw}{\partial z}=Y-\frac{1}{\rho}\frac{\partial P}{\partial y}+v\left[\frac{\partial^2 u}{\partial x^2}+\frac{\partial^2 v}{\partial y^2}+\frac{\partial^2 w}{\partial z^2}\right] \tag{2.32}$$

$$\frac{\partial w}{\partial t} + \frac{\partial uw}{\partial x} + \frac{\partial vw}{\partial y} + \frac{\partial w^2}{\partial z} = Z - \frac{1}{\rho}\frac{\partial P}{\partial z} + v\left[\frac{\partial^2 u}{\partial x^2} + \frac{\partial^2 v}{\partial y^2} + \frac{\partial^2 w}{\partial z^2}\right] \quad (2.33)$$

where t is the time, x, y and z are the Cartesian coordinates: u, v and w are the stream-wise, transverse and vertical velocity components of the fluid respectively; X, Y and Z are the external components force per unit mass; P is the fluid pressure; ρ is the fluid density (density of seawater ρ = 1025 kg/m³); and v is the kinematic viscosity.

The momentum equations are derived from Newton's laws of motion and describe the action of forces applied to the fluid that results in changes to the flow. The main assumption is that the stress in the fluid is the sum of a diffusing viscous term and a pressure term, enabling the characterisation of viscous flow.

Three types of models are used to conduct a resource assessment. These are typically defined by the number of dimensions that they can resolve. Firstly, one dimensional (1D) numerical models are used to assess energy extraction from channels (Garrett and Cummins, 2005; Vennell, 2011). These models require parameters such as the bed friction, channel dimensions, head difference between the end of the channel and the peak volume flow. However, 1D models cannot account for varying bathymetry in the transverse direction, changes in the channel geometry, or asymmetrical energy extraction.

Two dimensional (2D) models overcome several limitations of 1D models, in that they can account for local changes in bathymetry, variable coastal geometries and asymmetrical tidal energy extraction. 2D models using depth-averaged velocities carry a reduced computational overhead in comparison to three dimensional (3D) models, and the error introduced has been shown to be small compared to the uncertainties associated with calculating the mean velocity value (Blunden and Bahaj, 2006). 2D models are typically applied in medium to large scale resource assessment studies and can be used to identify far field effects due to tidal energy extraction (Pérez-Ortiz, Pescatore and Bryden, 2013; Lewis *et al.*, 2015; Haverson *et al.*, 2018)

3D models increase the accuracy of resource assessment because they calculate the velocity profile of the water column, and can include effects of flow diversion and blockage due to the presence of tidal turbines (Baston and Harris, 2011). However, the improved accuracy is achieved at the cost of computational overhead, and so 3D models are usually restricted to small-scale applications (Rahman and Venugopal, 2015; Chatzirodou, Karunarathna and Reeve, 2017; Togneri *et al.*, 2017).

This study focusses on the impact of uncertainty on resource assessment provided by 2D models. The results should be useful to financers and developers involved with tidal energy yield predictions.

Within the marine industry there are a wide range of hydrodynamic codes available. Some codes are open source (i.e. there is no initial cost to use the software). Other codes have been developed for commercial gain and require licences and payments to use them. In practice, such codes go through vigorous calibrating and validation processes. As an example, DNV GL (previously GL Garrad Hassan) initiated the development of the TidalFarmer software tool and underwent further developments through the Performance Assessment of Wave and Tidal Array Systems (PerAWaT) project. The project provided numerical and experimental data for model validation (Rawlinson-smith *et al.*, 2010). Table 2.7 outlines details of several available numerical software tools for tidal energy resource assessment, and provides references to academic papers where each one has been implemented.

Table 2.7: Hydrodynamic models available for tidal energy resource assessment

Hydrodynamic Model	Developed by	Model capability	Accessibility	Examples of use in academia
ADCIRC	The University of North Carolina	2D/3D	Open source	(Lynch and Davies, 1995; Hench and Luettich, 2003)
Delft3D	Deltares	2D/3D	Open source	(Rahman and Venugopal, 2015; Chatzirodou, Karunarathna and Reeve, 2017; Waldman *et al.*, 2017)
Fluent	ANSYS	2D/3D	Commercial	(Bai, G Spence and Dudziak, 2009; Hunter, Nishino and Willden, 2013; Zhang *et al.*, 2017)
FVCOM	The University of Massachusetts-Dartmouth	3D	Open source	(Chen, Liu and Beardsley, 2003; Yang *et al.*, 2013; Murray and Gallego, 2017)
MIKE (11, 21, 3)	DHI	1D/2D/3D	Commercial	(Warren and Bach, 1992)
POLCOMS-WAM	National Oceanography Centre	3D	Open source	(Holt *et al.*, 2005; Bolanos *et al.*, 2009; Walkington and Burrows, 2009; Bolaños *et al.*, 2011)

Hydrodynamic Model	Developed by	Model capability	Accessibility	Examples of use in academia
ROMS (Regional Ocean Modelling System)	Rutgers University, The University of California (UCLA)	2D/3D	Open source	(Lewis *et al.*, 2015; Togneri *et al.*, 2017)
SUNTANS	Stanford University	2D/3D	Open source	(Fringer, Gerritsen and Street, 2006)
Telemac-Mascaret	Artelia, BAW, CEREMA, EDF, HR Wallingford, Daresbury Laboratory	2D/3D	Open source	(Hervouet, 2000; Brière *et al.*, 2007; Moulinec *et al.*, 2011; Pérez-Ortiz, Pescatore and Bryden, 2013; Haverson *et al.*, 2018)
TidalFarmer	DNV GL	3D	Commercial	(Thomson, Whelan and Gill, 2011; Stock-Williams, Parkinson and Gunn, 2013)
TideModeller	ANSYS	3D	Commercial	(Crammond *et al.*, 2013)

2.3.3 Review of Hydrodynamic Modelling for Tidal Energy Yield

A review is now given of literature concerning the analysis of energy extraction from a tidal channel. Previous studies have considered analytical models of tidal power extraction from channels (Garrett and Cummins, 2004, 2005; Bryden and Couch, 2007; Blanchfield *et al.*, 2008), numerical models of site specific coastal regions (Blunden and Bahaj, 2006; Sutherland, Foreman and Garrett, 2007; Karsten *et al.*, 2008) and numerical models of general coastal regions (Bryden *et al.*, 2007; Polagye *et al.*, 2008). These studies have typically considered the maximum power that can be extracted from a coastal site and the impact of tidal devices on tidal variables such as the local tidal range and tidal current. As a result, a reasonably complete understanding has been developed of the power potential of well-bounded tidal streams, such as tidal flow through a single channel between two basins.

Previous numerical models have all been based on approximations to the Shallow Water Equations (SWEs), with the effects of tidal devices typically introduced through an added roughness or a general source term (Sutherland, Foreman and Garrett, 2007; Karsten *et al.*, 2008). This approach to represent tidal devices is valid as a first order approximation given that an enhanced bed roughness value cannot be related to a particular tidal device configuration. Nevertheless, this

method is useful for the purposes of this study. In each of these studies, the presence of tidal devices is modelled by an additional bed friction source term. For example, in both Sutherland et al. (2007) and Karsten et al. (2008), the friction coefficient is defined as

$$C_d = k_o + k_t \tag{2.34}$$

where k_o is related to the natural bed roughness and k_t represents an additional friction term due to the presence of tidal turbines. Bryden and Couch (2007) considered tidal flow around an island and used the same approach to represent idealised turbines by means of an added roughness value. Polagye et al. (2008) simulated uniform flow in a channel with one open boundary and one closed boundary. An alternative method to represent the turbines was implemented through the use of two discontinuous changes in width defining an internal extraction zone across the complete width of the channel.

Several ways are available by which to represent the effects of a tidal turbine in a shallow flow model. One approach is to evaluate a local drag coefficient which represents a resistance to the flow due to the presence of the turbines. By simulating an equivalent depth-averaged bed roughness over an area of the seabed, this method can provide a first approximation to modelling tidal energy devices. In practice, tidal turbines can be introduced over several strips of element in a tidal farm assumed to be uniform over each strip. The natural bed shear stress coefficient, C_d, in the vicinity of tidal devices is augmented to

$$C_{Tot} = C_d + C_T \tag{2.35}$$

where C_T is the roughness coefficient representing the increased roughness due to the presence of tidal turbines, per unit area of seabed. The energy dissipated directly from the presence of turbines otherwise described by the instantaneous power, P_t, extracted by the devices is

$$P_t = \frac{C_T}{C_d + C_T} P \tag{2.36}$$

where, P, is the potential power extracted from a 'farm' of turbines in a channel, defined in Equation 5.5. The use of Equation 2.36 to model tidal devices has been adopted in several studies on tidal energy extraction reported in the literature. For example, (Sutherland, Foreman and Garrett, 2007) and (Karsten *et al.*, 2008) use Equation 2.36 to calculate the potential power of two prospective tidal sites in Canada: the Johnstone Strait and the Minas Passage, Canada.

Other methods to model turbines include the use of Linear Momentum Actuator Disc Theory (LMADT) as discussed in (Garrett and Cummins, 2007; Houlsby, Draper and Oldfield, 2008;

Draper, 2011; Houlsby and Vogel, 2016) and the electrical circuit analogy as discussed by Draper (2011) and Draper et al. (2013).

Two approaches are used to model the local hydrodynamic effects of a tidal turbine in a hydrodynamic model: the actuator disk method, where the influence of a turbine is modelled through a head drop; or through an increased drag force induced by a turbine opposing the flow. The latter approach can be thought of as being similar to increasing the bed friction, and has been successfully applied in Telemac-2D (Joly et al. 2013, 2015). The drag force, F_D, on a tidal turbine is defined by

$$F_D = -\frac{1}{2}\pi R^2 \rho C_D \, U_r |U_r| \tag{2.37}$$

where R is the radius of the tidal turbine swept area, ρ is the fluid density, C_D is the drag coefficient of the turbine (usually provided by the developer and confirmed by the manufacturer), U_r is the velocity along the central axis of the turbines ($U_r|U_r|$ is used instead of ${U_r}^2$so that the directionality of the flow is properly included).

The mechanical power, P, extracted by a tidal turbine can be calculated from:

$$\mathrm{P} = \frac{1}{2}\pi R^2 C_P \rho \, {U_r}^2 |U_r| \tag{2.38}$$

where C_p is the coefficient of power, a dimensionless number which represents the efficiency of a turbines' power.

Garrett and Cummins (2005) considered flow through a channel with a variable cross-section, as shown in Figure 2.16. The flow velocity, $u(x,t)$, in the channel was assumed to be a function of time, t, as well as position, x, along the channel, but independent of the cross-channel position. Blanchfield et al. (2008) also investigated the maximum theoretical extractable power from a tidal stream turbine in a channel linking a bay to the open ocean. In both cases, the 1D shallow water momentum equation was considered within the theoretical model to define the flow as

$$\frac{\partial u}{\partial t} + u\frac{\partial u}{\partial x} + g\frac{\partial \zeta}{\partial x} = -F \tag{2.39}$$

where $F(x,t)$ represents an opposing force associated with the natural bed friction and possibly the presence of turbines and ζ is the slope of the surface elevation.

Garrett and Cummins (2005) developed an analytical model to describe energy extraction from a tidal turbine in a channel. The maximum average power, $\bar{P}$, that can be extracted from the channel when subjected to a driving tide with amplitude, a, either end of the channel is shown to be

$$\bar{P} = \gamma \rho g a Q_{max} \tag{2.40}$$

where Q_{max} is the maximum flow rate in the undisturbed channel, ρ is the density, g is acceleration due to gravity and γ is a dimensionless factor that varies between 0.19 and 0.26. The range of γ is representative of the dynamic balance in the channel, with a value of 0.21 in both models.

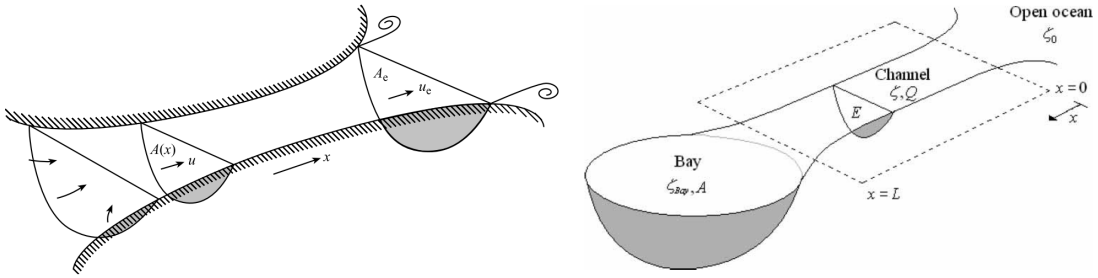

Figure 2.16: A channel connecting two basins with different tidal elevations (left), from (Garrett and Cummins, 2005)**. A channel connecting a bay to the open ocean (right),** (Blanchfield *et al.*, 2008)

Draper (2011) used a discontinuous Galerkin numerical model, a form of numerical method for solving differential equations (Cockburn and Shu, 1998), to solve the shallow water equations, with LMADT representing a turbine fence. Draper then assessed 12 cases of idealised channel geometry to evaluate the maximum extractable power from tidal turbines. The dimensions of the channel cases are detailed in Table 2.8 and a schematic of the mesh used is shown in Figure 2.17. The channels varied in scale from relatively short channels and shallow water depths, to longer and deeper channels.

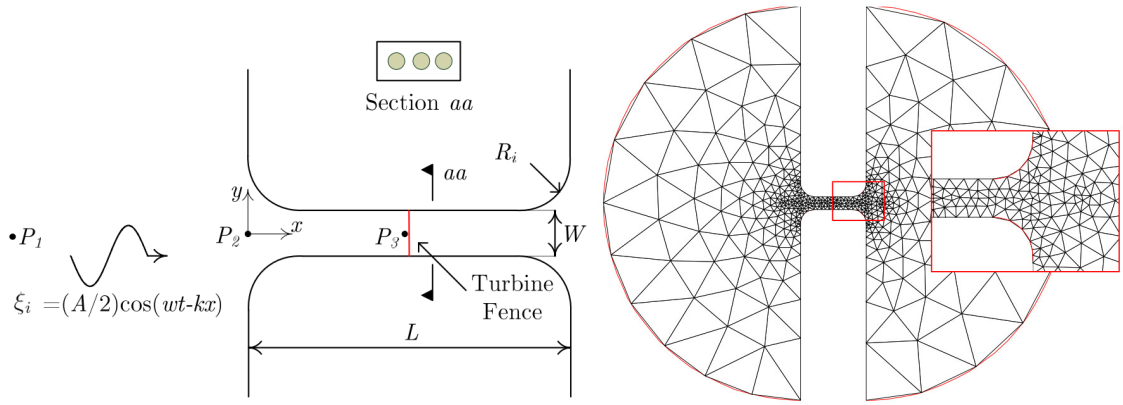

Figure 2.17: Scott Draper channel schematic (Draper, 2011)

Each modelled case was designed so that the Froude Number, *Fr*, had a value between 0.10 and 0.21. The Froude Number is a dimensionless parameter which is a measure of the ratio between the inertia force on an element of fluid to the weight of the fluid element, such that

$$Fr = \frac{v}{\sqrt{g h_m}} \tag{2.41}$$

where *v* is the mean flow velocity in the channel, *g* is the acceleration due to gravity and h_m is the hydraulic mean depth. In a wide, rectangular channel, the hydraulic mean depth tends to the depth of the channel.

Draper showed that the maximum extractable tidal power from a channel, for a given driving tide, is affected by the shape of the channel and that wide, deep channels provide the least impedance to the flow, thereby increasing the power that can be extracted by tidal devices (Draper, 2011).

Table 2.8: Draper (2011) channel parameters

Case	L [km]	W [km]	H_o [m]	C_d	A [m]	A/h_o	σ	Fr	ωL/U	C_dL/h
5-1	6	1.2	40	0.025	0.7	0.01	52°	0.21	0.25	0.375
5-2	6	1.2	80	0.01	1.75	0.02	20°	0.15	0.2	0.8
5-3	6	1.2	25	0.025	0.4	0.02	42°	0.13	0.4	0.6
5-4	6	1.2	25	0.01	1.1	0.04	15°	0.13	0.4	2.4
5-5	20	4	80	0.025	1.5	0.02	68°	0.11	0.90	0.625
5-6	20	4	80	0.01	4	0.05	28°	0.13	0.75	2.5
5-7	20	4	35	0.025	1.7	0.05	50°	0.10	0.95	1.4
5-8	20	4	35	0.01	2.5	0.07	21°	0.11	0.90	5.7
5-9	1	0.2	80	0.025	0.5	0.01	34°	0.19	<0.1	<0.1
5-10	1	0.2	80	0.01	0.6	0.01	14°	0.16	<0.1	0.1
5-11	1	0.2	10	0.025	0.15	0.02	15°	0.21	<0.1	0.2
5-12	1	0.2	10	0.01	0.3	0.03	8°	0.17	<0.1	1.0

Draper's model and analysis of energy extraction from a channel between two large bodies of water was verified against alternative results obtained by Bryden et al. (2004) for quasi-steady flow using 1-D momentum and continuity equations (with Bryden et al. using enhanced roughness

to model the energy extraction). Further verification against the analytical model by Garrett and Cummins (2005) was also carried out (Draper, 2011).

2.4 Chapter Conclusions

This chapter has addressed the methods used to assess uncertainty, including an overview of the terminology used and the key methods for uncertainty analysis. The normal distribution relies on assumptions from the central limit theorem, but helps ascertain levels of uncertainty when predicting future events. Other probability distributions can be used depending on the likelihood of occurrence and the characteristic of the uncertainty.

Probability distributions are an important part of the statistical analysis of data and for predicting future outcomes. Therefore, they are a critical component of uncertainty analysis. When estimating measurement uncertainty, it is important to use the correct probability distribution; otherwise the uncertainty value may be over or under estimated. The most common include the normal distribution as well as the rectangular, u-shaped and triangle distribution. There are many further distributions (Carta et al. 2009), however these are not considered in this thesis.

Uncertainties in forecasting are particularly important for predicting energy yield production. It allows financers to agree on the level of debt to provide for prospective renewable energy projects. Individual uncertainties are calculated and combined typically using the root-mean-square method, to give an overall uncertainty value. How this is implemented in the wind energy industry is discussed in more detail in Chapter 3, with implications for the tidal energy industry.

When simple assumptions regarding the standard deviation of a measured value do not suffice, other methods can be adopted to assess uncertainties. These include: jack-knife methods, commonly used in the wind industry; conducting sensitivity studies to assess the impact of varying inputs to models; Monte Carlo analysis to repeat high quantities of iterations of equations; and the analysis of residuals between measured and modelled values. The information outlined in this chapter provides the foundations for the statistical methods used in the remainder of the thesis.

Chapter 3

A Comparison of Tidal and Wind Energy Yield Procedure

3.1 Introduction

This chapter compares methodologies for calculating energy yield prediction for typical tidal and wind energy projects. As the tidal industry moves towards array development, approaches are required to evaluate uncertainty and minimise risk. This topic has been addressed in detail by the wind energy industry, and experience has shown that resource assessment is complex and subject to inherent uncertainty (Lackner, Rogers and Manwell, 2007; Kwon, 2010; Lira *et al.*, 2014). Historically, wind farm performance has been overestimated, adversely affecting investment and impacting sector growth (Johnson, White and Jones, 2008; Bruce Bailey, 2016; Blair Walter, 2017). Present wind resource assessment methods allow uncertainty in project return estimates to be determined. The process to achieve standardisation has been extensive, over many years, with areas to reduce uncertainty still being researched, and potential solutions continuing to be debated.

The following work proposes a transfer of existing experience and knowledge of uncertainty estimation from established processes at Wood and within the wind industry to the nascent tidal industry, based on similarities in annual energy yield calculations. Results detailed in this chapter show that there are significant analogies between the processes underpinning wind and tidal yield assessments. There is significant overlap within resource modelling, power performance assessment, and wake effect analysis. Knowledge and processes can be modified from wind techniques to better evaluate the tidal resource and estimate the yield output.

Section 3.2 outlines the importance of uncertainties in the financing of renewable energy projects. Section 3.3 introduces energy yield assessment in the context of the wind industry with a focus on its progression to its current established state. Section 3.4 outlines the importance of standardisation and how the tidal industry is already beginning to learn from the experience of the wind industry. Section 3.5 provides an outline of the wind energy yield procedure, which is then compared with the tidal energy yield procedure. Section 3.6 provides more detail on the similarities and differences between wind and tidal energy site assessments and summarises analogies and lessons that can be learnt. Section 3.7 discusses how long term estimates of the resource for the

tide and the wind are conducted using very different methods. This section also covers key areas in which processes could be transferred from the wind methodology to tidal. Section 3.8 outlines the similarities and differences in spatial modelling and the important part these play in evaluating the variation to the behaviour of the resource at a site. Section 3.9 compares losses typically applied to a wind energy yield assessment to losses for a typical tidal project. Section 3.10 outlines analogies in uncertainty classification, and, where possible, their quantification.

3.2 Uncertainty in Renewable Energy Financing

A typical renewable energy yield assessment aims to derive the gross generation by combining resource with a power conversion relationship. For a nominal wind energy site, the gross energy is calculated by combining the wind speed frequency distribution with the power curve from a wind turbine generator. The power curve defines the relationship between wind speed and power output. Technical loss factors are applied to estimate the net energy generation. Finally, an uncertainty analysis is conducted to determine the probability distribution of net energy production.

Every energy yield prediction is subject to uncertainty. Even the most thorough resource assessment campaign will give an imperfect knowledge of the resource at the site. This uncertainty grows when trying to extrapolate the outputs of the resource assessment in space and time, and is compounded again by uncertainties in plant performance and other losses. The purpose of an uncertainty assessment is to define the probability limits of the energy yield. In this context, energy yield uncertainty is the degree of precision with which an energy yield is predicted.

Uncertainties are particularly important to financiers since energy yield uncertainty translates directly into uncertainty in the revenue that a project will generate. Consider a project funded by debt finance. If the project revenues are roughly as expected, the loans are serviced and the owners make a modest return. If the project does better than expected, the owners of the project reap the benefit, but the debt providers do not see any additional return. However, if the project does not do as well as expected, the development company may be unable to service its debt and the debt providers will lose out. Debt providers are therefore exposed to the downside risks of uncertainty but would not see any upside benefits.

Investors need to understand energy yield uncertainty to gauge the risks associated with their investments. A process for assessing uncertainties has become well-developed in the wind industry. This involves working through a “taxonomy” of potential sources of uncertainty, and assigning a value to each one. These uncertainties are usually then combined using a root-sum-squares method to determine an overall energy yield uncertainty for a project (Joint Committee

For Guides In Metrology, 2008). Finally, this uncertainty is used to calculate energy yields that have specific exceedance probabilities.

In the planning and financing stage of a wind farm project an uncertainty assessment is required, quantifying all uncertainties related to the wind farm financing. Financial modelling requires a comprehensive understanding of the project assumptions in combination with an assessment of their sensitivities in order to define an agreed base case. One of the risks for renewable developers is the variability of the resource. While forecasting is continually improving, no developer is able to guarantee that a project with a strong energy estimate will not underperform for a period. Therefore, to protect themselves from such underperformance, investors have developed a way to put production requirements on projects and thereby de-risk the loan. These requirements involve the calculation of probabilities for energy production which are expressed as P values (where 'P' stands for 'Probability').

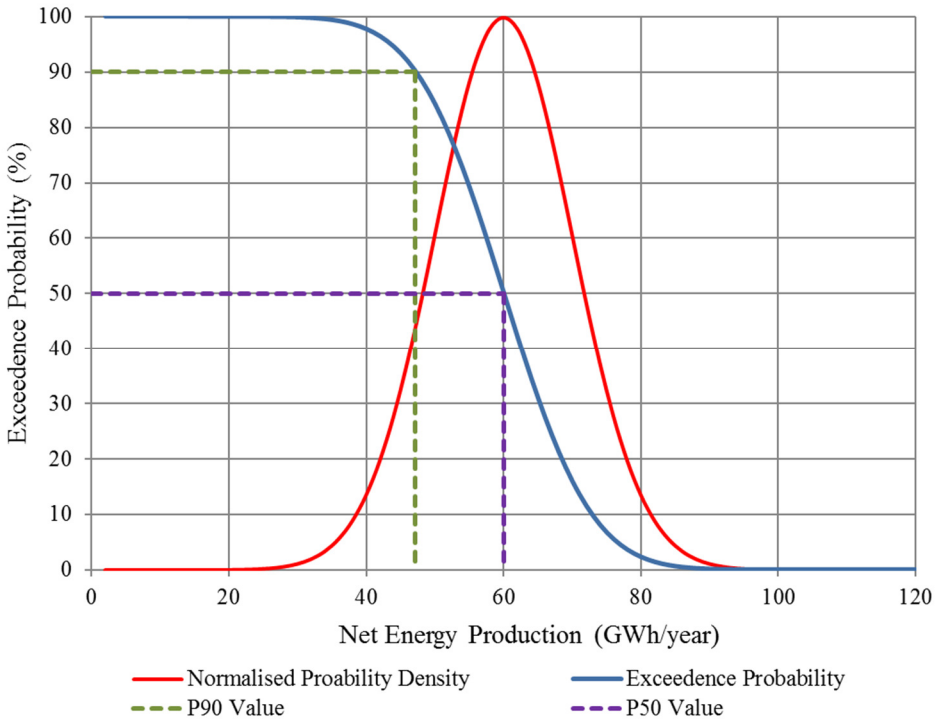

Figure 3.1 - Normal distribution graph showing difference between P90 and P99 for renewable energy financing

The result of an energy yield prediction in terms of an annual energy production (AEP) is called the P50 defined such that the probability of the AEP being higher or lower than this value is 50:50. An uncertainty assessment includes the quantification of the project-specific uncertainties and the whole range of exceedance probabilities, Pxx (where 'xx' is an integer between 1 and 100), of the wind farm's AEP. Other common probability values used include the P75 and P90 values. The

P75 value is the AEP with a probability of exceedance of 75%. Similarly, the risk that an AEP of P90 is not reached is 10%. Both values are widely used by banks and investors as a base in their financing decisions (Deloitte, 2014). Once the P50 value and the level of uncertainty are derived, a normal distribution is applied allowing any probability of exceedance value to be calculated (as shown in Figure 3.1). The reason for applying the normal distribution is discussed in more detail in Chapter 2.

Project developers use and promote a given project based on its P50 value, given that it is the most likely outcome in any given year. A P90 value is the level of generation that is forecast to be exceeded 90% of the year. This is a conservative estimate and for an investor, the P90 value gives a lower level of risk. For 90% of the time, the forecast generation will be exceeded and therefore the project will more likely meet its financial performance targets. This creates a dilemma where project developers want to use the P50 estimate, but their investors push them to deliver project that are viable based on the P90 estimates. The difference between the P50 and the P90 value is the level of the combined uncertainty. Therefore, reducing the level of uncertainty will give a higher P90 estimate for the same P50 value, as shown in Figure 3.2.

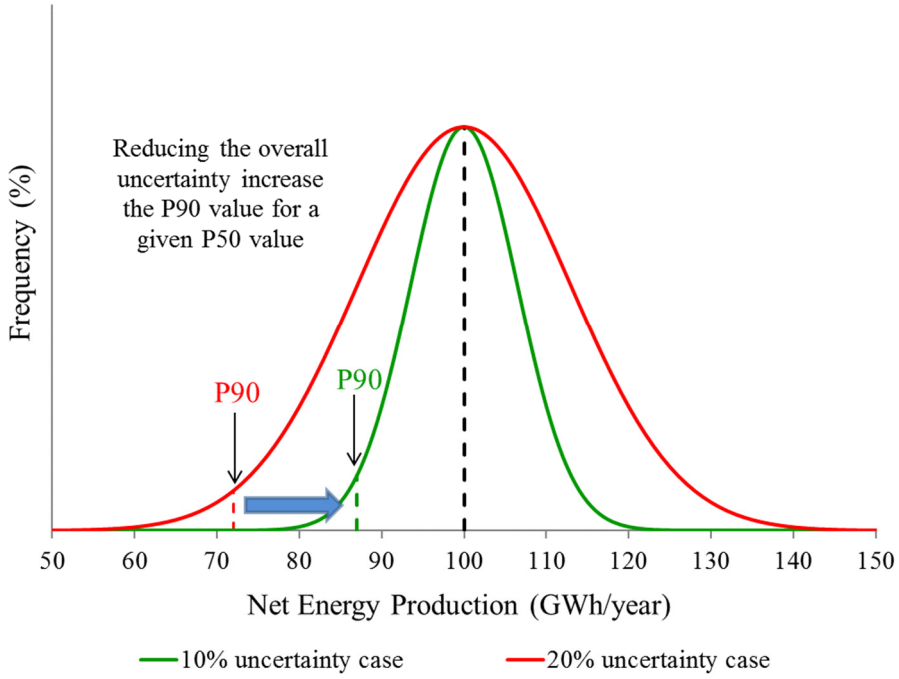

Figure 3.2 - Graphical visualisation of energy yield estimates for two hypothetical projects with differing uncertainty values

Finance arrangements vary from project to project. However, for debt finance of wind energy projects in Europe, it is typical that investors will determine the maximum loan size they are willing to extend based on the P90 value. An investor will size a loan such that the annual revenue

at the P90 level is a certain factor greater than the interest payments on that loan. This factor is known as the Debt Service Coverage Ratio (DSCR) and a DSCR of 1.4 based on the P90 is typical for onshore wind projects in the UK, whereas certain American investors use a DSCR of 1 based on the P99; the energy yield that has a 99% chance of being exceeded (Deloitte, 2014). The lower the uncertainty on a project, the closer the P90 and P99 are to the P50, so the greater the proportion of the development cost that can be covered by debt finance. This means that equity investors require a smaller investment, but will probably achieve a greater return on that investment.

It is important that uncertainties are quantified correctly in order to put the accuracy of the energy estimate into an appropriate context for project finance. Projects seeking finance from lenders will generally decide their lending value based on the P90 value. Project developers, therefore, want to minimise uncertainty in the assessment, in order to maximise the amount of money they can receive from lenders.

There are two approaches within the wind industry to estimating uncertainty: 'Type A' and 'Type B' evaluations. 'Type A' uncertainty is evaluated using statistical methods, usually determined from repeated readings. 'Type B' uncertainty is estimated using other methods, namely: calibration certificates, manufacturer's specifications, calculations, published information, and past experience of the analysis (Bell, 1999). For more information, please refer to Chapter 2.

3.3 Energy Yield Assessment

An energy yield assessment is an estimate of the energy production for a renewable energy project. Prior to planning, it is essential to determine where the most abundant resource exists. Producing more accurate estimates, through reduced uncertainty, helps developers acquire finance for their projects. Without high-quality assessments of renewable energy resources, the risks of projects are greatly magnified, and private financing will be correspondingly harder to obtain (The World Bank and Climate Investment Funds, 2013). In calculating the yield of a project, there are many factors which influence the final output. Understanding these factors and calculating the uncertainty around the yield estimate can be a challenge.

The wind energy industry is approximately 30 years ahead of the tidal stream industry and experience has shown that wind resource assessment is complex and uncertain (Kaldellis and Zafirakis, 2011; Garrad, 2012). Through the development of the wind energy industry, any issues identified were met with significant research efforts to resolve them. For example, in the UK, as the number of onshore wind project has increased and planning permission to develop on land became more difficult to obtain, many developers focussed their effort offshore to capture the benefit of higher wind speeds. Understanding how the resource differed offshore was important and particular attention was given to researching the effect of wakes on turbines in an offshore

environment. This area of research has benefited from many years of work and is still ongoing (Gribben and Frazer-Nash Consultancy, 2012; Adams and Frazer-Nash Consultancy, 2014; Moriarty *et al.*, 2014; Mortensen, Nielsen and Ejsing Jørgensen, 2015; Platis *et al.*, 2018). Many banks and lenders were first hit by energy predictions being overestimated. This was due to the use of low height meteorological (met) masts in resource measurement and the fact that wind shear is greater nearer the ground. This led to an overestimation in hub height wind speed from the extrapolation of wind speed from masts that were not high enough (Hodgetts and GL Garrad Hassan, 2012).

Wind resource assessment methods have developed since the first arrays were deployed, and the high levels of production data now available allow comparisons to pre-construction predictions. The development of uncertainty analysis enables developers and investors to have more confidence in their project return estimates. As the tidal stream industry moves towards array deployment, similar approaches are needed to evaluate uncertainty and minimise risk. At present, there is little known about tidal yield uncertainties and attempts to quantify them has shown that they are currently large (Adams *et al.*, 2015).

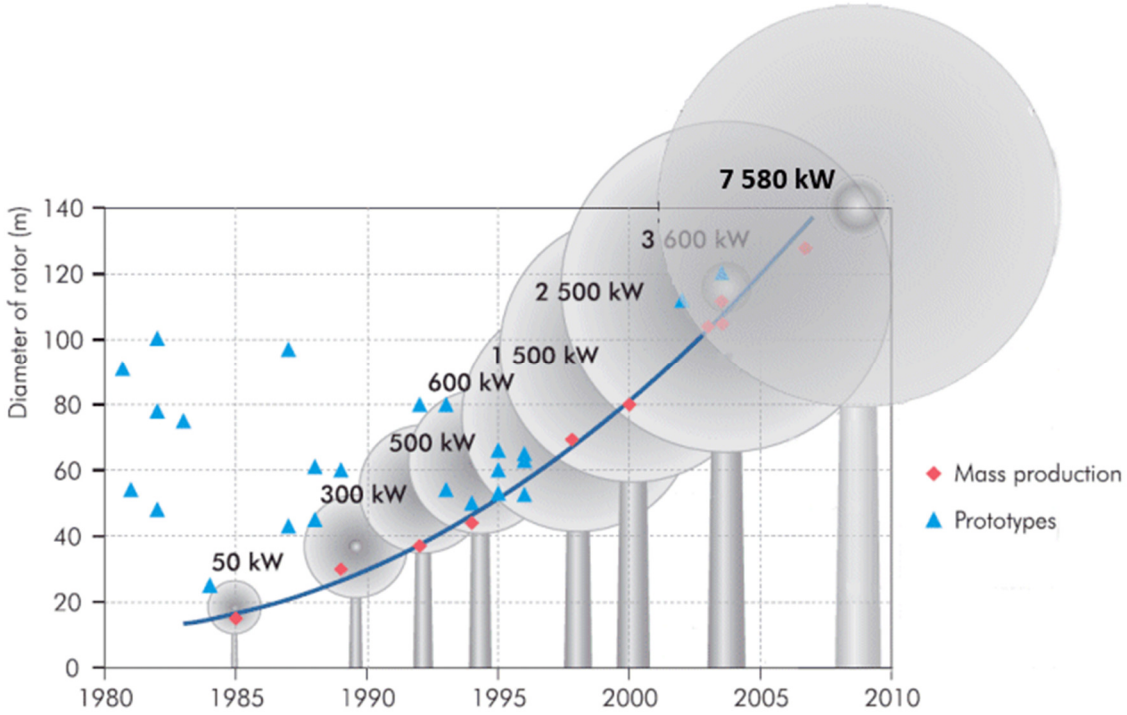

Figure 3.3 - Size and power evolution of wind turbines over time (National Renewable Energy Laboratory, 2012)

The wind industry has seen rapid increases in the size and scale of installations and, as offshore sites become more easily available and cheaper, wind turbines get larger. Early stage wind development saw the largest turbines being developed as prototypes by public/government

funding. Commercial wind began at small scale and increased slowly, through better understanding of the resource and incremental improvements in design, as shown in Figure 3.3. Since 1980, the diameter of the rotors of wind turbines has doubled each decade, and the turbine heights increased correspondingly. Each generation of turbines was predicted to be the biggest, but turbines keep evolving in an effort to capture the stronger winds accessible at higher elevations, and improve performance.

The economics of a wind farm project are crucially dependent on the wind resource at a site. A robust assessment of the energy production is essential in supporting investment and financing decision. In 2011, during a workshop at the European Wind Energy Association (EWEA) conference, 36 organisations from 16 countries participated in a cross-company study, where each organisation was asked to conduct an independent pre-construction energy yield assessment of a wind farm. The assessment results were compared and presented anonymously. The aim was to discover how organisations across the wind industry differ in the analysis of the same wind farm and hence to identify the areas with the largest discrepancies which required further standardisation. Table 3.1 shows the main results from the workshop, broken down into each part of the energy yield process.

Table 3.1- Summary of the results across the 36 organisations at the EWEA energy yield workshop in 2011 (Mortensen and Jørgensen 2011)

	All values are in GWh				
	Mean	Standard deviation	Coefficient of variance	Min	Max
Reference yield	116	7.7	6.6	98	131
Gross energy yield	121	3.5	2.9	113	127
Potential yield	113	3.6	3.2	104	120
Net energy yield (P_{50})	103	4.5	4.4	91	113
Net energy yield (P_{90})	89	6.4	7.2	73	99

The reference yield is calculated from the wind speed at the mast location, using the long-term wind distribution and the power curve for the turbine. The gross yield is calculated from the reference yield and includes the terrain or topographic effects from the flow model.

$$Gross\ AEP = Reference\ AEP \pm terrain\ effects \quad (3.1)$$

The potential yield is the gross yield value minus wake losses from wake modelling.

$$Potential\ AEP\ =\ Gross\ AEP\ -\ wake\ losses \tag{3.2}$$

The net energy yield (P_{50}) is the potential yield minus the estimated technical losses.

$$Net\ AEP\ (P50)\ =\ Potential\ AEP\ -\ losses \tag{3.3}$$

And the net energy yield (P_{90}) is the P_{50} yield value minus the uncertainties.

$$Net\ AEP\ (P90)\ =\ Net\ AEP\ (P50)\ -\ 1.282\ \times\ (uncertainty) \tag{3.4}$$

The results of the workshop show that despite the fact that the wind industry is well established, with approximately 540 GW of installed capacity worldwide in 2017 (Global Wind Energy Council, 2017), there are still inherent variations in the way that energy yields are calculated. In particular, this effects the calculation of the P90 value, which gives the largest variance across the whole process. The results from the study show that even within the wind energy industry, there are still large variations in how different companies calculate uncertainties. With this knowledge, the tidal industry needs to anticipate a similar issue and learn from experience in wind.

3.4 Uncertainty Categorisation

To date, considerable effort has been directed towards better understanding of uncertainties in wind energy yields. The International Electrotechnical Commission (IEC) is responsible for the development and publication of standards across all electrical, electronic and related technologies, including renewable electricity. Several technical committees work on the standardisation of best practices for wind energy. The most relevant to this work is Working Group 15, which intends to define a framework (IEC 61400-15) for the assessment and reporting of the wind resource, energy yield and site suitability input conditions for both onshore and offshore wind power plants. This technical group has been active since October 2013 and continues to work on developing a standard approach across the industry.

In 2013, DNV KEMA published a document, in collaboration with key industry organisations, to standardise loss factors and the uncertainty categories for wind. This was a significant milestone because the work clearly defined how to classify losses and uncertainties. Prior to this, organisations would use in-house definitions of uncertainty categories, which made it difficult when comparing different energy yields. Obviously, it was important to recognise that each project is different and requires site-specific considerations; and so the use of these clear categories would help compare uncertainty quantification. The report states that “the definitions are not an attempt to standardise the values of losses and uncertainties used in an assessment, but instead aim to provide a framework for the definitions” (DNV KEMA, 2013). The main limitation was that the

definition was only qualitative and there was no attempt to standardise the quantification of uncertainties. As the EWEA workshop case study shows, there are still variations in how organisations calculate wind uncertainties and energy yield values.

Two years later, the Offshore Renewable Energy Catapult (OREC) completed a study which aimed to replicate a similar framework categorising losses and uncertainties but for the marine energy industry. A comparison between the wind and marine categories can be found in Section 3.9.3. Collaboration with various industry stakeholders, through consultation, enabled an industry-wide standardisation for the definition of the uncertainties in marine energy yield estimates (ORE Catapult, 2015a). Similar to the DNV KEMA report for wind, this study primarily provided a framework for categorising uncertainties and failed to provide values or outline methods to quantify these uncertainties. Later, OREC commissioned Frazer Nash to develop a framework for these uncertainties (ORE Catapult, 2015c). The 3-month project involved conducting a literature review highlighting current knowledge and understanding of uncertainties, as well as producing a reference document including example projects, with some indicative uncertainty values associated with them. This proved useful in setting guidelines for applying uncertainties, but did not quantify explicit levels of uncertainty, but only went as far as providing uncertainty ranges for each category. This is discussed further in Section 3.10.

The next section presents an outline of the wind energy yield process and compares the tidal energy yield methods at each stage of the process. The subsequent sections then explore uncertainties in wind and tidal yield assessment, including an evaluation of lessons that can be learnt from the many years of experience and production of wind energy. It is anticipated that a fuller understanding and assessment of the wind industry methodology for conducting resource assessments and uncertainty analysis will help accelerate the maturing tidal industry by presenting uncertainties affecting the wind industry in a manner familiar to financiers.

3.5 Comparison of Wind and Tidal Energy Yield Methodology

It is important to state from the outset that there are inherent differences between wind and tidal resources. Fundamentally, wind is stochastic in nature, driven by differences in atmospheric pressure, whereas tides are deterministic, driven by the combined effects of the gravitational forces exerted by the Moon and the Sun and the rotation of the Earth. However, the methodology to calculate each resource is generally analogous and the energy is captured in a similar way; from the flow of a fluid (whether that is air or water) through a typically horizontal axis turbine.

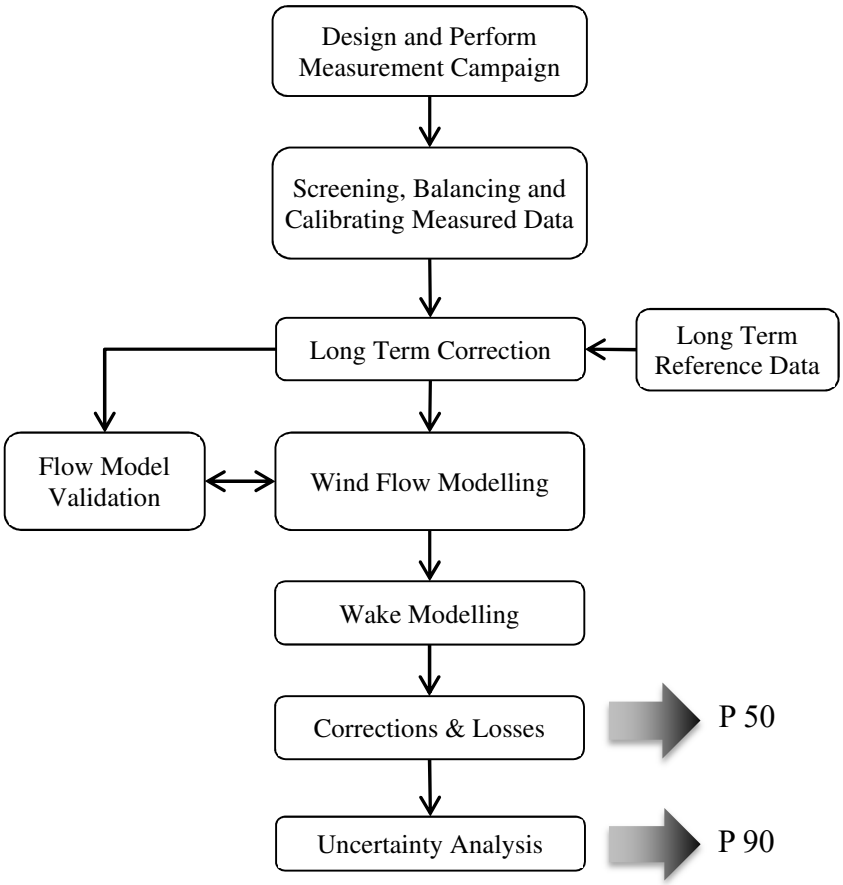

Figure 3.4 - Wind energy yield procedure diagram

This section outlines the simplified step-by-step methodology for completing a standard wind and tidal energy yield. Figure 3.4 shows a flow diagram of the processes involved in conducting a resource assessment for a wind energy project, adapted from Wood Group's wind energy methodology (Wood Plc, 2016).

Figure 3.5 shows the methodology for completing a tidal energy yield adapted from Wood's wind methodology and compared against the IEC technical specification 62600-201:2015. The energy yield assessment process for tidal energy shares many similarities with the wind energy process. This chapter details a complete comparison of the two methodologies and identifies the analogies that can be drawn at each stage, with an overall summary outlined in Section 3.10.1.

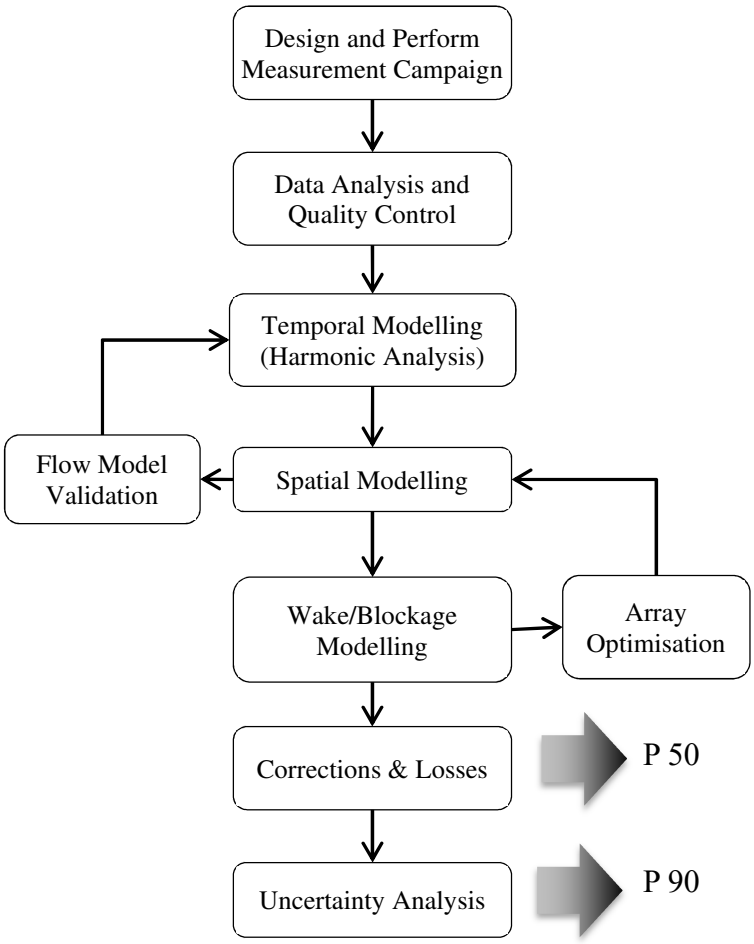

Figure 3.5 - Tidal energy yield procedure diagram

The measurement campaign is the first step in the process for both technologies. This involves installing a number of instruments at the site to measure the characteristics of the resource, the most important being the speed and direction of the air or water flow. Once the data have been successfully collected, post-processing and screening are required. These involve removing erroneous data and preparing the measurements for further analysis. For both wind and tidal assessments, the measurement campaign is conducted over a relatively short period compared to the length of the project. Therefore, the next stage is to conduct temporal modelling to predict how the resource will fluctuate over a longer period.

In order to determine how the resource varies across the site, spatial modelling is required. This step is similar for both technologies and involves the use of numerical models to perform the analysis. Temporal and spatial modelling should inform the optimal resource locations for the turbine farm. A gross energy yield value can then be estimated from the available information. The next steps are synonymous for wind and tidal. Losses are then applied; either calculated or estimated based on experience, and used to account for lost energy from production. This is the net energy yield value and typically has a 50% chance of being exceeded. The final energy yield

values incorporate uncertainties and allow a probability of exceedance value to be defined as detailed in Section 3.4. The following sections examine the processes in greater detail and aim to highlight important comparisons and establish lessons that can be learnt.

3.6 Site Assessment

Collecting raw site data is vital when conducting a resource assessment. This process can often take a long time and incur high costs but is an essential step. Although obtaining high quantities of quality data is the best approach to achieve an accurate energy yield value, cost and time constraints mean that data are usually collected over a relatively short time period.

3.6.1 Wind Energy Measurement Campaign

MEASNET is a consortium of companies which are engaged in wind energy to ensure high quality measurement, uniform interpretation of standards and recommendations as well as interchangeability of results. For much of the last decade, the most reputable European wind test centres have been involved in developing measurement standards to ensure that measurements are performed to a high quality. Over the same period, several national and international recommendations, standards and requirements for measurement procedures for wind velocity and wind turbine generator systems have been developed or are still under development. Consequently, for certain measurements, several different formal procedures for gathering and evaluating the data exist and have led to different measurement results. Experience also showed that measurements, performed by different institutes did not lead to comparable results, even if they took into account the same recommendations.

To improve this situation the most experienced wind energy institutes therefore decided to work together in a Measuring Network of Wind Energy Institutes called MEASNET with the goal of setting rules and requirements to ensure high quality measurements are achieved. The necessary creation of the network rules and the establishment of commonly agreed measurement methods were subsidised by the European Commission in two jointly performed projects. For the first time, institutes already in commercial competition agreed to work together for the benefit of their clients, with the objective to perform measurements of equal quality which are sufficient for the mutual comparison and acceptance necessary for the industry in an open worldwide market. Recommendations and information presented in this section are developed from the MEASNET procedure document titled ‘Evaluation of Site-Specific Wind Conditions’ (Measnet, 2009).

For the wind industry, measured wind data are collected at a proposed turbine site. Many sites can experience significant variations in resource, therefore it is important to measure on-site data as close to the proposed wind turbines as possible. This is achieved by installing one or more met

masts, depending on the size of the site, to measure the characteristics of the wind at multiple heights. A met mast will provide information on the wind speed from anemometers, wind direction using a wind vane, and sometimes atmospheric characteristics including temperature, humidity and air pressure.

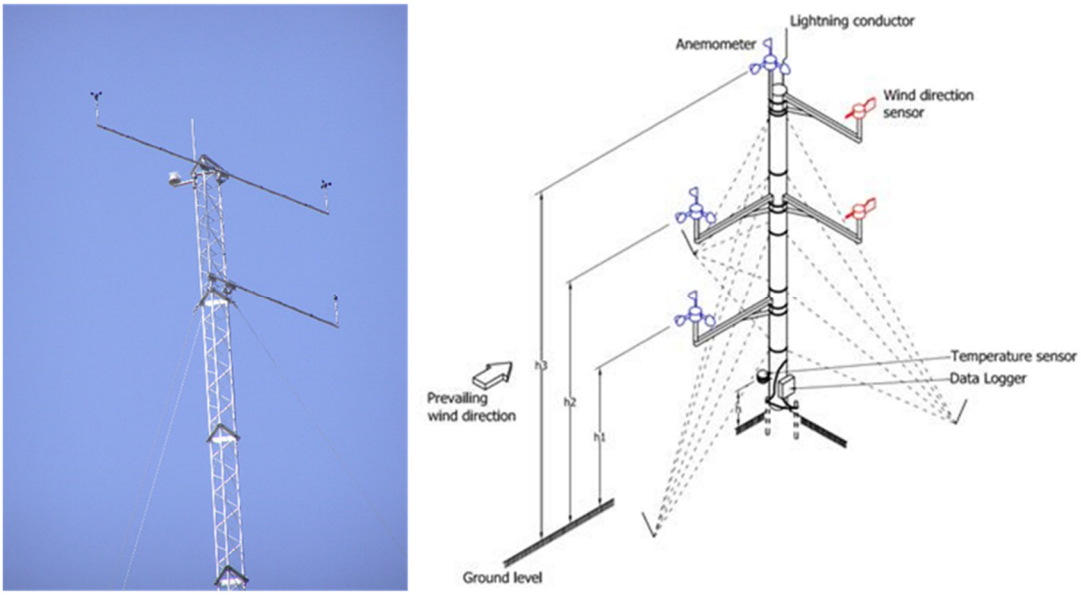

Figure 3.6 - Met mast configuration (Green Power Development, 2017; KONA, 2017)

Figure 3.6 shows the typical configuration of an onshore met mast. Cup anemometers are widely used across the wind industry to measure wind speed. Conventionally, an anemometer consists of three hemispherical or conical cups, arranged in a horizontal rotor configuration around a vertical shaft that drives a signal generation device. They are well suited to measure mean wind speed in a wide range of terrain and tend to be cost effective and robust in comparison to other types of instrument (International Energy Agency Technology Collaboration Programme, 2003).

The number of masts required depends on the size of the wind farm and the complexity of the site, but is ultimately at the discretion of the project developer. Whether the site is classified as simple or complex is influenced by factors such as the steepness of the slopes and the amount of forestry and areas of surface roughness at the site. Areas of open fields and water are allocated with low surface roughness values, while areas of forestry and built-up areas are given high roughness values.

Topographical data are typically supplied by the client for the project; however such data can be obtained from a number of sources depending on the country. In the UK for example, topographical data is sourced from Ordnance Survey maps and provided at 10 m resolution (Ordnance Survey, 2018). For larger sites it is advisable to have multiple met masts on the site. This may be due to the layout of the wind farm. If the wind turbines are positioned in clusters, then

it is often advisable to install a met mast within each cluster to represent the characteristics of the wind within the area of the cluster. Another example where it is beneficial to install multiple met masts at a site is where there are large variations in roughness, namely in a forest. It is useful, in this case, to use a different met mast for different types of exposure. Overall, the main advantage of having multiple masts is to validate the wind flow model and thereby reduce the horizontal extrapolation uncertainty. However, this adds expenditure to the measurement campaign. It should be noted that in most cases, spending more capital to ensure the measurement campaign is as robust and accurate as possible, will reduce the energy yield uncertainty and therefore increase the level of funding for the project, as discussed in Section 3.2.

To keep the uncertainty level below 1% (in wind speed), the MEASNET recommendation is to install met masts within 10 km of every wind turbine generator location for a simple site, and within 2 km for a complex site. However these figures do not have universal agreement in the wind industry, with various companies stating different values (Hodgetts and GL Garrad Hassan, 2012).

The length of the measurement period is another factor which will affect the final yield estimation. Typically, site data are collected for at least 1 year (12 consecutive months), to incorporate the seasonal variations of weather. A longer measurement period of data, collected by an onsite met mast, will result in a lower uncertainty value. However, this is affected by the costs and timescales of projects and it is not usually economically feasible to keep the met mast up for extended periods of time.

The type of anemometer used, the quality of the calibrations and the set-up of the met mast are all key factors which impact the uncertainty in the measurement campaign. Using well calibrated industry standard instruments that are mounted according to standard MEASNET practices and others such as IEC 61400/UKAS 17025 (British Standards Institution, 2017) will ensure that the uncertainty value is below 2%. The wind industry has largely adopted the MEASNET calibration system which, rather than a generic calibration standard, is one that is tailored to the requirements of the wind industry in order to minimise the measurement uncertainty. One of the checks of a wind energy yield assessment is to assess whether the met mast is compliant with the IEC specification. The requirement is that the booms connecting the anemometer to the mast are at minimum lengths so that the mast does not distort the wind flow.

In most cases the met mast will not reach the same height as the wind turbine hub height, especially considering the increase in capacity, rotor size and hub height of wind turbines the industry has seen in recent years. Therefore, vertical extrapolation of the wind shear is required to estimate the wind characteristics at the hub height. This introduces an uncertainty value dependent on the vertical distance from the anemometers to the turbine hub height. Wind shear is discussed in more detail in Section 3.6.1.2. The IEC standard for wind states that the mast height should be at least

2/3 of the hub height, whereas industry best practice typically recommends 3/4 of hub height. Overall, to keep uncertainty levels low (below 1%), it is recommended to install the met mast to a height within 10m of the proposed hub height of the wind turbine generator.

As the wind industry has developed, wind turbines have increased significantly in size, with longer blades and therefore higher hubs. This requires higher met masts which are more cumbersome and expensive to install, especially in areas with mountainous and complex terrain. As wind turbine rotor planes extend 150 m in diameter or wider, is it clear that the incoming wind field over the entire rotor plane is not measured representatively from a single cup anemometer mounted at hub height.

Accurate measurements of the inflow to the large wind turbines currently being installed will require multi-point, multi-height wind measurements within the entire rotor plane, to fully characterise the wind speed and wind shear. This can be achieved by using remote sensing devices such as SODAR (Sonic Detection and Ranging) or LIDAR (Light Detection and Ranging) as shown in Figure 3.7. These devices are commonly used in conjunction with a met mast for larger or more complex sites (Simley and Pao, 2012; Chaurasiya, Ahmed and Warudkar, 2017). In many cases the use of remote sensing, in combination with a met mast, allows wind speeds across a wider area to be evaluated.

Figure 3.7 - Images showing the applicability of LIDAR for wind energy (onshore-left, offshore-right) (Mitsubishi Electric, 2017)

These devices can be used for further validation of the characteristics of the wind at the site and to validate numerical models. Conducting resource assessments solely with LIDAR or SODAR is not fully accepted in the industry yet. However there have been a small number of projects which have been financed using LIDAR, for example Beatrice offshore wind farm (Froese, 2017). These projects have to meet specific standards of validation or the uncertainty levels will be much higher. Remote sensing devices are used more widely in conjunction with met masts to conduct power performance assessments (Khan and Tariq, 2018; Rehman, Mohandes and Alhems, 2018).

The subsequent sections highlight some of the areas that are involved in the analysis of the measured site data for a wind energy yield assessment.

3.6.1.1 Data Screening

Before the raw data are screened, it is important to check the calibration certificates of the measurement devices. Where incorrect calibrations have been applied, it is necessary to correct this. Calibrations are typically valid for two years, which means that longer measurement periods require ongoing maintenance and anemometer replacement, at least every 2 years, to maintain low levels of uncertainty.

Once the raw data are compiled and calibrated, the dataset requires screening. The aim is to identify and remove any anomalous data in the time series. The screening of the dataset is a key element of any reliable wind analysis process and failure to identify erroneous data may have a significant influence on the energy yield results. Software tools such as Windographer (AWS Truepower, 2018) allow the user to interrogate measured data in a range of ways. However, it is the job of the wind analyst to identify and remove inconsistent data, therefore the screening process should not be automated in any form. Anomalies in the data may occur for any of the following reasons:

Inconsistent wind shear profile

Wind speed should increase with distance from the ground in general. It should be noted that inverse shear (wind speed decreasing with elevation) is possible, just uncommon. Genuine negative shear can result from steep slopes in terrain in close proximity to a mast or from thermal effects. If there is some irregularity for an anemometer, this may be a directional effect (from instrument mounting). This can be checked by plotting a mast shadow graph as discussed in Section 3.6.1.2.

Intermittent instrument faults

An instrument may stop working for a period of time. This can easily be checked by comparing with another similar instrument. Careful consideration should be given as to whether the data are reliable, and data may be removed if deemed to be due to an instrument intermittent fault.

Inconsistent directional data

If the directional data for the different wind vanes do not match then they should be compared to reference data (see Section 3.7.1.1) in order to determine which are correct. The wind direction at the site may not be the same as the reference data source due to local topographic effects at the site or meteorological reference point, but it is generally a good indication. Consideration of mast

shadowing effects relative to the installation can also be used to verify any measurement direction offset.

Instrument icing

In cold climates, the temperature may drop below zero. This can cause anemometers or vanes to stick or slow down due to icing. If the mast has a thermometer installed, then erroneous data can be identified and removed. Complete icing is easy to identify, but anemometer slow down due to icing is more difficult to discern. An instrument may stop for a period of time and this can be checked by comparison with similar instruments. In many cold climates, anemometers and direction vanes may stick or slow down due to icing. Affected data should be removed. The issue of icing on masts can be mitigated by using heated anemometers. However, heated devices are more expensive and are used at the discretion of the project developer.

Data screening is an important part of the post-processing of the raw data. Removal of anomalous data caused by battery failure, icing effects, or potential instrument damage is vital to improve the validity of the data analysis. Data integrity is defined as the representational faithfulness of information to the true state of the object that the information represents (Boritz, 2004). Careful consideration should be given as to whether the data are reliable, and they should be removed if deemed otherwise.

3.6.1.2 Wind Analysis

Mast Shadow

Mast shadow is the physical effect of the mast on the anemometer, whereby wind coming from particular directions will be sheltered from the anemometer by that mast. Other obstructions, such as lighting devices, can also interfere with the wind as it travels across the mast. Installing more than one anemometer at the same height but orientated in a different direction allows the mast shadow effects to be identified and removed.

Anemometer Drift

A further check that is typically carried out in data analysis relates to anemometer drift. This is the gradual change in response of an anemometer to a given wind speed over a long period of time, caused by the wear and tear of the anemometer. Any apparent drift over time can increase uncertainty and it may be more appropriate to discard data where significant degradation is apparent.

Measured Wind Shear

Wind shear defines the variation in wind speed with height. Wind shear may be influenced by many factors, such as mast shadow, roughness, and topography. Ideally for wind farm sites, the IEC typical design wind shear exponent of 0.2, should not be significantly exceeded. Typically, wind shear follows a power law profile with higher wind speeds experienced at higher heights. The equation used to calculate the wind shear coefficient, α, for two prescribed heights z_1 and z_2 is:

$$ln\left(\frac{V_{z2}}{V_{z1}}\right) = \alpha\, ln\left(\frac{z_2}{z_1}\right) \tag{3.5}$$

where V_{z1} and V_{z2} are the average wind speeds from the seasonally balanced dataset. The magnitude of a wind shear component can be categorised as follows:

- $\alpha < 0.1$ - low wind shear;
- $> \alpha < 0.2$ - moderate wind shear;
- $> \alpha > 0.3$ - high wind shear, and
- $\alpha > 0.3$ - very high wind shear.

Wind shear is especially important when considering the fatigue loading of wind turbine generators (Corscadden *et al.*, 2016; Werapun, Tirawanichakul and Waewsak, 2017).

Data Synthesis

When data coverage for anemometers is reduced due to missing or erroneous data, data synthesis may be used to maximise the data available for evaluating the long term wind distribution at the site. Data synthesis is the creation of artificial time series for filling in gaps due to missing data. The most common methods include the autoregressive moving average method (Box, Jenkins and Reinsel, 2008), Markov chains (Manwell *et al.*, 2006) and the Shinozuka method (Shinozuka and Jan, 1972). Through the synthesis procedure, gaps in each mast dataset are filled, using data from instrumentation mounted on the same mast. This is known as intra-mast synthesis. It is also possible to extend a measured dataset from other masts installed at the site. This is known as inter-mast synthesis.

3.6.2 Tidal Energy Measurement Campaign

This section outlines the procedure for conducting the measurement campaign at a typical tidal energy site. Information is adapted from the IEC Technical Specification for Tidal Energy Reosurce Assessment and Characterisation (IEC, 2015).

Tidal flow is typically measured using an Acoustic Doppler Current Profiler (ADCP) or a velocimeter, similar to an anemometer. ADCPs are oceanographic instruments which measure the velocity of the water flow through the water column. Typically, they are anchored to the seabed and obtain measurements at a single location. However, ADCPs can also be attached to vessels to enable mobile analysis over a wider area.

When conducting any measurement campaign, it is important to comply with relevant industry guidelines or specifications, if they are available. This is to ensure that results are kept within acceptable uncertainty levels. When industry standards are not met, then the uncertainty level will increase. The minimum requirements from the IEC technical specification for tidal resource (IEC, 2015) is to measure the flow for 35 days, if the data are used to calibrate/validate a hydrodynamic model. This is to capture a typical spring and neap tidal cycle which recurs approximately twice every month. This raw data can then be extrapolated over longer periods using harmonic analysis (see Section 3.7.2 and Chapter 4). The technical specification also states that it is possible to use the raw data to compute directly the annual energy production (AEP). However, to achieve this, a minimum of 90 days of measured data are required. ADCPs used for such surveys are typically bottom mounted on a structure anchored on the seabed, to give the flow measurements at a fixed location across the water column. To complement this, vessel mounted ADCPs can be used to gather data over a wider area. The best way to reduce uncertainty is to use accurate devices and to complete all the necessary surveys in accordance with IEC guidelines.

ADCP manufacturers provide specification for the devices, which give bias and single ping error values. These give an indication of the accuracy of the device to measure the flow. The ADCP measures water currents by transmitting sound waves and measuring the frequency change from the reflections of the pulse by water-suspended particulates. The main assumption is that the particulates themselves have very little mass and, therefore, act as Lagrangian tracers. For a Lagrangian tracer particle, the position and physical properties of the particles are described in terms of the material or reference coordinates and time (Mahdavimanesh *et al.*, 2013). An ADCP measures the velocity (speed and direction) using the principle of the Doppler Effect as shown in Figure 3.8. A sound wave has a higher frequency, or pitch, when it is moving towards the device than when it is moving away. The ADCP transmits “pings” of sound into the water at a constant frequency (approximately 2 Hz) and a very high acoustic frequency (up to and above 1000 kHz). As the sound waves travel, they are scattered by particles suspended in the water column and moving with the speed of the current, with some of the signal reflected back to the instrument. Sound waves reflected back from a particle moving away from the profiler, have a slightly reduced frequency when they return. Particles moving towards the instrument send back higher frequency waves. The difference in frequency between the transmitted waves and the received waves is called the Doppler shift (Doppler, 1842). The instrument uses this shift in frequency to calculate the speed

of the particle in the water and the direction of the flow is derived from the particles moving across multiple beams.

It should be noted that there are other sensors and devices that can be used to measure the flow speed of water, such as a velocimeter. These devices are capable of measuring the flow speed at a single position in the water, with relatively high-frequency. One of the major advantages of ADCPs over single point velocimeter devices is that the measurements are collected across the whole water column. Sound waves that hit particles far from the profiler take longer to come back than the waves that are reflected closer. By measuring the time it takes for the wave to rebound, and the Doppler shift, the profiler can measure current speed at many different depths with each series of pings. This is useful as the ADCP can simultaneously measure the speed and direction of the water across many depths in the water column.

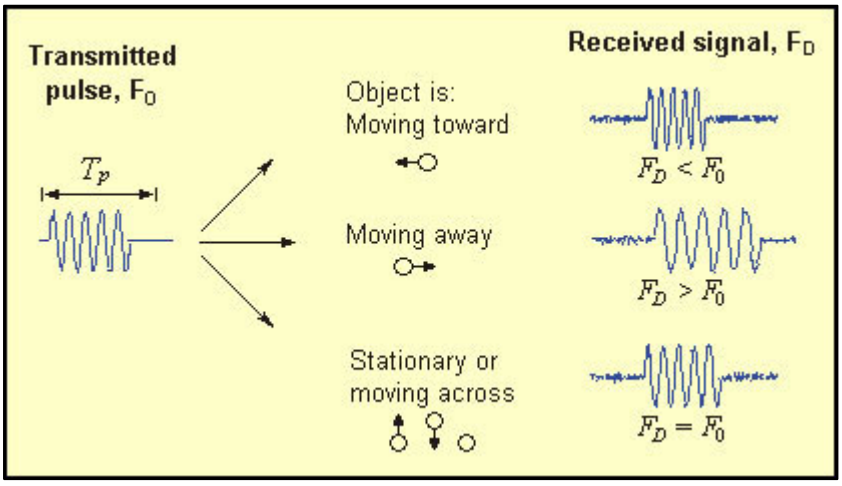

Figure 3.8 - Principle of Doppler Shift, illustrating how the frequency of a wave changes depending on the objects relative direction of travel (Sontek, 2001)

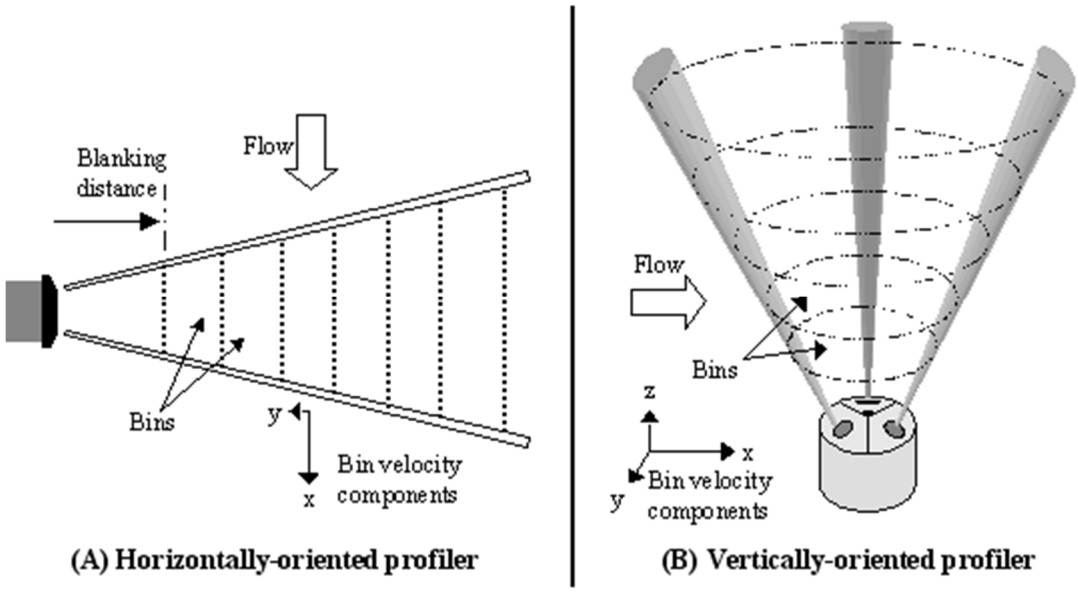

Figure 3.9 - Illustration of ADCP operation and cells along the beams (Levesque and Oberg, 2012)

Each transducer on an ADCP transmits and receives its own Doppler shift pulse and therefore only measures the velocity normal to its corresponding transducer head. In order to estimate the velocity relative to the ADCP, measurements are taken from three beams orientated at different angles. As the acoustic beams extend further away from the device, they diverge. Current techniques to process ADCP data (Epler, Polagye and Thomson, 2010; Parsons *et al.*, 2013; Vermeulen, Sassi and Hoitink, 2014; Zhu *et al.*, 2014) assume homogeneous flow between the measured radial components of velocity. The homogeneity assumption is often questionable (Marsden and Ingram, 2004), but it is widely applied. This is discussed in more detail in Section 3.6.2.1. When the device uses four beams (e.g. the Teledyne RDI workhorse) an estimate of horizontal velocity and two independent estimates of vertical velocity are made. The difference between the two vertical velocity estimates is termed "error velocity" and is indicative of horizontal homogeneity.

Each ADCP "ping", or acoustic transmission, captures a velocity profile. A velocity profile is a set of velocity measurements in a sequence of depth cells. The cell size specifies the vertical length of each depth cell in the profile as shown in Figure 3.9. However, (Gunawan, Neary and McNutt, 2011) showed that a single ADCP ping can have an uncertainty as high as 45%, due to large fluctuations on single velocity data output. Averaging multiple single-ping data reduces these fluctuations and thereby reduces the uncertainty. ADCP single ping random error can range from a few mm/s to as much as 0.5 m/s. The magnitude of this error depends on internal factors such as frequency, depth cell size, number of pings averaged together and beam geometry. The error is also influenced by external factors such as turbulence, internal waves, and the motion of the ADCP

(Teledyne RD Instruments, 2011). Random error can be reduced by ensemble averaging but does not affect the bias, as seen in Figure 3.10.

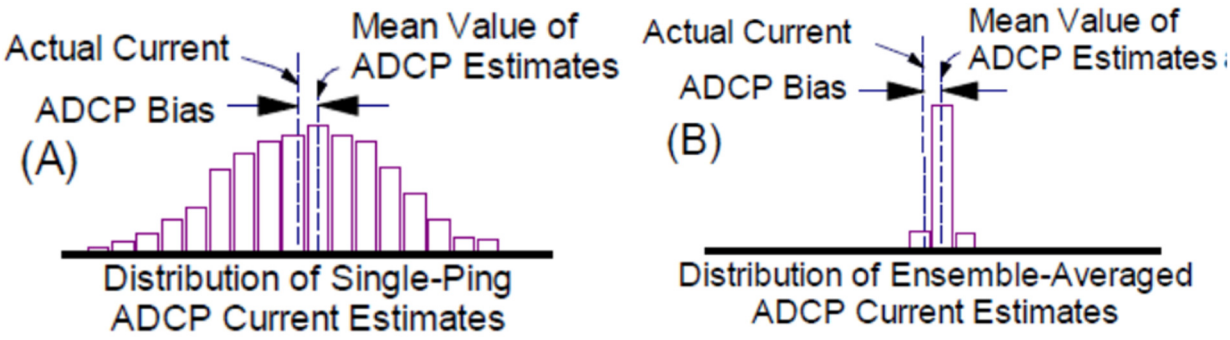

Figure 3.10 - The distribution of single-ping data (A) compared with the distribution of 200-ping averages of the same data (B) (Teledyne RD Instruments, 2011)

Ensemble averaging reduces random error in the velocity measurements by minimising the error of a single ping. This can be achieved by internally programming the ADCP to average the pings during post processing of the data. Averaging the data reduces the standard deviation of the velocity error by $N^{-0.5}$, where N is the number of pings averaged together. However, ensemble averaging assumes that the velocity field is stationary over the averaging period, which may result in long data periods smoothing out actual variations in the measured current. The bias in the measurement cannot be reduced with ensemble averaging and is therefore considered to be a constant, long-term measurement error.

When configuring an ADCP for a stationary deployment, there are a number of trade-offs between range, temporal resolution, and random noise. An ADCP measures the speed and direction of the flow across predefined cells or sections of the water column, as shown in Figure 3.11. The range is the vertical resolution of the profile and the total profiling distance from the ADCP. Selection of an appropriate cell size depends on the objective of the deployment. For deployments in shallow water, where the aim is to obtain as much information across the water column as possible, then a small cell size is appropriate. For deeper water deployment, where achieving a large range is the goal, then increasing the cell size to the maximum may be a good approach. This allows much larger distances to be reached, however the resolution of the beam profile will be reduced due to the larger cell size.

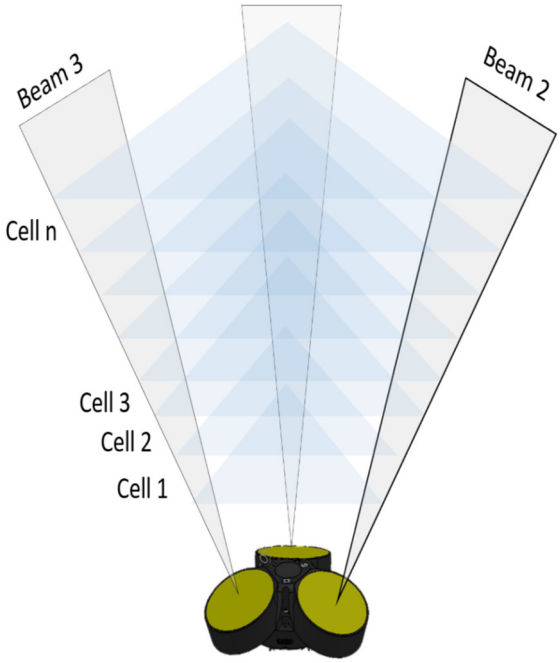

Figure 3.11 – An ADCP measurement profile, split into cells (Nortek AS, 2017)

High temporal resolution increases the amount of data which need to be stored and requires high sampling rates, which can drain battery life faster than desired. Random error is reduced through ensemble averaging, which has a negative effect on the battery life, or through increasing the cell size, which results in a loss of vertical resolution (Epler, 2010).

Vessel-mounted ADCP surveys have no power limitations, allowing for maximum resolution, ping rate, and data storage of individual pings (Teledyne RD Instruments, 2011). However, there is the additional expense associated with hiring a vessel and the personnel costs to operate it. Furthermore, the data will have been gathered over a larger area with high spatial variability, instead of a single location. A moving vessel current profiler survey usually traverses a single line or a circuit, for at least one full diurnal or semi-diurnal tidal cycle. The objective is to revisit each part of the circuit with sufficient frequency to resolve variations in the tidal current amplitude and phase (Vermeulen, Sassi and Hoitink, 2014). This condition typically restricts circuit times to a maximum of a few hours. Therefore, mobile survey design involves consideration of the trade-offs between spatial and temporal coverage and resolution related to the practical limitations of vessel speed and instrument operational limits in terms of vessel speed (Epler, 2010). The results are difficult to interpret but can play a crucial role in mapping the spatial variability of tidal currents at a site.

To fully understand the characteristics at a tidal site, it is also necessary to conduct bathymetry surveys using multi-beam echo sounders. These are typically attached to vessels and allow the mapping of the seabed, as shown in Figure 3.12. The hull-mounted multibeam transceiver sends

out a beam of sound waves which are reflected off the seafloor, back to the receiver on the ship (National Institute of Water and Atmospheric Research Ltd., 2016). The information gathered in this type of survey is used as input to numerical models, as well as helping to inform the optimum location for placing the tidal turbines.

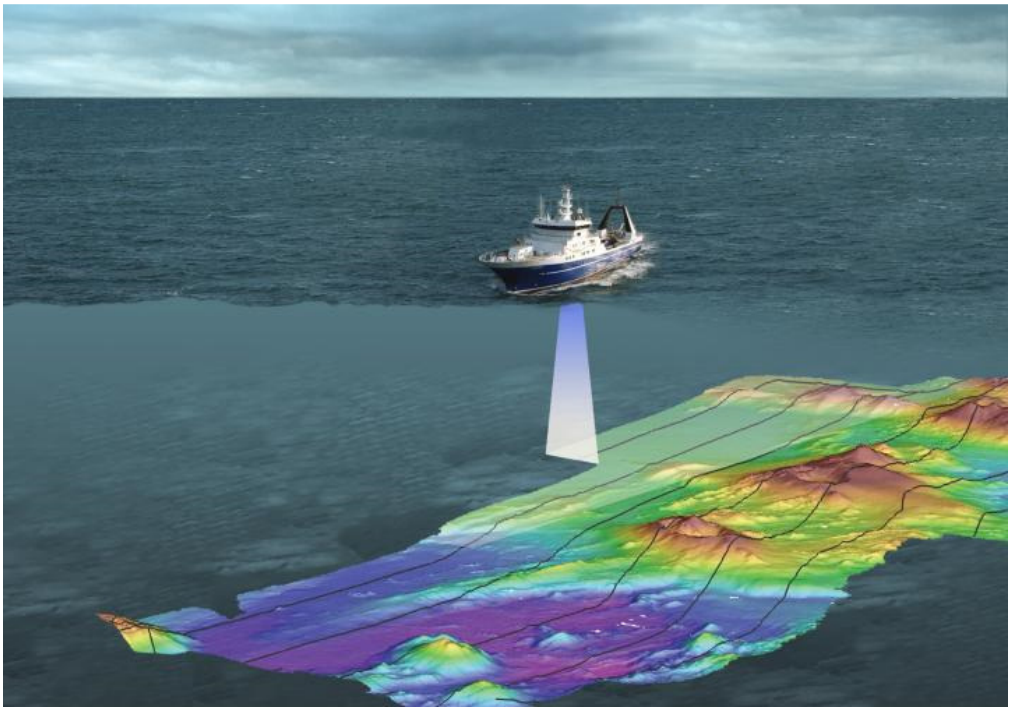

Figure 3.12 - Multibeam echo sounder tracing an image of a seabed (National Institute of Water and Atmospheric Research Ltd., 2016)

3.6.2.1 Analysis of Measured Data

Similar to wind, the measured data require post-processing. One aspect of the analysis is removing erroneous data. There are a number of effects associated with ADCPs that can reduce the quality of the data, such as:

Side-lobe interference

The acoustic beams focus most of the energy in the centre, but a small amount leaks out in other directions. Side lobe interference is caused when the leaked energy strikes a boundary before the main lobe has finished travelling the measurement range and back. Low energy signals that travel straight to the surface can produce sufficient echo to contaminate the desired signal. The angle between the main lobe and the side lobe is typically around 30°-40°. Reflections at the water surface, from the side lobes, interfere with water particles reflections from the main beam, causing part of the measurement height to be contaminated. Equation 3.6 gives an approximate estimate of the amount of near-surface contamination:

$$R_{max} = A \times cos(\theta) - Cell\ Size \tag{3.6}$$

where R_{max} is the range of valid data, A is the distance to the surface and θ is the angle of the beam relative to the vertical, and *Cell Size* is the distance between adjacent cells. This means, for an ADCP deployed in 100 m deep water, with a cell size of 1 m and a side beam angle of 25°, the contaminated region is expected to be the top 10% of water closest to the surface (Nortek AS, 2017). For side lobes orientated at 20° to the main beam, the contaminated region is usually considered to be the top 6% of the water column, and for a 30° angle this is thought to increase to 15%.

Side lobe interference may be mitigated by the use of bistatic transducers, such as acoustic Doppler velocimeters (ADVs), similar to the configuration shown in Figure 3.13(a). These devices are most commonly used to measure turbulence, as they focus their beams on a single point in the water column. However most commercially available ADCPs use monostatic diverging beams as shown in Figure 3.13(b). They transmit pulse and receive echoes with the same transducer, whereas bi-static profilers receive the returning echoes from multiple transducers.

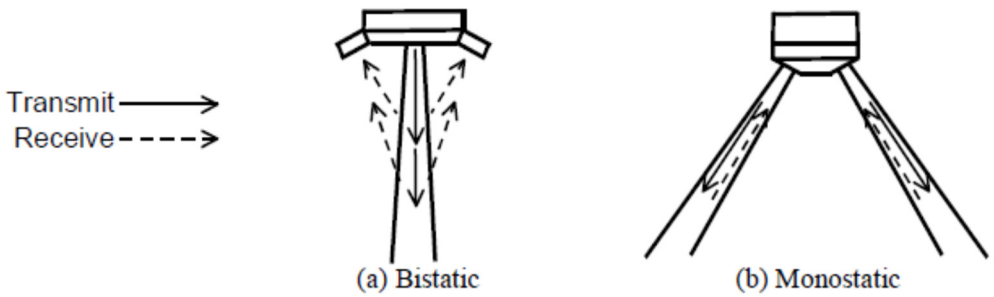

Figure 3.13 – Schematic diagram of two-dimensional bistatic (a) and monostatic (b) profilers (Nystrom, Oberg and Rehmann, 2002)

In rougher sea conditions, the contaminated regions are likely to be lower due to the scattering of the side lobe signals as they reflect off the uneven water surface (Gunawan, Neary and McNutt, 2011). The impact of side-lobe interference may be removed through appropriate quality control procedures to identify and remove affected data points. When analysing the data, an assessment of the vertical velocity near the surface should typically give a value close to zero, otherwise the data are likely affected by interference. As locating the affected data is difficult, it is more advisable to discard the data from the contaminated region of the water column.

Transducer ringing

When ADCP transducers transmit sound pulses into the water column, they continue to vibrate. The vibrations (ringing) interfere with the returning sound waves, causing data from locations close to the ADCP to be considered erroneous. For a typical ADCP operating at 300 kHz (e.g. Teledyne Sentinel), data measured up to 2 m from the ADCP are considered to be contaminated by the transducer ringing and should therefore be removed (Teledyne RD Instruments, 2011).

Non-homogenous flow

The uncertainty stated by manufacturers of ADCPs is based on the assumption of homogenous flow across layers of constant depth. However, in practice there may be spatial variations across a site due to shear, as outlined in Section 3.6.2.2. Instrument uncertainty does not account for the error caused when separate beams detect spatially varying flows (IEC, 2015). However, ADCPs do report an "error velocity" which can be used to evaluate whether the assumption of non-homogenous flow is reasonable, and this is an important built-in functionality to evaluate data quality. Similar issues are encountered in the wind industry when using LIDARs in complex terrain. These measurements can be used to validate models through comparison of shear over a larger area (Harris *et al.*, 2010). This process could be applied to tidal currents in the future. However, it is important to note that models should not be used to adjust measured data.

Positional uncertainty

During the deployment of an ADCP, the desired location of the device may change due to installation conditions and external environmental factors. This could result in a change in the position of the ADCP, when it is lowered through the water column. In other words, it is important to verify where the ADCP is deployed on the sea-bed, as this will differ from the sea surface location. This does not directly cause measurement uncertainty, but may affect the interpolation of the results, and would be manifested as a spatial extrapolation uncertainty.

Pitch and Roll

If the ADCP is not aligned vertically, with a zero-tilt angle, then the acoustic beams will measure at different depths, resulting in cells (determined by time delay of the returned signal) not measuring the same horizontal plane. A non-zero tilt angle can be adjusted using a method known as "bin mapping" which uses the beam velocity nearest the nominal bin centre. However, this method can result in omitting or duplicating data and does not correct for the fact that the beam velocities averaged over different depth ranges are combined to calculate the flow field. One study (Ott 2001) reports that typical errors for the standard method are approximately 0.01 m/s, although these can be reduced by a factor of 10 or so by linearly interpolating the beam velocities from the measured values.

Proximity to ferrous materials

Ferrous materials are ones that contain iron (ferrite). If ADCPs are deployed in close proximity to materials of this kind, then the magnetic compass inside the device may be affected. This can introduce biases in flow directional measurements (Ó'Catháin, 2012). The way to mitigate this issue is to calibrate the device before the survey, whilst it is mounted in the deployment frame (IEC, 2015), and also checking the compass calibration when the survey is completed.

These effects are usually accounted for by removing anomalous data in the analysis. An automated approach to screening ADCP data is outlined by Wanis et al. 2015.

3.6.2.2 Tidal Analysis

Measured Tidal Shear

In the same way that the wind resource varies with height from the ground, the tidal resource changes with depth in the water column. This is due to frictional interaction of water with the seabed which slows the flow closer to the seabed. Typically, this results in a power or log profile across the water column as illustrated in Figure 3.14.

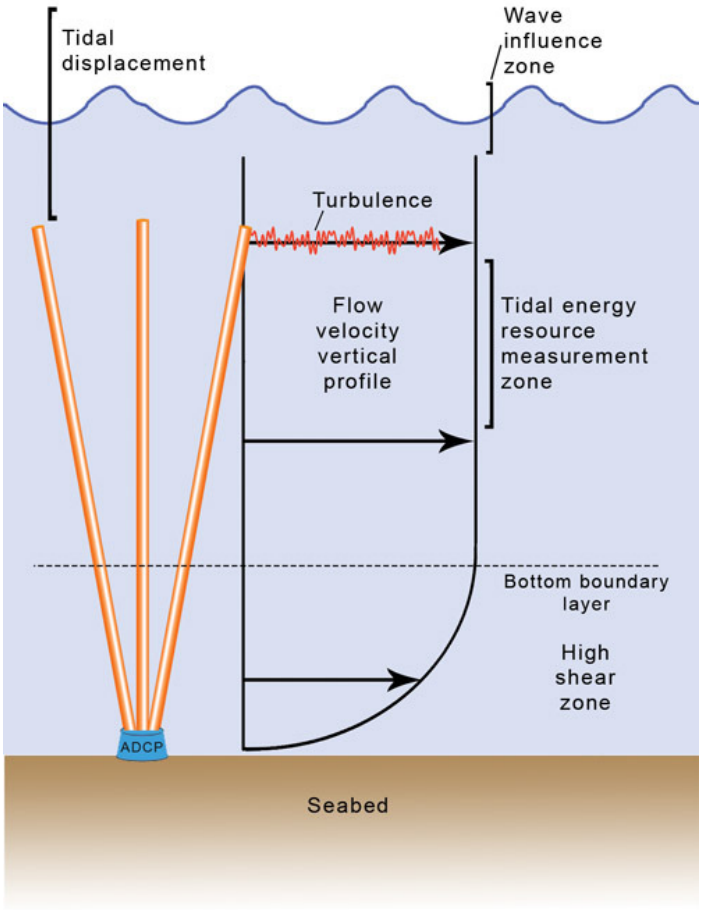

Figure 3.14 – Schematic diagram showing the vertical current velocity profile at a typical tidal energy site (Wilson, 2009)**.**

The fastest tidal flow is in the region towards the top of the water column and the flow speed reduces as the depth increases. Ideally the tidal turbine would be positioned in a flow region where the profile is relatively linear and vertical, i.e. not within the bottom boundary layer, where bed friction retards the flow (Qing and Qian-Lu, 2015). Furthermore, the region close to the sea surface is affected by wave action, which can increase unwanted forces on the device. Therefore, ensuring the turbine is positioned away from these two regions will minimise shear across the turbine blades and in theory will produce a steadier power output (Lewis *et al.*, 2017a).

Turbulence

Turbulence is often used to include all unsteady motion in a flow of fluid. However, not all unsteady effects are strictly turbulent, such as tidal flux and wave motion. Turbulence at tidal sites can originate in several different ways:

- Inflow – the nature of any wall-bounded flow at high Reynolds Number primarily affecting the boundary layer flow.
- Bed Roughness – eddies caused by bathymetry and the profile of the seabed, which modifies the turbulent boundary layer and causes turbulence structures with strong coherency.
- Channel Slope – the shape of the channel (e.g. headlands or bays) may generate specific coherent structural content in the flow such as vortex streets or affects the density of different eddy types.
- Stratification – vertical gradient in temperature and/or density introduce buoyant effects and may affect the stability.
- Wind Shear – shear stress applied to the surface of the sea by the wind generates a velocity shear profile and consequent generation of turbulence.

When considering energy yield, turbulence affects the recovery of wakes downstream of a turbine, as well as the kinetic energy flux through a turbine. This can therefore affect the performance of the power curve and contributes significantly to device fatigue loading, affecting the cost and availability of the tidal devices (Clark, 2015).

An extensive review of issues relating to turbulence has been undertaken as part of the Turbulence in Marine Environments (TiME) project. When considering the implications of turbulence on tidal turbines, is it useful to define the different scales of turbulent motions (small-scale, mid-scale and large-scale) to help understand their resulting effects:

1. **Small-scale eddies** are typically defined as turbulent fluctuation having characteristic length scales less than a typical blade chord length. Turbulence at this scale usually affects the hydrodynamic performance of the device without exerting direct loadings, since its scale is much smaller than the equipment itself and direct loading averaged out over the surface of the blade.
2. **Mid-scale eddies** have a characteristic length scale larger than a typical blade chord length, but smaller than the diameter of the turbine rotor.
3. **Large scale eddies** have a characteristic length scale greater than a turbine rotor area. These eddies usually exert a fairly uniform gust over a turbine rotor area but describe intermittency and fluctuation on a large scale. For example, over the proposition length of a turbine wake or on the scale of turbine separations with an array.

Studies have shown that ADCPs can provide reasonable estimates of turbulence and have been used to calculate parameters such as turbulence intensity and kinetic energy (Nystrom, Oberg and Rehmann, 2003). However, there are only a few published results of measurements from high-

energy tidal sites (Thomson *et al.*, 2012). To measure turbulence using an ADCP the raw data from individual "pings" must be retained, as averaging obscures the velocity variance. Also Doppler noise must be removed from the velocity variance statistically (Clark *et al.*, 2017). The accuracy of using ADCPs to measure turbulence is often poor when compared to other measurement techniques (e.g. Acoustic Doppler Velocimetry). This is because ADCP measurements capture Doppler noise and the devices assume homogenous flow between beams, which causes measurement inaccuracies.

ADCPs typically have poor temporal and spatial resolutions due to the size and width of the cells and the pinging frequency that are used. To measure turbulence accurately, measurement devices require faster sampling rates and less spatial averaging. There is also a need for the correlation of turbulence measurements to statistically, if not directly, correlate with blade load data from the turbine blades (Sutherland, Sellar and Bryden, 2012). However, it has been shown that turbulent statistics calculated from ADCP data will not capture the whole spectrum (Guion and Young, 2015). The filtering process used in ADCPs means that some frequencies are attenuated completely while others will be amplified. Ultimately, this means that a turbulence spectrum will be skewed by an ADCP. This also highlights that other measurement techniques (e.g. hot-wire anemometer) should be used to calibrate the ADCP data.

Data Synthesis

Data synthesis may be required if data coverage is considered poor. In the same way that wind data are synthesised, periods of missing tidal data may be synthesised, requiring interpolation of data between measured data points. Data packages such as ProcED, available through MATLAB, are able to process and synthesise gaps in data to improve data coverage (Genz, Cirano and Lessa, 2010).

3.6.3 Measurement Campaign Analogies

Within measurement uncertainty there are many similarities between the methodology to collect wind and tidal data. Despite differences between the instruments used to measure the resource, uncertainty in the accuracy of the instrument is calculated in the same way based on the uncertainty tolerances provided from the device calibration tests. Wind resource is typically measured using an anemometer, i.e. a single point measurement device, in combination with a LIDAR emitting a pulsed laser light, whereas tidal resource is typically measured using an ADCP which emits sound pulses into the water. The instrument uncertainty for tidal energy can be calculated in a similar way to wind energy as the value is dependent on the quality of the device and the accuracy of the measurements collected in the resource campaign.

Interference with the measurements can be caused by the methods of installation as well as environmental factors. For wind, the presence of the mast can affect the anemometer measurements in particular wind directions. When measuring tidal flow, there are a number of factors caused by interference that can increase the uncertainty, as discussed in Section 3.6.2.1. To mitigate the effects of measurement interference the methods are the same for wind and tidal. It is common practice to remove affected data from any analysis. The uncertainty due to measurement interference is dependent on the ability to locate and remove erroneous data. If this can be done effectively, following the correct guidance, then uncertainty can be considered lower. The uncertainty value will be calculated relative to the average flow speed, i.e. an uncertainty value of 2% in flow speed. This means that sites with higher wind speeds will incur a higher measurement uncertainty value. Data synthesis and quality uncertainty are expected to be similar for tidal cases because they are dependent on the amount of data synthesis required and the quality of the correlation between the data. This is discussed in Section 3.6.1.2.

3.7 Temporal Modelling

The next stage in the energy yield procedure for both wind and tidal energy is to use the short-term site data and perform an analysis to predict the long-term trends. The method to conduct temporal modelling is fundamentally different between wind and tide, and this section aims to highlight the processes involved in more detail.

3.7.1 Wind Long Term Estimation

Generally, the results of a wind measurement campaign are too short to be considered representative of the long-term wind climate. In an ideal situation, a site would benefit from a long-term data set of over 10 years, measured at hub-height. In some cases this is available, but it is very rare, due to time and cost constraints for most projects. Therefore, it is necessary to use limited short-term site data and longer term reference data from a fixed mast to analyse the correlation (known as the Measure-Correlate-Predict method) between the two sources in order to create a long-term prediction.

3.7.1.1 Reference Data Selection

For accurate prediction of the energy available at a site, long-term wind data are required to account for inter-annual variations. These data should be collected over a period for which measurements are consistent, but ideally a minimum of 15-20 years (Lileo *et al.*, 2013). The methodology behind long-term assessment aims to determine the relationship between concurrent site and reference wind data and apply this relationship to extrapolate the site data over longer time

periods. Uncertainty in the long-term reference data (σ_{LT}) is related to the interannual variation of the wind speed as well as the length of the measurement period. The equation to calculate this is:

$$\sigma_{LT} = \frac{\delta}{\sqrt{\lambda}} \tag{3.7}$$

where δ is the interannual variation as a percentage, and λ is the number of years of long-term reference data. For this, data are gathered from third party sources, usually in the form of measured, mesoscale modelled, or reanalysed data. The UK Met Office collects meteorological data from a wide network of stations and is therefore able to provide long-term wind data for the UK. Data from the Met Office are considered to have low associated uncertainties, because the masts are generally well maintained. However they have proved to be very expensive for project developers and are now rarely used. Most recent projects consider modelled or reanalysis data as a cheaper alternative, especially considering the advance in accuracy in recent years (Brower *et al.*, 2013; Sharp *et al.*, 2015)

For every energy yield assessment, two or more independent sources of measured reference data should be considered, in addition to a minimum of one reanalysis or mesoscale reference data set. If no suitable measured reference data are available, reanalysis or mesoscale data may have to be used in isolation. The main factors to be considered when selecting suitable reference data include:

- Proximity to the site – this is ideally within 50 km of the site, but anything up to 100 km could be considered.
- Exposure from surrounding trees and slopes to avoid significant sheltering.
- Consistency of the measurements over time.
- Quality of the correlation between the measured and reference site data.
- Accuracy of the short term measurements – the mast should be equipped with a good quality, well maintained, appropriately mounted anemometer.

If a close relationship (good correlation) between the site data and a reference mast can be established, then it is possible to use the long-term reference data and the relationship to predict the wind speeds at the site. This is a very powerful technique if a good correlation exists, but if the correlation is weak, it can be misleading and therefore must be used with caution.

When considering the correlations between wind site data and long term reference data, it is important to balance concurrent datasets over different seasons. This involves characterising the number of data points that occur in summer and winter months. The summer period is defined as March 21st and September 21st and winter months between September 21st and March 21st. The aim is to balance the data by removing additional data so that the percentage of summer and winter

months is the same, or as close as possible to be half summer and half winter. The reason for this step is that in certain climates, such as Europe, winter months experience higher wind speeds than summer months in a typical year. Therefore, a dataset with more winter months present will introduce a bias, producing a higher average wind speed. Once the concurrent data has been seasonally balanced, then the analysis can proceed.

To create a long-term wind speed and directional distribution, relationships are established between the short-term measured site data and short-term reference data. This is known as a Measure-Correlate-Predict (MCP) analysis, and consists of a comparison of the short-term site data with the reference data during the concurrent period. The prediction is the application of the determined relationship to extrapolate the short-term data to the long-term period. If a sufficient length of on-site data is available (typically more than four years) then no MCP adjustment may be required.

A simplified visualisation of the MCP process can be seen in Figures 3.15 to 3.17. Figure 3.15 shows an idealised short-term site data set, with 12 months of measured data. Figure 3.16 shows an idealised reference data set, with approximately 20 years of data. The concurrent data for the two sites, which is the one year of overlapping data, can be seen in the scatter plot in Figure 3.17. This plot shows the target site data on the *y*-axis and the reference site data on the *x*-axis. To decide on the MCP method to use, it is common to assess the resulting uncertainty and use the option which gives the lowest uncertainty. There are a number of MCP correlation methods that can be used, as discussed by Klinkert (2012) and Jonsson (2010a). The chosen correlation method can then be applied to the short term site data, yielding a prediction of the long-term wind resource at the proposed site.

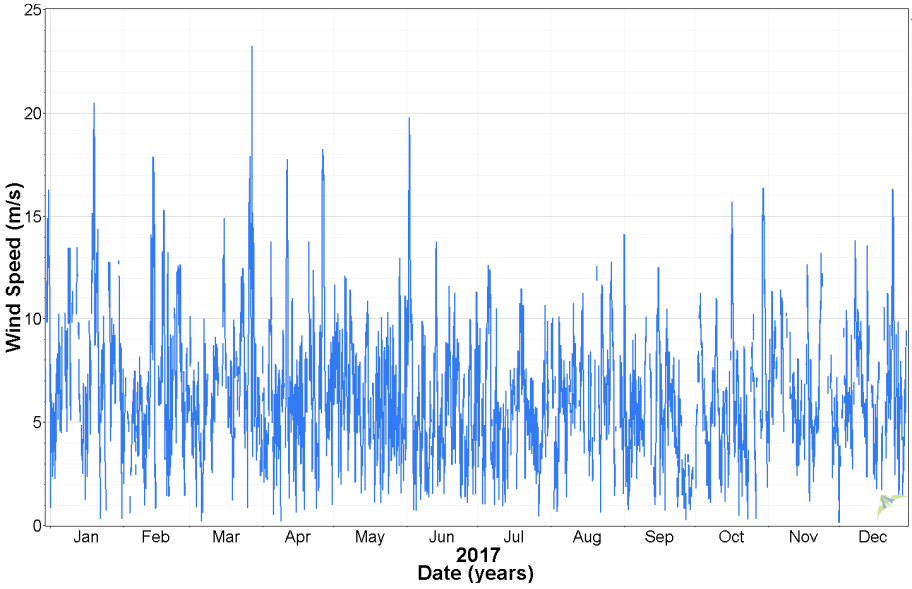

Figure 3.15 - Sample 12 months of site measured data

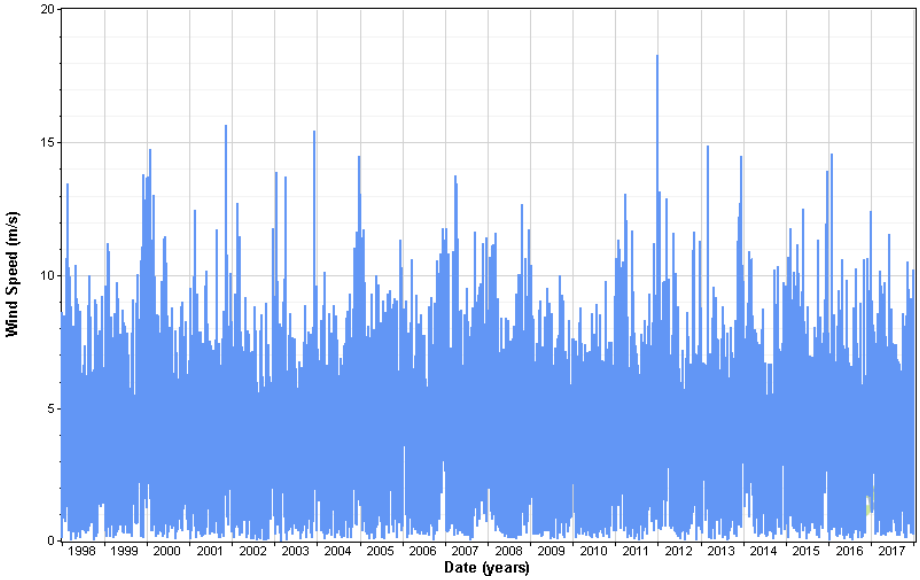

Figure 3.16 – Sample 20 years of reference data

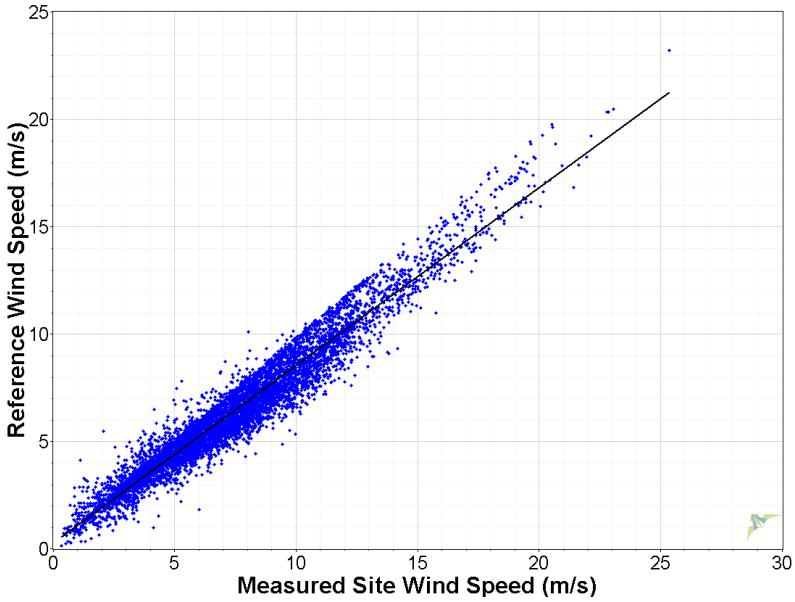

Figure 3.17 - Sample MCP relationship

The types of models used in MCP include: linear models (Bardsley and Manly, 1983), non-linear models (Mortimer, 1994; Riedel, Strack and Waldl, 2001), artificial neural networks (Addison *et al.*, 2000; Bechrakis, Deane and McKeogh, 2004), Markov chain models (Nfaoui, Essiarab and Sayigh, 2004), joint probability models (García-Rojo, 2004) as well as others. Rogers et al. (2005a) and Anderson (2004) provide detailed reviews of a variety of MCP methods, as well as a comparison of the performance of several methods. Anderson points out that the more complex non-linear and neural network models do not perform substantially better than the simple 2-

parameter linear models. Rogers et al. also develop a linear model, the "Variance Ratio" method, which performed well compared to the other models. For a linear regression model, (Derrick, 1992) outlines an approach for estimating the uncertainty of an MCP prediction . However, as shown by Rogers et al., this approach significantly underestimated the actual uncertainty of the predictions (Rogers, Rogers and Manwell, 2005b). This is because the wind data relationship between two sites is serially correlated, and so linear regression theory cannot be used to estimate the uncertainty associated with the MCP prediction.

An alternative approach to estimate correlation uncertainty uses a jack-knife method to estimate the variance (Rogers, Rogers and Manwell, 2005b). This was introduced in Chapter 2 and is discussed further in Chapter 4. This method splits the dataset into subsets by removing a small subset of the data each time. The MCP is then re-run for each subset of the data, and the difference in long-term mean wind speeds is used to calculate the uncertainty. For a standard dataset with one or more years, four subsets are usually created. The results of the investigation by Rogers et al. indicate that the jack-knife prediction provides a better estimate of uncertainty over linear regression theory methods associated with the MCP procedure (Measnet, 2009). This has also been seen in other studies conducted to analyse long term correction methods for wind (Jonsson, 2010).

3.7.2 Tidal Harmonic Analysis

This section outlines the approach to harmonic analysis which is the process by which long-term variations can be predicted for tides. A more in-depth description and evaluation of harmonic analysis for long-term tidal flow prediction is outlined in Chapter 4. Wind is stochastic in nature, whereas tides are deterministic. What this means in practice is the wind has a random probability distribution and aperiodic fluctuations that may be analysed statistically, but may not be predicted precisely. Tides, on the other hand, can be explained by the relative astronomical movements of the Earth, Moon and Sun in their various orbits, rotations, and axis tilts. The tidal forcing can be attributed to different tidal frequencies that are resolved using the mathematical method known as harmonic analysis.

As for wind, it is essential to gather as much on-site data as possible. However, the measurement campaign at a tidal site using ADCPs, as outlined in Section 3.6.2, is primarily constrained by the trade-off between resolution of the data and the battery life of the instrument. This means that if high resolution data are required, then only a short time period of data can be collected in one deployment. Temporal modelling can be used as an alternative to multiple deployments, which would be expensive. Typically, this is achieved using harmonic analysis techniques which extract tidal constituents from the short-term site flow data. The main assumption of harmonic analysis is

that the tidal variations, *h*, can be represented by a finite number of harmonic terms, or constituents, *n*, that combine together, illustrated by the simplified equation:

$$h(t) = A_n \cos(\omega_n t - \phi_n) \tag{3.8}$$

where $A_n$is the amplitude of the tide, ω_n is the tidal frequency, ϕ_n is the phase lag, usually called the epoch, and *t* is time.

The amplitude and epoch of each tidal constituent are required to make a prediction. A study conducted by the National Oceanic and Atmospheric Administration (Parker, 2007) reported that there are a total of 149 known tidal constituents. However a study (Lu and Lueck, 1999) indicates that over 91% of the flow characteristics at a site can be predicted using only the dominant constituents outlined in Table 3.2. However, this may vary depending on the site. The subscript of each constituent symbol indicates the approximate number of daily cycles associated with that constituent.

Table 3.2 - Principal Harmonic Constituents

Harmonic Constituent		Period (hr)	Frequency (°/hr)
Symbol	Name		
M_2	Principal lunar semidiurnal	12.421	28.984
S_2	Principal solar semidiurnal	12.000	30.000
O_1	Lunar diurnal	25.819	13.943
K_1	Lunar diurnal	23.934	15.041

The harmonic analysis process then applies the same tidal constituents to a longer time period to give an estimate of the long-term behaviour of the tide. The length of the measured dataset will affect the accuracy of the harmonic analysis. The guidelines set out by EMEC (European Marine Energy Centre) state that 3 months of data are required from the site for a full detailed analysis, especially if no modelling is carried out (EMEC, 2009). This is discussed in more detail in Chapter 4.

3.7.3 Temporal Modelling Analogies

Methods used to estimate historic and future wind and tidal energy resource are very different, making analogies between the two methods inappropriate. Due to the stochastic nature of the wind, statistical methods are used to estimate long-term variations, primarily by assessing the correlation between short-term site data and long-term reference data. Due to the deterministic nature of the

tides, harmonic analysis is an effective method widely used to estimate the tidal variations over a long-time period. In harmonic analysis, Fourier transforms are used to decompose a tidal signal into individual astronomical frequencies. MCP and harmonic analysis methods are fundamentally different, and so the uncertainty prediction methodology for this aspect of the assessment is not transferable. A deeper understanding of harmonic analysis and the available tools for its application is required to determine the inherent uncertainty within the methods. This is one of the aims of this thesis and is discussed in more detail in Chapter 4.

3.8 Spatial Modelling

The next sections outline the spatial modelling requirements for wind and tidal and address the similarities and differences in the modelling procedures.

3.8.1 Wind Flow Modelling

The temporal modelling for wind, discussed in the previous section, predicts the long-term wind speeds and direction at the site mast. The next stage is to determine the wind speed and direction at each wind turbine location. This could be achieved by installing a met mast at each wind turbine generator location; however, this would be expensive and time consuming. A much more efficient way of predicting the wind characteristics at each location is to build a numerical model. The model will provide an estimate of the wind speed variability across the site. It also enables the evaluation of topographic effects and wake losses from other neighbouring wind turbine generators.

For the wind industry, there are a number of tools and software that can be used, depending on the characteristics of the site. Due to the variation in wind speed across a site, there is a need to model how the wind varies spatially. The requirement is to extrapolate the wind climate at a specific point, namely the hub height location of each proposed wind turbine generator. For projects on complex terrain, or in a forestry, computational fluid dynamics (CFD) models are used such as Meteodyn (Ayala et al. 2017; Balakrishna Moorthy & Deshmukh 2016). For less complicated sites, CFD is usually not required and simpler linear models, such as Wind Atlas Analysis and Application Program (WAsP) can be used. The WAsP suite of software is industry-standard for wind resource assessment, siting, and energy yield calculations for wind turbines and wind farms (Carvalho *et al.*, 2013; Chancham, Waewsak and Gagnon, 2017; Murthy and Rahi, 2017).

Information required to run a WAsP model is usually provided by the Client or is sourced online. The basic requirements include:

Terrain and roughness map

Detailed topographical information is required to understand the shape and features of land around the site. The purpose of the map is to provide an accurate description of the terrain and surface roughness for the project site and surrounding area. Whilst topography in an area is usually static, with the exception of quarries, roughness can change over time, particularly when there is managed forestry in the area. Therefore, more than one roughness and topography map may be required. Roughness values are assigned to define terrain surface conditions. For example, high roughness values would be given to built-up areas with tall buildings or forestry. Lower values are assigned to areas of bare ground and open water is assigned a value of zero.

WAsP advises that the topography should extend to at least 100 times the height modelled (usually hub height) from the site, and the roughness to at least 10 km from the project site. It is recommended that 10 km from every wind turbine generator location is modelled. If the site is near the sea (within 20 km), the roughness map should extend further to include this significant roughness change.

Mast location co-ordinates

This information should include the geographic coordinate location of the mast at the site that has measured the raw data.

Long-term wind rose at the mast location

This is the calculated/modelled wind rose following the MCP analysis.

Project wind turbine generator locations and hub heights

This includes the coordinates and hub heights of each turbine at the site that makes up the wind farm array

Any neighbouring wind farm wind turbine generator locations and hub heights

This information includes any wind turbine locations of farms in close proximity to the project wind farm, usually within 5 km, but for larger wind farms it may be as far as 10 km from the site.

Wind turbine generator power curve, thrust coefficient and rotor diameters

The power curve and thrust curves are required for the wind turbine generator. These are usually tested in laboratory conditions to calculate the power production for each wind speed bin.

3.8.1.1 Validation of the Wind Flow Model

Wind flow modelling is only as accurate as the input data and the model's underlying assumptions. To assess the validity of the model used, it is common to review aspects of the modelled wind flow output against measured data. This review comprises a comparison of the wind shear at the site masts, assessment of the wind speed cross prediction errors between site mast locations, and the sensitivity of the model to operator adjustable parameters (Clerc, Anderson and Stuart, 2012). The model calculates the wind shear profile based on orography and roughness, using internal boundary layer techniques. A check can then be made to compare the measured and modelled shear at the site and whether they are in good agreement.

If there are multiple met masts installed at the site, it may be possible to check the accuracy of wind speed using cross predictions. To limit errors in the energy yield assessment, which could arise from the use of data from a single met mast location, wind flow models can be created using concurrent datasets for each of the met mast locations. Comparison between measured and modelled wind speeds at each mast enables an assessment to be made of the accuracy of the wind flow model in the horizontal extrapolation of wind speeds across the site. Using cross prediction values, it is possible to calculate the percentage error of the wind speed predictions and thereby identify whether the model under or over predicts the wind speed at each location.

A final step in the validation of the model is to conduct a sensitivity analysis. The final model configuration is selected in order to minimise the sensitivity of the model output to the model input parameters. This is estimated by comparing the relative influence of each of the final model configuration parameters with the next nearest value, using the model calculated gross wind farm output. This analysis indicates whether the model is particularly sensitive to any of the input parameters and how the energy output varies. These components are all considered in the calculation of the model validation.

3.8.1.2 Wind Wake Modelling

As well as modelling the wind flow across the site, it is also important to model the wake effects of the wind turbine generators. The wake behind turbines reduces the wind speed and increases turbulence encountered by downstream wind turbines. As wind turbine generators are often positioned closely together, energy extraction from one wind turbine generator produces a wake or flow deficit behind it, so that any downstream wind turbine generators will experience a reduced wind speed. This has a direct impact on the energy production of the wind farm and is therefore important to understand as part of the energy yield prediction.

There are two main types of wake models that can be used to evaluate more accurately wake effects on wind farm performance. The most common are semi-empirical models that apply model-calculated freestream wind speeds such as the Ainslie (eddy viscosity) model (Ainslie, 1988) and the Jensen Park model (Jensen, 1983). Other models are firmly rooted in flow physics. Computational fluid dynamics models such as Meteodyn (Moorthy and Deshmukh, 2016; Ayala *et al.*, 2017) and WindModeller (Montavon and ANSYS, 2010) use actuator disk models that incorporate the wake in the simulation such that there is no freestream wind speed calculation. These have shown promising results in the modelling of wakes (Montavon, 2011), but they are computationally expensive.

Until recently, validation of offshore wake effects was scarce. However, measured data, from wind farms such as Horns Rev, have been used to develop and tune models. Uncertainties tended to be high – typically 50% of the predicted wake loss. Work conducted by the Offshore Wake Accelerator programme (Walker *et al.*, 2016) demonstrated the predictive power of the models, which allowed a reduction in the typical wake loss uncertainty from 50% to 25% of the predicted wake loss. This performance was achieved by models of all types, demonstrating that semi-empirical models can be set up in a way that provides reliable wake loss predictions for a range of wind farms, and that physics-based models capture the physics accurately enough to give satisfactory estimates of wake loss. The increase in confidence of offshore wind wake models was only possible through validation against production data from large wind farms.

3.8.2 Tidal Flow Modelling

Spatial modelling is important to understand how tidal flow varies across a site if multiple turbines are to be deployed at locations remote to the ADCP deployment. For smaller arrays (< 10 MW), no spatial modelling may be required if ADCPs are deployed at each turbine location. For larger arrays this is not feasible, therefore spatial modelling is required.

The first step is to select an appropriate model. For early stage site suitability studies, either 2D (depth averaged) or 3D models, which resolve vertical velocity variations, may be used. 2D models will only provide the flow speed and direction as an average over the water depth. Therefore, to understand how the flow varies across the depth of the water column, 3D models are required to resolve the vertical dimensions. Each vertical bin should be sufficiently fine to resolve boundary layers and to include several vertical bins in the cross-sectional area of expected turbine deployments (IEC, 2015).

There are a number of industry models that are currently used across academia and the industry. For more information on the different types of models used for tidal resource assessment, see Chapter 5.

The tidal industry has not yet converged on the use of a standard model in the same way that the wind industry has with the use of WAsP. To date, each developer has typically built their own hydrodynamic model using one of the modelling software packages outlined above and has validated it in-house. The tidal industry is not at the same stage as the wind industry where a third party conducts the model study which is independently validated and verified. This may be a future requirement for the tidal industry, particularly when similar investment and debt finance to that of the wind industry is required.

To evaluate the spatial variation in flow, tidal models require input information on the site bathymetry, the boundary conditions of the model and the required resolution of the mesh. Using more detailed input data in the model (i.e. with a higher resolution) will result in a lower overall uncertainty associated with the accuracy of the model. However, there is often a compromise between the level of detail and the computing power required to run the model. The seabed roughness input is more difficult to define and is commonly used to adjust or calibrate the model to fit the measured data. In the wind industry, roughness is a defined input to the wind flow model as described in Section 3.8.1. It has a large effect on the variation and characteristics of the resource within the model and is sometimes used as to adjust the model outputs to the measured data, through adjusting the modelled shear profile to better match the measured shear profile.

The simplest method to implement a tidal turbine in the model is to apply a thrust force in the form of an equivalent drag force term (Kramer and Piggott, 2016; Vennell, 2016). In depth-averaged models (2D), this typically requires an increased bed roughness value that represents a tidal device located over an area of the seabed. An early estimation of the power potential of a tidal energy site (Garrett and Cummins, 2004) showed that the power cannot simply be estimated by evaluating the average kinetic energy flux in the undisturbed state. A more detailed approach to represent tidal turbines is known as linear momentum actuator disk theory (LMADT). This methodology was applied to open channel flow in 2008 by Houlsby et al. (2008). Another method considers tidal channels as an electrical circuit and when applied to a Pentland Firth scenario, shows good agreement to depth averaged numerical models (Draper *et al.*, 2013b). These methodologies are described in more detail in Chapter 5.

The gross energy yield is then determined by combining the tidal resource at each turbine location with the device performance curve.

3.8.2.1 Wake & Blockage Modelling

When there are multiple turbines being deployed, it is important to understand how each of the turbines will interact as part of an array. There are two primary areas which significantly influence tidal turbine arrays. These are:

- Wake effects – which relate to the velocity deficit of the flow behind a turbine, and therefore the reduced inflow speed a downstream turbine would experience
- Blockage – which relates to the influence of the turbine's thrust causing the flow to be re-directed from its natural flow and bypass the turbine altogether.

These effects are closely linked, however there are resource interactions which blur the boundary between them. For example, the flow immediately outside the wake regions downstream of a turbine may be accelerated by the presence of the turbine. Some array layouts, for both wind and tidal turbines, feature staggered grids in an attempt to take advantage of this effect. It could be classified as a local-scale blockage effect, however, it is also a result of the turbines' wake.

Currently there are only a few operational tidal arrays, namely the MeyGen project in the Inner Sound, Pentland Firth, and Nova's Bluemull Sound array in Shetland. Validation of the wake effects of the arrays are possible, but are not yet public. The IEC specification states that if an array is extracting less than 10 MW, or 2% of the theoretical resource, large-scale blockage effects are not significant. Many of the first arrays will fall into this category, however this means that blockage effects will not be validated until array capacity exceeds this threshold.

For tidal energy yield assessments, it is necessary to try to capture both wake and blockage effects through modelling. This requires the use of 3D models because 2D models cannot accurately capture wake interactions between turbines and lack sophisticated turbulence modelling capabilities. For these reasons, different types of models need to be combined to capture all of the relevant flow physics (Thomson, Whelan and Gill, 2011). The process of coupling 1D, 2D and/or 3D models is complex (Sufian, Li and O 'connor, 2017). The specific approach taken in any study would need to be reviewed to understand whether all of the relevant physical processes were being captured by an appropriate model, and whether this influence could be transmitted through the modelling chain so that feedback mechanisms were captured.

3.8.3 Spatial Modelling Analogies

The industry standard software for completing a wind energy yield is WAsP (Wind Atlas Analysis and Application Program). The tidal industry does not currently have an industry standard software for modelling. The IEC Technical Specification (IEC, 2015) provides detail on setting up a model and the input requirements (e.g. coverage, resolution, boundary conditions etc.), however it does not specify which model to use. As the tidal industry develops, use of models that have been applied widely and validated against measured data will increase confidence and assist in developing a consistent standard approach to modelling.

Blockage is a factor that the wind industry does not need to consider. Tidal flows are constrained by the free surface, whereas wind farms can draw down momentum from the geostrophic wind above the farm. This influences the flow around the device, accentuating the acceleration around the wake and fundamentally changing the mechanism that limits array efficiency for large farms. Large wind farms' array efficiencies are limited by the rate at which they can draw down this energy and momentum from the geostrophic wind (Frandsen, 2007; Calaf, Meneveau and Meyers, 2010), whereas tidal arrays are expected to be limited by the driving head acting on the flow (Adcock *et al.*, 2013). This also has more local effects, influencing the actuator disk solution for an individual turbine and hence its power and thrust coefficients (Nishino and Willden, 2012).

Tidal flows tend to have one dominant direction in flood and one in ebb, whereas wind resource is more smoothly distributed over the full 360°. This is particularly significant because many wind wake effect models perform well when averaged over large directional sectors (e.g. 30°) but poorly over narrow sectors (e.g. 5°) (Ott, Berg and Nielsen, 2011). Tidal resource assessments will be much more susceptible to the uncertainty associated with narrow directional sectors.

3.9 Losses

The gross energy yield value represents a hypothetical situation where all the turbines are performing at 100% all the time. In reality, this will never be the case. The solution is to apply corrections and losses to account for energy lost during operation of the technology. The corrections and losses outlined in the subsequent section are taken from the DNV KEMA (2013) categorisation document. They are site specific and some are calculated, and others are estimated based on experience.

3.9.1 Wind Losses

A correction is applied to the gross energy yield to make the prediction more representative of the actual wind turbine generator power produced. Losses are effects that detract or reduce the power output at the wind turbine generator (Tamura, 2012). An example of some of the corrections applied to a typical wind energy yield include:

- Weibull correction to account for the fact that the model uses a Weibull fit distribution rather than the measured data.
- Topographic and roughness correction to account for the extrapolation of measured data from the mast location to the wind turbine generator locations in the model.
- Air density correction to account for the difference in power curve density, for which the power curves used as input to the wind flow models are valid

The industry consensus is to apply losses to the energy yield value in the following areas:

i. Availability loss, which accounts for the time that the turbines are not active, usually caused by breakdown or routine maintenance. This includes availability loss from the balance of plant and the grid.
ii. Wake loss, which is applied to account for the effects of other turbines altering the wind behaviour (speed and turbulence) for the site. Typical wake models consider the influence of other wind turbine generators in terms of energy reduction only. A separate model, known as a Sten Frandsen model (Frandsen, 2007), is used to calculate the influence of other wind turbine generators in terms of turbulence.
iii. In order for a power curve to be warranted it is required to undergo rigorous testing. A loss is applied to account for the difference between the test conditions of the power curve and the actual conditions at the site. This is dependent on a number of factors such as the mean wind speed, the steepness of the slopes, the roughness complexity, the wind shear and the turbulence intensity at the site. This is still under investigation in the wind industry.
iv. Electrical losses are applied to account for the electricity lost between the wind turbine generator and the point of connection, which typically considers the loss associated with the transformers, cables and substation.
v. Environmental losses are applied to account for changes in the environment that affect the turbine. These include issues such as blade degradation, icing and extreme temperature change. Site access is also a factor which needs to be accounted for. For offshore wind, where site access losses are much higher, these are commonly included in the overall availability loss. The result is that the manufacturers are taking on this risk through the availability guarantee. This is something that the marine industry may adopt.
vi. Curtailment losses include any circumstances in which a wind farm may is not allowed to operate at the full power curve level. These instances generally fall into one of three categories: wind sector management, to limit loading; grid curtailment, which limits the export of electricity; and environmental curtailment, due to noise, shadow flicker or ecological issues. It is noted that for environmental curtailment the loss calculated should ideally consider the capability of the wind turbine generator to implement the curtailment strategy.

3.9.2 Tidal Losses

Losses are applied to the tidal energy yield value in the same way as the wind industry. Typical losses include:

i. Availability – to account for any downtime in operation of the turbines. This value is difficult to quantify at the current stage in the industry as there are insufficient operational turbines.
ii. Array interactions – including wake loss and blockage effects as discussed in Section 3.8.2.1.
iii. Power curve performance loss - applied to account for the difference between the test conditions of the power curve and the actual conditions at the site. This also includes performance degradation from biofouling or corrosion.
iv. Electrical losses - applied to account for the electricity lost between the point of generation and the metering point.
v. Environmental - The main difference here is that environmental losses include factors such as marine vessel proximity and/or impacts on marine life.
vi. Curtailment losses - include any circumstances in which a tidal farm is not allowed to operate. This is generally caused by grid constraints, or operational management in extreme wave conditions.

3.9.3 Analogies Between Wind and Tidal Losses

In order to compare the losses for wind and tidal, the various loss categories are outlined in Table 3.3. The losses that are similar for both wind and tidal are detailed, as well as those specific to each energy resource.

Table 3.3 - Comparison of loss categories for wind and tidal energy

Loss Categories	Analogies between wind and tidal	Wind specific losses	Tidal specific losses
Availability	• Lost energy due to routine maintenance as well as maintenance from component failures and faults with the turbines. • Losses due to downtime in components between the turbine circuit breakers up to and including substation transformer and project-specific transmission line • Losses due to power grid downtime		
Array interactions	• Losses due to wake effects: • Internal to array • External to array • Future to array		• Losses due to blockage effects
Turbine Performance	• Power curve • Flow conditions • Hysteresis • Sub optimal		• Biofouling
Electrical	• Losses to the point of metering, including, transformers, collection cabling, substation and transmission • Facility parasitic consumption		

Loss Categories	Analogies between wind and tidal	Wind specific losses	Tidal specific losses
Environmental	• Site access from remote project location (now included in availability)	• Icing • Blade degradation due to blade soiling • Performance degradation due to icing • Shutdown due to icing, lightening, hail • High and low temperature • Tree growth and felling • Site access and other force majeure events	• Marine vessel proximity • Marine life proximity
Curtailment	• Operational management curtailment • Grid constraint and ramp-rate • Off taker curtailment	• Environmental (noise, visual, bird/bats)	• Environmental (marine life migration)
Other	• Resource speed-energy relationship	• Air density	• Water density

As Table 3.3 illustrates, there are a large number of transferable losses from wind to tidal. Despite the resource being different, the methods to calculate the energy yield losses can be translated across. The main differences within the losses concern environmental losses. The environmental conditions that the turbines are deployed in differ greatly. For example, the density of the fluid is approximately 800 times greater, which has positive impacts on energy generation but introduces many difficulties for operation and maintenance efforts. Marine growth on blades has the potential to cause substantial performance degradation and is dependent on a number of different factors such as geographical location, season of the year, water chemistry, temperature, salinity, sunlight, distance from the shore and turbulence. In the same way that wind turbine blades can be degraded by icing or soiling, the performance of tidal turbine blades is affected by the added roughness of marine biofouling (Song *et al.*, 2019). In some cases, blade roughness was found to reduce the power coefficient by almost 20% (Walker *et al.*, 2014).

3.10 Uncertainty

Energy yield predictions are only useful if their uncertainty is well defined. Uncertainties play an important role in financing renewable projects as described in Section 3.2. Unless the energy yield assessment can offer a degree of confidence to the resource prediction, it is not possible to construct a sound financial model for a project investment. Financial models depend on understanding and capturing risk. For a renewable energy project, risk depends strongly on the uncertainty in the resource. Table 3.4 lists uncertainties which are typically included in a wind energy yield assessment, categorised into the four main areas covered in this chapter: site measurement, temporal extrapolation, spatial extrapolation, and losses.

An attempt to quantify the uncertainty range values has been conducted. These values should be considered as a guide only and should not be used commercially without the advice of a trained wind analyst. The values are stated as a percentage of the wind speed at the site. However, in order to transfer the uncertainties to an energy uncertainty it is necessary to calculate the energy gradient. This value illustrates the relationship between the wind speed and the power production at the site. A typical energy gradient is between 1.5 and 2. Therefore an uncertainty of 2% in wind speed will have an approximate value of 4% in energy yield. The uncertainties calculated as a percentage of energy are then transferred to an energy production value and are used to predict the P90 value from the P50 (see Section 3.2).

Table 3.5 outlines a summary of the uncertainties from hypothetical tidal energy projects. These values are taken from (ORE Catapult, 2015c) and are used as indicative values for comparison.

Table 3.4 – Summary of uncertainty sources for a typical wind energy project

Energy Yield Uncertainty Categories		Typical Wind Energy Uncertainty Range		Source/Reference
		% of Wind Speed	% of Energy	
Site Measurement	Instrument Accuracy	1.5 - 3.0		Wind tunnel tests (Lockhart and Bailey, 1998; Pedersen, 2004; Pedersen, Dahlberg and Busche, 2006)
	Measurement Interference	0.5 - 1.0		Physical effects of mast on measurements
	Data Synthesis	0.0 - 1.5		Amount of data synthesised, correlation of data used
	Data Quality and Metadata	0.0 - 2.0		Removed or missing data (Jung, Arda Vanli and Kwon, 2013)
Temporal Extrapolation	Historic Variation	1.0 - 4.0		MCP correlation, consistency, jack-knife (Miller, 1974)
	Future Variation	0.0 - 2.5		Weibull correction, future wake & forestry effects
	Climate Change	0.5 - 1.0		Nominal figure applied (SgurrEnergy and Solórzano, 2006)
Spatial Extrapolation	Model Inputs	0.0 - 3.0		Accuracy of input data, terrain and roughness complexity
	Horizontal Extrapolation	1.0 - 5.0		Extrapolation distance between wind turbine generator and mast for model (Clerc *et al.*, 2012)
	Vertical Extrapolation	0.0 - 3.0		Shear and vertical extrapolation

Device Performance & Losses	Availability		0.5 - 3.0	Nominal value
	Array Interactions		0.3 - 0.5	Percentage of wake loss
	Power Performance		3.0 - 5.0	Nominal value
	Electrical Losses		0.1 – 0.5	Percentage of electrical loss
	Performance Degradation		0.0 - 2.0	Percentage of icing loss
	Curtailment		0.0 - 2.0	Percentage of curtailment loss

Table 3.5 – Summary of uncertainty sources for a typical tidal energy project (ORE Catapult, 2015c)

Energy Yield Uncertainty Categories		Typical Tidal Energy Uncertainty Range	
		% of Wind Speed	% of Energy
Site Measurement	Instrument Accuracy	1.0 - 5.2	
	Measurement Interference	0.5 - 1.0	
	Data Synthesis	0.0 - 1.5	
	Data Quality and Metadata	0.0 - 2.0	
Temporal Extrapolation	Historic Variation	1.0 – 2.0	

	Future Variation	0.0 - 1.0	
	Climate Change	0.0 – 1.0	
Spatial Extrapolation	Model Inputs	0.0 - 3.0	
	Horizontal Extrapolation	5.0 - 10.0	
	Vertical Extrapolation	0.0 - 5.0	
Device Performance & Losses	Availability		0.0 - 1.2
	Array Interactions		1.5 - 3.2
	Power Performance		2.2 - 5.2
	Electrical Losses		0.5 - 1.0
	Performance Degradation		0.0 – 3.0
	Curtailment		0.0 – 2.0

3.10.1 Analogies Between Wind and Tidal Uncertainty

This section compares common uncertainties present in tidal energy yield assessments with those in wind energy yield assessments.

Within measurement uncertainty there are many similarities between wind and tidal. Even though the instruments used to measure the resource are fundamentally different, the uncertainty in the accuracy of the instrument is based on manufacturing tolerances given in the technical specification (Lockhart and Bailey, 1998; Pedersen, 2004; Pedersen, Dahlberg and Busche, 2006). When assessing the technical specifications of ADCPs, accuracies of velocity measurements are commonly stated to be between 0.3 – 1.0% in flow speed (Nortek AS, no date; Teledyne RD Instruments, 2013). However, the uncertainty in ADCP instrument accuracy has been assessed through experiments of two laboratory and two field tests. The uncertainty was estimated to be 4.55%, in flow speed, under laboratory conditions and 5.24% for field measurements (Lee *et al.*, 2013). The uncertainties in the study represent standard deviations of the differences between mean values of FlowTracker ADV and StreamPro ADCP in the repeated measurements at the same points over the vertical, and are labelled as instrument accuracy uncertainties. However, it should be noted that these estimated uncertainties are only valid for low flow speeds (velocities ranging between 0.12 – 0.50 m/s). The study also provided a breakdown of the factors that affect the accuracy of ADCP measurements, including resolution, operational conditions, sampling time etc. It was shown that the largest contributors to overall ADCP measurement uncertainty were the accuracy of mean velocity measurements (32%) and the accuracy of depth measurements (49%). The combined standard uncertainty was calculated to be approximately 2.15%.

Interference with the measurements is usually caused by the methods of installation. For wind, this includes the effect of the mast on the anemometer measurements. For tidal, interference may be caused by a number of factors including the arrangement and installation of the ADCP at the site as well as issues such as side lobe interference, which are a by-product of using an acoustic instrument to measure flow velocity. The issue of measurement interference can be mitigated in the same way for tidal energy yields as for wind energy yields. It is common practice to remove as much of the affected data from the analysis as possible. This requires robust quality control checks to be implemented throughout the post-processing of the data.

It may not always be possible to remove all of the disturbed data. For example, in wind, if only one anemometer is used, it will be shadowed by the mast in one direction, but usually this is not in the prevailing wind direction. With only one anemometer, it is not possible to correct for the shadowing effect, which results in the removal of data from one directional sector which is not representative. In some cases, the data that are distorted in a direction are not removed as it could

be in a sector that is not the prevailing wind direction. This may result in lower wind speeds overall and therefore yield a more conservative value. This may be acceptable if removing the data will produce high uncertainties.

For wind, there are a number of long-term sources of reference data which can be used to predict the long-term variations of the wind resource. However, for tidal these do not exist. Due to the deterministic nature of the tides, harmonic analysis is an effective method to estimate the tidal variations over a long period. Therefore, the uncertainty prediction methodology for this aspect of the assessment cannot be transferred to tidal from wind. A deeper understanding of harmonic analysis and the available tools for its application are required to determine the uncertainty within the methods. This is discussed further in Chapter 4.

Climate change is also considered within the uncertainties for wind resource prediction and accounts for a small uncertainty within yield assessment (SgurrEnergy and Solórzano, 2006). Local and global climate change patterns are not fully understood for tidal flow. Sea level rise can influence tidal hydrodynamics through increased tidal ranges, surge heights, and inundation of present day shorelines. In addition, it has the potential to change circulation and sediment transport patterns, which may result in changes to habitats and their organisms. Increased tidal ranges have the potential to increase tidal current velocities (Passeri *et al.*, 2015); however the effects of this have not been calculated and the magnitude of the increase is difficult to quantify. There is no evidence at present to suggest that climate change will cause a significant change in tidal resource. There has been some research into the effects of climate change on sea-level rise and the occurrences of storm surges. For example, the UK Climate Impacts Programme 2009 (Jenkins, Perry and Prior, 2009), predicts absolute sea-levels could rise by between 100mm and 300mm by 2030 and that there is likely to be a significant increase in extreme high sea levels resulting in increased storms. This could have an effect on the energy yield of tidal devices through decreased availability but this uncertainty is not fully understood. As a result, the effect of climate change on the future variability of tidal resource is not discussed further, but is mentioned as a minor issue for the readers' information.

There are many similarities between wind and tidal modelling techniques. The main aim of creating models is to analyse how the dynamics of the fluid, whether air or water, vary over a spatial domain. This involves extrapolation of measured data from a known location to another position of interest within the model, usually the proposed turbine locations. Even though the tools to model wind and tidal flows are different, the uncertainties are transferable. There are uncertainties with the model inputs, the boundary conditions and with the user defined inputs such as resolution and the setup of the domain. The uncertainties can be quantified using validation with multiple measurement devices.

The uncertainties arising from losses and corrections applied to the gross energy yield value are similar. Both wind and tidal farms will experience plant performance losses. Generally, Monte Carlo simulations are carried out for every component failure rate and accessibility factor, to give an appropriate availability estimate. This method is more commonly applied to offshore wind accessibility calculations but can be applied to tidal devices too. It is common in the wind industry to manage this through a turbine supply contract which defines an agreed availability value.

Turbine power performance uncertainty for the wind industry can be calculated through testing outlined in the IEC standard for Power Performance Measurement of Wind Turbines 61400-12-1-2005 (IEC, 2005). This technical standard outlines a methodology for quantifying the overall uncertainty and the specific parameters which should be assessed. The performance of the turbine is usually tested within typical operating conditions and ranges of wind shear, turbulence intensity and temperature. This can be applied directly to tidal energy and has helped to inform a similar IEC standard for tidal turbine testing.

Many of the loss uncertainties are similar for wind and tidal and can be assumed to be a percentage of the overall loss. However, the factors that affect performance degradation losses differ from wind energy to tidal. Wind energy has to combat blade degradation from soiling and other extreme weather effects, whereas tidal turbines are affected by marine growth and bio-fouling (Walker *et al.*, 2014; Song *et al.*, 2019). Corrosion protection is essential to mitigate degradation from sea water. This loss is difficult to quantify and the associated risk is commonly pushed onto the turbine supplier who must carry out sufficient inspections and cleaning of blades to maintain the warranted power curve.

The final loss uncertainty accounts for the impact of curtailment on an energy project. For the wind industry, this has been considered as a percentage of the loss and this method could be applied to the tidal industry. It varies from project to project as the developer's exposure to this risk depends on the terms of the Power Purchase Agreement they have in place.

3.11 Chapter Conclusions

For the tidal industry to become commercially viable, a better understanding is required of the uncertainties affecting energy yields. This chapter has analysed the methods and techniques that the wind industry uses to evaluate uncertainties and drawn comparisons to improve knowledge of tidal uncertainties. There are some key similarities where the tidal industry can learn from the wind industry. Namely, these include: calculating measurement uncertainty for site assessments; uncertainty in modelling for evaluating spatial extrapolation variations; and methods to evaluate power performance uncertainty for tidal turbine testing.

There are areas where the tidal industry can take lessons learnt from the mature wind industry. The wind industry has benefitted from the standardisation of modelling. WAsP linear flow modelling is commonly used across the industry and this enables results from different assessments to be compared more easily. As the tidal industry develops, the use of standard hydrodynamic models will enable better understanding of uncertainties to apply. Another area to highlight is the use of the bed roughness parameter in hydrodynamic modelling. A single bed roughness value is currently used to adjust the modelled outputs to available measured data; however, this approach is not considered robust. The use of a distribution of bed roughness value and its effect on the expected power is investigated in Chapter 5. As more tidal arrays become operational, models and other pre-construction estimates can be verified using operational data.

A key milestone for the wind industry occurred when several organisations came together to compare methods and results in energy yield assessments. The resource assessment workshop, at EWEA in 2011, shed light on the different approaches and the resulting variation in energy yield predictions from different sources (Mortensen and Jørgensen, 2011). The tidal industry would greatly benefit from a similar collaborative study to evaluate how developers, consultants and academics are approaching tidal resource assessment and share knowledge on the best practices to use. This would lead to a better understanding of energy yield techniques and an industry wide convergence on the most appropriate approaches to use.

Early stage wind development saw the largest turbines being developed as prototypes by public/government funding (MacGillivray, 2016). Commercial wind began at the smaller scale and increased slowly, through better understanding of the resource and incremental improvements in design. A similar approach for the tidal approach would be advisable, in order to keep deployment costs low and enable better understanding of the turbine performance at each incremental scale.

Finally, the wind industry has benefitted from the creation of the MEASNET organisation, which has developed a collection of standard guidelines (Measnet, 2009). The setup of an equivalent organisation for the tidal industry would help align new methods and techniques and assist in standardising procedures.

Chapter 4

Uncertainty in the Prediction of Temporal Variations in Tidal Flow Velocity

4.1 Introduction

This chapter introduces new methods and practices for predicting long-term variations in tidal energy flow and assesses statistical methods to quantify uncertainty in harmonic analysis procedures. Section 4.2 introduces a case study, using measured site data from two acoustic Doppler current profiler's (ADCP's) deployed at a prospective tidal energy site in the UK. Section 4.3 outlines the methodology and results of the harmonic analysis work conducted, using the open source Matlab code UTide. Section 4.4 investigates three methods to evaluate uncertainty in long term tidal predictions which are applied to the harmonic analysis conducted on the measured site data. Section 4.5 discusses some of the techniques used to evaluate uncertainty in the wind industry and investigates their applicability to the quantification of uncertainty in harmonic analysis.

4.2 The Sound of Islay Measurement Campaign

This section introduces a tidal energy case study, using measured site data from two acoustic Doppler current profilers (ADCPs), deployed at a prospective tidal energy site in the UK. An appraisal of current procedures and methods for conducting harmonic analysis is presented as an example of how to use harmonic analysis to predict long term tidal variations.

The Sound of Islay is a narrow strait between the islands of Jura and Islay, off the west coast of Scotland, as shown in Figure 4.1. The strait runs roughly north to south and is approximately 21 km long and 1.4 km wide, at its narrowest point. Consent for a tidal turbine project was given by Marine Scotland on 17 March 2011 (Iyer, 2010). Tidal turbines were first proposed for deployment at the site by Scottish Power Renewables, but the site was then purchased by Atlantis Renewables in 2016.

Figure 4.1 – Map showing the Sound of Islay, the strait between the island of Jura and Islay, off the west coast of Scotland (Ayack, 2008)

The site has highly favourable characteristics for the development of tidal turbines; namely because the tidal flow through the channel is highly bi-directional with flow speed exceeding 2.5 m/s. This is discussed further in Section 4.2.2 . Furthermore, the channel is orientated in a north-south direction and is therefore protected from waves generated from the prevailing wind direction (south-west) and the Atlantic fetch. The channel is approximately 60 m deep at its deepest point as shown by the image of the bathymetry at the site in Figure 4.2. Two ADCPs were deployed at the site in 2009 to measure tidal flow. The positions of the two ADCP deployments are also shown in Figure 4.2.

The high tidal current speeds in the channel has resulted in the seabed consisting predominantly of exposed bed rock, with some boulders and patches of coarse sand (DP Marine Energy Ltd, 2009). Some of the exposed rocks are in excess of 30 cm in diameter. Benthic survey work was conducted and found that the seabed in the Sound had large quantities of boulders and uneven terrain. However flat sandy patches were discovered and considered to be ideal locations to deploy ADCP's to measure the flow in the channel.

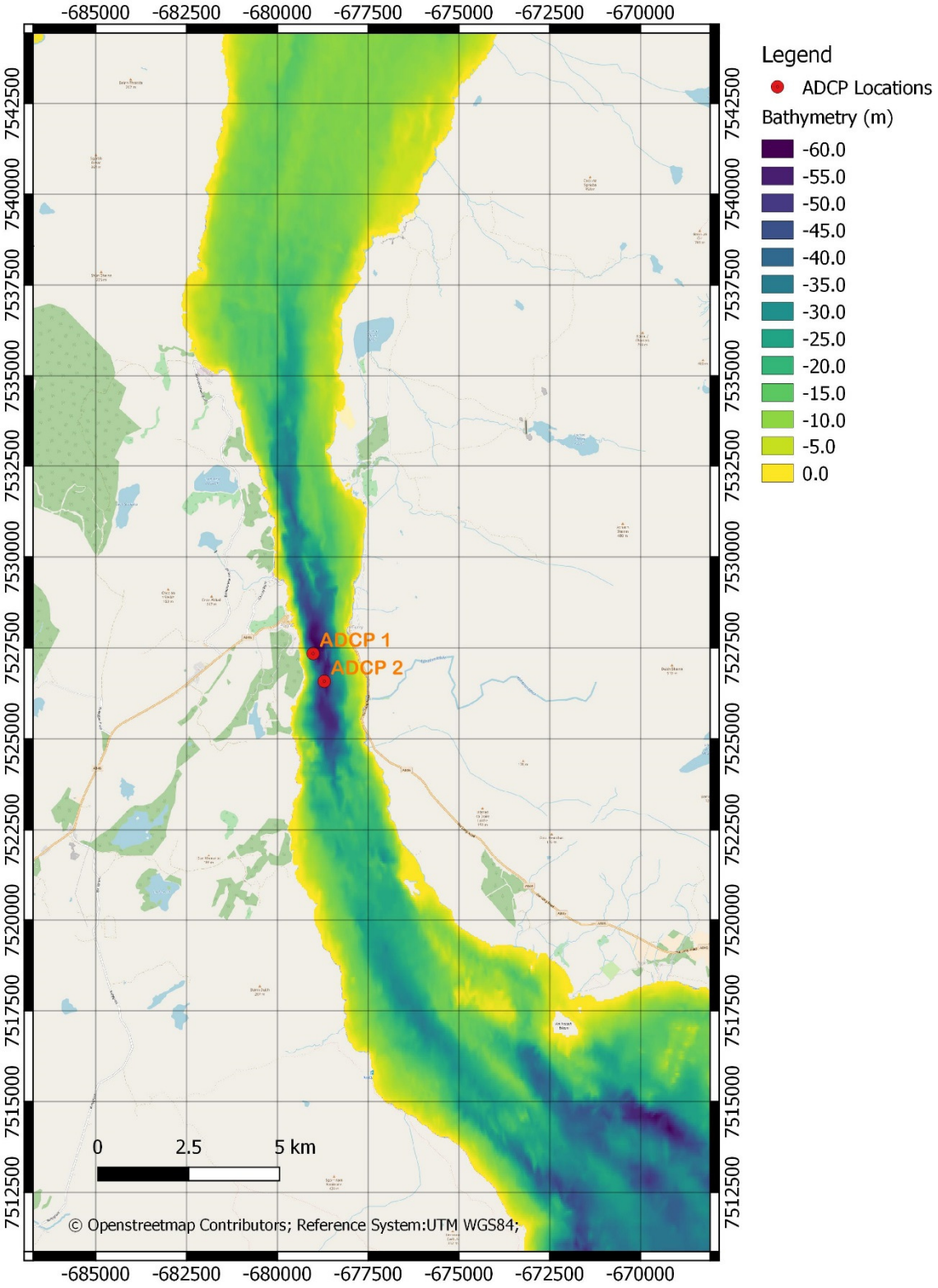

Figure 4.2 - Sound of Islay bathymetry plot, showing ADCP deployment locations within the channel, with the island of Jura to the east and the island of Islay to the west.

4.2.1 Analysis of Measured Data

Measured data was recorded by two ADCPs deployed at the site. The ADCPs were installed by Partrac on 15 June 2009 and each ADCP measured data for approximately 32 days, from 15 June 2009 to 17 July 2009. The distance between the devices was calculated to be approximately 820 m. After the data had been collected, the ADCPs were then retrieved and the data received for analysis. Table 4.1 provides a summary of the ADCP instrumentation and configuration during the measurement campaign.

Table 4.1 – Summary of ADCPs Instrumentation Configuration

Data Category	ADCP 1	ADCP 2
Instrument Type	RDI Sentinel ADCP	
Instrument Mounting	Frame	
Start Time	15/06/09 15:53:00	15/06/09 14:57:00
End Time	17/07/09 06:09:00	17/07/09 16:44:59
Sampling Interval (s)	0.73	0.73
Averaging Interval (s)	60	60
Parameters Measured	Current Speed, Current Direction, Data Quality, Pitch, Roll, Depth, Standard Deviation	
Location	Latitude 55°50’37.031”N	Latitude 55°50’23.2”N
	Longitude 6°5’58.69”W	Longitude 6°5’48.703”W
Sensor Height ABL (m)	0.8	0.8
Erroneous data (%)	7.3	7.4
1st Bin Range (m)	3.21	3.2
Bin size (m)	1	1
Number of bins	52	50
Depth to Chart Datum (m)	62.0	59.1

The ADCPs were deployed in depths of water ranging from 52 to 61 m and were pre-configured for a 31 day deployment. In order to ensure that the equipment was positioned reasonably level (within a tolerance of 7 degrees) on the seabed, a camera system (with lights) was used to monitor

a level attached to the stainless-steel frames of the ADCPs. The time window for deploying the frames, during each slack tide, was 45 minutes.

Each ADCP measured the flow across the water column in 1 m bins. The number of bins at each location was 52 and 50 for ADCP 1 and ADCP 2 respectively. The ADCP was programmed to take into account the 0.8 m distance between the sea bed and the transducers on top of the device. A value of 0.8 m was added to the depth values to take into account the height of the instrument above the seabed. Data was removed if the percentage of good data was less than 80%. This value was calculated using a combination of criteria including correlation, error velocity and fish detection and is used as an indicator of quality control. This criterion was applied to the data by Partrac.

4.2.2 Review of Measured Data

The data were initially converted into the east and north components of the flow using the depth averaged speed, $\overline{U}$, and direction, θ, at each timestamp. The east component defines the flow in the east-west direction and the north flow defines the flow in the north-south direction. The east, *u*, and north, *v*, components of the flow were calculated using Equation 4.1 and Equation 4.2, respectively.

$$u = \overline{U} sin\, \theta \tag{4.1}$$

$$v = \overline{U} cos\, \theta \tag{4.2}$$

Figure 4.3 shows a comparison of the raw data from ADCP 1 and ADCP 2. The data is separated into the east and north components and is averaged over the depth. Observations of the raw data show that the tide can be characterised as semi-diurnal, meaning there are two high and two low waters each tidal day, with relatively small differences in the respective highs and lows. The spring and neap cycle can also be observed over the month of data, where the spring tide reached its maximum around 25th June and 11th July.

An evaluation of the effect of using depth averaged flow speeds against rotor averaged or hub height velocities was carried out. Using the turbine parameters of the SIMEC Atlantis Resources AR1500 tidal turbine (Atlantis Resources, 2019), the average velocity values were calculated and are shown in Table 4.2. The turbine is a bottom mounted, three bladed horizontal axis turbine, with a hub height of 15 m and a rotor diameter of 9 m. Therefore, the rotor averaged velocity is averaged between 6 m and 24 m in the water column.

Table 4.2 - Comparison of spatial averaging options of ADCP velocities based on the Atlanstis Resources AR1500 tidal turbine

Flow Velocity (m/s)	ADCP 1	ADCP 2
Depth Averaged Velocity	1.415	1.409
Rotor Averaged Velocity	1.360	1.376
Hub Height (15 m)	1.407	1.391

From the results it can be seen that the depth averaged velocity is higher than the rotor averaged for this turbine type and configuration. The hub height velocity is closer to the depth averaged velocity at both ADCP locations. The analysis in this chapter was carried out using the depth averaged velocity, as defining a turbine type and size will skew the results.

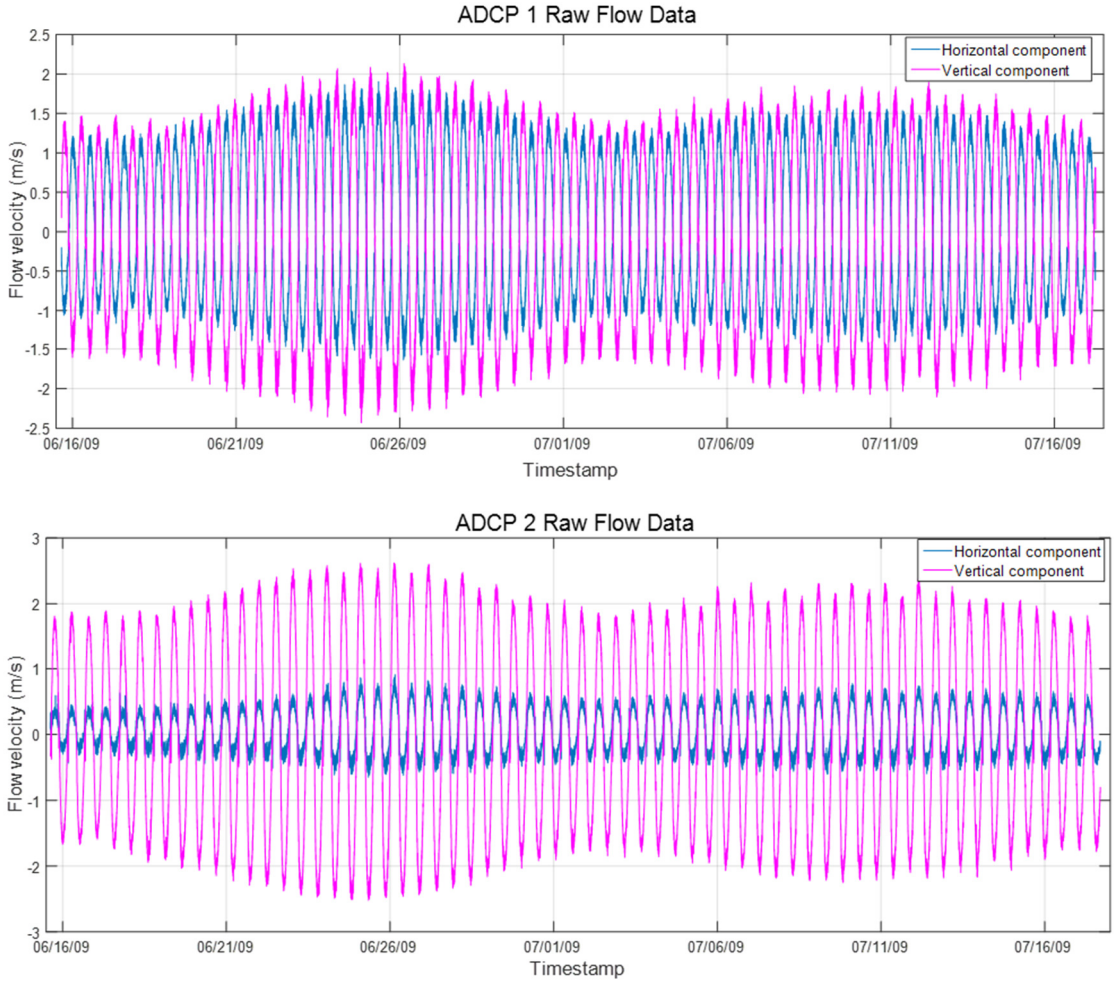

Figure 4.3 - Sound of Islay plot of raw measured data

It can be seen that the north-south component of the tide is greater than the east-west component for both ADCP's, but ADCP 2 has a much more pronounced difference between the east and north

tidal signal, as seen in Figure 4.3. This is because the channel is orientated in a north to south direction. ADCP 2 is located towards the centre of the channel and therefore there is not much east-west flow. For ADCP 1, the flow is greater in the southerly direction reaching a maximum of approximately 2.4 m/s compared to a maximum of 2.1 m/s in the northerly direction. This means that the tidal flow is stronger on the flood tide when tide is moving towards the south of the channel. For ADCP 2, the flow component in the east-west direction is significantly smaller than the north-south component, showing that the tide flows mostly in the north/south direction. To get a better understanding of the directionality of the flow at each location, polar plots of the data were produced, as shown in Figure 4.4.

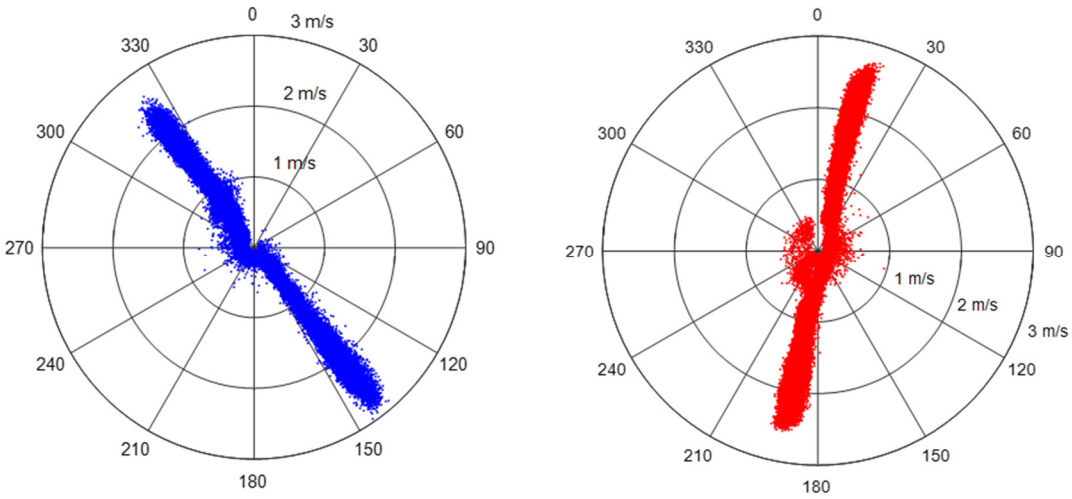

Figure 4.4 – Polar plot of raw data (left – ADCP 1, right – ADCP 2)

The flow in both locations can be classed as bi-directional, which means the flow moves primarily in two directions, 180° apart. The main variations in the direction occur at low flow speeds. This is most likely due to the flow during slack tide, when the tide is turning, but may also be due to fluctuations in the turbulence at the site. An assessment of the location of each ADCP suggests that the difference in principal current direction is caused by the local bathymetry effects at each location. As Figure 4.2 shows, ADCP 2 is positioned towards the centre of the channel compared to ADCP 1 being positioned towards the west side of the channel.

4.2.3 Data Availability

The data coverage was considered to be high quality, with only 7% removed as unusable. The majority of this bad data was found in the upper bins, caused by side-lobe echoes and returns from the water surface.

An assessment of the availability of the data measured at each ADCP was conducted. The average availability of data in each ADCP cell was plotted against the normalised depth of the cell, as

shown in Figure 4.5. Data availability is considered poor below a value of 80%. The availability data, for both ADCP 1 and ADCP 2, shows that availability is below 80% in the top 12% and 7% of the water column for ADCP 1 and ADCP 2 respectively. The region close to the sea surface is typically disregarded as it is usually affected by wave interactions. Furthermore, ADCP data near the surface is usually removed due to contamination from side lobe interference. This is discussed in Chapter 3 (Section 3.6.2.1). To determine the amount of near-surface contamination, Equation 4.3 can be used. The ADCPs used in this measurement campaign are both RDI Sentinel ADCPs, which have a beam angle, θ, of 20°. Therefore, the maximum distance, R_{max}, that should be considered is:

$$= [A \times cos(\theta)] - Cell\ Size \tag{4.3}$$

$$R_{max} = [52\ \times cos\,20] - 1 \tag{4.4}$$

$$R_{max} = 47.9m \tag{4.5}$$

A is the depth of water and the cell size is equal to the bin size of the ADCP data. This results in omitting approximately the top 8% of the water column for both ADCPs. For most fixed tidal turbines, the region towards the centre of the water column is the most desirable location to fix the turbine. The data availability, in this region, between 10% and 70% of the water depth, has high availability (above 95%). This is because the tidal flow lower in the water column isn't influenced by wave-current interactions, but the profile of the tidal flow speed shows that the velocity remains high, as is discussed in the next section.

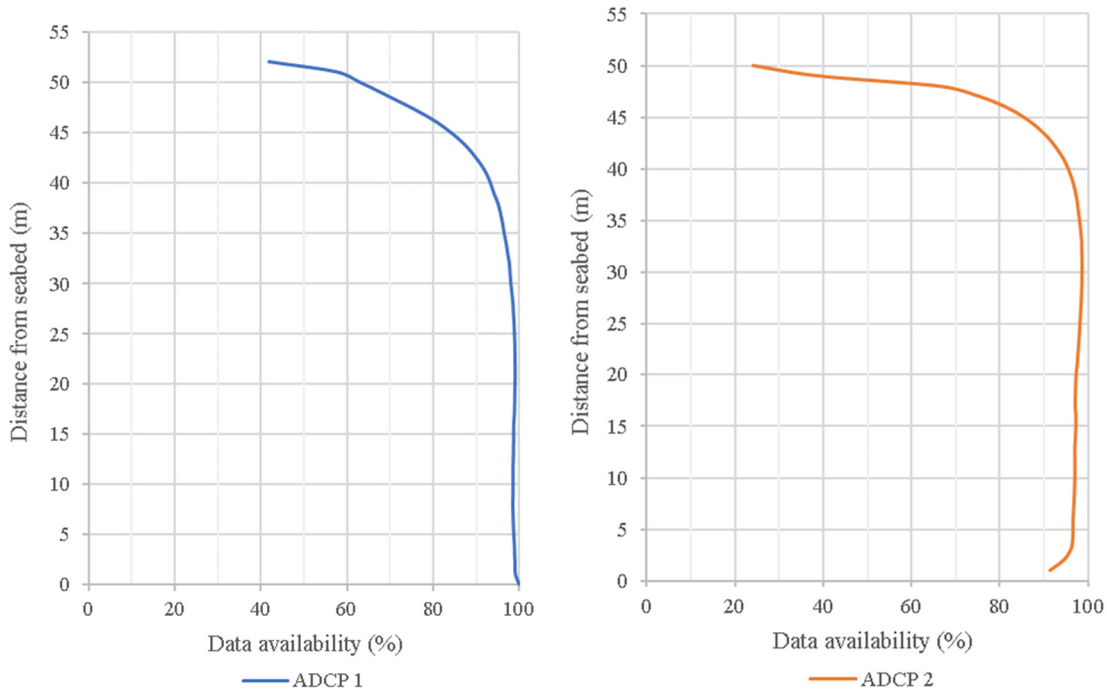

Figure 4.5 – Graph showing the availability of measured ADCP data with respect to the normalised depth of water

4.2.4 Measured shear

An evaluation of the measured shear at the site was conducted by plotting the average flow speed values at each depth in the water column, shown graphically in Figure 4.6. The shear exponent provides an indication of how the flow varies across the water column. A high shear value suggests that the flow has a high variation with water depth and a low shear value indicates that the flow is relatively uniform across the depth. This is particularly important when considering the flow across turbine blades and the corresponding variation in forces from flow speed variations. The average shear at the two locations was calculated to be 0.11. However, the profile shows some variation over the depth. Data from ADCP 1 shows that the average maximum flow speed of 1.50 m/s was measured at a height of 34 m from the seabed. Similarly, data from ADCP 2 shows that the average maximum flow speed of 1.48 m/s was measured at a height of 39 m from the seabed. The effect of the water surface is evident at both locations, as the flow speed is significantly reduced where the water meets the free surface and wave-current interactions occur most prevalently.

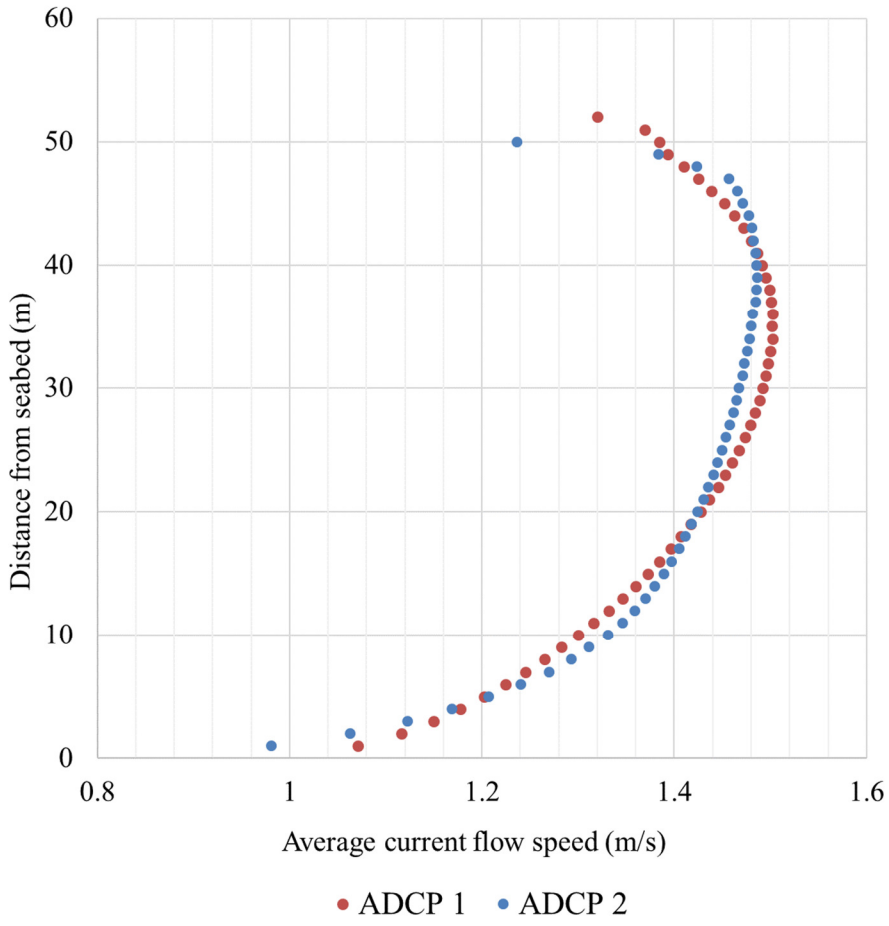

Figure 4.6 –Mean flow speed in each depth bin, for both ADCP locations, showing the flow variation across the water column

Friction from the seabed results in reducing tidal velocity near to the seabed, which is characterised using the power law (Soulsby, 1997). The power law exponent characterises the rate at which the speed changes with height above the seabed. The flow speed varies with the height above seabed according to the following equation

$$U(z) = \left(\frac{z}{\beta h}\right)^{\frac{1}{\alpha}} \bar{U} \tag{4.6}$$

Where the velocity profile (the velocity at height, z, above the seabed, $U(z)$) is described using the power law, α, and the bed roughness coefficient, β, with water depth, h, and depth averaged velocity, $\bar{U}$.

It should also be noted, that the logarithmic (log) law can also be used to characterise the velocity profile (Soulsby, 1997). The log-law states that the speed varies logarithmically with the height above the seabed according to the following equation

$$U(z) = \begin{cases} \frac{U^*}{k} ln\left(\frac{z}{z_0}\right) & if\ z > z_0 \\ 0 & if\ z \leq z_0 \end{cases} \quad (4.7)$$

Where U^* is the friction velocity (m/s), k is the von Karman's constant (=0.4) and z_0 is the surface roughness (m) and the remaining symbols are the same as the power law exponent values. However, the power law, which is derived from shelf-sea oceanographic research, is typically used to characterise the velocity profile in tidal energy research (Batten *et al.*, 2008; Myers and Bahaj, 2010; O'Doherty *et al.*, 2010). For tidal energy resource assessments, depth-averaged shallow water-equation models are often used, with an assumed velocity profile using the 1/7th power law and a bed roughness (β) of 0.32 (Batten *et al.*, 2008; Serhadlioğlu *et al.*, 2013). Other studies (Lewis *et al.*, 2017b) have suggested that other power laws may be more applicable (e.g. 1/8th or 1/10th power laws).

Figure 4.7 and Figure 4.8 show the average velocity profile compared to different power law and bed roughness values for ADCP 1 and ADCP 2 respectively. The plots show how the power law value affects the steepness of the velocity profile and that for this site a power law (α) value of 8 is more suitable. The profiles for varying bed roughness (β) values is also depicted. This value greatly affects the velocity profile, by reducing the flow near the seabed and therefore reducing the flow across the whole water column. The bed roughness value of 0.4 shows the greatest agreement with the measured data at the site. This value fits with the value suggested in other studies (Ward *et al.*, 2015; Lewis *et al.*, 2017b), which suggest that this enhanced bed roughness coefficient is due to coarser sediment types (or larger bed forms) in these tidally-energetic environments. This shows that using a higher bed roughness value of 0.4 may be more suitable and where possible the value should be calculated from ADCP velocity profiles in future studies of turbine interaction with the resource.

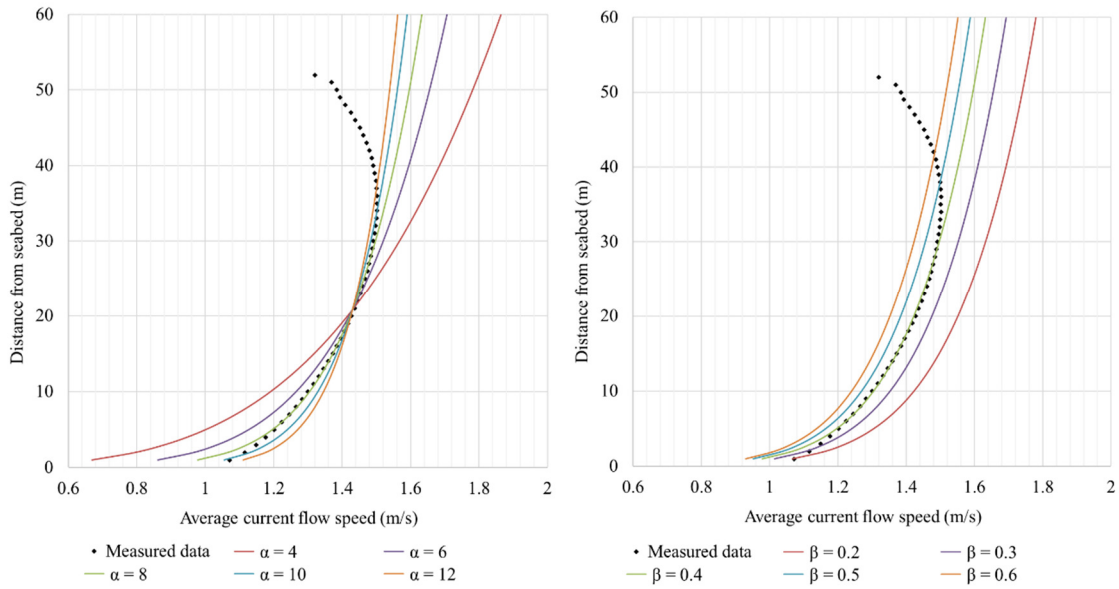

Figure 4.7 – Velocity profile variability due to varying power law (α) and bed roughness (β) coefficients, compared against measured data at ADCP 1 location

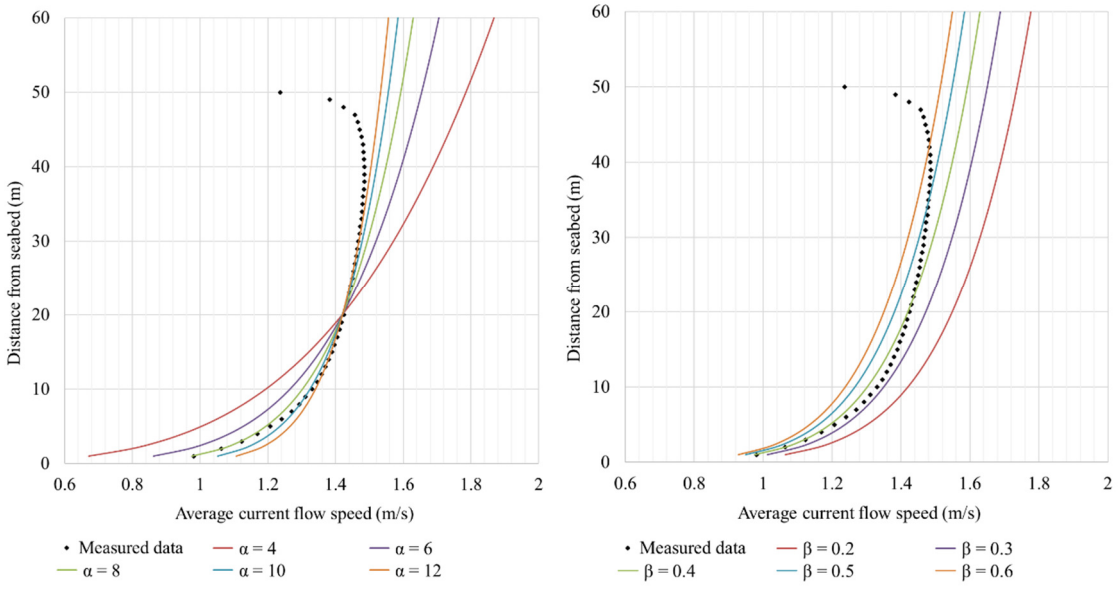

Figure 4.8 – Velocity profile variability due to varying power law (α) and bed roughness (β) coefficients, compared against measured data at ADCP 2 location

4.3 Harmonic Analysis Methodology

4.3.1 UTide - Unified Tidal Analysis and Predictions Functions

There are several numerical codes created to conduct harmonic analysis. The most common are outlined in Section 2.2.4. The UTide harmonic analysis code was selected as the most appropriate tool for this investigation. UTide is a freely available tidal analysis code which built upon previous codes; namely T_Tide (Pawlowicz, Beardsley and Lentz, 2002), r_t_tide (Leffler and Jay, 2009), and "versatile" (Foreman, Cherniawsky and Ballantyne, 2009). It is therefore considered one of the most advanced open source tidal analysis codes and is recommended in the IEC tidal resource technical specification (IEC, 2015). For this study, the UTide package was used through the Matlab numerical programming software. The UTide package can be downloaded directly from the Mathworks website (Codiga, 2011). A similar package can be accessed for use in the numerical software Python (Bowman, 2018).

UTide consists of a pair of Matlab functions: *ut_solv*, to perform the harmonic analysis; and *ut_recontr*, which uses the *ut_solv* results to reconstruct the time series for hindcast or forecast prediction. Taking the raw time series data, the aim is to deconstruct and extract the harmonic constituents and then the code enables the user to recreate a tidal variation over longer time periods.

For this analysis, the two ADCP datasets discussed in Section 4.2 were used. The measurement period consists of approximately a month (31.59 days) of tidal speed and direction data. The flow was measured every 0.73 seconds to give 82 measurements per minute. The post-processing of the data, conducted by Partrac, involved averaging the data to give measurements at 1-minute intervals. The flow data was measured over the depth of the channel and binned into 52 bins. The data was then averaged over the depth to give a single value of the flow speed and direction every minute. Each time step can therefore be described as a vector with a magnitude and a direction of the flow. To comply with the required UTide input format, the data at each time step was converted into an east, F_u, and north, F_v, component of the flow, calculated using

$$F_u = V_i \cos\theta \text{ and } F_v = V_i \sin\theta \tag{4.8}$$

where V_i is the magnitude of the depth averaged velocity, and θ is the direction of the depth averaged flow. The data was then input into the UTide functions. The Matlab syntax for the two-dimensional raw input is

coef = ut_solv (t_raw, u_raw, v_raw, lat, cnstit, {options})

- **t_raw** represents the timestamp as a column vector, which must be input as date number format. If the timestamp is in a string format (i.e. dd/mm/yyyy hh:mm:ss), then it can be converted to the date number format using the MatLab function **datenum**

- **u_raw** and **v_raw** represents the easterly (u) and northerly (v) components of the tide. The easterly component is associated with the longitude direction and the northerly component is associated with the latitude direction. This should be input as a column vector the same size at the timestamp vector

- **lat** represents the latitude of the location of interest. This should be input as a scalar input, in decimal degrees (north is positive and south is negative)

- **cnstit** is the input to specify which constituents should be included in the harmonic analysis. The user can either select the default setting 'auto' which will solve the constituents based on LSS or select the constituents manually depending on the requirements for the analysis. The constituents can be selected manually by creating a cell array with any of the 146 constituents outlined in the 'ut_constants.mat' as part of the UTide package. The constituents are input as a character string using the symbols defined for each constituent (letters and numbers).

There are a number of additional user-defined variables that can be selected to modify the analysis. For more information see the UTide user guide (Codiga, 2011).

For an individual constituent, the tip of the velocity vector in the complex plane traces out an ellipse during each full period, as discussed in Section 2.2.3. Current ellipse parameters are expressed in terms of the magnitudes and phases of the complex amplitudes as:

$$L_q^{smaj} = \left(A_q^+ + A_q^-\right) \tag{4.9}$$

$$L_q^{smin} = \left(A_q^+ - A_q^-\right) \tag{4.10}$$

$$\theta_q = mod\left[\frac{\varepsilon_q^+ + \varepsilon_q^-}{2}, \pi\right] \tag{4.11}$$

$$g_q = -\varepsilon_q^+ + \theta_q \tag{4.12}$$

And are defined as the semi-major axis length L_q^{smaj}, the semi-minor axis length L_g^{smin}, the orientation angle θ_q and the Greenwich phase lag g_q, where A_q^+ and A_q^- are the magnitudes of the tide and ε_q^+ and ε_q^- are the associated phases.

Random realisations of the current ellipse parameters (L^{smaj}, L^{smin}, θ and g) are generated through Monte Carlo uncertainty propagation within the code. Standard errors, σ, of current ellipse parameters are computed using the median-averaged-deviation formulation:

$$\sigma_{L^{smaj}=Median[|\{L^{smaj}\}-Median[\{L^{smaj}\}]|]/0.6745} \quad (4.13)$$

$$\sigma_{L^{smin}=Median[|\{L^{smin}\}-Median[\{L^{smin}\}]|]/0.6745} \quad (4.14)$$

$$\sigma_{\theta=Median[|\{\theta\}-Median[\{\theta\}]|]/0.6745} \quad (4.15)$$

$$\sigma_{g=Median[|\{g\}-Median[\{g\}]|]/0.6745} \quad (4.16)$$

Finally, the 95% confidence intervals, CI, is calculated as 1.96 times these standard errors, such that, for example, it is 95% probable that L^{smaj} lies between L^{smaj} - CI(L^{smaj}) and L^{smaj} + CI(L^{smaj}). Each of the four key parameters defined in Equations 4.9 to 4.12 are presented as outputs from the code with a 95% confidence interval.

4.4 Three Methods to Evaluate Uncertainty

When analysing tidal currents, Parker (2007) defines three main approaches to assess the accuracy of harmonic analysis predictions. The three approaches are:

(1) directly comparing the speeds, directions, and times of maximum floods, maximum ebbs, and slack waters (or minimum flows) in the predicted series versus an observed time series;

(2) carrying out and examining a spectral analysis of the residual time series; and

(3) examining the residual time series itself for periods with transient tidal current oscillations.

The first approach, comparing the overall tidal variations between the measured and predicted variations, is addressed in Section 4.4.2. The second approach, evaluating spectral analysis of the residuals, is investigated in Section 4.4.3. The third approach is covered is Section 4.4.5 which aims to evaluate the residuals by using statistical methods to calculate the error.

4.4.1 Initial UTide Results

A summary of the initial harmonic analysis results for ADCP 1 and ADCP 2 are shown in Table 4.3 and Table 4.4, respectively. The major and minor axis lengths are provided, along with the direction of the major axis and the phase angle of the constituent. Each value is shown with a corresponding 95% confidence interval calculated through UTide, as described in Section 4.3.1. The signal-to-noise ratio (SNR) is used to compare the strength of a desired signal to the level of

background noise. For UTide a SNR value of 2 is typically used when resolving constituents. Therefore, any constituents with a SNR lower than 2 are not included in the results.

The percent energy (PE) is a value that indicates the relative importance of a constituent. For constituent q, the percent energy is

$$PE_q = \frac{E_q}{\sum_{q=1}^{n_{allc}} E_q} * 100 \tag{4.17}$$

where

$$E_q = \left(L^2{}_{smaj} + L^2{}_{smin}\right) \tag{4.18}$$

E_q is proportional to the kinetic energy. The value indicates the importance of the constituent in an amplitude-weighted sense. The PE results in Table 4.3 and Table 4.4 show that the M2 tidal constituent is the most dominant at the site, corresponding to approximately 91% of the signal at both ADCP locations. The N2 and S2 constituents have high signal to noise ratios and each contribute to an additional 4% of the energy of the tide. Therefore, it can be seen that the top 3 constituents (M2, N2 and S2) represent approximately 99.5% and 98.5% of the tidal variations at the ADCP 1 and ADCP 2 locations, respectively. These values show how important these first three constituents (especially the M2 constituent) are at this site.

Another useful parameter is The 'PTVallc' value is the percent tidal variance captured by the model solution. This is a useful parameter, calculated by the UTide code, to assess how well the harmonic prediction fits the measured data. The PTVallc value for the ADCP 1 and ADCP 2 harmonic analysis were calculated to be 91% and 89% respectively. This value provides an overall value of how well the predicted harmonics fit to the measured variation when you consider all of the constituents and their combined contributions. Therefore approximately 10% of the tidal variations are not captured by the harmonic fit. The resulting residuals may result from wave current interactions and turbulence caused by bathymetric effects, which are difficult to quantify.

Table 4.3 – ADCP 1 UTide Harmonic Analysis Results

Constituent ID	Major axis length (m/s)	Minor axis length (m/s)	Angle (θ)	Phase (°)	Signal to Noise Ratio	Percent Energy (%)
M2	2.16 ± 0.003	-0.0043 ± 0.0009	127 ± 0	21.3 ± 0.08	1,900,000	91.35
N2	0.474 ± 0.003	-0.0061 ± 0.001	128 ± 0	360 ± 0.41	110,000	4.43
S2	0.432 ± 0.002	-0.0035 ± 0.0008	127 ± 0	74.1 ± 0.37	110,000	3.68
M6	0.1 ± 0.003	0.0089 ± 0.0011	130 ± 1	265 ± 1.56	4,100	0.20
2MN6	0.074 ± 0.002	0.0068 ± 0.0011	129 ± 1	246 ± 2.3	2,900	0.11
K1	0.06 ± 0.002	0 ± 0.0009	127 ± 1	236 ± 2.23	2,600	0.07
2MS6	0.058 ± 0.003	0.0063 ± 0.0011	128 ± 1	313 ± 2.55	1,300	0.07
M4	0.031 ± 0.003	0.012 ± 0.0016	155 ± 4	219 ± 4.7	460	0.02
O1	0.028 ± 0.002	-0.0013 ± 0.0008	130 ± 2	100 ± 4.7	460	0.02
MS4	0.027 ± 0.003	0.0049 ± 0.0009	128 ± 2	223 ± 5.84	410	0.02
MN4	0.024 ± 0.002	0.0043 ± 0.0015	148 ± 4	209 ± 6.63	330	0.01
MSF	0.016 ± 0.003	0.0058 ± 0.001	132 ± 5	198 ± 9.43	120	0.01
MK3	0.014 ± 0.003	-0.0013 ± 0.0009	130 ± 4	147 ± 12.7	98	0.00
NO1	0.013 ± 0.003	-0.0004 ± 0.0011	113 ± 5	38.6 ± 14.7	60	0.00

Constituent ID	Major axis length (m/s)	Minor axis length (m/s)	Angle (θ)	Phase (°)	Signal to Noise Ratio	Percent Energy (%)
2SM6	0.013 ± 0.003	0.0008 ± 0.0009	126 ± 5	30.9 ± 13.1	56	0.00
M8	0.012 ± 0.003	-0.0044 ± 0.001	136 ± 10	133 ± 16.6	73	0.00
2MK5	0.012 ± 0.003	0 ± 0.001	126 ± 4	99 ± 11.6	74	0.00
ETA2	0.012 ± 0.002	-0.0008 ± 0.0006	123 ± 3	146 ± 8.64	160	0.00
MO3	0.011 ± 0.003	-0.0004 ± 0.0009	121 ± 4	333 ± 12.8	51	0.00
2Q1	0.009 ± 0.002	-0.0011 ± 0.0007	118 ± 6	207 ± 15.5	57	0.00
Q1	0.008 ± 0.003	-0.001 ± 0.0008	128 ± 5	51.1 ± 15	36	0.00
UPS1	0.008 ± 0.002	-0.0005 ± 0.0006	129 ± 6	356 ± 19.3	81	0.00
M3	0.006 ± 0.003	0.0003 ± 0.001	125 ± 8	216 ± 26.2	15	0.00
3MK7	0.006 ± 0.003	-0.0005 ± 0.0009	132 ± 10	21.4 ± 24.9	14	0.00
OO1	0.005 ± 0.002	0.0006 ± 0.0007	124 ± 9	253 ± 26.3	20	0.00
S4	0.005 ± 0.002	0.0008 ± 0.0009	127 ± 11	220 ± 31.1	18	0.00
J1	0.004 ± 0.002	-0.0002 ± 0.0008	115 ± 11	0.54 ± 96.1	12	0.00
SK3	0.003 ± 0.002	-0.0001 ± 0.0011	101 ± 20	299 ± 33.4	7	0.00
2SK5	0.003 ± 0.003	0.0012 ± 0.0009	118 ± 29	258 ± 61.5	5	0.00

Table 4.4 – ADCP 2 UTide Harmonic Analysis Results

Constituent ID	Major axis length (m/s)	Minor axis length (m/s)	Angle (θ)	Phase (°)	Signal to Noise Ratio	Percent Energy (%)
M2	2.13 ± 0.002	0.0111 ± 0.001	77.4 ± 0	22.5 ± 0.04	4,800,000	90.61
N2	0.455 ± 0.002	0.0242 ± 0.0009	79.1 ± 0	359 ± 0.19	240,000	4.14
S2	0.434 ± 0.002	-0.0209 ± 0.001	75.3 ± 0	75.2 ± 0.19	190,000	3.76
L2	0.179 ± 0.001	0.0204 ± 0.0008	73.6 ± 0	60 ± 0.48	58,000	0.65
M6	0.108 ± 0.002	0.0038 ± 0.0011	78 ± 1	281 ± 0.86	11,000	0.23
M4	0.082 ± 0.002	-0.0068 ± 0.001	65.7 ± 1	90.1 ± 1.1	6,100	0.13
2MN6	0.076 ± 0.002	0.0043 ± 0.0009	79.5 ± 1	267 ± 1.12	6,300	0.12
2MS6	0.067 ± 0.002	0.0021 ± 0.0009	77.2 ± 1	327 ± 1.14	4,500	0.09
K1	0.063 ± 0.001	-0.0003 ± 0.0008	76.1 ± 1	233 ± 1.29	7,800	0.08
MU2	0.049 ± 0.002	-0.0209 ± 0.0011	69.4 ± 2	180 ± 2.65	2,900	0.06
MS4	0.035 ± 0.002	0.0041 ± 0.001	69.6 ± 2	168 ± 2.61	1,300	0.02
MN4	0.033 ± 0.002	-0.0023 ± 0.001	65.6 ± 2	71.1 ± 2.58	1,300	0.02
O1	0.031 ± 0.001	-0.0003 ± 0.0009	75.2 ± 2	114 ± 2.78	1,800	0.02
EPS2	0.026 ± 0.001	-0.0095 ± 0.001	89.4 ± 3	148 ± 3.74	1,100	0.02

Constituent ID	Major axis length (m/s)	Minor axis length (m/s)	Angle (θ)	Phase (°)	Signal to Noise Ratio	Percent Energy (%)
ETA2	0.023 ± 0.001	0.0061 ± 0.0006	76.2 ± 2	126 ± 2.64	1,500	0.01
MM	0.019 ± 0.002	0.0069 ± 0.001	78.3 ± 4	153 ± 5.01	430	0.01
M8	0.017 ± 0.002	-0.0054 ± 0.0011	50.8 ± 4	336 ± 5.44	280	0.01
MSF	0.014 ± 0.002	0.0094 ± 0.001	55.5 ± 10	135 ± 12.4	320	0.01
MO3	0.015 ± 0.001	-0.0014 ± 0.0008	79.2 ± 4	1.54 ± 8.96	370	0.00
SN4	0.014 ± 0.002	-0.0025 ± 0.001	59.9 ± 5	317 ± 6.95	230	0.00
NO1	0.012 ± 0.002	0.0007 ± 0.0011	68.4 ± 6	45.9 ± 10.4	150	0.00
2SM6	0.011 ± 0.002	0.0007 ± 0.0011	75.2 ± 5	20.1 ± 8.26	120	0.00
MK3	0.01 ± 0.002	-0.0011 ± 0.0008	73.9 ± 5	191 ± 8.29	120	0.00
2MK5	0.009 ± 0.002	-0.0006 ± 0.001	81.2 ± 5	118 ± 9.26	85	0.00
ALP1	0.008 ± 0.001	0.0002 ± 0.0007	72.7 ± 6	53.8 ± 7.82	120	0.00
Q1	0.007 ± 0.001	-0.001 ± 0.0008	72.3 ± 8	68.1 ± 11	72	0.00
M3	0.007 ± 0.002	0.0007 ± 0.001	74.6 ± 9	222 ± 12.9	45	0.00
2Q1	0.006 ± 0.001	-0.0004 ± 0.0008	84.2 ± 9	253 ± 11.3	44	0.00
J1	0.005 ± 0.001	0.0002 ± 0.0008	86.2 ± 8	13.8 ± 13.7	45	0.00

Constituent ID	Major axis length (m/s)	Minor axis length (m/s)	Angle (θ)	Phase (°)	Signal to Noise Ratio	Percent Energy (%)
UPS1	0.005 ± 0.001	-0.0009 ± 0.0006	79.9 ± 7	359 ± 48.9	88	0.00
S4	0.004 ± 0.001	0.0007 ± 0.0009	76 ± 12	204 ± 21.9	23	0.00
3MK7	0.004 ± 0.002	0.0002 ± 0.0008	94 ± 13	68.9 ± 19.8	20	0.00
OO1	0.004 ± 0.001	0.0007 ± 0.0006	80 ± 13	256 ± 20.9	32	0.00
2SK5	0.002 ± 0.001	-0.0004 ± 0.0009	101 ± 25	302 ± 34	10	0.00
SK3	0.001 ± 0.001	-0.0005 ± 0.0012	143 ± 97	24 ± 107	2	0.00

4.4.2 Comparison of Modelled & Measured Data

This section compares the raw ADCP data with the reconstructed modelled data from harmonic analysis. Figure 4.9 and Figure 4.10 show plots comparing the measured ADCP 1 data to the reconstructed data, for the northerly and easterly components of the flow, respectively. The green line indicates the residual, the difference between the raw and reconstructed data. From a visual observation of the result, it is clear to see that there are significant errors in the reconstructed fit. The graph shows that the model is able to predict the frequency of the tidal flow and account for spring and neap tidal variations. However, the magnitude of the flow variation is not captured as accurately. The tidal flow during spring tide is shown to be overpredicted by the harmonic analysis and underpredicted during neap tidal periods.

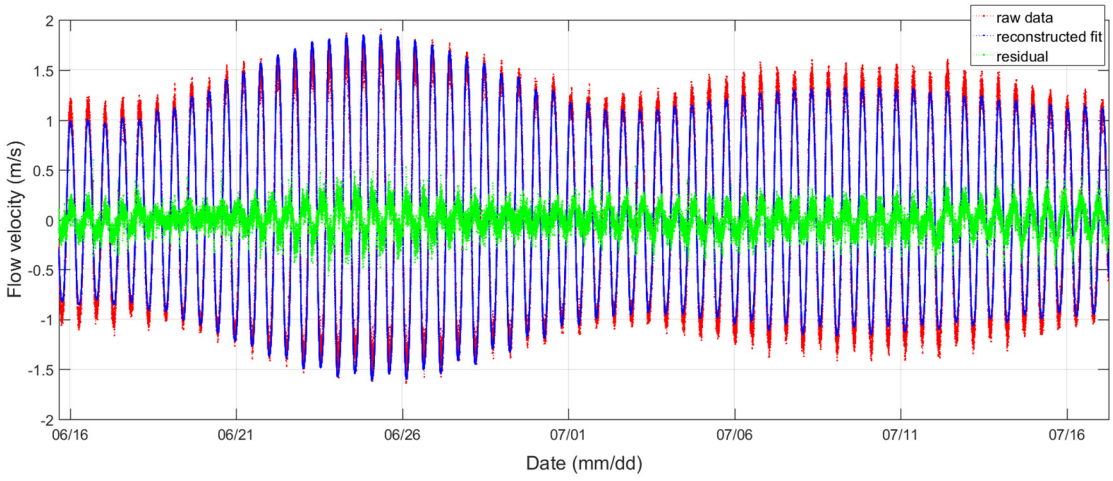

Figure 4.9 - UTide Plot of ADCP1 Flow in East-West Direction

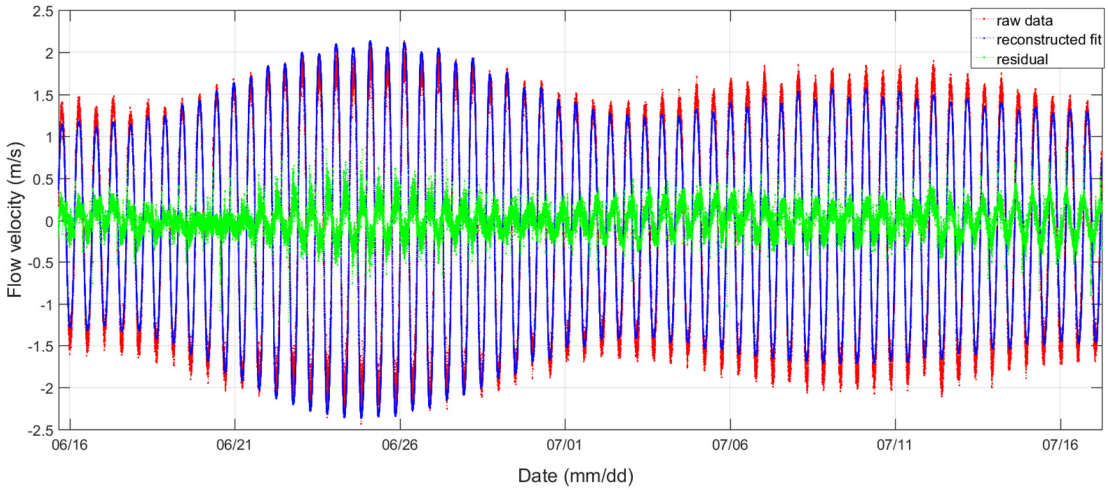

Figure 4.10 - UTide Plot of ADCP 1 Flow in North-South Direction

The plot of the northerly flow shows a similar result with the spring times being overpredicted and the neap times are under predicted. Having split the data into its vertical and horizontal components, it helps to characterise the flow at this point. When these plots are compared to the polar plot in Figure 4.4, it is evident that the flow is stronger in the north/south direction which corresponds to north-south orientation of the Sound of Islay channel site. ADCP 1 is deployed to the west of the channel, as shown in Figure 4.2, which results in an alteration to the direction of the flow from an influence of the bathymetry and channel. This becomes more obvious when compared with the results of ADCP 2.

Figure 4.11 and Figure 4.12 show the harmonic results for ADCP 2. The plots show that the residuals in the east-west direction are much larger. The tidal signal for this direction component is also much smaller, with the largest flow speed being approximately 0.7 m/s. The flow in the north-south direction is much stronger, reaching speeds of approximately 2.5 m/s. The harmonic prediction for this component is much more accurate and the resulting residuals are significantly reduced.

The location of the second ADCP is further into the centre of the channel. The polar plot, Figure 4.4, shows that the flow is very close to flowing along a north/south direction. By comparing the graphs from the harmonic analysis of the raw data, it is clear that the flow is much larger in the vertical direction, reaching velocities of over 2.5 m/s compared to less than 1 m/s in the horizontal direction. One further observation from the harmonic analysis plots is that the vertical flow of ADCP 2 has much smaller residuals. The flow is much stronger in this direction than the horizontal direction, similar to ADCP 1. Therefore, this highlights that results based on a single ADCP cannot be relied on, as the effectiveness of harmonic analysis is based on a number of site factors including bathymetry, turbulence and flow speed. In this case, the harmonic analysis was more accurate at predicting the higher flow speeds in the north-south direction than the lower flow speeds in the east-west direction.

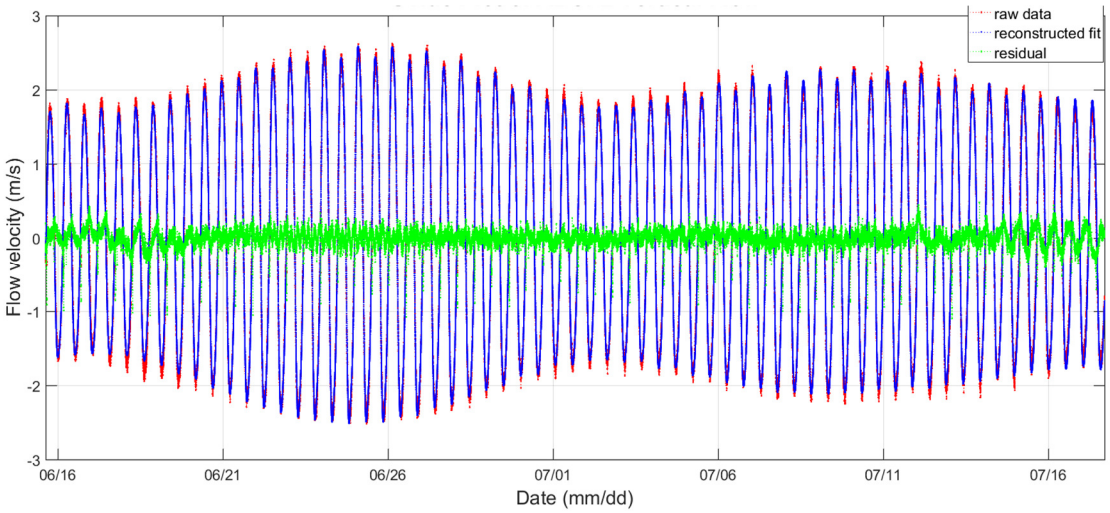

Figure 4.11 - UTide Plot of ADCP 2 Flow in North-South Direction

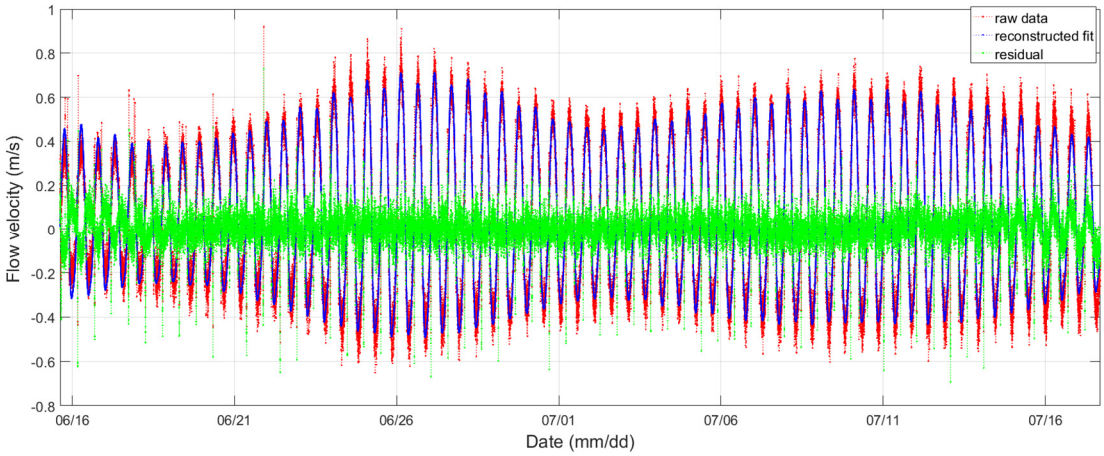

Figure 4.12 - UTide Plot of ADCP 2 Flow in East-West Direction

Table 4.3 and Table 4.4 show the breakdown of the tidal constituents for ADCP 1 and ADCP 2 respectively, detailing both the major axis length and the minor axis length. For ADCP 1 60% of the flow variation is caused by the principle semidiurnal lunar constituent M2. The two other main constituents are N2 and S2 which make up a further 25% of the flow variation. When compared with ADCP 2, the M2 constituent contributes approximately 52% of the flow variations with the N2 and S2 constituents providing a further 22% to the variation. The flow in the centre of the channel (at the ADCP 2 location) is influenced by a greater number of constituents with a total of 35 being resolved from the data, compared to 29 at the ADCP 1 location.

For each of the results, a weighted uncertainty value was calculated by taking the 95% confidence interval (*CI*) of each constituent which is equal to two standard deviations. This value was then divided by two to give one standard deviation for each constituent value. The standard deviation was then divided by the actual result to give an uncertainty percentage:

$$Ls_{maj} \pm CI_{95\%} \tag{4.19}$$

$$Uncertainty = \frac{\left(\frac{CI_{95\%}}{2}\right)}{Ls_{maj}} \tag{4.20}$$

After further investigation, it was clear that some of the smaller constituents contributing towards the tidal variations were introducing very large uncertainties compared to the actual value of the constituent. Therefore, a weighted method was adopted which is used in the wind industry when combining more than one input that is used to characterise a site. The method uses a weighted uncertainty relating to the quality of the correlation between the measured data and the reference/modelled data to combine and give an overall uncertainty value.

The uncertainty values, in this case, were weighted by the percentage that the constituent contributed to the overall flow variation. Each constituent uncertainty was then summed to give an overall uncertainty value for that prediction. This was done for ADCP 1 and an uncertainty value of 0.998% was calculated. For ADCP 2, a greater number of constituents were resolved which resulted in a lower uncertainty value calculated of 0.64%. This may suggest that uncertainty is linked directly to the number of tidal constituents that can be resolved by the harmonic analysis. An increase in the number of constituents that can be resolved should correspond with a lower uncertainty value. These results are as expected, where a lower uncertainty is calculated for a higher number of tidal constituents. These uncertainty values are lower than values previously stated by ORE Catapult (2015c), where it was suggested that harmonic analysis conducted with a 28-day data set gives an uncertainty value of 2%. The report also stated that this value can be reduced to 1% uncertainty, providing a minimum of 90-days of data are used. The harmonic analysis was first run using the 'auto' setting, which aims to resolve any harmonic constituents with a SNR larger than 2. The number of constituents resolved for ADCP 1 and ADCP 2 are 29 and 35, respectively.

Figure 4.13 and Figure 4.14 show the correlation of the measured and modelled flow speed for ADCP 1 and ADCP 2, respectively, using the 'Auto' harmonic constituent setting. The plots shows that the quality of correlation (R^2) between the measured and modelled data was 0.92 and 0.98 for ADCP 1 and ADCP 2, respectively. Figure 4.13 shows that at higher flow speeds at ADCP 1, the model over predicts the measured data values. The modelled data for ADCP 2 may show a higher correlation possibly due to the fact that the flow at the ADCP 2 position, is aligned in a north-south direction. This means that the northerly component of the flow is aligned well to the major axis for resolving the harmonic constituents. This can be observed when comparing the 95% confidence intervals in Table 4.3 and Table 4.4. The confidence intervals in the prediction of the major axis of each constituent are slightly lower for ADCP2 than ADCP 1.

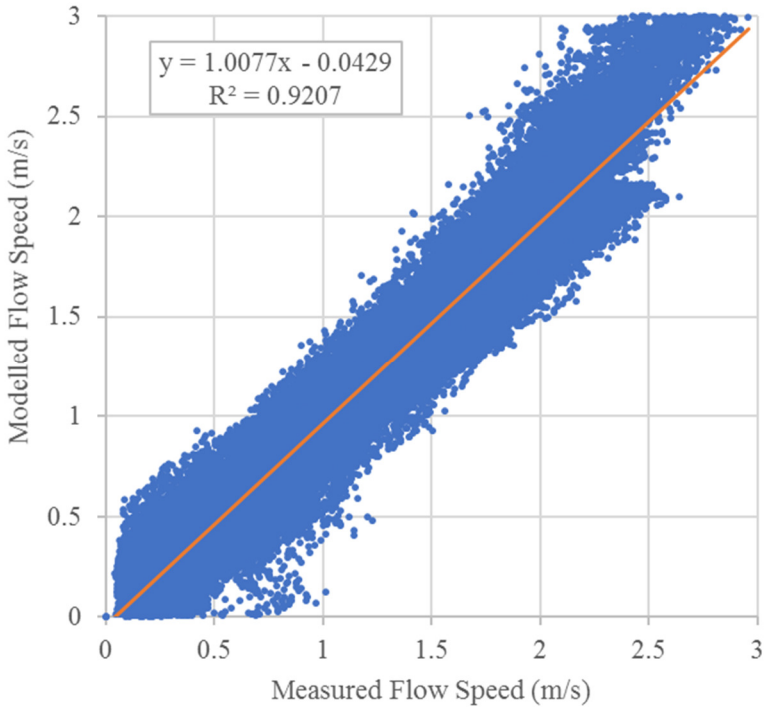

Figure 4.13 – Correlation of flow speed measured by ADCP 1 and flow speed as predicted by harmonic analysis methods using UTide – using 'Auto' setting

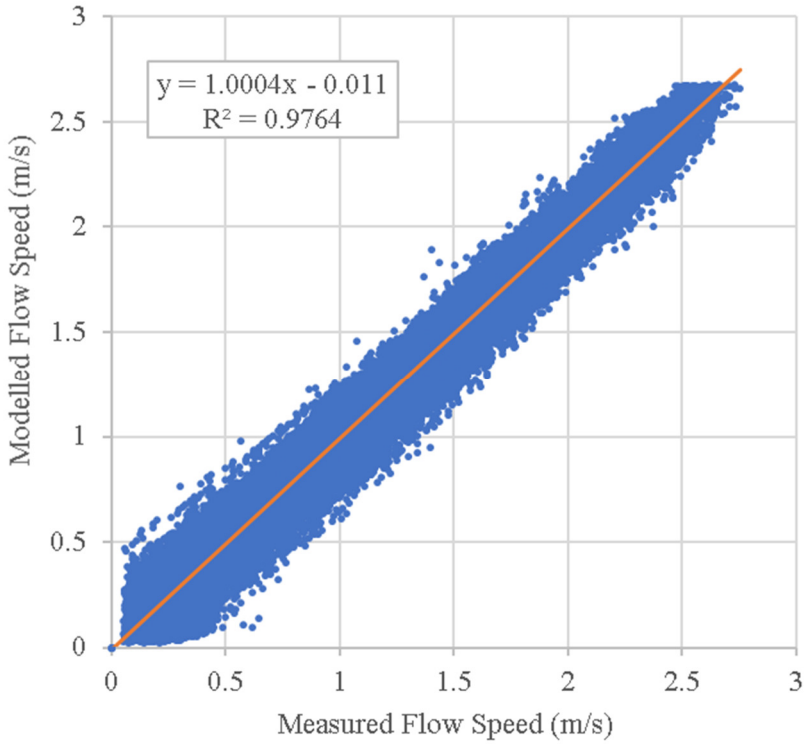

Figure 4.14 – Correlation of flow speed measured by ADCP 2 and flow speed as predicted by harmonic analysis methods using UTide – using 'Auto' setting

It was noted that the L2 constituent was resolved for ADCP 2 and was shown to be the fourth most important tidal variation of the tide. However, the harmonic analysis for ADCP 1 did not resolve the L2 constituent. Therefore, the harmonic analysis was re-run for ADCP 1 to include the L2 constituent. The results showed that including this constituent, reduced the overall residuals between the measured and modelled signals. In order to investigate whether the L2 constituent is important for predicting the flow at the ADCP 1 location, the harmonic analysis was re-run using pre-defined harmonic constituents. The harmonic constituents that were selected included the constituents resolved using the 'Auto' setting, as well as the L2 constituent. The resulting modelled fit was plotted against the measured data and is shown in Figure 4.15. Here it can be observed that the quality of correlation has increased from 0.92 to 0.96. Therefore, it can be concluded that the L2 constituent improves the modelled prediction of the flow.

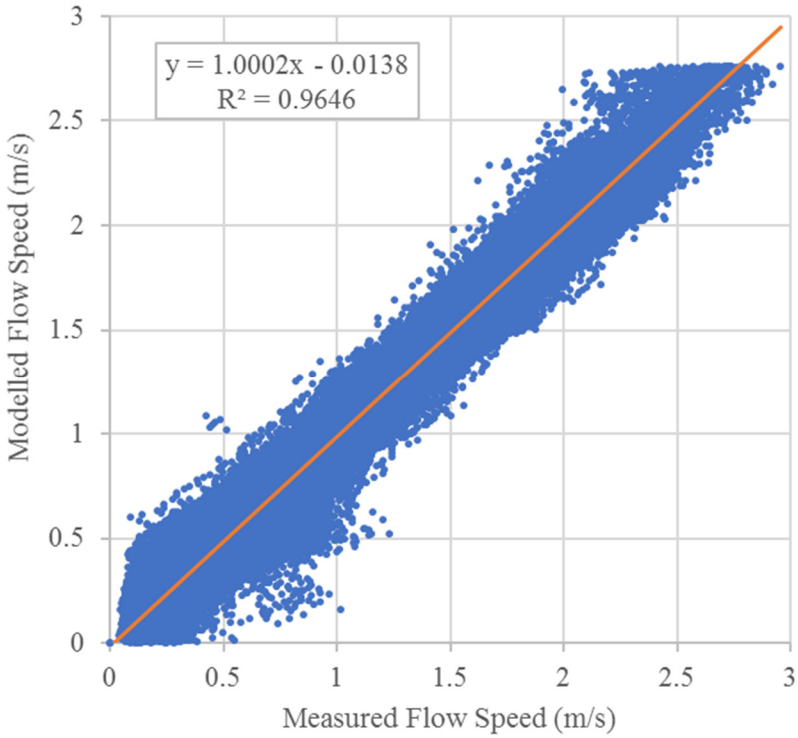

Figure 4.15 – Correlation of flow speed measured by ADCP 1 and flow speed as predicted by harmonic analysis methods using UTide – manual selection of constituents (including L2)

A key finding of this analysis shows the importance of evaluating the modelled fit and the resulting constituents resolved not relying on the 'Auto' function within the UTide code. It is recommended that the 'Auto' setting is used first and then additional constituents introduced to the prediction to

evaluate whether they improve the modelled prediction. This is also made easier through Fourier analysis of the residuals, which is discussed further in the following section.

4.4.3 Spectral Analysis of Residuals

This section outlines the methodology used to conduct spectral analysis of the residual time series. Taking the time series of the residuals between the measured and modelled data and conducting a Fast Fourier Transform (FFT) on the data, it is possible to evaluate the frequencies that make up the residual signal and determine if any astronomic variations are omitted from the harmonic analysis. The Matlab code used to evaluate this is detailed in Appendix A. This investigation aims to characterise the "noise" in the signal. Any large peaks suggest that there are periodic fluctuations in the residuals which may represent harmonic constituents that were not included in the harmonic analysis.

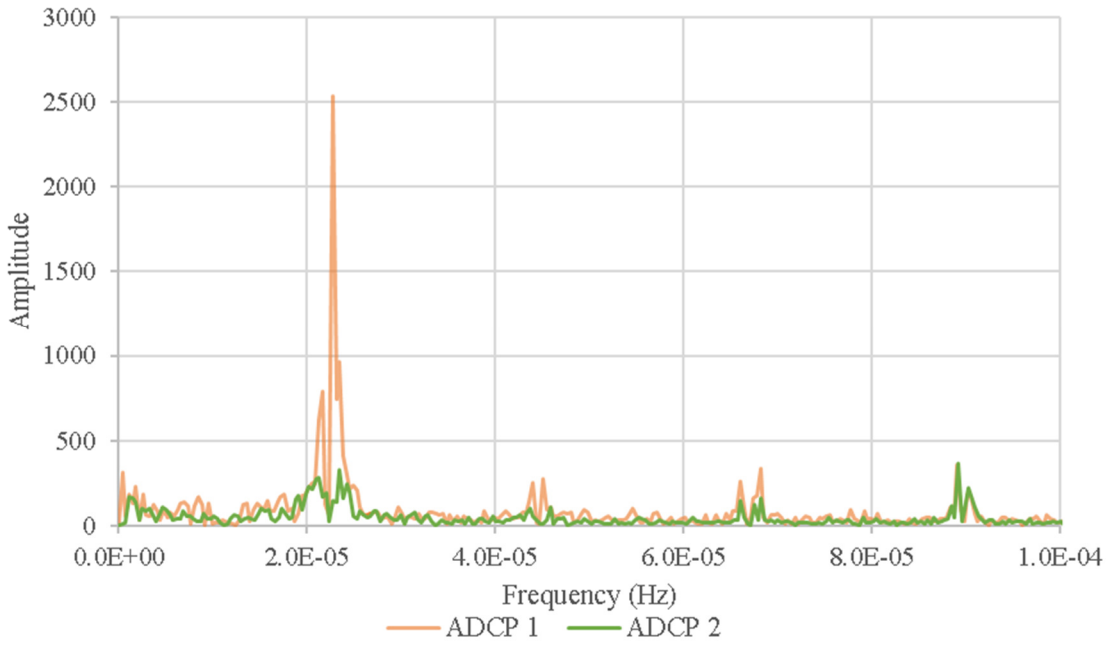

Figure 4.16 - Magnitude response of the Fast Fourier Transform on the residuals of ADCP 1 & 2 harmonic prediction

The FFT results for ADCP 1 and ADCP 2 are shown in Figure 4.16. It is clear from the peaks in the graph that there are a number of periodic fluctuations in the signal that have not been captured by the harmonic analysis conducted on the data. The large peak occurs at approximately 2.2715 x 10^{-5} Hz. This corresponds to approximately 0.5095 cycles per day or 29.44 deg/hour. The constituent with the closest corresponding frequency is the L2 constituent which has a frequency of 29.528 deg/hour. To reduce the magnitude of the residuals, the UTide code was run by manually defining the constituents to be used, as opposed to selecting the 'auto' setting. 30 harmonic

constituents were selected, which included the 29 originally resolved, with the addition of the L2 constituent.

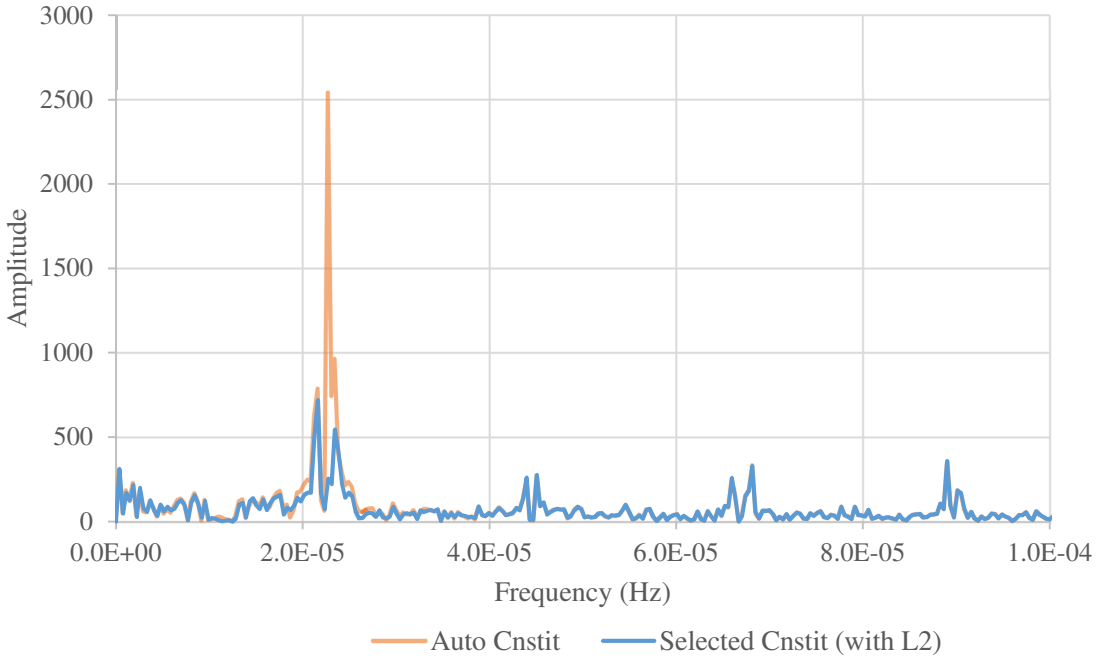

Figure 4.17 - ADCP 1: Comparison the response of the Fast Fourier Transform on the residuals of harmonic prediction using 'Auto' and 'Manual'

Figure 4.17 compares the results of the FFT analysis for the residuals using the 'Auto' function for selecting harmonic constituents and for the residuals when the constituents were manually selected. The amplitude of the residual signal, which was evident at approximately 2.2715 x 10^{-5} Hz, has been reduced from 2539.6 to 254.2. Through an assessment of the FFT of the residuals, it was found that the largest magnitude response was produced by the L2 constituent missing from the original harmonic analysis, which confirms the results outlined in Section 4.4.2. The residuals were reduced, therefore decreasing the overall error in the analysis.

4.4.4 Evaluation of Stochastic Nature of the Tide

4.4.4.1 Turbulence Intensity

Turbulence intensity is a ratio of the mesoscale fluctuation to the background velocity. These fluctuations are characterised as turbulent structures caused by flow conditions and the local bathymetry. Turbulence or eddy intensity, I, can be calculated as

$$I = \left\langle \frac{v'}{\bar{v}} \right\rangle - \left\langle \frac{n}{\bar{v}} \right\rangle \tag{4.21}$$

Where $\bar{v}$ is a 15 minute centred moving velocity average, v' is the velocity anomaly where $v' = v - \bar{v}$ represents the velocity with its temporal mean removed. The value of *n* is the intrinsic noise in the ADCP measurements, which depends on the device set up (frequency, bin size and pings per ensemble). The angle brackets imply a mean over the entire dataset The value of *n*, the intrinsic noise, can be calculated using the formula

$$n = \frac{1}{\sqrt{N} \times h} \times \alpha \tag{4.22}$$

Where *N* is the number of pings per ensemble (which is 82 for this ADCP set up), *h* is the bin size (1 m) and α is the single-ping standard deviation (12.8 mm/s, obtained from the Workhorse Sentinel ADCP datasheet (Teledyne RD Instruments, 2013)**.** Computing these values gives a value of n = 1.416 cm/s. Between ADCP 1 and 2, *n* is reported as being constant so direct comparison between them is acceptable. The value is only computed for bin 15 at a n approximate hub height of a tidal device.

Figure 4.18 and Figure 4.19 show the turbulence intensity at ADCP 1 and 2 respectively. It can be seen that the turbulence intensity is much higher at lower flow speeds t both locations. The overall turbulence intensity value was calculated to be 5.27% and 3.88% for ADCP 1 and 2 respectively. These values are within the same range as (Gooch *et al.*, 2009)**.** It is unclear as to why the turbulence intensities are different between the two ADCP's. One possibility is due to difference in the mean velocity for ebb and flood, although the root cause of differences are likely die to local topographic and bathymetric features. ADCP 1 is located to towards the edge of the channel, compared to ADCP which is located towards the centre. This is a potential reason why the turbulence is greater at the location of ADCP 1, where the flow interacts with the steeper bathymetry and flow effects from the side of the channel.

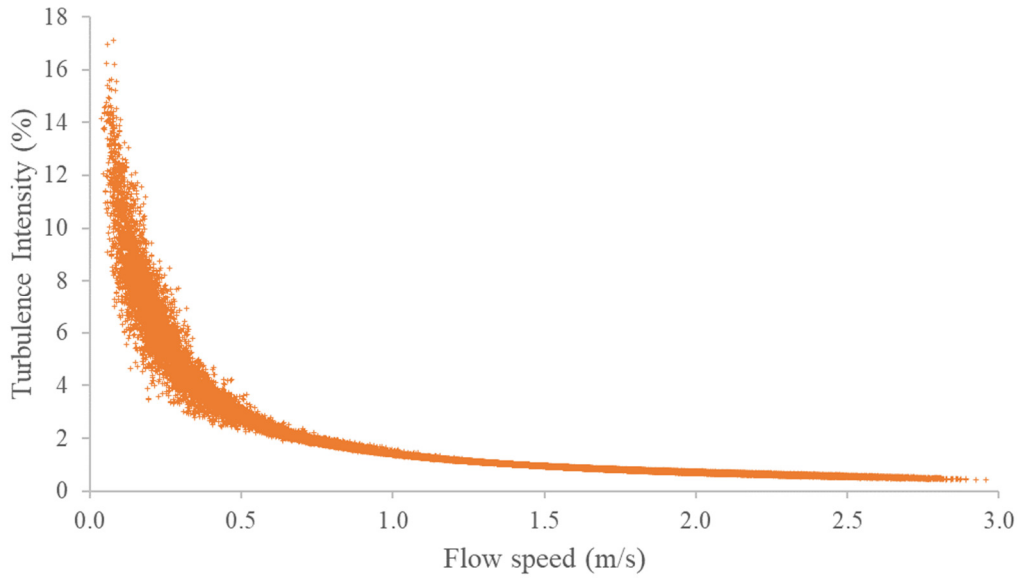

Figure 4.18 - Plot of turbulence intensity at ADCP 1 against flow speed

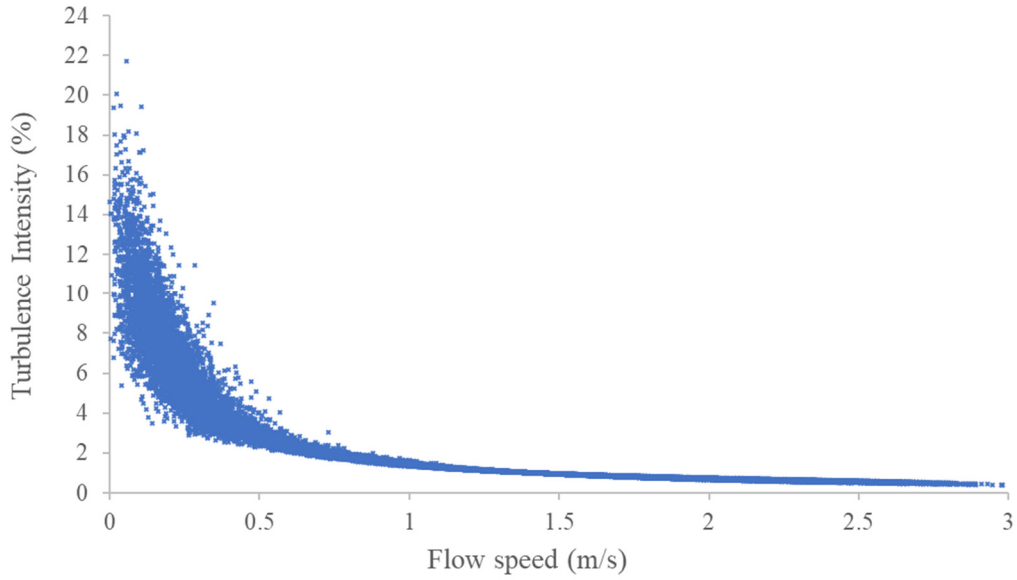

Figure 4.19 - Plot of turbulence intensity at ADCP 2 against flow speed

4.4.4.2 Non-Harmonic Tidal Influences

In order to better understand the stochastic nature of the tidal signal, it is necessary to look at the sources of the stochastic element of the data and potential causes of the residuals. As well as turbulence, discussed above, other sources from wind, wave and pressure provide useful insights.

Wave data at the site was collected from an Acoustic Wave and Current (AWAC) device that was deployed between 16th June 2009 and 17th July 2009. A Nortec AWAC device uses the same acoustic principle as an ADCP, but it has an additional beam which is orientated vertically to

measure wave characteristics as well as current. The wave data collected by the AWAC had a temporal resolution of 2 hours. Figure 4.20 shows the significant wave height (H_{m0}) and the maximum wave height (H_{max}) over the measurement campaign. The significant wave height is defined as the mean wave height (trough to crest) of the highest third of the waves, sometimes denoted as $H_{1/3}$.

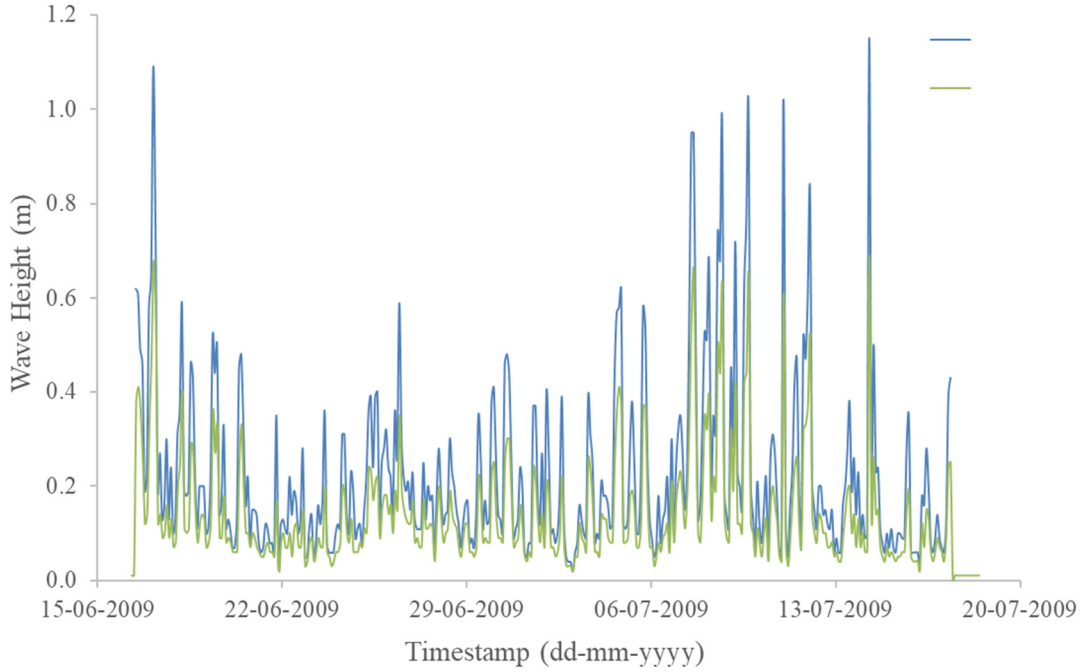

Figure 4.20 - Plot of wave data (H_{max} and H_{m0}) collected from a Nortec AWAC device in the Sound of Islay over the period of June – July 2009

Similarly, meteorological data was acquired from the Met Office from Port Ellen, approximately 20 km from the site and provided wind speed and pressure data on an hourly basis. Figure 4.21 shows the data collected, measured from 15th June 2009 to 17th July 2009.

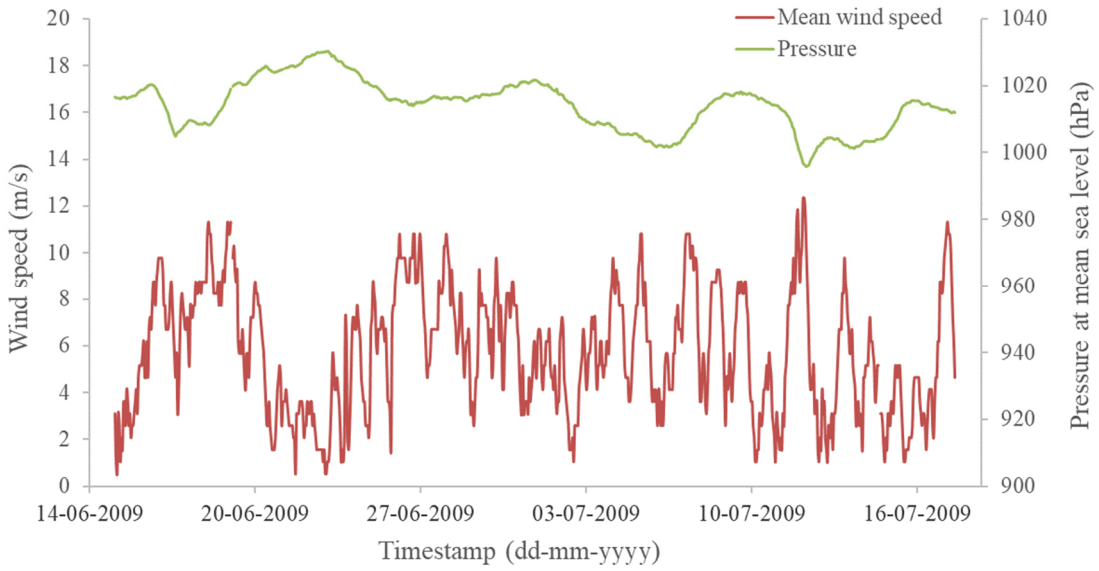

Figure 4.21 - Plot of wind speed and pressure data from Met Office Port Ellen station on the Sound of Islay

From an assessment of the wind speed and pressure data, there doesn't seem to be any extreme storm events during the period. The highest wind speed is 12.4 m/s which occurs on 12th July 2009. To understand the residuals of the harmonic analysis, an evaluation of the correlation between the residuals and the wind and wave conditions was conducted. The temporal resolution of the meteorological data (wind speed and pressure) taken from Port Ellen was on an hourly basis and the wave height data had a resolution of two hours. Therefore, in order to evaluate the correlations, the residual data was averaged to hourly and two hourly temporal resolutions.

Figure 4.22 shows scatter plots of the magnitude of the ADCP residuals, against the wave height, wind speed and pressure data. A trendline was created and the relationship between the data was evaluated. It can be seen that none of the meteorological data gathered showed any correlation with the magnitude of the residuals. Due to the averaging of the residuals, some of the higher magnitude values were lost through averaging to longer periods.

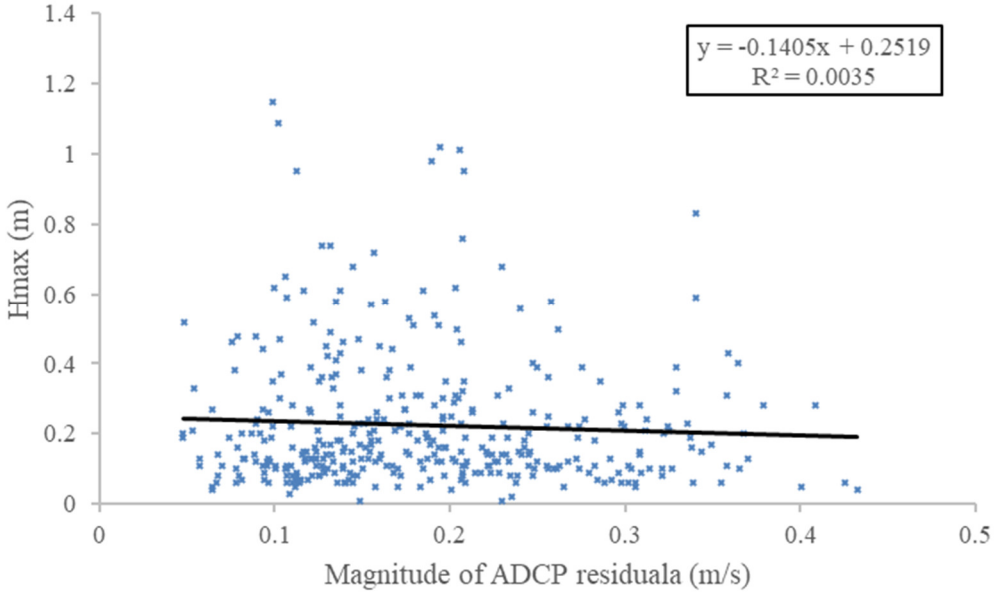
y = -0.1405x + 0.2519
R² = 0.0035
Hmax (m)
Magnitude of ADCP residuala (m/s)
0
0.2
0.4
0.6
0.8
1
1.2
1.4
0.1
0.3
0.5

[a]

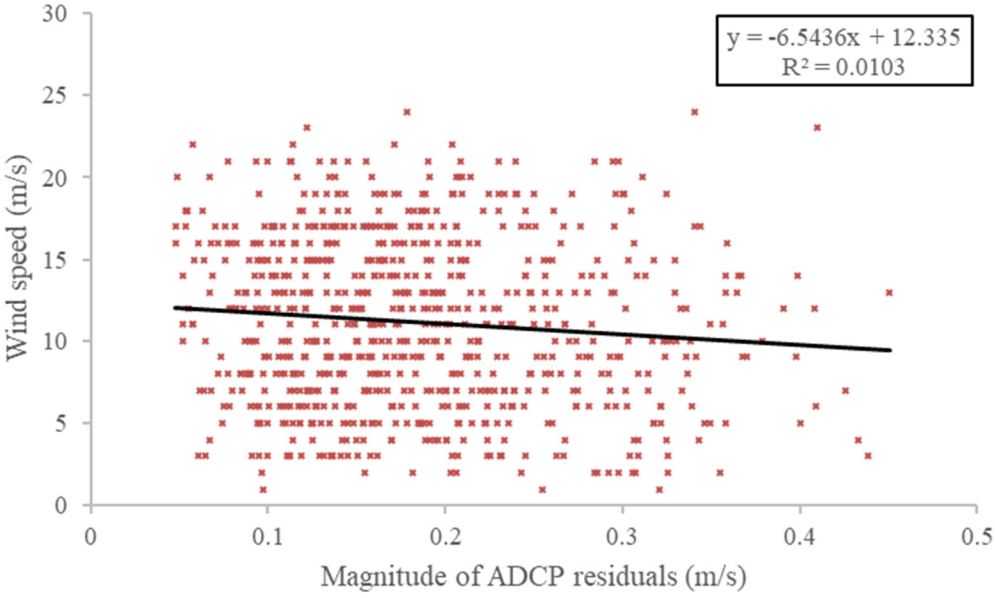
y = -6.5436x + 12.335
R² = 0.0103
Wind speed (m/s)
Magnitude of ADCP residuals (m/s)
0
5
10
15
20
25
30
0.1
0.2
0.3
0.4
0.5

[b]

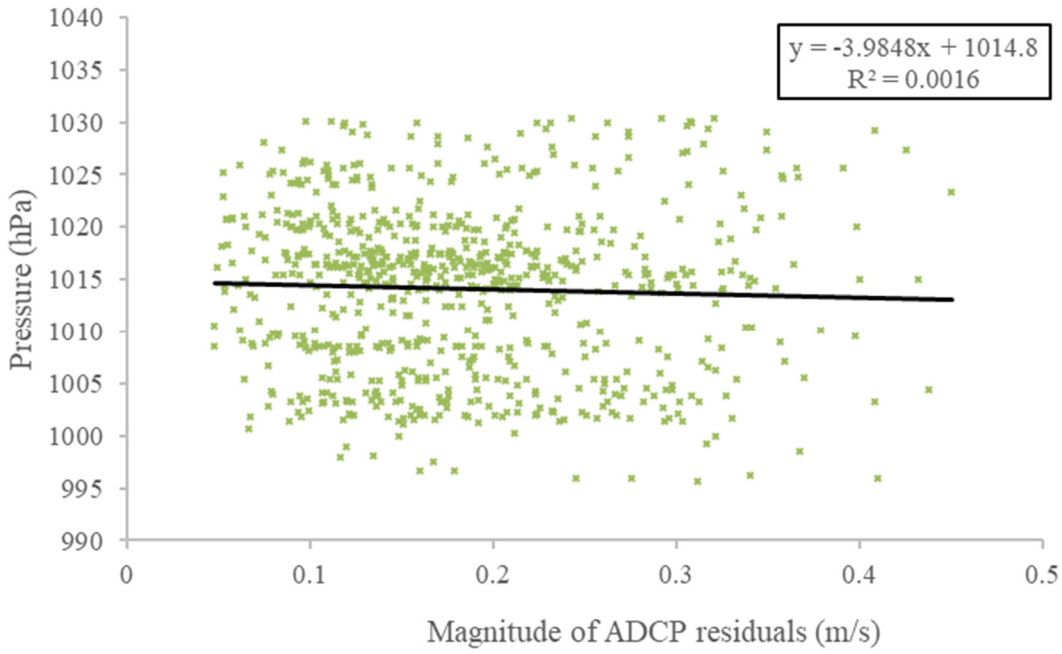

[c]

Figure 4.22 – Plot of temporally averaged harmonic analysis residuals compared with [a] wave height data, [b] mean wind speed and [c] mean sea level pressure for the same temporal period & resolution. The graphs aim to identify if any correlations are present but may not show individual large residual values visible in Figure 4.23, due to the temporal averaging of the data.

There were no direct correlations between the residuals and the meteorological conditions as none produced an R^2 value above 0.01. This investigation has shown that there is no statistical relationship between the ADCP residual data and the meteorological data. Furthermore, it is not possible to suggest that the residuals are higher when wind speed or wave height are larger. However, an assessment of the residuals was carried out by overlaying the magnitude of the residuals onto the met-ocean data. Figure 4.23 shows the results of the residuals and the corresponding met-ocean data, for the 12th July 2009 period, when the wind speed is high and the pressure is lowest.

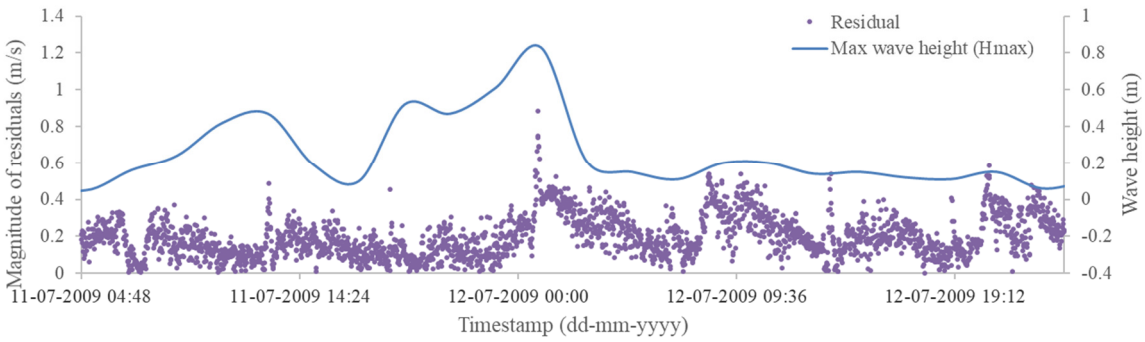

[a]

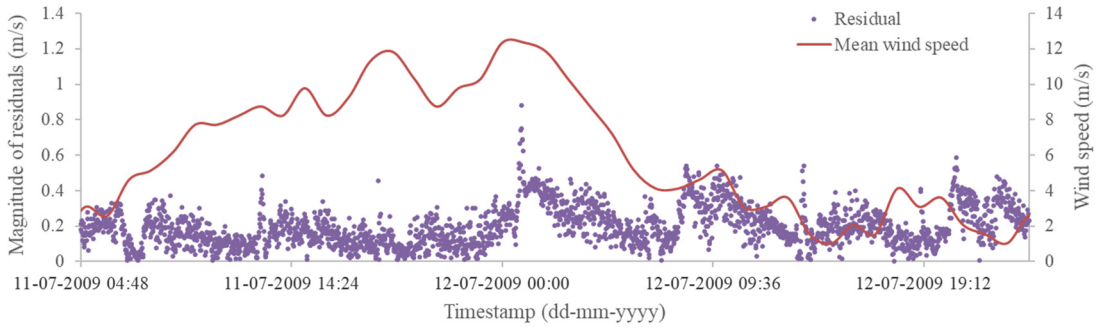

[b]

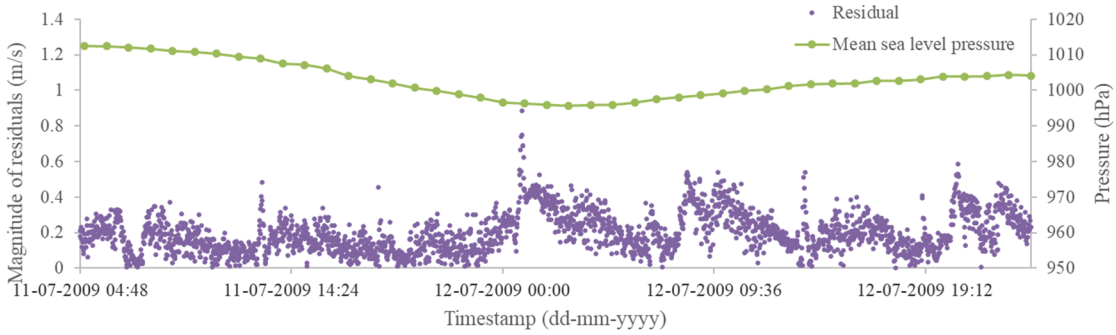

[c]

Figure 4.23 - Plot of harmonic analysis residuals against [a] wave height data, [b] mean wind speed and [c] mean sea level pressure during period of strong wind and wave conditions.

It can be seen that the high wind speed and the high wave height correspond with the low pressure in the region, which occurs at approximately 1:00 am on the 12th July. From the plots, it can also be seen that this corresponds to a period when there are large residuals in the data. The overall correlation between the datasets was poor, as discussed previously. However, it can be suggested that in this instance, the higher residuals may be influenced by the higher wind and wave conditions. A quantitative assessment of the correlations showed no statistical relationship, however the timeseries plots above, suggests that there may be times when the magnitude of the ADCP residuals are related to meteorological effects. This implies that a qualitative method based on observations between the residuals and meteorological data can provide insight into the magnitude of the stochastics uncertainties. In order to evaluate this in more detail, higher resolution data for wind speed, and wave height would be required. The hourly resolution of the wave and wind data means that correlations made would potentially miss periods of higher residuals due to averaging the data to an hourly basis.

An evaluation of the tidal flow characteristics was carried out by splitting the flow into the flood and ebb components. The mean flow speed and eddy intensity was calculated for each part of the flow.

Table 4.5 - Tidal characteristics at ADCP 1 and 2, with flow separated into flood and ebb components

Flow Velocity (m/s)	ADCP 1	ADCP 2
Datapoint count	45495	46192
Mean flow speed (m/s)	1.39	1.41
Eddy Intensity (%)	5.27	3.88
Flood		
Datapoint count	23717	23776
Mean flow speed (m/s)	1.47	1.64
Eddy Intensity (%)	3.97	2.24
Ebb		
Datapoint count	21778	22416
Mean flow speed (m/s)	1.64	1.51
Eddy Intensity (%)	3.69	2.42

The results show that the higher the average flow speed, the lower the eddy intensity for both ADCPs. The eddy intensity is higher at ADCP 1 for both the flood and ebb tidal components.

4.4.5 Quantifying the difference between harmonic-based tidal predictions and in-situ measurements

Another method to assess the uncertainties involves calculating the statistical error between the predicted values, f_i, and the measured values, y_i. There are a few standard error measures used in statistics that can be applied to help inform the uncertainty of the harmonic analysis. These include the mean absolute error, mean absolute percentage error, the root mean squared error and the coefficient of determination. Detail of how each value can be calculated is outlined in Chapter 2.

After conducting the harmonic analysis, the reconstructed data was used to compare with the raw data. The residuals were evaluated, for the north and east components of the flow, and various statistical error values were calculated with the results shown in Table 4.6.

Table 4.6 - Error estimates of the residuals between the raw ADCP data and the reconstructed UTide data

Error value	ADCP 1		ADCP 2	
	Easterly flow (u)	Northerly flow (v)	Easterly flow (u)	Northerly flow (v)
R^2	0.982	0.981	0.951	0.994
RMSE	0.125	0.173	0.076	0.114
MAE (m/s)	0.102	0.140	0.054	0.083
MAPE (%)	50.9	38.5	52.7	59.4

It can be seen that harmonic analysis is not a perfect solution. The results indicate that there are some errors when comparing the raw measured data and the harmonic analysis fit. The R^2 value indicates how well the harmonic fit represents the measured data. The results show that the correlation between the measured data and the modelled data are above 0.95 for each component of tide measured by both ADCPs. This indicates a strong correlation between the measured and modelled values. Furthermore, the correlation for the northerly component of ADCP 2 is as high as 0.99. This shows that harmonic analysis, using the UTide tool, is able produce a tidal variation fit that represents the measured variation with a high level of correlation.

The Root Mean Squared Error (RMSE) is used to measure the differences between measured and modelled values, known as residuals. A value of zero would indicate a perfect fit to the data, however this is never achievable in practice. The closer the value is to zero, the lower the error and better the model is. An RMSE value of 0.21 was achieved in the literature (Stock-Williams, Parkinson and Gunn, 2013) for a similar study of the uncertainties in harmonic analysis using T_Tide and UTide. The RMSE values shown in Table 4.6 need to be combined together as they represent the error on each of the horizontal and vertical components of the tide. When combined in quadrature, ADCP 1 produces an RMSE value of 0.21, whereas ADCP 2 produces a value of 0.14.

Some researchers recommend the use of the Mean Absolute Error (MAE) instead of the RMSE (Pontius Jr, Thontteh and Chen, 2008). This is because it is understood to be easier to interpret as each error influences the MAE in direct proportion to the absolute value of the error, which is not the case for the RMSE. The values shown in Table 4.6 are shown in the same units as the tidal flow; therefore, it is easier to interpret. The average flow speed measured at each location was 1.35 m/s and 1.34 m/s at ADCP 1 and 2, respectively, as discussed in Section 4.2.4.

The tidal flow at the site varies over short periods due to meteorological and turbulent effects. These are not fully evaluated by the harmonic analysis, as the modelled fit smooths out the tidal flow. Many of the smaller fluctuations caused by turbulence and other interactions are not able to be resolved by harmonic analysis. When evaluating each individual residual, the results seem to show large errors. Many of the flow fluctuations are not captured, as harmonic analysis will only resolve the astronomical variations.

To calculate a predicted energy yield output from harmonic analysis, the flow speed predictions can be combined with a power curve for a tidal turbine. The simplest method to assess this is to evaluate the tidal flow on a frequency distribution basis. This involves sorting each measured flow speed into a flow speed bin, which shows the number of times a particular flow speed occurs. A turbine power curve will describe how much power will be produced for each flow speed. Therefore, a simple way to predict the power production is to combine the frequency distribution of the flow with the power value at each flow speed and then sum the values.

4.4.5.1 SeaGen Case Study

Another method to assess the variation between the measured and modelled tidal values is to evaluate the estimated power output using a frequency-based approach. Figure 4.24 shows a theoretical power curve, adapted from the SeaGen tidal turbine, which had a rated capacity of 1.3 MW. The measured flow was binned into individual flow speed bins and combined with the theoretical power curve. The resulting value gives a gross energy yield prediction, which doesn't account for losses, assuming that the turbine was placed at the location of ADCP 1. The value was calculated to be 203.2 MWh over the measurement period.

The same was completed for data predicted using harmonic analysis. The predicted flow data from the temporal model was binned and combined with the same power curve. The power output using the modelled data was 198.6 MWh over the same period, which gives a 2% underprediction using the data estimated from harmonic analysis. This shows that if the data from harmonic analysis was used solely to estimate the power production of a tidal turbine at this site, the prediction would be 2% lower over a 32 day period. This may vary from site to site and harmonic analysis may produce an over prediction at other locations. This highlights that performing an energy yield prediction using only data from harmonic analysis will likely result in an over or under prediction. Therefore, this data should complement the measured data to evaluate long term trends.

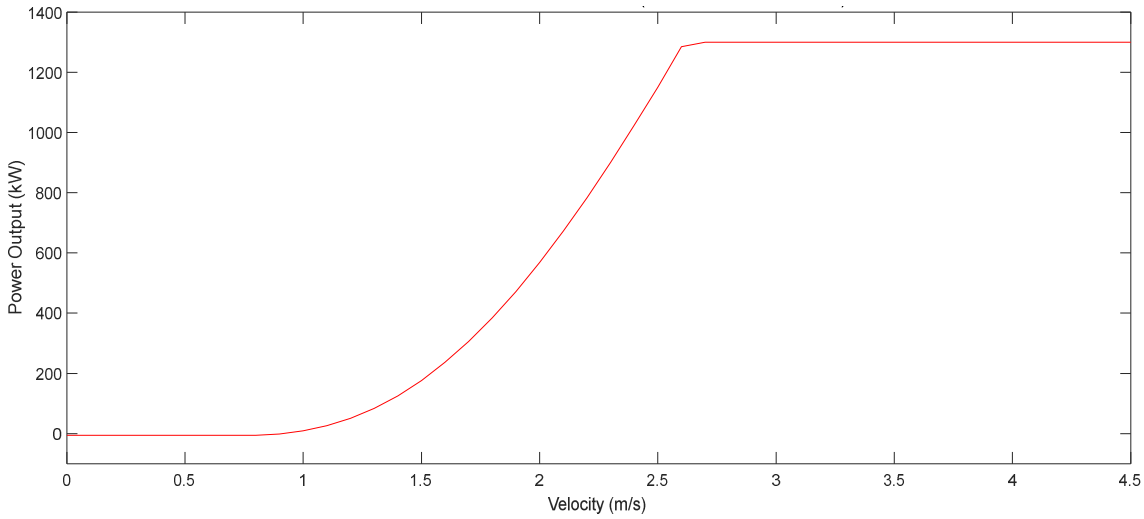

Figure 4.24 - Theoretical tidal turbine power curve, based on SeaGen turbine (Iyer, 2010)

4.4.5.2 Temporal Resolution Uncertainty

A further investigation aimed to compare the temporal resolution of the input data and the resulting effects on the output. From the dataset, three different resolutions of data were analysed. The raw data was originally provided at one-minute resolution. This data was then averaged over 10 minutes and 1 hour. The harmonic analysis code was run using each of the three datasets as inputs. The results of the 7 most prominent tidal constituents are shown in Table 4.7. Each constituent is shown along with the associated 95% confidence interval on the prediction. The root-mean-square error is calculated for the whole result using Equation 2.12 in Section 2.1.2.4.

The uncertainty value was calculated by converting the 95% confidence interval into a standard deviation. The 95% confidence interval of a prediction, CI_{Lmaj}, is linked to the standard deviation, σ, as

$$\sigma = \frac{CI_{Ls_{maj}}}{2} \tag{4.23}$$

Therefore, the standard deviation can be calculated to be half of the 95% confidence interval value. The standard error, δ, which is a measure of uncertainty, can be calculated as

$$\delta = \frac{\sigma}{Ls_{maj}} \tag{4.24}$$

The total uncertainty for the prediction could then be calculated by summing the uncertainties in quadrature:

$$\sigma_{tot} = \sqrt{\sum_{i=1}^{n} {\sigma_i}^2 + {\sigma_{i+1}}^2 + \cdots {\sigma_n}^2} \tag{4.25}$$

It was noted that some of the smaller constituents had very large uncertainty values. In some cases, the standard uncertainty was as high as 45% of the magnitude of the constituent. These constituents had a very small influence on the overall variation, but were contributing to very high uncertainty values when they were combined. A modified approach was used which introduced a weighting to each constituent based on the magnitude of the response.

The total uncertainty value was then calculated by using

$$\sigma_{tot} = \sqrt{\sum_{i=1}^{n} (\beta_i \sigma_i)^2 + (\beta_{i+1} \sigma_{i+1})^2 + \cdots (\beta_n \sigma_n)^2} \tag{4.26}$$

where β is the weighing for each constituent, calculated as $\beta_i = Ls_i / \sum Ls_i$.

The results are presented in Table 4.7. The first observation is that using 10-minute averaged data produces very similar major axis results to the one minute resolution data. Most values are within 0.002 m/s of the original value. The big difference comes when we look at the 95% confidence interval. For each constituent, the confidence intervals increased by at least double and in some cases, triple the original value. It is, therefore, possible to conclude here that using 10-minute averaged data is as accurate at estimating the main tidal constituents, but gives an increased uncertainty associated with the predictions.

The 1 hour averaged data is quite different; in most cases the predictions are lower than the original values. The confidence intervals are also much larger than 10 minute averaged as well as the predictions using the full data set. The uncertainty in the predictions is much greater when the data is averaged every hour; the results show almost double the uncertainty compared to when 10-minute resolution data is used. From the results it is clear that using hourly data is not a good representation of the data as smaller constituent variations are missed out, creating inaccuracies in the prediction. However, using 10-minute data is an accurate way to calculate long term variations without having to measure the flow every minute.

Table 4.7 - A comparison of the tidal harmonic constituents for varying input resolutions

Constituent	1 minute raw data		10 min averaged data		1 hour averaged data	
	Major axis (m/s)	Phase (deg)	Major axis (m/s)	Phase (deg)	Major axis (m/s)	Phase (deg)
M2	2.160 ± 0.003	21 ± 0.1	2.160 ± 0.009	19 ± 0.2	2.130 ± 0.019	7.25 ± 0.5
S2	0.432 ± 0.002	74 ± 0.4	0.432 ± 0.007	72 ± 1.1	0.428 ± 0.018	59.8 ± 2.1
N2	0.474 ± 0.003	360 ± 0.4	0.474 ± 0.010	358 ± 0.9	0.468 ± 0.019	346 ± 2.4
K1	0.060 ± 0.002	236 ± 2.2	0.060 ± 0.007	235 ± 7.0	0.059 ± 0.020	229 ± 18.1
M4	0.031 ± 0.003	219 ± 4.7	0.033 ± 0.007	218 ± 18.8	0.091 ± 0.009	22.9 ± 6.6
O1	0.028 ± 0.002	100 ± 4.7	0.028 ± 0.007	99.4 ± 14.7	0.027 ± 0.015	94.8 ± 37.5
M6	0.100 ± 0.003	265 ± 1.6	0.101 ± 0.008	258 ± 5.3	0.094 ± 0.009	225 ± 12.0
RMS error or re-prediction (m/s)	0.21		0.22		0.25	
Uncertainty value (%)	1.0%		2.8%		5.5%	

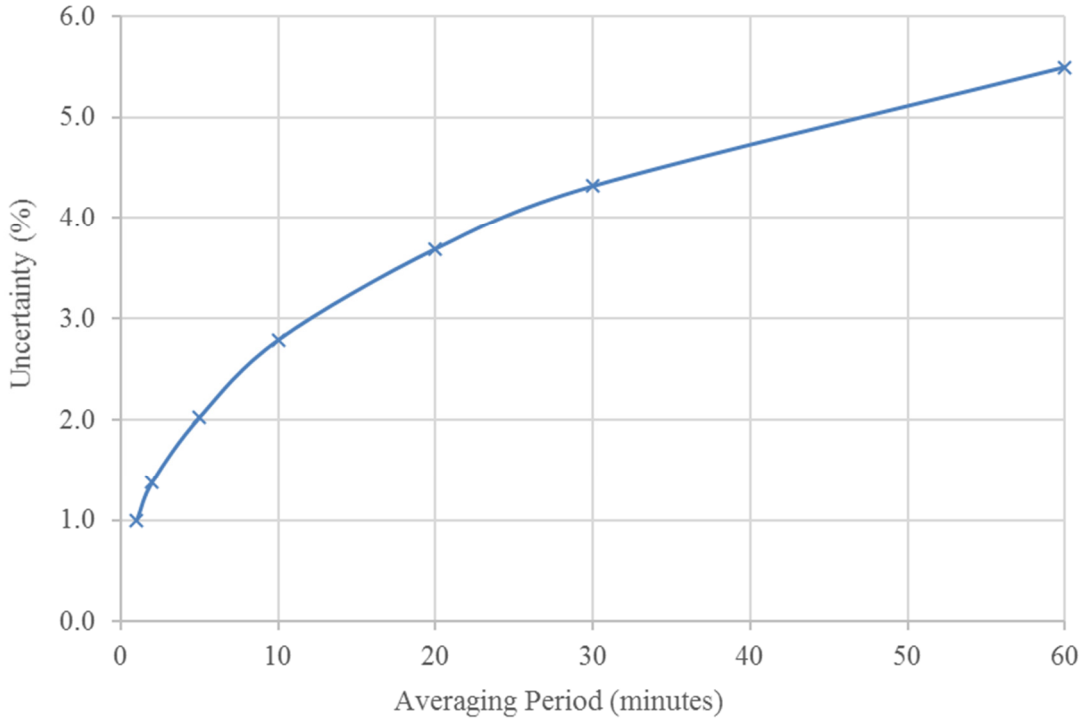

Figure 4.25 – Harmonic Analysis uncertainty with varying averaging periods of input data

The uncertainty was also calculated for additional averaged data periods and the results were plotted as shown in Figure 4.25. The results show that as the data is averaged over longer periods, the calculated uncertainty increases. Using data with a minute resolution gives the lowest uncertainty of approximately 1%. If the data is averaged over a 10 minute period, then the harmonic analysis results will give an increased uncertainty of 2.8%. Therefore, to produce results with the lowest possible uncertainty value, harmonic analysis should be conducted with high resolution data. Given the relatively short period measurement campaign, typically conducted at a prospective tidal site, it is feasible to conduct the analysis without further averaging.

The IEC technical specification (IEC, 2015) recommends that the averaging period should be between 2 and 10 minutes to filter the majority of turbulence from observations and that the sampling frequency should be maximised with the constraint of battery life and memory storage. However, the results included here show that uncertainty can be reduced slightly by using an averaging period of 1 minute. If the battery life and memory storage can facilitate this then it is recommended that the lowest possible averaging period is used.

4.4.6 Annual Variability

One of the most significant tidal variations occurring over periods longer than a year is the nodal cycle. The nodal cycle, or factor, is related to the obliquity of the Moon's orbit. Further information can be found in the literature (Oost *et al.*, 1993; Jeuken *et al.*, 2003; Haigh, Eliot and Pattiaratchi, 2011) and is discussed earlier in the Chapter in Section 2.2.

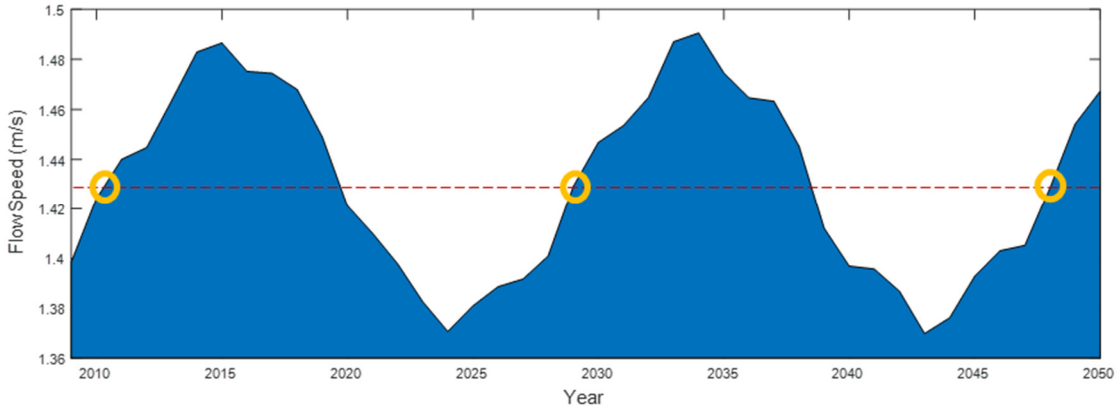

Figure 4.26 – Plot of annual variation of tidal flow at ADCP 1 location, showing the average annual flow speed over 40 years, with the average flow speed plotted as a red dotted line and the regression of the lunar node (18.6 nodal cycle) highlighted by the yellow circles.

The effect of this variations becomes clear when the annual mean flow speed is compared over the life time of a project. The measured ADCP data was used to evaluate tidal variations over a 40-year period. The average flow speed for each year was calculated and is shown in Figure 4.26. The red line represents the mean flow speed, over the 40 year period and the orange circles show the beginning of each nodal cycle, which occurs in the years 2010, 2029 and 2048.

This variation, which occurs approximately every 18.6 years, has a particular impact when considering tidal projects built with a design life of approximately 20-25 years. For example, a tidal project commissioned in 2019 will have a different energy yield prediction to a tidal project commissioned in 2024.

Analysis of the variation in the average flow speed across the project's life can vary by ±4.2% maximum percentage change between a mean year, such as 2010, 2029, 2048, to either extreme is approximately. Similar variations have also been reported by (Iyer, 2011; Passeri *et al.*, 2015). Since power is proportional to velocity cubed, even small variations can have significant changes, as high as 13% in the energy output.

It is important that the variations resulting from the 18.6 year nodal cycle are included in any long term assessment of tidal flow. This study verifies that harmonic analysis using UTide is able to capture this effect.

4.5 Jack-Knife Uncertainty Analysis

The jack-knife method determines the variability of the prediction by dropping out segments of the concurrent data set. More detail on the jack-knife procedure is outlined in Chapter 2. The data was split into various subsets and an iterative process uses proportions of the full data set to calculate the long-term wind speed using the MCP procedure. This method has been applied to the data to assess its suitability and the effect on uncertainty quantification.

Once this is completed, the output is a number of predicted mean wind speeds based on the subsets of short-term data used to calculate it. The variance was then determined by calculating the difference between the known mean wind speed and the estimated speeds from the jack-knife subset. The total jack-knife variance (σ_{jk}) is calculated using Equation 2.13 in Section 2.1.3.1.

Table 4.8 shows the results of the jack-knife analysis with the data split into 4 subsets. This means that for each assessment, there is only 24 days of data out of 32 being used. Using the methodology described above, which is the same for wind energy, an uncertainty value of 6.91% in flow speed was calculated. This value is very large, especially when you consider the energy yield uncertainty is usually around double the value of the flow speed uncertainty.

Table 4.8 - Jack-knife analysis (4 subsets)

JK Set	Full	1	2	3	4	Variance	Uncertainty (%)
Mean flow speed (m/s)	1.4293	1.3831	1.5235	1.3847	1.4296	0.00975	6.91

The data was then split into 8 subsets and the analysis was repeated. The results are shown in Table 4.9 showing an overall reduction in the jack-knife uncertainty to 5%. In this case, each assessment is using 28 days of data out of the complete 32-day dataset.

Table 4.9 - Jack-knife analysis (8 subsets)

JK Set	Full	1	2	3	4	5	6	7	8	Variance	Uncertainty (%)
Mean flow speed (m/s)	1.4293	1.4174	1.4501	1.4873	1.4401	1.4224	1.4000	1.3997	1.4256	0.00512	5.01

Table 4.10 – Islay Data Jack-Knife Analysis Results

Number of subsets	Average flow speed for each subset (m/s)								Uncertainty (%)
	1	2	3	4	5	6	7	8	
Full	1.3988								
2	1.3054	1.4568							5.56
3	1.3498	1.4525	1.4149						4.35
4	1.3540	1.4898	1.3579	1.3999					6.77
5	1.3582	1.5009	1.4066	1.3445	1.3904				7.87
6	1.3625	1.4744	1.4299	1.3846	1.3531	1.3826			6.71
7	1.3656	1.4438	1.4494	1.4004	1.3727	1.3597	1.3800		6.01
8	1.3869	1.4194	1.4550	1.4090	1.3929	1.3708	1.3694	1.3953	4.97

4.5.1 Falmouth Bay Measurement Campaign

Due to the relatively short measurement period of the Islay ADCP data, an investigation into using a longer dataset was conducted. Data from an ADCP deployed in Falmouth Bay was acquired covering a period of approximately 90 days. The site is not being considered for a tidal energy device deployment, but the data was collected to measure the current speed and direction at the South West Mooring Test Facility site, operated by the University of Exeter. A summary of the ADCP instrumentation and configuration during the measurement campaign is provided in Table 4.11.

Table 4.11 – Summary of Falmouth Bay ADCPs Instrumentation Configuration

Data Category	Falmouth Bay ADCP
Instrument Type	RDI Sentinel ADCP
Instrument Mounting	Frame
Start Time	10/12/2010 12:34
End Time	09/03/2011 12:18
Sampling Interval (s)	0.5
Averaging Interval (s)	600
Parameters Measured	Current speed, current direction
Location	Latitude 50° 04.75' N
	Longitude 5° 2.85' W
Sensor Height ABL (m)	0.7
1st Bin Range (m)	1.61
Bin size (m)	0.5
Number of bins	76
Depth to Chart Datum (m)	27

The raw depth averaged flow data measured by the ADCP is shown in Figure 4.28, which shows that the flow at the peak flow speed at the site approximately 0.5 m/s. The flow is not as bi-directional as the Sound of Islay site, as it is located approximately 2 km east of the mouth of the Helford River in South Cornwall.

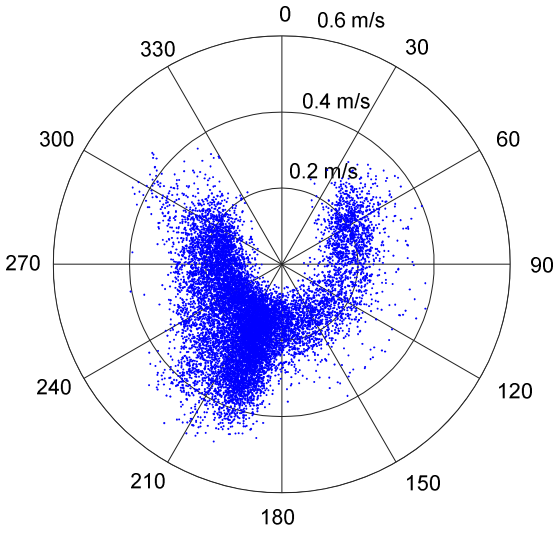

Figure 4.27 – Polar plot of raw data from the Falmouth Bay ADCP

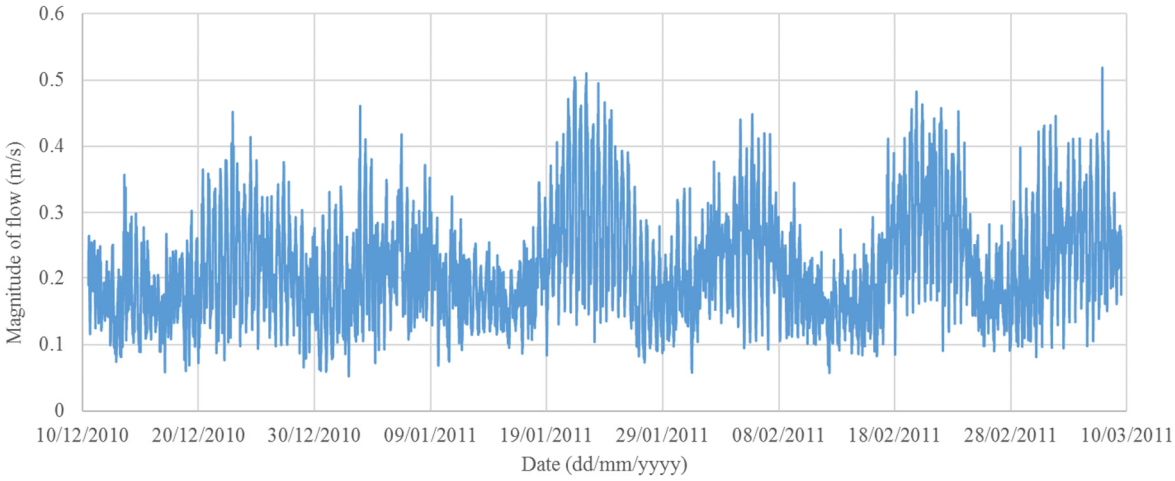

Figure 4.28 – Falmouth Bay ADCP timeseries plot of magnitude of measured data

For the final jack-knife investigation, the short term ADCP data at both the Islay site and the Falmouth Bay was analysed using harmonic analysis and reconstructed over a one-year period. The resolution of the long-term period was set to be 10 minutes. Harmonic analysis was performed using UTide and the average flow speed was calculated to be 1.40 m/s and 0.13 m/s over the annual period for the Islay and Falmouth Bay sites respectively.

The short-term data was then split into a number of subsets and UTide was re-run with one of these subsets missing (see Jack-knife approach in Section 2.1.3.1) and the annual average flow value calculated. The results from the Islay and Falmouth Bay data are shown in Table 4.10 and Table 4.12, respectively. Each row shows the results for a different number of subsets and the number of each column corresponds to the subset of data that was missing from the analysis. The long-term

average flow speed was then calculated for each analysis run and compared with the long-term average using the whole dataset. The uncertainty is calculated using the variance between the values using Equation 2.14. The jack-knife uncertainty for each number of subsets was plotted and is shown in Figure 4.29 for both datasets.

Table 4.12 – Falmouth Bay Data Jack-Knife Analysis Results

Number of subsets	Average flow speed for each subset (m/s)								Uncertainty (%)
	1	2	3	4	5	6	7	8	
Full	0.1309								
2	0.1408	0.1268							5.35
3	0.1402	0.1288	0.1290						5.83
4	0.1361	0.1331	0.1309	0.1280					3.45
5	0.1363	0.1338	0.1296	0.1307	0.1285				3.74
6	0.1354	0.1352	0.1296	0.1306	0.1303	0.1298			3.19
7	0.1347	0.1337	0.1331	0.1288	0.1310	0.1296	0.1297		2.70
8	0.1339	0.1333	0.1344	0.1297	0.1316	0.1299	0.1299	0.1287	2.20

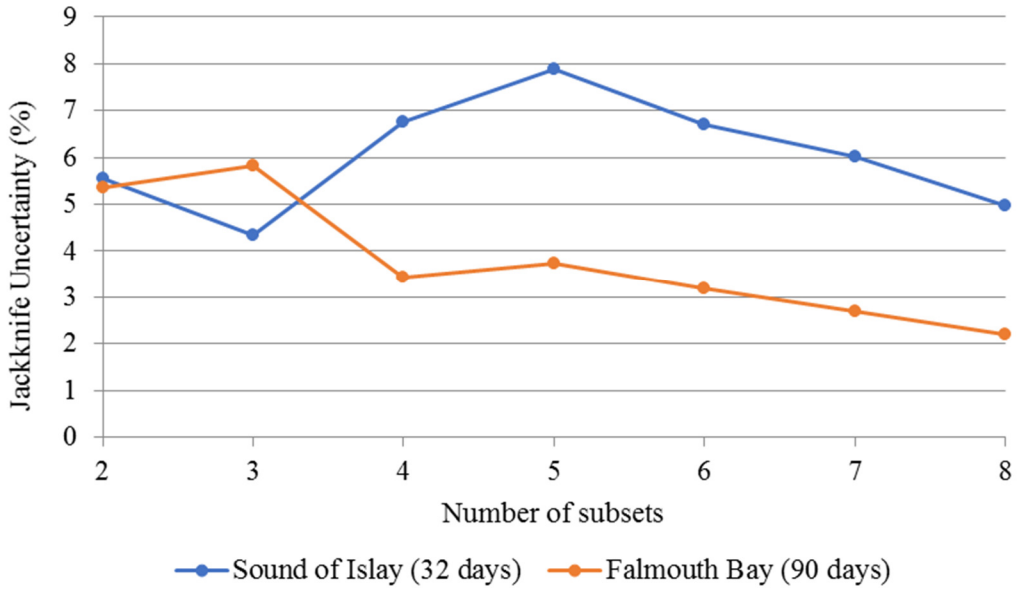

Figure 4.29 - Plot of Jack-knife uncertainty variation

The overall results show that the higher the number of subsets used, the lower the resulting uncertainty using the jack-knife approach. This is in-line with the expected results as each increase in the number of subsets, is including a higher proportion of the data in the analysis. However, for the lower number of subsets, where large periods of the data are being removed, it is shown that for the Sound of Islay data set, the largest uncertainty corresponds to the analysis using 5 subsets. Similarly, the lowest uncertainty value is achieved when conducting the analysis using 3 subsets. However, when using the Falmouth Bay, which had a total of 90 days, the jack-knife uncertainty is highest using 3 subsets and lowest using 8.

Within the calculation of wind energy uncertainty, the jack-knife uncertainty analysis is typically used for at least a year of wind data. It is known that the wind is very stochastic in nature and the wind resource one day is not linked to the wind resource the day before. On the other hand, however, tides are much more deterministic and periodical in nature. Therefore, when data is removed, a sub-section of the tidal cycle is removed, which greatly affects the harmonic analysis ability to evaluate the astronomic constituents. The resulting mean value calculated from the jack-knife analysis is greatly impacted, leading to such high uncertainty values.

4.6 Chapter Conclusions

This study has shown how harmonic analysis can be used to predict tidal flow variations over longer periods. Using short-term data measured at a site, tools such as UTide can accurately predict how the flow will vary many years into the future. This is due to the fact that tidal variations are

deterministic and are reasonably well understood. There are a few methods to evaluate the accuracy of the harmonic analysis techniques. The methods covered in this research include a direct comparison of the modelled data with the measured site date; statistical evaluations of the residuals to give error values for simple comparisons; and a technique used in the wind industry that has been applied for the first time to tidal data, known as the jack-knife method.

The direct comparison of the reconstructed fit showed that harmonic analysis does include many different tidal variations including the spring/neap cycle as well as the 18.6-year nodal cycle, however, it is not able to predict the smaller variations which are caused by turbulence and other site interactions. An evaluation of the residuals between the data showed that the harmonic analysis fits the data with a minimum of 0.95 R^2 value, which suggests a good correlation. A high correlation of 0.99 was achieved for the vertical component of ADCP 2, due to the high flow speed in this direction.

Finally, an investigation of the jack-knife uncertainty method for tidal analysis was conducted. The results suggest that uncertainties are very large for predicting long-term estimates. The research has shown that the jack-knife method is not the most appropriate method to evaluate uncertainties for tidal energy. This is due to the fact that it involves taking out sections of the data which are vital for the harmonic analysis to accurately resolve the constituents that are causing the many variations in the tide. An evaluation of the residuals through fast Fourier analysis was shown to be a more effective way to evaluate uncertainties in harmonic analysis.

Chapter 5

Uncertainty in Hydrodynamic Modelling for Tidal Stream Energy

5.1 Introduction

This chapter investigates the propagation of uncertainty in a hydrodynamic model for tidal stream resource assessment, through an investigation using Telemac-2D, a widely used open source software (Moulinec *et al.*, 2011; EDF R&D *et al.*, 2014). A step by step description is given, in Appendix E:, of the methodology required to build the Telemac model. However, there are limits to how far models can be used to replicate real environments, as errors and uncertainties are introduced (Adcock *et al.*, 2013).

A discussion is included of several common issues that may be encountered when developing a model. The chapter concludes with an application of a numerical methodology for estimating the effect of bed friction uncertainty on tidal power statistics using a procedure proposed by Kreitmair (2018). The chapter presents an introduction to tidal stream power assessment, a description and review of hydrodynamic models, an outline of Telemac and how it is applied to a strait between the ocean, and results from a parameter study examining how bed friction uncertainties affects the expected power and its variance for a fence of tidal turbines in a strait. This the first time that the methodology is applied to estimate the uncertainty in power of a tidal stream turbine using a model developed in Telemac. The methodology presented here could be adapted and applied to consider uncertainty arising from other model inputs, such as eddy viscosity, turbine drag and turbulence.

Section 5.2 introduces Telemac-2D, the hydrodynamic modelling software used in this chapter to assess the power potential and associated uncertainties of modelling tidal turbines in tidal flow. A methodology to build a theoretical model of a strait between two oceans in Telemac 2D and how the expected power can be calculated is included in Appendix E:. It also includes a model validation exercise to confirm the initial model results. Section 5.3 discusses the main results of how uncertainty in bed roughness influences the uncertainty associated with the expected power of a tidal stream turbine. Section 5.4 provides conclusions and implications for the marine industry as well as ideas for future work in this area.

5.2 Telemac 2D

Telemac is a finite element shallow flow solver that has been successfully used to model the hydrodynamic effects of tidal turbines. Examples include the studies by Pérez-Ortiz et al. (2013), Haverson et al. (2018) and Piano et al. (2015). The flow of water from tidal stream currents is complicated, but can be simplified by flow speed averaged vertically over the water column to reduce it to a two-dimensional problem.

The Telemac-2D code solves the depth-averaged free surface flow equations as first derived by Barre de Saint Venant in 1871 (EDF R&D *et al.*, 2014). Here shallow water is defined as having a depth less than one tenth of the width of the domain it occupies. At this small aspect ratio, scale studies have shown that vertical velocities are negligible compared to streamwise and transverse velocities (Bailey, 2010). With the assumption of hydrostatic pressure distribution, the continuity and Navier-Stokes momentum equations, detailed in Section 2.3.2, can be reduced to the unsteady shallow water equations through depth integration.

The Telemac-2D code solves the following shallow water equations simultaneously:

Continuity

$$\frac{\partial h}{\partial t} + u \cdot \vec{\nabla}(h) + h div(\vec{u}) = S_h \tag{5.1}$$

Momentum along x

$$\frac{\partial u}{\partial t} + \vec{u} \cdot \vec{\nabla}(u) = -g \frac{\partial Z}{\partial x} + S_x + \frac{1}{h} div\left(h v_t \vec{\nabla} u\right) \tag{5.2}$$

Momentum along y

$$\frac{\partial v}{\partial t} + \vec{u} \cdot \vec{\nabla}(v) = -g \frac{\partial Z}{\partial y} + S_y + \frac{1}{h} div\left(h v_t \vec{\nabla} v\right) \tag{5.3}$$

in which h is the depth of water, u and v are velocity components in the x and y horizontal directions, g is gravitational acceleration, v_t is the momentum diffusion coefficient, Z is the free surface elevation, t is time, x, y are the horizontal space coordinates, S_h is the source or sink of fluid, and S_x, S_y are the source or sink terms in dynamic equations. In this case h, u, and v are the unknowns that the code solves for.

The process to create and undertake a resource assessment using Telemac-2D is outlined in Figure 5.1. BlueKenue (Canadian Hydraulics Centre, 2011) software is typically used for pre- and post-

processing of the data and the steering file can be created most efficiently using the software FUDAA (Telemac, 2007). A more detailed methodology is outlined in Appendix A:.

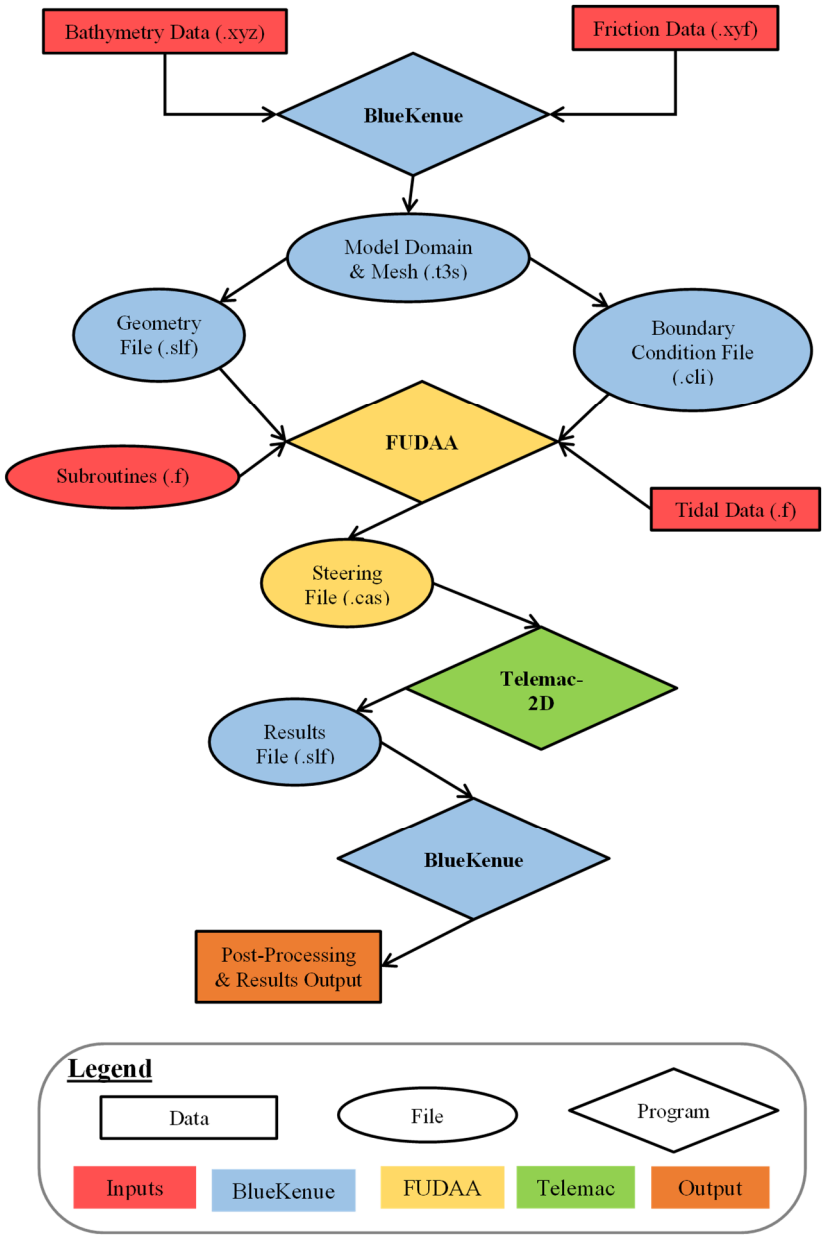

Figure 5.1: Process of conducting a resource assessment in Telemac-2D, adapted from Pérez-Ortiz et al. (2013)

5.2.1 Model Validation

In order to validate the initial model, a comparison of the primary outputs was made with Draper's (2011) Case 5-8. First, it was important to ensure that the maximum flow rate through the channel remained consistent. This validation method was used by Draper (2011) to ensure that the momentum of the water is conserved between different models with different dimensions and

attributes. Therefore, the amplitude of the initial tidal force was changed and the maximum velocity and maximum flow rate recorded. In the numerical simulations, the tide is introduced as a linear incident wave at the left boundary as

$$\xi_i = \left(\frac{A}{2}\right)\cos(\omega t - kx) \tag{5.4}$$

where A is the amplitude of the tide at the entrance to the channel if the channel did not exist and non-linear effects were negligible, $k = \omega\sqrt{gh_o}$ is the wave number, h_o is the uniform mean depth, and ω is the frequency of the tide, taken to be 0.00014 rad/s to represent the principal M2 component. To implement the tide numerically at the open boundary, the sum of the incident wave and its reflection, in the absence of the channel, are specified using a characteristic non-reflecting boundary condition (i.e. $h_b = h_o A\cos(\omega t)\cos(kx)$, $u_b = \sqrt{\frac{g}{h_o}}h_b$ and $v_b = 0$). At the right open boundary $h_b = h_o$ and $u_b = v_b = 0$. The model was tuned in an iterative way as depicted in Figure 5.2 until the target flow rate of 4.40 x 10^5 m^3/s was achieved. This was reached when the amplitude of the input tide was 5.225 m, a slightly larger value than Draper's input amplitude of 4.4 m, as shown in Figure 5.2.

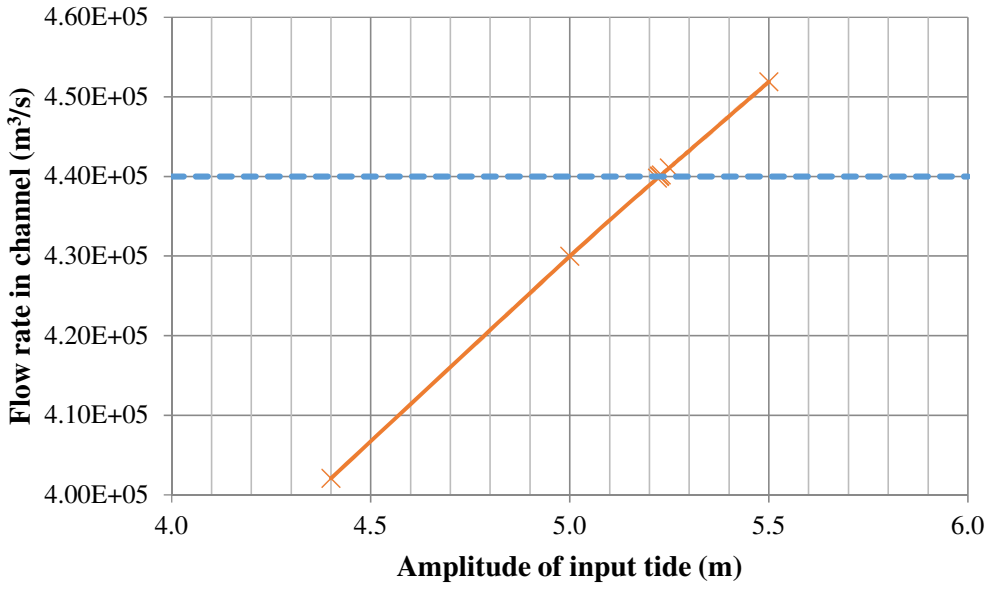

Figure 5.2: Iterations of initial model tidal amplitude (*A*) to achieve target flow rate (*Q*)

The average flow velocity in the channel was calculated to be 3.14 m/s for an input tidal amplitude of 5.225 m. Figure 5.3 shows a contour plot of the undisturbed velocity in the channel before the theoretical tidal turbines were added. The velocity across the channel is relatively uniform, with

the flow reaching a maximum towards the end of the channel before radially dissipating as it enters the ocean on the downstream end.

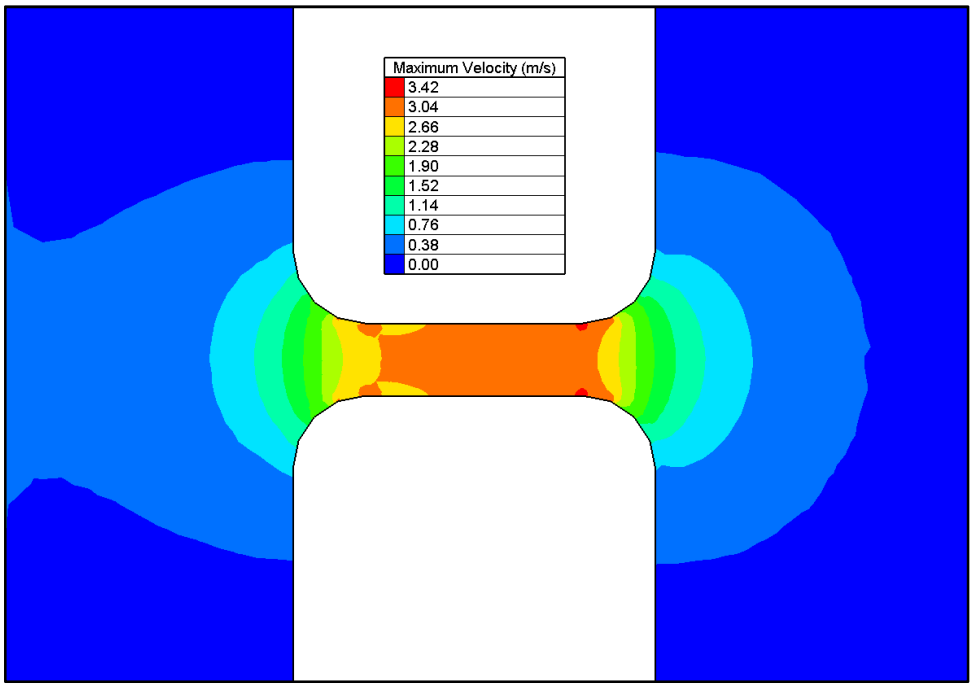

Figure 5.3: BlueKenue plot of maximum velocity contours from outputs of model with no turbines included.

The final validation exercise was to calculate the expected value of power from the model. This was calculated using Equation 5.5 for varying bed roughness values as shown in Figure 5.4. The power was calculated as:

$$P = \rho \cdot C_t \cdot \int_{y_1}^{y_2} v^3 \, dy \cdot dx \tag{5.5}$$

Where, ρ, is the water density, assumed to be 1025 kg/m^3, *dx* and *dy* are the width and length of the turbine array area, respectively.

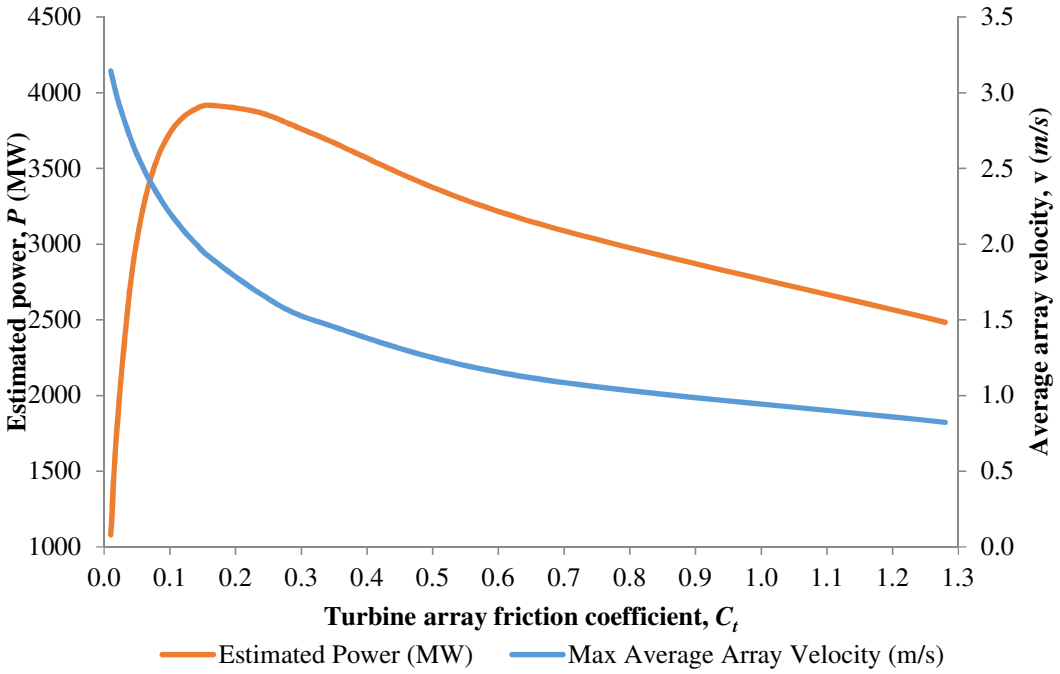

Figure 5.4: Variation in average velocity, v, and estimated power potential, P, through a channel with varying turbine friction, C_t, and constant C_d value of 0.2 across the model domain

The maximum power measured in the channel was 3917 MW, which is almost the same as the value of 3900 MW calculated by Draper (2011). The calculated power reaches the maximum value at a turbine friction value of 0.16 and then gradually decreases for higher friction coefficient values. The increase in the bed friction coefficient causes the flow speed to decrease exponentially from a maximum value of 3.14 m/s in the undisturbed case to a value of 1.92 m/s when the power is maximised. The flow speed continues to reduce and tends to converge towards a flow speed of 0.8 m/s. This validation exercise gives confidence that the Telemac model gives accurate predictions of tidal stream power in a strait.

Once the geometry of the model was defined, the next step was to create a computational mesh with BlueKenue. The number of mesh elements and the edge length Δx will influence the computational time. The time step is related to the Courant-Friedrichs-Lewy (CFL) condition, which is a necessary prerequisite for computational stability while solving certain partial differential equations numerically by the method of finite differences. In two dimensional cases, the dimensionless CFL number is defined as

$$CFL = \frac{u_x \Delta t}{\Delta x} + \frac{u_y \Delta t}{\Delta x} \leq C_{max} \tag{5.6}$$

where u is the magnitude of the velocity, Δt is the time step and Δx is the spatial increment. CFL is a stability criterion, prescribing the maximum in time step commensurate with a given mesh or

grid size so that the time step is not greater than the fluid travel time across an element. The value of C_{max} depends on whether the method used to solve the discretised equation is explicit or implicit. For an explicit solver, then typically $C_{max} = 1$. Implicit solvers are usually less sensitive to numerical instability and so larger values of C_{max} may be acceptable. In Telemac-2D, recommended CFL values are typically between 0.1 and 2 (Hervouet, 2007).

Using the maximum velocity in the channel, the Froude number, *Fr*, can be calculated using Equation 2.41. The Froude number for the Telemac-2D model is calculated to be 0.17 which is higher than Draper's value of 0.11 for the same case.

5.3 Results Discussion

Once the theoretical model was created and validated to represent a simple channel between two large basins, and spanned by a fence of turbines, a series of simulations was undertaken to calculate the expected power that could be extracted by the tidal turbines. The model was run systematically for an array of different C_d and C_t values. The resulting power output was calculated using Equation 5.5 and recorded as a look up table. In this case, *dx* is 2000 m and *dy* is 4000 m, C_t is the localised turbine drag value applied as an increased bed roughness over the turbine array area, and *v* is the velocity of the flow at each node in the turbine array. Table 5.1 lists the resulting power outputs for varying C_d and C_t values.

Table 5.1: Look up table of power output from turbine array in a strait

Power (MW)	C_d Value												
C_t Value	0.0055	0.0070	0.0080	0.0090	0.0100	0.0120	0.0150	0.0180	0.0200	0.0250	0.0300	0.0400	0.0550
0.005	1469.0	1070.5	894.4	761.6	658.7	510.7	372.4	286.8	246.3	178.1	136.3	89.1	55.4
0.010	2578.7	1922.0	1623.8	1395.3	1215.7	953.7	704.0	546.8	471.7	343.8	264.6	174.2	109.0
0.050	6338.6	5210.6	4632.1	4153.9	3753.2	3122.3	2458.5	2001.3	1769.9	1352.3	1076.5	741.3	482.5
0.100	7302.5	6336.7	5805.7	5346.0	4944.7	4279.8	3529.7	2977.5	2685.2	2132.6	1747.2	1252.3	846.0
0.300	6783.0	6320.4	6041.1	5782.7	5542.9	5112.4	4566.8	4114.7	3854.3	3313.4	2890.1	2274.2	1686.6
0.500	5968.7	5686.0	5510.4	5344.4	5187.3	4897.0	4512.9	4179.4	3980.4	3549.1	3192.9	2639.9	2066.6
1.000	4727.8	4593.1	4507.6	4425.5	4346.4	4196.8	3990.9	3804.0	3688.4	3426.5	3196.5	2811.1	2366.5
1.500	4039.4	3952.4	3897.1	3843.8	3792.4	3694.4	3558.1	3432.5	3353.8	3172.4	3009.1	2725.9	2381.9
2.000	3590.5	3525.8	3484.9	3445.6	3407.6	3335.2	3234.2	3140.7	3081.9	2945.0	2820.3	2600.0	2324.5

The results in Table 5.1 show that the expected power decreases as the value of bed roughness increases. This is due to the speed reducing as higher bed friction coefficients impede the flow. However, the initial results also show that as the localised turbine drag is increased, the power increases to a maximum and then decreases. Figure 5.5 shows graphically, the effect of increasing

the bed roughness on the extracted power is similar for all C_d values. The plot shows that increasing the effective drag coefficient of the turbine fence initially increases the extracted power, until the turbines begin to slow the flow rate to such an extent that a reduction in extracted power results. The present results are in good agreement with values from Draper's numerical model (2011).

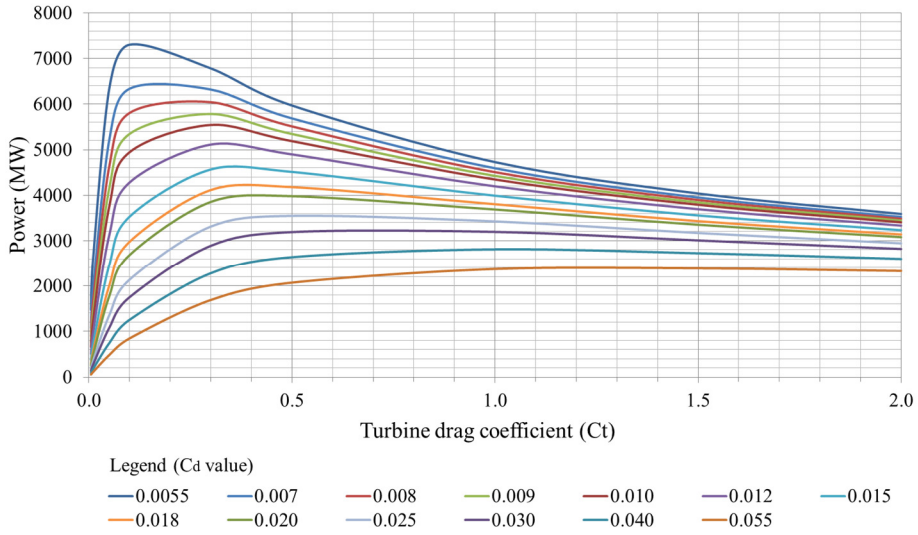

Figure 5.5: Variation in power with varying bed roughness value, C_d, and turbine drag coefficient, C_t.

These results provide insight into the relationship between the bed roughness value of the model, the localised turbine drag, and the expected power output from the turbines. However, calculations of expected power become unreliable if the actual bed roughness at the site is unknown. Moreover, it is often that case, in practice, that the bed roughness value is often used simply as a tuning parameter to calibrate predicted values with any known measured values.

In order to understand how uncertainty in the bed roughness influences the expected power of a turbine (and higher statistical moments), an investigation was carried out using the power output look up table (Table 5.1). The methodology is taken from Kreitmair (2018) who proposed a numerical technique for uncertainty propagation that can be generally applied to problems in hydraulic engineering.

The first step is to use a two-dimensional cubic spline to refine the look up table and hence acquire additional interpolated power output values. This was carried out in MATLAB using the interp2 function. The ranges of bed roughness and turbine drag values selected for the interpolation were:

- C_d – 0.005 to 0.055 in intervals of 0.001
- C_t – 0.0 to 2.0 in intervals of 0.01

The results of the cubic spline interpolation gave a surface plot of refined power values for different bed and turbine roughness values, shown in Figure 5.6. The interpolated results show a similar relationship to the values presented in Figure 5.5, but presented as a surface. For each value of bed roughness, C_d, the expected power increases to a maximum and then decreases more gradually.

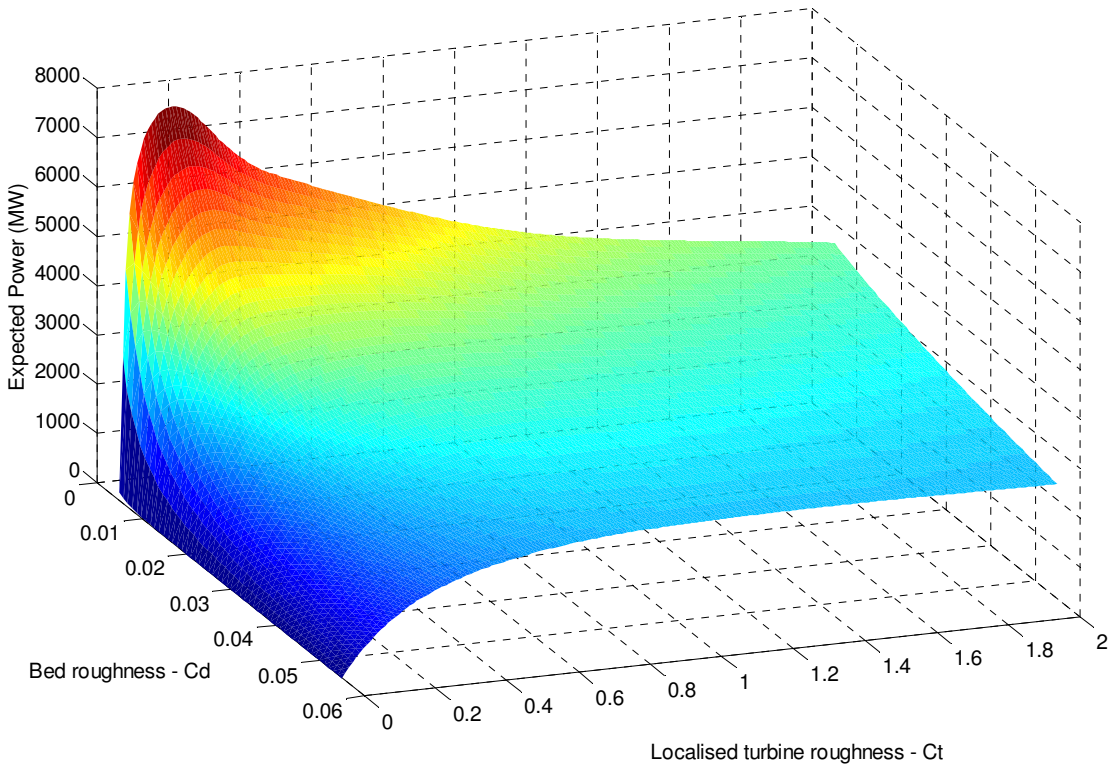

Figure 5.6: Interpolated variation in power with varying bed roughness value, C_d, and turbine drag coefficient, C_t

The next step involved defining a probability density function (pdf) for the bed roughness value, C_d, with a specified mean, μ_{C_d}, and variance $\sigma^2_{C_d}$. Initially a mean C_d value of 0.02 was selected with a variance of 0.005. The probability density function (pdf) and cumulative density function (cdf) for this variation of the roughness coefficient (C_d) is shown in Figure 5.7 (a) and (b) respectively. The variation is represented as a normal distribution as discussed in Chapter 2.

The pdf and cdf were split into 10 equally spaced bins in C_d intervals of 0.004. Figure 5.7 (b) shows the CDF value and the 10 bins, with the central value marked with an 'x'.

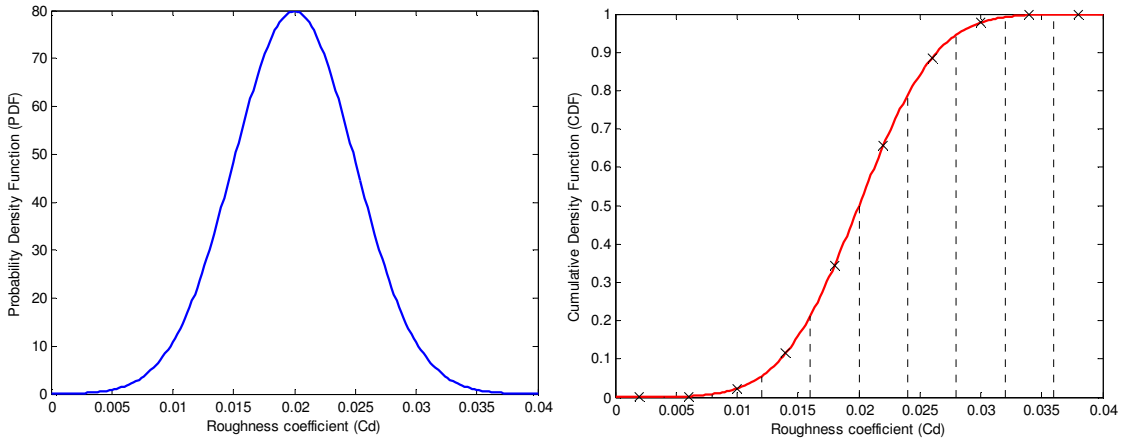

(a) (b)

Figure 5.7: (a) Bed roughness (C_d) probability distribution function (pdf) and (b) cumulative distribution function (cdf) – right.

The probability of $C_{d,i}$ is then calculated by integrating the pdf over the area of each bin, i.e:

$$Pr(C_{d_i}) = Pr(C_{d,i-1/2} < C_d < C_{d,i+1/2}) = \int_{C_{d,i-1/2}}^{C_{d,i+1/2}} \text{pdf}\, dC_d \tag{5.7}$$

For a known pdf, this is simply the cumulative distribution function (cdf) of the distribution between the defined boundary values of the bin, designated by $C_{d,i\pm1/2}$. This equals the probability of power for this value of bed roughness coefficient $P_i = f(C_d = C_{d_i})$ because probability is conserved (Kreitmair, 2018). Table 5.2 shows the value of C_d at the centre of each bin and the corresponding probability for each bin, Pr $(C_{d,i})$, taken as the difference between the probability at the beginning and end of each bin. $P_i(C_{d,i})$ is the power for each value of $C_{d,i}$. The expected power, E[P], is then calculated as

$$E[P] = \sum_i P_i\,(C_{d_i}) \cdot Pr(C_{d,i}) \tag{5.8}$$

and the variance as

$$\sigma_P^2 = \sum_i \left(P_i(C_{d_i}) - E[P]\right)^2 \cdot Pr(C_{d,i}) \tag{5.9}$$

where σ_P is the standard deviation. Higher, n^{th} order, statistical moments such as the skewness and kurtosis can be calculated by

$$\mu_n = \sum_i \left(P_i\left(C_{d_i}\right) - E[P]\right)^n \cdot Pr\left(C_{d,i}\right) \tag{5.10}$$

where $n = 3$ gives the skewness of a distribution (a measure of asymmetry) and μ_4 gives the kurtosis (a measure for the "peakedness" or "tailedness") of a distribution. For more information, see Kreitmair (2018) . The results in Table 5.2 show that the expected power distribution has a positive skew of 0.79 which indicates that the mean value and the mass of the distribution is skewed to the left. The results also show that the distribution has a kurtosis value of 4.20. This indicates that the distribution of power is less peaked than a typical normal distribution and that the data gradually reduces towards the tails.

Table 5.2: Base case results with C_d split into 10 bins and the probability of occurrence, Pr $(C_{d,i})$ and the power value $P_i(C_{d,i})$ for the centre of the bin.

Bin Number	$C_{d,i}$	Pr $(C_{d,i})$	$P_i(C_{d,i})$ [MW]
1	0.002	0.0007	7243.11
2	0.006	0.0075	6203.82
3	0.010	0.0466	5376.60
4	0.014	0.1571	4723.76
5	0.018	0.2881	4197.72
6	0.022	0.2881	3765.15
7	0.026	0.1571	3403.84
8	0.030	0.0466	3097.78
9	0.034	0.0075	2835.00
10	0.038	0.0007	2608.42
		Expected Power (E[P]) [MW]	4040.21
		Variance (σ_P^2)	3.45 x 10^5
		Standard deviation (σ_P) [MW]	587.10
		Skewness (μ_3)	0.79
		Kurtosis (μ_4)	4.20

From the results, it is then possible to plot the pdf and cdf for the power. Figure 5.8 shows the how the probability density can be transferred from a defined pdf for the bed roughness (C_d) to a pdf in power (P).

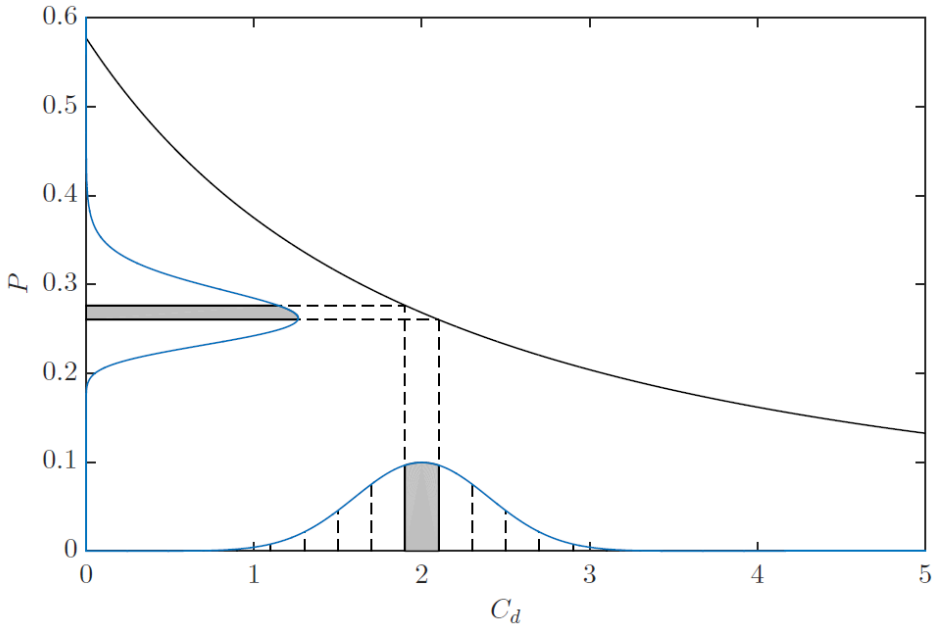

Figure 5.8: Probability density transfer from a pdf for C_d to a pdf in P via a function $P = f(C_d)$. The pdf for C_d has been subdivided into discrete bins indicated by the dashed lines. The shaded areas represent the same area, by conservation of probability (taken from (Kreitmair, 2018)**).**

The resulting pdf and cdf for the power is calculated by evaluating the power value at the beginning and the end of each bin.

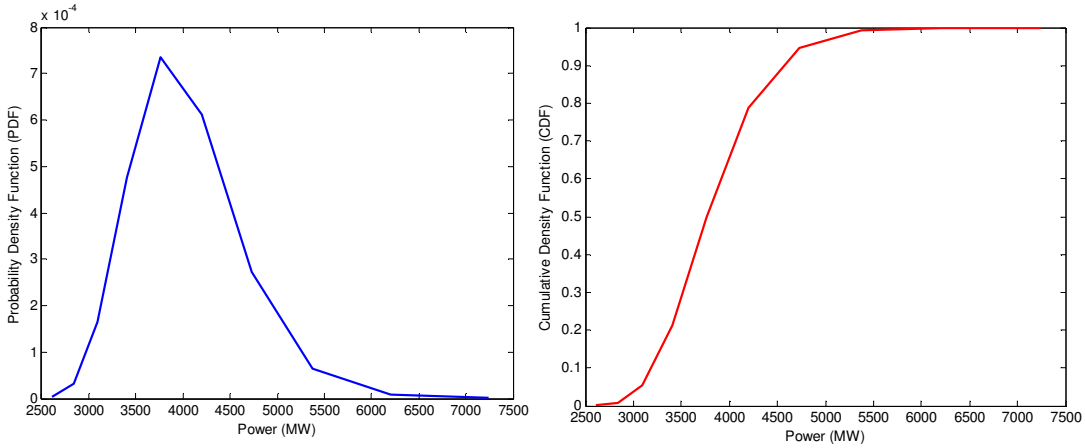

(i) PDF 10 bins

(ii) CDF 10 bins

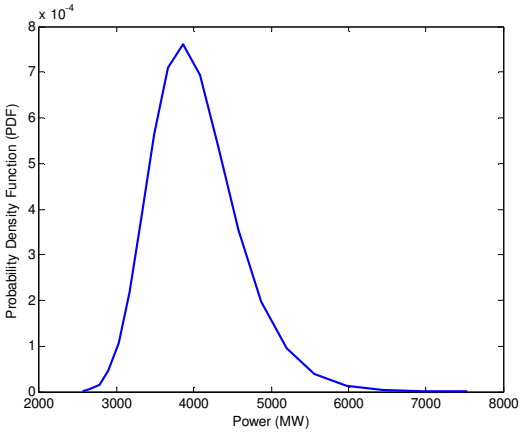

(iii) PDF 50 bins

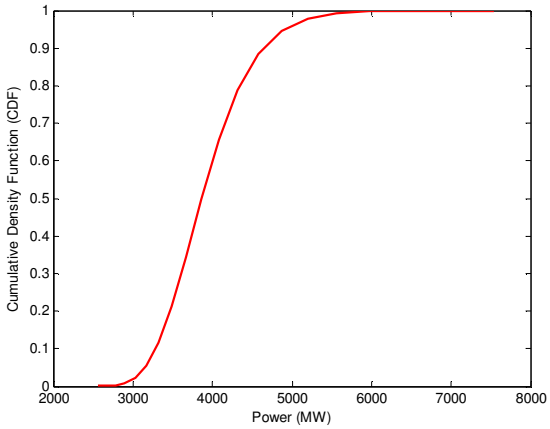

(iv) CDF 50 bins

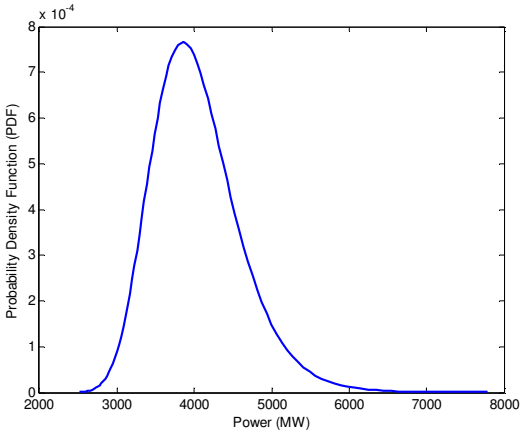

(v) PDF 100 bins

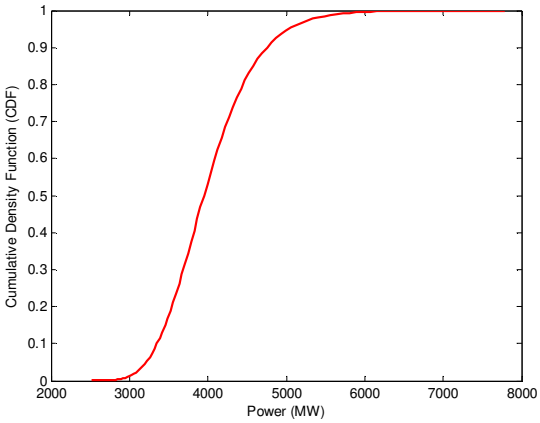

(vi) CDF 100 bins

Figure 5.9: Resulting probability distribution function and cumulative distribution function of the expected power for different numbers of bins.

An evaluation of the impact of the number of bins on the predicted values of expected power was investigated, and the results are presented in Table 5.3. It is shown that an increase in the number of bins results in convergence of each variable. Use of 100 bins provides an acceptable approximation. Figure 5.9 shows the effect of increasing the number of bins on the shape of the distributions. The results become smoother as more bins are used. From this convergence test, it can be taken that 100 bins are sufficient to give accurate statistical estimates.

Table 5.3: Effect of varying the number of bins on expected power and other statistical uncertainty results

Number of bins	Expected Power – E[P] (MW)	Variance (σ_P^2)	Standard deviation (σ_P)	Skewness (μ_3)	Kurtosis (μ_4)
10	4040.21	3.45 x 10^5	587.10	0.79	4.20
20	4037.49	3.30 x 10^5	574.56	0.77	4.16
50	4036.73	3.26 x 10^5	571.01	0.77	4.15
100	4036.62	3.25 x 10^5	570.51	0.77	4.15
150	4036.62	3.25 x 10^5	570.51	0.77	4.15

A further study was carried out to compare the expected power when the standard deviation of C_d was changed. Table 5.4 shows that a reduction in the standard deviation of C_d gives a lower value of expected power. In other words, a larger uncertainty associated with the bed roughness tends to over predict the power. Furthermore, the code was run for different mean values of natural bed friction, C_d, with the standard deviation kept constant. The results show that the standard deviation of power decreases as the mean value of bed roughness increases. It should be noted that the ratio between the mean and standard deviation of power is greater than the ratio of the bed roughness for each case.

Table 5.4: Summary of expected power for different values of mean and standard deviation in bed roughness C_d.

Case	Bed roughness (C_d)			Expected Power (E[P])			
	Mean (μ)	Standard deviation (σ)	Ratio ($\frac{\mu}{\sigma}$)	Mean (μ)	Normalised Power	Standard deviation (σ)	Ratio ($\frac{\mu}{\sigma}$)
Base Case	0.02	0.005	4	4036.62	1.00	570.51	7.1
Case-σ1	0.02	0.02	1	5310.95	1.32	4230.00	1.3
Case-σ2	0.02	0.01	2	4258.12	1.05	1348.79	3.2
Case-σ3	0.02	0.001	20	3962.86	0.98	107.76	36.8
Case-σ4	0.02	0.0005	40	3960.99	0.98	54.06	73.3
Case-μ1	0.005	0.005	1	6572.79	1.63	1266.11	5.2
Case-μ2	0.01	0.005	2	5491.53	1.36	968.25	5.7
Case-μ3	0.03	0.005	6	3139.96	0.78	368.10	8.5
Case-μ4	0.04	0.005	8	2528.34	0.63	252.25	10.0

As well as understanding how uncertainty in bed roughness affects the expected power, the effect on the flow velocity was investigated. Figure 5.10 shows the interpolated variation in flow velocity when the bed roughness and enhanced turbine roughness is changed. The results show that an increase in the mean roughness value causes a steep decrease in the flow speed in the channel. Even increasing the bed roughness from 0.01 to 0.02 reduces the flow speed from 2.60 m/s to 1.85 m/s, when the turbine roughness value is 0. It is also shown that the turbine roughness can reduce the flow speed to a minimum value of 0.52 m/s when the turbine roughness and bed roughness values are maximised at 2 and 0.055, respectively. It should be noted that the water in this case has no alternative route to take, whereas in a real tidal channel, an increase in roughness caused by the number of turbines reaching the blockage threshold may result in the water taking an alternative route and bypassing the channel altogether.

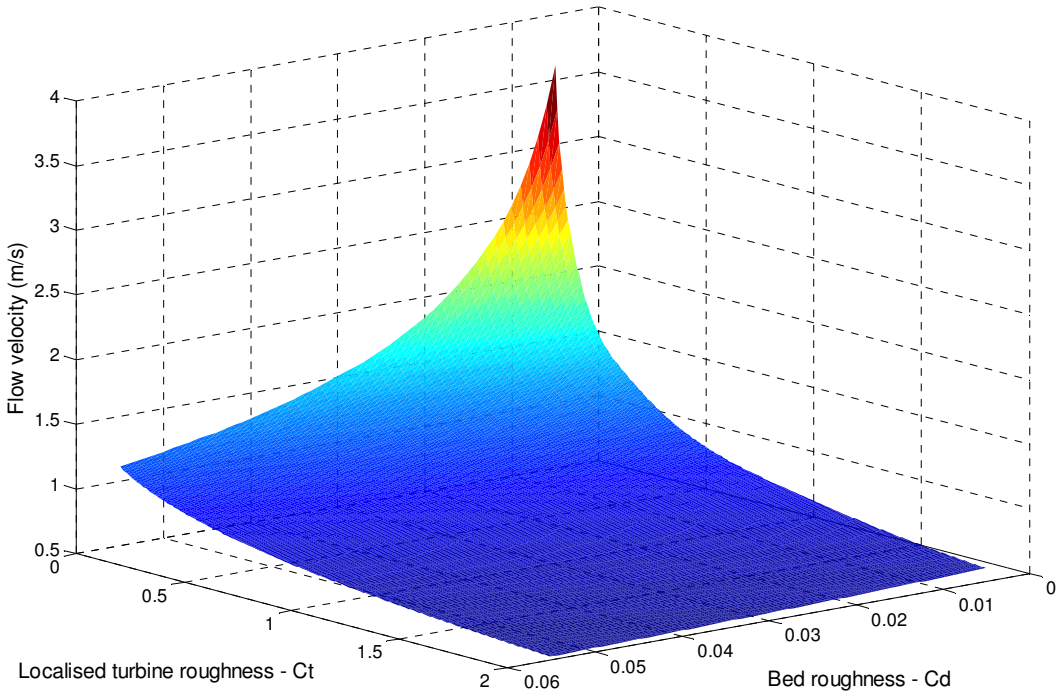

Figure 5.10: Interpolated variation in flow velocity with varying bed roughness value, C_d, and turbine drag coefficient, C_t

The same distribution of bed roughness shown in Figure 5.7 was input into the model and run to evaluate the impact on the velocity of the flow. The resulting distribution is shown in Figure 5.11.

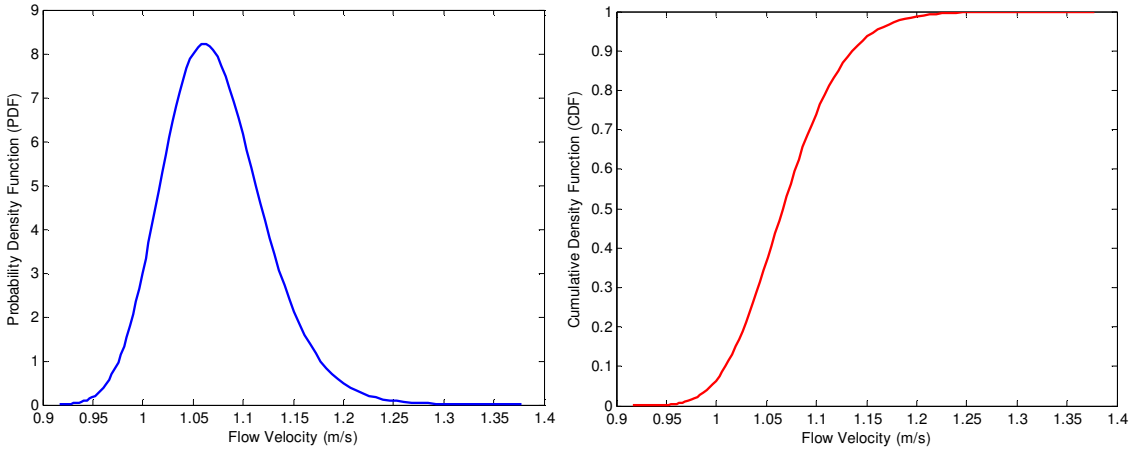

(a) (b)

Figure 5.11: Resulting flow velocity probability distribution function (a) and cumulative distribution function (b).

Table 5.5: Effect of varying the number of bins on expected velocity in the channel and associated uncertainty values

Case	Bed roughness (C_d)			Flow Velocity (v)			
	Mean (μ)	Standard deviation (σ)	Ratio $\left(\frac{\mu}{\sigma}\right)$	Mean (μ)	Normalised velocity	Standard deviation (σ)	Ratio $\left(\frac{\mu}{\sigma}\right)$
Base Case	0.02	0.005	4	1.072	1.00	0.051	21.07
Case-σ1	0.02	0.02	1	1.196	1.12	0.504	2.37
Case-σ2	0.02	0.01	2	1.087	1.01	0.119	9.14
Case-σ3	0.02	0.001	20	1.067	1.00	0.009	108.30
Case-σ4	0.02	0.0005	40	1.068	1.00	0.005	215.66
Case-μ1	0.005	0.005	1	1.282	1.20	0.106	12.06
Case-μ2	0.01	0.005	2	1.194	1.11	0.078	15.33
Case-μ3	0.03	0.005	6	0.985	0.92	0.038	25.65
Case-μ4	0.04	0.005	8	0.917	0.86	0.031	30.09

The effect of varying the mean and standard deviation of bed roughness on the flow velocity statistics was explored, and the results shown on Table 5.5. The same cases were considered as those used to investigate the impact on the power in Table 5.3. Here it can be seen that as the uncertainty in bed roughness increases, the expected flow velocity in the channel increases. Furthermore, Case-σ3 shows that reducing the uncertainty in the mean value of bed roughness, has a minimal impact on the mean value of flow velocity, but does reduce its standard deviation and thereby its uncertainty.

5.4 Chapter Conclusions

This chapter has investigated the influence of bed friction uncertainty propagation on the power output statistics of a tidal stream turbine. The study provides a useful numerical investigation of the quantification of uncertainty in power due to an uncertainty in an input parameter that may be unknown, from a deterministic perspective (provided a suitable pdf is available). This process is demonstrated via an investigation of the influence of bed roughness uncertainty on the expected power from a tidal stream turbine in a channel joining two infinite oceans. The model used a simplistic tidal turbine analogy whereby an enhanced bed roughness value is used to represent an increased turbine drag coefficient. The model was validated using results from Draper's Case 5-8.

Furthermore, this chapter has provided an overview of how to produce a hydrodynamic model of a tidal site using Telemac-2D, an open source numerical code widely used in industry. Modelling currently represents a significant proportion of overall energy yield uncertainty, see Chapter 3. The present work helps reduce the uncertainty in hydrodynamic modelling for tidal turbine applications, which is discusses in more detail in Chapter 6.

A new methodology, proposed by (Kreitmair, 2018) for assessing model uncertainty was applied to the case of a tidal fence in a strait between two oceans. The methodology is based on first conducting sensitivity studies by varying a parameter in the model and calculating the power. Then using a mean and standard deviation for the input parameter, the impact of the uncertainty can be transferred to the estimate of power. The results show that a larger uncertainty associated with the bed roughness tends to over predict the estimate of power. Similarly, a greater uncertainty in bed roughness results in an over prediction of the velocity. One of the uncertainty cases showed that reducing the uncertainty in the mean value of bed roughness didn't affect the prediction of the flow velocity but did reduce the standard deviation and as result reduced its associated uncertainty. The results emphasis the need to better understand how uncertainties propagate through models. Also, that uncertainties in bed roughness have an effect on the predicted velocity and power, and that the bed roughness could be calculated from evaluating the geology of the seabed and assessing the shear profile of the flow – as described in Chapter 3.

Kreitmair's methodology could be applied to other inputs to models where uncertainty may be present. Future work includes extending this model to consider uncertainty arising from other input variables such as eddy viscosity, turbine drag, and turbulence size and the resolution of the mesh.

Chapter 6

Industry Recommendations

6.1 Summary of recommendations for tidal energy yield uncertainties

Uncertainty is present whenever a measurement or a prediction is made. When seeking finance for renewable energy projects, an understanding of uncertainty in energy yield assessment allows financers to make decisions which affect the funding of projects. The tidal industry is currently building towards commercialisation and there is an opportunity to increase the understanding of energy yield uncertainty to inform tidal resource assessment.

The work in this thesis has developed understanding of tidal resource uncertainty and evaluated methods to quantify and reduce the effects of certain sources of uncertainty. An overview of the categories for assessing uncertainties in tidal energy yield assessments with a summary of methods to calculate and reduce them is included here, in Table 6.1, to provide procedural recommendations to the industry going forward.

Table 6.1 - Summary of tidal energy yield uncertainty recommendations

Uncertainty Category		Level of Uncertainty	Methods to Calculate Uncertainty	Recommendations to Reduce Uncertainty
Measurement Uncertainty	Instrument Accuracy	1.0 - 5.2	Uncertainty associated with the accuracy of the measurement instrument can be calculated from the device manufacturer specifications. The uncertainty in the measurements will vary based on the configuration of the instruments (e.g. the number and size of the bins for a current profiler).	It is recommended that the device manufacturers are consulted to ensure they are correctly set up with appropriate settings, and the device technical specifications are assessed to determine the appropriate uncertainty contribution to use. Ensure that the devices have been calibrated and even validated alongside other measurement devices (such as velocimeters)
	Measurement Interference	0.5 - 1.0	Measurement uncertainty also includes any uncertainty caused by interference as a result of physical instrument support/mooring structure, gross movement, rocking or environmental interference.	This uncertainty can be removed by discarding affected data through error checking. The device manufacturer should be consulted to ensure that the configuration of the measurement device is suitable for the site. If data is deemed to be affected by interference (e.g. side lobe interference, transducer ringing, etc.) this data should be removed and reported during the post-processing analysis.
	Data Synthesis	0.0 - 1.5	When data synthesis is conducted, an uncertainty value should be applied based on the percentage of synthesised data used compared to the total amount of data.	The methodology used to synthesis the data should be recorded in the assessment. In order to reduce uncertainty, it is recommended that the use of synthesised data to “fill in” missing data should be avoided whenever possible, and only raw measured data should be used within the assessment.

Uncertainty Category		Level of Uncertainty	Methods to Calculate Uncertainty	Recommendations to Reduce Uncertainty
	Data Quality and Metadata	0.0 - 2.0	An uncertainty should be applied when the general quality of the data or the overall metadata is poor. This could apply to missing information or poorly recorded information.	Important to minimise this uncertainty by collecting and documenting all data correctly, in lines with relevant industry standards and guidelines (such as the IEC 62600-201 technical specification).
Temporal Extrapolation	Historic Variation	1.0 – 3.0	Calculated based on the confidence intervals reported by harmonic analysis tools, which is based on the quality of the harmonic fit to the measured currents.	Collect as much on-site data as possible, at least 35 days, but to reduce uncertainties to 1% use at least 90 days of measured data. Spectral analysis of residuals using Fast Fourier Transforms can identify missing constituents. Using 1 minute averaged data instead of 10 minute averaged data will reduce uncertainty from approximately 3% to 1%.
	Future Variation	0.0 - 1.0	Uncertainty associated with long-term variations of the tides and how a project timescale may fit with the 18.6 year lunar nodal cycle.	Important to evaluate the long-term variations over at least an 18.6-year period. The sensitivity of an unknown start/commissioning date should be considered in the model.
	Climate Change	0.0 – 1.0	This uncertainty considers the local impacts of long-term global climate change, which for tidal turbines mainly considers the increase in sea level.	This uncertainty can be considered low as it will have a negligible impact on the energy yield of a tidal turbine over its lifecycle.
Spatial Extrapolation	Model Inputs	0.0 - 3.0	Uncertainties associated with the data inputs to hydrodynamic or other numerical models. The uncertainty could be calculated by conducting sensitivity analysis on inputs such as bathymetry, bed-roughness and boundary conditions.	To reduce uncertainties, the assessment should use high resolution data Use high resolution data Ensure the model domain is large enough to cover the resource in the region and consider smaller domain inside the larger domain Conduct sensitivity analysis

Uncertainty Category		Level of Uncertainty	Methods to Calculate Uncertainty	Recommendations to Reduce Uncertainty
	Horizontal Extrapolation	5.0 - 10.0	This uncertainty can be calculated based on the distance required to extrapolate the measured data to the turbine locations in the model.	Increasing the number of datasets will reduce the extrapolation distance and the associated uncertainty. For sites with 2 or more datasets, the horizontal extrapolation uncertainty should be guided by cross predictions at each location in the model.
	Vertical Extrapolation	0.0 - 5.0	The uncertainty is required is vertical extrapolation is required. Where a 2D model is used for resource assessment, an additional uncertainty should be quantified using a sensitivity study to assess the potential shear profiles relating hub-height to depth averaged flow speeds.	If hub-height data is used for energy yield calculations in conjunction with a 3D CFD model, then vertical extrapolation uncertainty can be considered minimal. It is important to ensure the resolution of the model includes a minimum of 3 layers over the turbine rotor area (in line with the IEC 62600-201 recommendations).
Plant Performance and Losses	Availability	0.0 - 1.2	This uncertainty is generally based on availability data provided by manufacturer, based on failure rates and associated repair times. For given failure rates, metocean conditions and vessel capabilities, the availability can be calculated using a time-domain event-based Monte Carlo analysis.	Ensure failure rates of key components are well understood and quantified and the availability provided by the turbine supply contract is well documented.
	Array Interactions	1.5 - 3.2	Uncertainty associated with wake and blockage modelling. The value of the uncertainty can be considered to be a percentage (likely 50%) of the wake and/or blockage loss.	Evaluate wakes and other array interactions using CFD or other advanced 3D modelling techniques. The wake uncertainty is likely to increase with the size of the array.
	Power Performance	2.2 - 5.2	The uncertainty in power performance should be calculated on a specific device basis. A power performance assessment should be carried out at the site and the uncertainty calculated using the IEC 62600-200 Technical Specification	Requires power performance tests to be carried out on deployed turbines. This uncertainty will decrease over time with an increase of device performance validation.

Uncertainty Category		Level of Uncertainty	Methods to Calculate Uncertainty	Recommendations to Reduce Uncertainty
	Electrical Losses	0.5 - 1.0	Uncertainty associated with transmission line loss estimation and electrical metering. This is typically specified by manufacturers.	Use good quality cables and power electronics with well documented and tested electrical systems.
	Performance Degradation	0.0 – 3.0	This uncertainty is based on the degree of biofouling or other forms of degradation that may affect performance.	Ensure device is suitably maintained, inspected and cleaned to maintain power curve.
	Curtailment	0.0 – 2.0	This uncertainty is applied if curtailment strategies are required and based on the extent of the curtailment.	Minimise curtailment required, if curtailment is required then the effects on production should be accurately quantified and documented.

6.1.1 Recommendations for evaluation long term effects using harmonic analysis

The work conducted in Chapter 4 has shown that the quality of the fitting of harmonic constituents to data can be evaluated by assessing the confidence intervals typically reported by harmonic analysis tools. The confidence interval on each tidal constituent prediction can be translated into a standard uncertainty value, as shown in Section 4.4.2 and can then be combined by the root-mean square (RMS) method, to arrive at an overall uncertainty value, defined as a percentage of the flow velocity.

Spectral analysis of residuals using Fast Fourier Transforms proved effective at identifying constituents that could not easily be extracted through harmonic analysis. Spectral analysis enabled additional constituents to be evaluated, which reduced the residuals, and hence uncertainty in the predicted variations.

The temporal uncertainty is also dependent on the level of non-astronomical variations present in the tidal signal such as flow variations caused by significant bathymetric or coastal features and non-harmonic forcing. These are uncertainties coming from aspects of the measured flow that are not captured in the model. This uncertainty can be determined by assessing the residuals between the measured ADCP data and the modelled harmonics, as discussed in Section 4.4. The turbulence intensity can be calculated using ADCP data, and the corresponding magnitude can be used to influence the level of uncertainty applied, as outlined in Section 4.4.4.1. Collecting meteorological and met-ocean data at the site can provide useful insights into the potential causes of residual. Section 4.4.4.2 outlined a method to assess the correlations of residuals and meteorological data, but showed that for this site, no statistical relationship could be found. An alternative qualitative method was suggested, to identify periods when the residuals may be influenced by stronger wind and wave conditions. Higher resolution wind and wave data should be collected in order to evaluate whether a statistical relationship between ADCP residuals and meteorological data exists.

An investigation into the uncertainty of calculating tidal constituents using input data of different resolutions showed that using 10-minute averaged data increased the uncertainty in the prediction from 1% to 2.8%. Given that raw site data used in tidal resource assessment is typically relatively short compared to wind resource assessment, it is recommended that the data resolution should be as high as possible when calculating long-term variations using harmonic analysis.

Finally, the temporal uncertainty due to the inter-year variations caused by the annual variations caused by the 18.6-year nodal cycle should be assessed. Harmonic analysis should be used to compute time series for the full 18.6 year cycle separately for each year to avoid nodal drift. The uncertainty related to deviation of the chosen typical year to the full range should be assessed for the annual velocity distributions.

6.1.2 Recommendation for evaluating uncertainty in hydrodynamic modelling

This uncertainty is associated with the validation of the hydrodynamic modelling, using measured site data. The uncertainty can typically be calculated through comparing the measurements to the modelled results. Sensitivity analysis should be used to evaluate the impacts of user defined inputs on the final model results. This is primarily linked with the model mesh resolution and the quality of the model inputs (which may include, but is not limited to, accuracy and resolution of bathymetry data and assigned boundary conditions). The number of model variables to be assessed should be defined by the user, but should include as a minimum, the resolution of the mesh (horizontal and vertical), the boundary conditions and the bed roughness value.

This uncertainty is associated with any hydrodynamic (or other) modelling required to extrapolate data from a "known" measurement point to a tidal energy convertor device location. This can include vertical or horizontal extrapolation.

The horizontal uncertainty is driven by the distance between the measured point and the proposed turbine locations. For sites, where the measurement devices are deployed at every turbine location, the spatial variation uncertainty is assumed to be negligible. For sites, where extrapolation is required from a measurement location to a proposed turbine location, the distance between the measured location and the unknown turbine location should be assessed when considering the spatial uncertainty. For projects with at least two concurrent periods of measurements from different sources, cross predictions should be carried out to predict and compare the modelled flow characteristics at each location to the measured flow characteristics.

To reduce uncertainty, this distance should be minimised by deploying additional measurement devices, or conducting transect surveys to characterise the flow variation across the site.

Although the bed roughness parameter is often used as a tuning parameter in model validation tests against measured data, small variations in bed roughness can have a significant impact on the output power from a turbine. Instead of using a single value for bed roughness, it is recommended in future that a probability density distribution should be used to evaluate the corresponding expected power and variation in power output. The latter would provide information on power uncertainty arising from uncertain input to the model equations.

A simple study demonstrated that propagation of uncertainty through a hydrodynamic tidal power assessment model can be quantified using a suitable probability density function fitted to the mean and standard deviation of an input parameter (e.g., the Manning coefficient). A principle of conservation of probability was utilised, following Kreitmair (2018), to obtain numerical estimates of the power probability density function and its statistical moments. The method essentially

quantified the uncertainty in expected power output from a turbine arising from uncertainty in bed friction.

The influence of bed friction uncertainty propagation on the power output statistics of a fence of tidal turbines showed that a reduction in uncertainty in bed friction gives a reduction in the expected power. Furthermore, an increase in bed friction coefficient, provided a power estimate with relatively lower uncertainty. Therefore, the uncertainty of a model to predict the power is dependent on the mean value of the bed friction coefficient used. This is important when considering model validation through altering the bed friction coefficient. A higher value of the bed friction coefficient will result in a more conservative estimate of power, but with a lower associated uncertainty.

Propagation of uncertainty through a model can be addressed through a parameter study to assess the sensitivity of any given input parameter on the power output. The numerical methodology presented herein (following Kreitmair 2018) can be extended further to assess other model parameters as well as site specific parameters for a real tidal site.

6.2 Tools to enhance incorporation of uncertainty quantification in tidal energy resource assessment

Through this study, several codes and tools have been developed to assess uncertainties. These are listed in the Appendices of the thesis, and are therefore available for the host company and the wider industry. These include:

- An enhanced UTide MATLAB code which incorporates quantification and evaluation of uncertainty in harmonic analysis (Appendix A)
- A procedure for using Telemac, FUDAA and BlueKenue to build, run and evaluate a hydrodynamic model for tidal resource assessment. This allows Wood and other industry users to develop models and understand how the three software's interact with each other. (Appendix B and Appendix E:)
- Matlab code for uncertainty quantification from hydrodynamic modelling outputs (Appendix D) and an example of the Telemac steering file detailing the required format (Appendix C)

Overall, the aim of improving understanding of uncertainty in tidal energy yield was achieved by three means: demonstration of the synergies between wind and tidal power, and the transfer of experience from wind to tidal energy assessment; evaluation of uncertainty in harmonic analysis, unique to tidal resource assessments; and assessment of uncertainty propagation in a shallow flow hydrodynamic model (a major contributor to overall uncertainty).

Through this, Wood has gained knowledge of harmonic analysis uncertainty, a hydrodynamic model of a tidal channel, and a statistics-based numerical means by to assess the sensitivity of the overall power estimate to uncertainty in input parameters.

6.3 Research Contributions

The research presented in this thesis has contributed to the advancement of knowledge as follows:

- Presented the first in-depth comparison between the approaches of the wind and tidal industries to energy yield assessment and uncertainty analysis, identified synergies where knowledge can be transferred, and highlighted analogous significant contributors to overall uncertainty.
- Developed methods for overall uncertainty quantification in UTide, beyond the 95% confidence interval provided for individual tidal constituents.
- Demonstrated that spectral analysis of residual of harmonic analysis is an effective method to identify missing harmonic constitutes, thereby increasing the accuracy of harmonic predictions.
- Applied a new methodology to evaluate uncertainty propagation within a widely used hydrodynamic model in the tidal industry.
- Showed that the impact of varying the bed roughness, typically used as a parameter to validate measured data, on predicted power was significant. The procedure outlined in the work provides a way for the uncertainty in power to be quantified, using a predefined mean and variance of a model parameter.
- Tools and guidance have been developed to assist with tidal energy resource assessment at Wood. These are designed to inform the calculation of tidal energy yield results and provide methods to quantify uncertainty.
- Finally, limitations in current published guidance have been identified when considering tidal energy yield uncertainties.
- This includes how to evaluate uncertainties in harmonic analysis using confidence intervals, as well as developing a methodology to assess the residuals of the assessment to guide uncertainty quantification. Additional work was carried out to conduct a sensitivity assessment of the bed roughness value and determine its impact on the expected modelled power output.
- To address these, recommendations were suggested to augment existing guidance and support the development of a revised technical specification. The work presented in this thesis is currently being used to inform uncertainty quantification in the IEC tidal resource technical specification. It is expected that this technical specification document will be

used worldwide to provide guidance to developers seeking to conduct and assess tidal resource assessment and quantify the corresponding uncertainty level in energy yield predictions.

6.3.1 Commercial Impact

It is likely that the work contained in this EngD thesis will deliver commercial impact for the host company plus the wider offshore renewable energy sector. Information in this project is already being used to inform and enhance resource assessment for tidal stream energy projects conducted by Wood. An understanding as to how tidal energy yield assessment differs from the (well-established) wind energy yield assessment is a clear benefit to the company and also the wider industry. The guidance developed for Wood highlights some of the complexities in calculating uncertainty in energy yield, particularly concerning harmonic analysis and hydrodynamic modelling. Wood has extensive experience in wind energy yield assessments and has begun transferring the knowledge to marine energy, most notably tidal energy. This thesis represents Wood's first stage in developing expertise on tidal energy yield assessment. Given Wood's extensive experience in wind energy and the transferability of much of this knowledge to the tidal industry, the present work should help Wood on its way to becoming an industry leader in tidal resource assessment and uncertainty analysis.

Tools and guidance have been developed to assist with tidal energy resource assessment at Wood. These are designed to inform the calculation of tidal energy yield results and provide methods to quantify uncertainty. The procedures and tools used for these software are very useful to Wood as it seeks to conduct independent energy yield assessments for tidal developers in the future. On a wider level, the work contained in this thesis is directly informing the development of a revised IEC technical specification. This document will be available to countries worldwide as a set of guidelines on how to conduct tidal resource assessment while quantifying and reducing energy yield uncertainty.

6.4 Recommendations for Future Work

The following topics are recommended for future work:

Developments in lidar and sodar

Improved instrumentation would help reduce uncertainty. Wind energy yield assessment usually relies on cup anemometers to measure wind speeds for a bank-grade energy yield report. In recent years, lidar and sodar devices have been used to complement measurement campaigns by providing measured wind characteristics over a larger range of heights. In certain cases, such remote sensing devices the only measurement devices available at a site to inform energy yield assessments, and this carries a high level of uncertainty. Given the similarities between sodar and ADCPs for tidal resource assessment, future analysis of sodar uncertainty would provide additional confidence in uncertainty attributed to ADCP in tidal energy yield assessments.

Longer measurement periods

Longer observational signal duration would benefit harmonic analysis. The analysis presented in Chapter 4 relied on ADCP data sourced from two sites in the UK. The data collected from the Islay tidal energy site was initially collected over a month-long campaign. However, this is simply not long enough to capture all the harmonic components. Although the data collected at Falmouth Bay was measured over a longer time period, the location is not representative of a typical tidal energy site. Future work is recommended to extend the harmonic analysis uncertainty study by obtaining observational data over longer time periods at a fast-flowing tidal site. In practice, longer data sets (up to 18.9 years, Pugh 1996) would facilitate much better site characterisation and improve the accuracy of harmonic analysis predictions.

Application to a real tidal site

The hydrodynamic modelling work considered a theoretical tidal site situated in a channel between two bodies of water. The strait is very simple idealisation, though applicable in principle to channel-like tidal sites. Given the easy of application of the numerical uncertainty propagation technique devised by Kreitmair (2018), it is recommended that the same methodology be applied to a real tidal energy site. In the present thesis, the methodology was applied to evaluating the effect of uncertainty in the input bed roughness value, a key model tuning parameter, which significantly impacts on model performance. Future work to assess the impact of other model parameters, such as turbine drag, energy dissipation through turbulence, etc. would further refine understanding. And investigations into the impact of uncertainty on hydro-environmental parameters such as sediment transport, flood risk, water quality, and biodiversity are well worth carrying out.

References

Abdi, H. and Williams, L. J. (2010) 'Jackknife', *Encylopedia of Research Design. Thousand Oaks, CA*, pp. 655–660.

ABPmer, The Met Office and Proudman Oceanograhic Laboratory (2008) *Atlas of UK Marine Renewable Energy Resources: Technical Report*. Southampton.

Achour, B. (2015) 'Chézy's Resistance Coefficient in a Rectangular Channel', *Journal of Scientific Research and Reports*, 7(5), pp. 338–347. doi: 10.9734/JSRR/2015/18385.

Adams, N. *et al.* (2015) 'Developing Best Practice in Uncertainty Assessment for Wave and Tidal Energy Projects', in *Proceedings of the 11th European Wave and Tidal Energy Conference*. Nantes, pp. 1–10.

Adams, N. and Frazer-Nash Consultancy (2014) 'Benchmarking of Offshore Wake Effects Models Background & Purpose', in *Wind Resource Assessment Workshop*.

Adcock, T. A. A. *et al.* (2013) 'The available power from tidal stream turbines in the pentland firth', *Proceedings of the Royal Society A: Mathematical, Physical and Engineering Sciences*, 469(2157). doi: 10.1098/rspa.2013.0072.

Addison, J. F. D. *et al.* (2000) 'A neural network version of the measure correlate predict algorithm for estimating wind energy yield', in *Proceedings of 13th International Congress on Condition Monitoring and Diagnostic Engineering*. Houston, Texas, pp. 917–922.

Ainslie, J. F. (1988) 'Calculating the flowfield in the wake of wind turbines', *Journal of Wind Engineering and Industrial Aerodynamics*. Elsevier, 27(1–3), pp. 213–224. doi: 10.1016/0167-6105(88)90037-2.

Anderson, M. (2004) *A Review of MCP Techniques*.

Arcement, G. J. and Schneider, V. R. (1989) 'Guide for selecting Manning's roughness coefficients for natural channels and flood plains', *US Geological Survey Water-Supply Paper*, 2339. doi: 10.3133/wsp2339.

Atlantis Resources (2019) *AR1500 Tidal Turbine Specification Brochure*. Available at: https://simecatlantis.com/wp-content/uploads/2016/08/AR1500-Brochure-Final-1.pdf.

AWS Truepower (2018) *Windographer Wind Resource Assessment Software*. Available at: https://www.windographer.com/ (Accessed: 24 March 2018).

Ayack (2008) *Sound of Islay Map*, *Wikipedia*.

Ayala, M. *et al.* (2017) 'Wind Power Resource Assessment in Complex Terrain: Villonaco Case-study Using Computational Fluid Dynamics Analysis', in *Energy Procedia*, pp. 41–48. doi: 10.1016/j.egypro.2016.12.127.

Bai, L., G Spence, R. R. and Dudziak, G. (2009) 'Investigation of the Influence of Array Arrangement and Spacing on Tidal Energy Converter (TEC) Performance using a 3-Dimensional CFD Model'.

Bailey, C. L. (2010) *Mathematical modelling of shallow water flows with application to Moreton Bay, Brisbane*. Loughborough University. doi: 10.1061/(ASCE)1090-0241(2008)134:1(79).

Bardsley, W. E. and Manly, B. F. J. (1983) 'Regression-Based Estimation of Long-Term Mean and Variance of Wind Speed at Potential Aerogenerator Sites', *Journal of Climate and Applied Meterology*, 22, pp. 323–327. doi: 10.1175/1520-0450(1983)022<0323:rbeolt>2.0.co;2.

Baston, S. and Harris, R. E. (2011) 'Modelling the Hydrodynamic Characteristics of Tidal Flow in the Pentland Firth', *EWTEC 2011 Proceedings*, pp. 1–7.

Batten, W. M. J. *et al.* (2008) 'The prediction of the hydrodynamic performance of marine current turbines', *Renewable Energy*. Pergamon, 33(5), pp. 1085–1096. doi: 10.1016/J.RENENE.2007.05.043.

Bechrakis, D. A., Deane, J. P. and McKeogh, E. J. (2004) 'Wind resource assessment of an area using short term data correlated to a long term data set', *Solar Energy*, 76(6), pp. 725–732. doi: 10.1016/j.solener.2004.01.004.

Bell, S. (1999) 'A Beginner's Guide to Uncertainty of Measurement', *National Physical Laboratory*, 11(2), pp. 586–587. doi: 10.1111/j.1468-3148.2007.00360.x.

Bennett, M. (2018) *Whatever happened to the Saltire Prize?*, *BBC News*. Available at: https://www.bbc.co.uk/news/uk-scotland-scotland-business-42832168.

Bergek, A. and Jacobsson, S. (2003) 'The emergence of a growth industry: a comparative analysis of the German, Dutch and Swedish wind turbine industries', in *Change, Transformation and Development*. doi: 10.1007/978-3-7908-2720-0_12.

Bhattacharya, A. (2019) 'Chapter 1 - Global Climate Change and Its Impact on Agriculture', in Bhattacharya, A. B. T.-C. C. and R. U. E. in P. (ed.). Academic Press, pp. 1–50. doi: https://doi.org/10.1016/B978-0-12-816209-5.00001-5.

Bissell, A. F. and Ferguson, R. A. (1975) 'The Jackknife--Toy , Tool or Two-Edged Weapon ?', *Journal of the Royal Statistical Society*, 24(2), pp. 79–100.

Blair Walter (2017) *Wind farm developments: Getting energy prediction right*.

Blanchfield, J. *et al.* (2008) 'The extractable power from a channel linking a bay to the open ocean', *Proceedings of the Institution of Mechanical Engineers, Part A: Journal of Power and Energy*, 222(3), pp. 289–297. doi: 10.1243/09576509JPE524.

Blunden, L. S. and Bahaj, A. S. (2006) 'Initial evaluation of tidal stream energy resources at Portland Bill, UK', in *Renewable Energy*, pp. 121–132. doi: 10.1016/j.renene.2005.08.016.

Bolanos, R. *et al.* (2009) *A comparison of wave-current interaction formulation using POLCOMS-WAM wave-current model*.

Bolaños, R. *et al.* (2011) 'Development of the POLCOMS–WAM current–wave model', *Ocean Modelling*. Elsevier, 36(1–2), pp. 102–115. doi: 10.1016/J.OCEMOD.2010.10.004.

Boritz, J. E. (2004) *IS practitioners' views on core concepts of information integrity*, *University of Waterloo Centre for Information Systems Assurance*. doi: 10.1016/j.accinf.2005.07.001.

Bowman, W. (2018) *Python UTide Project*, *Python Software Foundation*.

Box, G. E. P., Jenkins, G. M. and Reinsel, G. C. (2008) *Time series analysis: forecasting and control*. Fourth. Hoboken, NJ: John Wiley & Sons Ltd.

Brière, C. *et al.* (2007) 'Assessment of TELEMAC system performances, a hydrodynamic case study of Anglet, France', *Coastal Engineering*, 54(4), pp. 345–356. doi: 10.1016/j.coastaleng.2006.10.006.

British Standards Institution (2017) *BS EN ISO/IEC 17025:2017 General requirements for the competence of testing and calibration laboratories*.

Brower, M. C. *et al.* (2013) *A study of wind speed variability using Global Reanalysis data*.

Bruce Bailey (2016) *The State of Wind Farm Underperformance Syndrome*, *Wind Systems Magazine*.

Bryden, I. G. *et al.* (2007) 'Tidal current resource assessment', *Proceedings of the Institution of Mechanical Engineers, Part A: Journal of Power and Energy*, 221(2), pp. 125–135. doi: 10.1243/09576509JPE238.

Bryden, I. G. and Couch, S. J. (2007) 'How much energy can be extracted from moving water with

a free surface: A question of importance in the field of tidal current energy?', *Renewable Energy*. Pergamon, 32(11), pp. 1961–1966. doi: 10.1016/J.RENENE.2006.11.006.

Bryden, I. G., Grinsted, T. and Melville, G. T. (2004) 'Assessing the potential of a simple tidal channel to deliver useful energy', *Applied Ocean Research*, 26(5), pp. 198–204. doi: 10.1016/j.apor.2005.04.001.

Calaf, M., Meneveau, C. and Meyers, J. (2010) 'Large eddy simulation study of fully developed wind-turbine array boundary layers', *Physics of Fluids*, 22(1), p. 015110. doi: 10.1063/1.3291077.

Campbell, J. Y., Lo, A. W. and MacKinlay, A. C. (1997) *The Economics of Financial Markets*, *Princeton University Press*. doi: 10.1007/s13398-014-0173-7.2.

Canadian Hydraulics Centre (2011) 'Blue Kenue Reference Manual', *Organization*, (September), p. 204.

Carbon Trust (2011) *Accelerating Marine Energy, the potential for cost reduction*.

Cartwright, D. E. (1999) *Tides - A Scientific History*. Cambridge: Cambridge University Press.

Carvalho, D. *et al.* (2013) 'Wind resource modelling in complex terrain using different mesoscale-microscale coupling techniques', *Applied Energy*, 108, pp. 493–504. doi: 10.1016/j.apenergy.2013.03.074.

Chancham, C., Waewsak, J. and Gagnon, Y. (2017) 'Offshore wind resource assessment and wind power plant optimization in the Gulf of Thailand', *Energy*, 139, pp. 706–731. doi: 10.1016/j.energy.2017.08.026.

Chatzirodou, A., Karunarathna, H. and Reeve, D. E. (2017) 'Modelling 3D hydrodynamics governing island-associated sandbanks in a proposed tidal stream energy site', *Applied Ocean Research*, 66, pp. 79–94. doi: 10.1016/j.apor.2017.04.008.

Chaurasiya, P. K., Ahmed, S. and Warudkar, V. (2017) 'Wind characteristics observation using Doppler-SODAR for wind energy applications', *Resource-Efficient Technologies*, 3(4), pp. 495–505. doi: 10.1016/j.reffit.2017.07.001.

Chen, C., Liu, H. and Beardsley, R. C. (2003) 'An Unstructured Grid, Finite-Volume, Three-Dimensional, Primitive Equations Ocean Model: Application to Coastal Ocean and Estuaries', *Journal of Atmospheric and Oceanic Technology*. American Meteorological Society, 20(1), pp. 159–186. doi: 10.1175/1520-0426(2003)020<0159:AUGFVT>2.0.CO;2.

Clark (2016) *Tides - 8th Grade Science*. Available at:

https://clarkscience8.weebly.com/tides.html#.

Clark, T. *et al.* (2017) 'InSTREAM: Measurement, Characterisation and Simulation of Turbulence from Test Tank to Ocean', *Proceedings of the Twelfth European Wave and Tidal Energy Conference*, p. {1160\hyphen 1}--{1160\hyphen 7}.

Clark, T. H. E. (2015) 'Turbulence in Marine Environments (TiME): A framework for understanding turbulence and its effects on tidal devices .', *Proceedings of the 11th European Wave and Tidal Energy Conference*, pp. 1–10.

Clerc, A. *et al.* (2012) 'A systematic method for quantifying wind flow modelling uncertainty in wind resource assessment', *Journal of Wind Engineering and Industrial Aerodynamics*, 111, pp. 85–94. doi: 10.1016/j.jweia.2012.08.006.

Clerc, A., Anderson, M. and Stuart, P. (2012) 'A systematic method for quantifying wind flow modelling uncertainty in wind resource assessment.', *Journal of Wind Engineering and Industrial Aerodynamics*, 111, p. 85.

Cockburn, B. and Shu, C.-W. (1998) 'The Runge–Kutta Discontinuous Galerkin Method for Conservation Laws V: Multidimensional Systems', *Journal of Computational Physics*. Academic Press, 141(2), pp. 199–224. doi: 10.1006/JCPH.1998.5892.

Codiga, D. L. (2011) 'Unified Tidal Analysis and Prediction Using the UTide Matlab Functions', p. 59. doi: 10.13140/RG.2.1.3761.2008.

Coles, D. S., Blunden, L. S. and Bahaj, A. S. (2017) 'Assessment of the energy extraction potential at tidal sites around the Channel Islands', *Energy*, 124, pp. 171–186. doi: 10.1016/j.energy.2017.02.023.

Committee on Hydromechanics of the Hydraulics Division - ASCE (1963) 'Friction Factors in Open Channels', *Journal of the Hydraulics Division*, 89(2), pp. 97–143.

Cornett, A. (2008) *Guidance for Assessing Tidal Current Energy Resources*.

Cornett, A., Toupin, M. and Nistor, I. (2015) 'Appraisal of IEC Technical Specification for Tidal Energy Resource Assessment at Minas Passage, Bay of Fundy, Canada', in *Proceedings of the 11th European Wave and Tidal Energy Conference*, pp. 1–10.

Corscadden, K. W. *et al.* (2016) 'The Impact of Variable Wind Shear Coefficients on Risk Reduction of Wind Energy Projects', *International Scholarly Research Notices*, 2016, pp. 1–12. doi: 10.1155/2016/5790464.

Costello, K. W. (2018) 'Electrification: The nexus between consumer behavior and public policy', *The Electricity Journal*, 31(1), pp. 1–7. doi: https://doi.org/10.1016/j.tej.2018.01.005.

Crammond, S. *et al.* (2013) 'Meygen Tidal Energy Project, Numerical Modelling of Tidal Turbine Wake Interactions', *Proceedings Tenth European Wave and Tidal Energy Conference.*

Deloitte (2014) *Establishing the investment case Wind power*.

Department of Oceanography, N. P. S. (2018) *Basic Concepts in Physical Oceanography: Tides*.

Derrick, A. (1992) 'Development of the measure-correlate-predict strategy for site assessment', in *Proceedings of the British Wind Energy Association Conference*.

DNV KEMA (2013) *Framework for the Categorisation of Losses and Uncertainty for Wind Energy Assessments*.

Doodson, A. T. (1921) 'The harmonic development of the tide-generating potential', *Proceedings of the Royal Society of London. Series A*, 100(704), pp. 305 LP – 329.

Doppler, C. (1842) 'Über das farbige Licht der Doppelsterne und einiger anderer Gestirne des Himmels'.

DP Marine Energy Ltd (2009) *Islay Tidal Energy Project: Environmental Impact Assessment Report*.

Draper, S. (2011) *Tidal Stream Energy Extraction in Coastal Basins By Tidal Stream Energy Extraction in Coastal Basins*. University of Oxford.

Draper, S. *et al.* (2013a) 'An electrical analogy for the Pentland Firth tidal stream power resource', *Proceedings of the Royal Society A: Mathematical, Physical and Engineering Science*, (470), p. 20. doi: 10.1098/rspa.2013.0207.

Draper, S. *et al.* (2013b) 'An electrical analogy for the Pentland Firth tidal stream power resource', *Proceedings of the Royal Society A: Mathematical, Physical and Engineering Science*, 470. doi: http://dx.doi.org/10.1098/rspa.2013.0207.

EDF R&D *et al.* (2014) 'TELEMAC-2D modelling system - User manual'.

Elasha, F. *et al.* (2017) 'A hybrid prognostic methodology for tidal turbine gearboxes', *Renewable Energy*, 114, pp. 1051–1061. doi: https://doi.org/10.1016/j.renene.2017.07.093.

EMEC (2009) *Assessment of Tidal Energy Resource*. London: The British.

EMEC (2018) *Pathway to Commercialisation*.

EnFAiT (2017) ‘EnFAIT - Enabling Future Arrays in Tidal’. Available at: www.enfait.eu.

Epler, J. (2010) *Tidal Resource Characterization from Acoustic Doppler Current Profilers*. Washington.

Epler, J., Polagye, B. and Thomson, J. (2010) ‘Shipboard acoustic doppler current profiler surveys to assess tidal current resources’, *Oceans 2010 Mts/Ieee Seattle*. Ieee, 2(1), pp. 1–10. doi: 10.1109/OCEANS.2010.5664387.

Foreman, M. G. G., Cherniawsky, J. Y. and Ballantyne, V. A. (2009) ‘Versatile harmonic tidal analysis: Improvements and applications’, *Journal of Atmospheric and Oceanic Technology*, 26(4), pp. 806–817. doi: 10.1175/2008JTECHO615.1.

Foreman, M. G. G. and Henry, R. F. (1989) ‘The harmonic analysis of tidal model time series’, *Advances in Water Resources*, 12(3), pp. 109–120. doi: 10.1016/0309-1708(89)90017-1.

Foreman M.G.G (1996) ‘Manual for tidal heights analysis and prediction’, *Pacific Marine Science Report*, 77(77–10), p. 58.

Frandsen, S. T. (2007) *Turbulence and turbulence- generated structural loading in wind turbine clusters*, *Risoe National Laboratory. Risoe-R; No. 1188*. Roskilde, Denmark. doi: Riso-R-1188.

Fringer, O. B., Gerritsen, M. and Street, R. L. (2006) ‘An unstructured-grid, finite-volume, nonhydrostatic, parallel coastal ocean simulator’, *Ocean Modelling*. Elsevier, 14(3–4), pp. 139–173. doi: 10.1016/J.OCEMOD.2006.03.006.

Froese, M. (2017) *LiDAR becoming top choice as measurement tool for offshore wind sites*. Available at: https://www.windpowerengineering.com/business-news-projects/lidar-becoming-top-choice-measurement-tool-offshore-wind-sites/ (Accessed: 15 March 2018).

García-Rojo, R. (2004) ‘Algorithm for the estimation of the long-term wind climate using a joint probabilistic approach’, *Wind Engineering*, 28(2), pp. 213–223.

Garrad, A. (2012) ‘The lessons learned from the development of the wind energy industry that might be applied to marine industry renewables’, *Philosophical Transactions of the Royal Society A: Mathematical, Physical and Engineering Sciences*, 370(1959), pp. 451–471. doi: 10.1098/rsta.2011.0167.

Garrett, C. and Cummins, P. (2004) ‘Generating Power from Tidal Currents’, *Journal of Waterway, port, coastal and ocean engineering*, (June), pp. 114–118.

Garrett, C. and Cummins, P. (2005) ‘The power potential of tidal currents in channels’,

Proceedings of the Royal Society A: Mathematical, Physical and Engineering Sciences, 461(2060), pp. 2563–2572. doi: 10.1098/rspa.2005.1494.

Garrett, C. and Cummins, P. (2007) 'The efficiency of a turbine in a tidal channel', *Journal of Fluid Mechanics*, 588(2007). doi: 10.1017/S0022112007007781.

Genz, F., Cirano, M. and Lessa, G. C. (2010) 'ProcED: A MATLAB package for processing ADCP estuarine data', *Brazilian Journal of Geophysics*, 28(2), pp. 183–192. doi: 10.1590/S0102-261X2010000200004.

Gipe, P. (1995) *Wind Energy Comes of Age*. New York: John Wiley & Sons Ltd.

Global Wind Energy Council (2017) *Global Wind Statistics 2017*.

Godin, G. (1972) *The analysis of tides*. Toronto: Toronto University Press.

Gooch, S. *et al.* (2009) 'Site Characterization for Tidal Power'.

Green Power Development (2017) *Wind and its measurement in wind energy*.

Gribben, B. and Frazer-Nash Consultancy (2012) 'New Approaches to Offshore Wake Modelling : Validating Results and Driving Industry Acceptance', in *Wind Resource Assessment Workshop*.

Guion, R. U. G. and Young, A. M. (2015) 'The frequency response of acoustic Doppler current profilers: Spatiotemporal response and implications for tidal turbine site assessment', *2014 Oceans - St. John's, OCEANS 2014*. IEEE, pp. 1–10. doi: 10.1109/OCEANS.2014.7003057.

Gunawan, B., Neary, V. S. and McNutt, J. R. (2011) *ORNL ADCP Post-Processing Guide and Matlab Algorithms for MHK Site Flow and Turbulence Analysis*, *Ornl/Tm-2011/404*. Oak Ridge, Tennessee. doi: 10.2172/1034377.

Haigh, I. D., Eliot, M. and Pattiaratchi, C. (2011) 'Global influences of the 18.61 year nodal cycle and 8.85 year cycle of lunar perigee on high tidal levels', *Journal of Geophysical Research*, 116(C6), p. C06025. doi: 10.1029/2010JC006645.

Hamby, D. M. (1994) 'A review of techniques for parameter sensitivity analysis of environmental models', *Environmental Monitoring and Assessment*, (32), pp. 135–154.

Harris, M. *et al.* (2010) 'Validated adjustment of remote sensing bias in complex terrain using CFD', *Ewec 2010*, p. 7.

Hashemi, M. R. *et al.* (2015) 'Effect of waves on the tidal energy resource at a planned tidal stream array', *Renewable Energy*. Elsevier Ltd, 75, pp. 626–639. doi: 10.1016/j.renene.2014.10.029.

Haverson, D. *et al.* (2018) 'Modelling the hydrodynamic and morphological impacts of a tidal stream development in Ramsey Sound', *Renewable Energy*. Pergamon, 126, pp. 876–887. doi: 10.1016/J.RENENE.2018.03.084.

Hay, J. E. *et al.* (2016) 'Introduction to the special issue: Observed and projected changes in weather and climate extremes', *Weather and Climate Extremes*, 11, pp. 1–3. doi: https://doi.org/10.1016/j.wace.2015.08.006.

Hench, J. L. and Luettich, R. A. (2003) 'Transient Tidal Circulation and Momentum Balances at a Shallow Inlet', *Journal of Physical Oceanography*, 33(4), pp. 913–932. doi: 10.1175/1520-0485(2003)33<913:TTCAMB>2.0.CO;2.

Hervouet, J.-M. (2000) 'TELEMAC modelling system: an overview', *Hydrological Processes*, 14(13), pp. 2209–2210. doi: 10.1002/1099-1085(200009)14:13<2209::AID-HYP23>3.0.CO;2-6.

Hervouet, J.-M. (2007) *Hydrodynamics of Free Surface Flows: Modelling with the finite element method*. Chichester, UK: John Wiley & Sons, Ltd. doi: 10.1002/9780470319628.

Hodgetts, B. and GL Garrad Hassan (2012) 'Measurement campaigns – What have we learnt since the days of the 10 m masts?', in *Wind Resource Assessment Workshop*.

Högselius, P. and Kaijser, A. (2019) 'Energy dependence in historical perspective: The geopolitics of smaller nations', *Energy Policy*, 127, pp. 438–444. doi: https://doi.org/10.1016/j.enpol.2018.12.025.

Holt, J. T. *et al.* (2005) 'Error quantification of a high-resolution coupled hydrodynamic–ecosystem coastal–ocean model: Part 1 model overview and assessment of the hydrodynamics', *Journal of Marine Systems*. Elsevier, 57(1–2), pp. 167–188. doi: 10.1016/J.JMARSYS.2005.04.008.

Houlsby, G. T., Draper, S. and Oldfield, M. L. G. (2008) *Application of Linear Momentum Actuator Disc Theory to Open Channel Flow*.

Houlsby, G. and Vogel, C. (2016) *The power available to tidal turbines in an open channel flow*, *Proceedings of the Institution of Civil Engineers - Energy*. doi: 10.1680/jener.15.00035.

House of Commons Science and Technology Select Committee (2001) *Third Special Report*.

Huggett, R. J. (2007) *Fundamentals of Geomorphology*. Third. Oxon: Routledge, Taylor & Francis.

Hunter, W., Nishino, T. and Willden, R. H. J. (2013) 'Investigation of Tidal Turbine Arrays using

3D Reynolds-Averaged Navier-Stokes Simulations', *10th European Wave and Tidal Energy Conference*.

Hyndman, R. J. and Athanasopoulos, G. (2013) *Forecasting: principles and practice*. Monash University, Australia.

IEC (2005) *International Standard - IEC 61400-12-1 - Power performance measurements of electricity producing wind turbines*.

IEC (2015) *Technical Specification - Marine Energy - Part 201: Tidal Energy Resource Assessment and Characterization*.

International Energy Agency Technology Collaboration Programme (2003) *Wind Speed Measurement and Use of Cup Anemometry*, *Recommended Practices for Wind Turbine Testing*. doi: 10.1121/1.394734.

Iowa State University (2012) *Measurement Uncertainty*, *NDT Resource Center*.

IRENA (2018) *Renewable Power Generation Costs in 2017*, *International Renewable Energy Agency*. Abu Dhabi. doi: 10.1007/SpringerReference_7300.

ISO (2005) 'ISO/IEC 17025:2005 General requirements for the competence of testing and calibration laboratories'. International Organization for Standardization.

Iyer, A. S. (2010) 'TIDAL SITE CHARACTERISATION USING ADCP RECORD 1 AND 2'.

Iyer, A. S. (2011) 'New Methodologies and Scenarios for Evaluating Tidal Current Energy Potential', *Doctor of Philosophy Dissertation,The University of Edinburgh, Edinburgh*, (November).

Iyer, A. S. *et al.* (2013) 'Variability and phasing of tidal current energy around the United Kingdom', *Renewable Energy*, 51, pp. 343–357. doi: 10.1016/j.renene.2012.09.017.

Jenkins, G., Perry, M. and Prior, J. (2009) *The climate of the United Kingdom and recent trends*. Exeter.

Jensen, N. O. (1983) 'A note on wind generator interaction', *Riso National Laboratory Roskilde*, 2411, pp. 1–16. doi: Riso-M-2411.

Jeuken, M. C. J. L. *et al.* (2003) 'Morphological response of estuaries to nodal tide variation', in *International Conference on Estuaries and Coasts*. Hangzhou, China, pp. 166–173.

Johnson, C., White, E. and Jones, S. (2008) *Summary of Actual vs. Predicted Wind Farm*

Performance – Recap of Windpower 2008, *AWEA Wind Resource Assessment Workshop Presentation*.

Joint Committee For Guides In Metrology (2008) 'Evaluation of measurement data — Guide to the expression of uncertainty in measurement', *International Organization for Standardization Geneva ISBN*, 50(September), p. 134. doi: 10.1373/clinchem.2003.030528.

Joly, A. *et al.* (2013) *Tidal farm modelling : The Alderney Race , the Pentland Firth and the Paimpol-Bréhat sites modelled in Telemac software*.

Joly, A. *et al.* (2015) 'Using the DRAGFO subroutine to model Tidal Energy Converters in Telemac-2D', in *XXII TELEMAC-MASCARET User Conference*, pp. 182–189.

Jonsson, C. (2010) *Statistical analysis of wind data regarding long-term correction*. Uppsala.

Jung, S., Arda Vanli, O. and Kwon, S. D. (2013) 'Wind energy potential assessment considering the uncertainties due to limited data', *Applied Energy*, 102, pp. 1492–1503. doi: 10.1016/j.apenergy.2012.09.011.

Kaldellis, J. K. and Zafirakis, D. (2011) 'The wind energy (r)evolution: A short review of a long history', *Renewable Energy*, 36(7), pp. 1887–1901. doi: 10.1016/j.renene.2011.01.002.

Karsten, R. H. *et al.* (2008) 'Assessment of tidal current energy in the Minas Passage, Bay of Fundy', *Proceedings of the Institution of Mechanical Engineers, Part A: Journal of Power and Energy*, pp. 493–507. doi: 10.1243/09576509JPE555.

Khan, K. S. and Tariq, M. (2018) 'Wind resource assessment using SODAR and meteorological mast – A case study of Pakistan', *Renewable and Sustainable Energy Reviews*, pp. 2443–2449. doi: 10.1016/j.rser.2017.06.050.

Khare, V. *et al.* (2019) 'Chapter 7 - Tidal Energy Assessment and Economics', in Khare, V. et al. (eds). Elsevier, pp. 331–394. doi: https://doi.org/10.1016/B978-0-12-814881-5.00007-7.

Klinkert, R. (2012) *Uncertainty Analysis of Long Term Correction Methods for Annual Average Winds*. UMEA, Norway.

KONA (2017) *Met Mast Rental*. Available at: http://konastructures.com/met-mast-rental/ (Accessed: 14 June 2017).

Kramer, S. C. and Piggott, M. D. (2016) 'A correction to the enhanced bottom drag parameterisation of tidal turbines', *Renewable Energy*, 92, pp. 385–396. doi: 10.1016/j.renene.2016.02.022.

Kreitmair, M. (2018) *Uncertainty quantification in tidal energy resource assessment*. The University of Edinburgh.

Kwon, S.-D. (2010) 'Uncertainty analysis of wind energy potential assessment', *Applied Energy*, 87, pp. 856–865.

Lackner, M. A., Rogers, A. L. and Manwell, J. F. (2007) 'Uncertainty analysis in wind resource assessment and wind energy production estimation', *45th AIAA Aerospace Sciences Meeting and Exhibit*, pp. 1–16. doi: doi:10.2514/6.2007-1222.

Lamy, J. V and Azevedo, I. L. (2018) 'Do tidal stream energy projects offer more value than offshore wind farms? A case study in the United Kingdom', *Energy Policy*, 113, pp. 28–40. doi: https://doi.org/10.1016/j.enpol.2017.10.030.

Lee, K. *et al.* (2013) 'Uncertainty in open channel discharge measurements acquired with StreamPro ADCP', 509(2014), pp. 101–114.

Leffler, K. E. and Jay, D. A. (2009) 'Enhancing tidal harmonic analysis: Robust (hybrid L1 / L2) solutions', *Continental Shelf Research*, 29(1), pp. 78–88. doi: 10.1016/j.csr.2008.04.011.

Leopold, L. B. (1953) 'Downstream change of velocity in rivers', *American Journal of Science*, 251, pp. 606–624.

Levesque, V. A. and Oberg, K. A. (2012) *Computing Discharge Using the Index Velocity Method*, *U.S. Geological Survey Techniques and Methods 3–A23*. Reston, Virginia.

Lewis, M. *et al.* (2015) 'Resource assessment for future generations of tidal-stream energy arrays', *Energy*. Elsevier Ltd, 83, pp. 403–415. doi: 10.1016/j.energy.2015.02.038.

Lewis, M. *et al.* (2017a) 'Characteristics of the velocity profile at tidal-stream energy sites', *Renewable Energy*, 114, pp. 258–272. doi: 10.1016/j.renene.2017.03.096.

Lewis, M. *et al.* (2017b) 'Characteristics of the velocity profile at tidal-stream energy sites', *Renewable Energy*, 114, pp. 258–272. doi: 10.1016/j.renene.2017.03.096.

Li, W. *et al.* (2016) 'Review on the blade design technologies of tidal current turbine', *Renewable and Sustainable Energy Reviews*, 63, pp. 414–422. doi: https://doi.org/10.1016/j.rser.2016.05.017.

Liebowitz, D., Criminisi, A. and Zisserman, A. (1999) 'Creating Architectural Models from Images', 18(3).

Lileo, S. *et al.* (2013) 'Long-term correction of wind measurements. State-of-the-art, guidelines and future work', *Ewea*, (January), pp. 1–10.

Lira, A. G. *et al.* (2014) 'Uncertainties in the estimate of wind energy production', p. 12.

Lockhart, T. J. and Bailey, B. H. (1998) *The Maximum Type 40 Anemometer Calibration Project*, *NRG Systems*.

Lu, Y. and Lueck, R. (1999) 'Using a Broadband ADCP in a Tidal Channel. Part I: Mean Flow and Shear', *Journal of atmospheric and oceanic technology*, pp. 1556–1567.

Lynch, D. R. and Davies, A. M. (1995) *Quantitative Skill Assessment for Coastal Ocean Models*. Volume 47. Edited by D. R. Lynch and A. M. Davies. Washington, D. C.: American Geophysical Union (Coastal and Estuarine Studies). doi: 10.1029/CE047.

Lyndon Department of Atmospheric Sciences (2000) *Making Meteorological Measurements - Uncertainty*.

MacGillivray, A. (2016) *Economically Sustainable Development of Wave and Tidal Stream Energy Technologies*. The University of Edinburgh.

MacKay, D. J. C. (2008) *Sustainable Energy - Without the Hot Air*.

Mahdavimanesh, M. *et al.* (2013) 'Lagrangian particle tracking: Model development', *Life Science Journal*, 10(8), pp. 34–41.

Manning, R. (1895) 'On the flow of water in open channels and pipes', *Transactions of the Institution of Civil Engineers of Ireland*, (24), pp. 179–207.

Manwell, J. F. *et al.* (2006) *Hybrid2 - A hybrid system simulation model theory manual*. Massachusetts.

Marine Energy (2018) *MeyGen tidal array reconnects all four turbines to grid*. Available at: https://marineenergy.biz/2018/12/19/meygen-tidal-array-reconnects-all-four-turbines-to-grid/.

Marsden, R. F. and Ingram, R. G. (2004) 'Correcting for beam spread in acoustic Doppler current profiler measurements', *Journal of Atmospheric and Oceanic Technology*, 21(9), pp. 1491–1498. doi: 10.1175/1520-0426(2004)021<1491:CFBSIA>2.0.CO;2.

Marshall, T. (2015) *Prisoners of Geography*. Elliott & Thompson.

MathWorks (2018) *Matlab*.

McCombes, T. *et al.* (2010) 'Deliverable 3.4 - Best practice for tank testing of small marine energy devices', *EquiMar Project*, pp. 1–48.

Measnet (2009) 'MEASNET Procedure: Evaluation of Site Specific Wind Conditions', *Measnet*,

1(November), pp. 1–53.

Miftakhova, A. *et al.* (2019) 'Statistical approximation of high-dimensional climate models', *Journal of Econometrics*. doi: https://doi.org/10.1016/j.jeconom.2019.05.005.

Miller, R. G. (1974) 'The Jackknife - A Review', *Biometrika*, pp. 1–15.

Mitsubishi Electric (2017) *Doppler Lidar Systems*. Available at: http://www.mitsubishielectric.com/bu/lidar/lidar/applications/apps_01.html (Accessed: 2 August 2017).

Montavon, C. (2011) 'Offshore wind accelerator: wake modelling using CFD', in *EWEA Offshore Conference*.

Montavon, C. and ANSYS (2010) 'Wind Farm Flow Modelling Using CFD'. ANSYS. Available at: https://www.ansys.com/en-gb/resource-library/webinar/wind-farm-flow-modeling-using-cfd.

Moorthy, C. B. and Deshmukh, M. (2016) 'Wind Resource Assessment Using Computer Simulation Tool: A Case Study', *Energy Procedia*, 100, pp. 141–148. doi: 10.1016/j.egypro.2016.10.156.

Moriarty, P. *et al.* (2014) 'IEA-task 31 WAKEBENCH: Towards a protocol for wind farm flow model evaluation. Part 2: Wind farm wake models', *Journal of Physics: Conference Series*, 524(1). doi: 10.1088/1742-6596/524/1/012185.

Mortensen, N. G. and Jørgensen, H. E. (2011) 'Comparison of Resource and Energy Yield Assessment Procedures', in *EWEA Wind Resource Assessment Technology Workshop 2011*.

Mortensen, N. G., Nielsen, M. and Ejsing Jørgensen, H. (2015) *Offshore CREYAP Part 2 – final results*, *EWEA Technology Workshop*. Copenhagen, Denmark.

Mortimer, A. A. (1994) 'A New Correlation/Prediction Method for Potential Wind Farm Sites', in *16th British Wind Energy Conference*. Stirling, UK, pp. 259–265.

Moulinec, C. *et al.* (2011) 'TELEMAC: An efficient hydrodynamics suite for massively parallel architectures', *Computers and Fluids*, 51(1), pp. 30–34. doi: 10.1016/j.compfluid.2011.07.003.

Murphy, J. M. *et al.* (2004) 'Quantification of modelling uncertainties in a large ensemble of climate change simulations', *Nature*, 430(7001), pp. 768–772. doi: 10.1038/nature02771.

Murray, R. O. and Gallego, A. (2017) 'A modelling study of the tidal stream resource of the Pentland Firth, Scotland', *Renewable Energy*, 102, pp. 326–340. doi: 10.1016/j.renene.2016.10.053.

Murthy, K. S. R. and Rahi, O. P. (2017) 'A comprehensive review of wind resource assessment', *Renewable and Sustainable Energy Reviews*, 72, pp. 1320–1342. doi: 10.1016/j.rser.2016.10.038.

Myers, L. E. and Bahaj, A. S. (2010) 'Experimental analysis of the flow field around horizontal axis tidal turbines by use of scale mesh disk rotor simulators', *Ocean Engineering*. Pergamon, 37(2–3), pp. 218–227. doi: 10.1016/J.OCEANENG.2009.11.004.

National Institute of Water and Atmospheric Research Ltd. (2016) *How do we map the seafloor?* Available at: https://www.niwa.co.nz/coasts-and-oceans/faq/how-do-we-map-the-seafloor (Accessed: 30 September 2017).

National Renewable Energy Laboratory (2012) *IEA Wind Task 26: The Past and Future Cost of Wind Energy*, *IEA Wind*. Golden, CO.

Nfaoui, H., Essiarab, H. and Sayigh, A. A. M. (2004) 'A stochastic Markov chain model for simulating wind speed time series at Tangiers, Morocco', *Renewable Energy*, 29(8), pp. 1407–1418. doi: 10.1016/S0960-1481(03)00143-5.

Nikuradse, J. (1933) 'Gesetzmäßigkeiten der turbulenten Strömung in glatten Rohren (Nachtrag)', *Forschung auf dem Gebiete des Ingenieurwesens*, 4(1), pp. 44–44. doi: 10.1007/BF02716946.

Nishino, T. and Willden, R. H. J. (2012) 'The efficiency of an array of tidal turbines partially blocking a wide channel', *Journal of Fluid Mechanics*. Cambridge University Press, 708, pp. 596–606. doi: 10.1017/jfm.2012.349.

NOAA (2001) *Tidal datums and their applications*. Silver Spring, Maryland.

Noguera-Santaella, J. (2016) 'Geopolitics and the oil price', *Economic Modelling*, 52, pp. 301–309. doi: https://doi.org/10.1016/j.econmod.2015.08.018.

Nortek AS (2017) *Principles of Operation - Signature Manual*.

Nortek AS (no date) *Nortek Signature 1000/500 Datasheet*.

Nourani, V., Gökçekuş, H. and Umar, I. K. (2019) 'Artificial intelligence based ensemble model for prediction of vehicular traffic noise', *Environmental Research*, p. 108852. doi: https://doi.org/10.1016/j.envres.2019.108852.

Nystrom, E. A., Oberg, K. A. and Rehmann, C. R. (2002) 'Measurement of Turbulence with Acoustic Doppler Current Profilers - Sources of Error and Laboratory Results', *Hydraulic Measurements and Experimental Methods 2002*, pp. 1–10. doi: 10.1061/40655(2002)55.

Nystrom, E., Oberg, K. and Rehmann, C. (2003) 'Measurement of Turbulence with Acoustic

Doppler Current Profilers - Sources of Error and Laboratory Results'. doi: 10.1061/40655(2002)55.

Ó'Catháin, M. (2012) 'Towards increased confidence in wave and tidal energy production estimates', *4th International Conference on Ocean Energy*, pp. 2–7.

O'Doherty, T. *et al.* (2010) 'Considerations of a horizontal axis tidal turbine', *Proceedings of Institution of Civil Engineers: Energy*, 163(3), pp. 119–130. doi: 10.1680/ener.2010.163.3.119.

Ocean Energy Europe (2017) *Ocean energy project spotlight: Investing in tidal and wave energy*.

Offshore Renewable Energy Catapult (2014) *Financing solutions for wave and tidal energy*.

Olivecrona, C. (1995) 'Wind energy in Denmark', in *Green Budget Reform*, pp. 55–68.

Oost, A. P. *et al.* (1993) 'The 18.6 yr nodal cycle and its impact on tidal sedimentation', *Sedimentary Geology*, 87(1–2), pp. 1–11. doi: 10.1016/0037-0738(93)90032-Z.

Open University (1989) *Waves, Tides and Shallow Water Processes*. Elsevier. doi: 10.1016/C2009-0-24331-5.

Ordnance Survey (2018) *Mapping data and georgraphic information from OS*. Available at: https://www.ordnancesurvey.co.uk/opendatadownload/products.html (Accessed: 26 March 2018).

ORE Catapult (2015a) *Framework for the Categorisation of Losses and Uncertainty for Wave and Tidal Energy Assessments*.

ORE Catapult (2015b) 'Wave and Tidal Energy Yield Uncertainty - Literature Review', (July), pp. 385–396. doi: 10.1016/B0-12-176480-X/00344-2.

ORE Catapult (2015c) *Wave and Tidal Energy Yield Uncertainty - Reference Document*.

OREC (2018) *Tidal stream and wave energy cost reduction and industrial benefit*.

Ott, M. W. (2002) 'An improvement in the calculation of ADCP velocities', *Journal of Atmospheric and Oceanic Technology*, 19(10), pp. 1738–1741. doi: 10.1175/1520-0426(2002)019<1738:AIITCO>2.0.CO;2.

Ott, S., Berg, J. and Nielsen, M. (2011) *Linearised CFD Models for Wakes*, *Risø Nationallaboratoriet for Baeredygtig Energi.* Roskilde, Denmark: APAEN.

Palisade Corporation (2015) *User's Guide @RISK Risk Analysis and Simulation Add-In for Microsoft*. Available at: http://www.palisade.com/downloads/documentation/7/EN/RISK7_EN.pdf (Accessed: 4 February

2018).

Parker, B. B. (2007) *Tidal Analysis and Prediction*, *NOAA Special Publication*. Silver Spring, Maryland. doi: 10.1017/CBO9781139235778.007.

Parsons, D. R. *et al.* (2013) 'Velocity Mapping Toolbox (VMT): A processing and visualization suite for moving-vessel ADCP measurements', *Earth Surface Processes and Landforms*, 38(11), pp. 1244–1260. doi: 10.1002/esp.3367.

Passeri, D. L. *et al.* (2015) 'The dynamic effects of sea level rise on low-gradient coastal landscapes : A review', *Earth's Future*, 3, pp. 1–23. doi: 10.1002/2015EF000298.Received.

Pawlowicz, R., Beardsley, B. and Lentz, S. (2002) 'Classical tidal harmonic analysis including error estimates in MATLAB using T_TIDE', *Computers & Geosciences*, 28(8), pp. 929–937. doi: 10.1016/S0098-3004(02)00013-4.

Pedersen, T. F. (2004) *Characterisation and Classification of RISØ P2546 Cup Anemometer*, *Risø National Laboratory*. Roskilde. doi: Risø-R-1364.

Pedersen, T. F., Dahlberg, J.-Å. and Busche, P. (2006) *ACCUWIND - Classification of Five Cup Anemometers According to IEC61400-12-1*, *Risø National Laboratory*. Roskilde. doi: Risø-R-1556(EN).

Pérez-Ortiz, A., Pescatore, J. and Bryden, I. (2013) 'A Systematic Approach to Undertake Tidal Energy Resource Assessment with Telemac-2D', *10th European Wave and Tidal Energy Conference*, p. 9.

Piano, M. ; *et al.* (2015) 'Characterizing the tidal energy resource of the West Anglesey Demonstration Zone (UK), using TELEMAC-2D and field observations', in *XXIIth Telemac-Mascaret User Conference*. Daresbury, pp. 202–210.

Pilkey, O. H. and Pilkey-Javis, L. (2007) 'Useless arithmetic: Why environmental scientists can't predict the future', *Integrated Environmental Assessment and Management*, 3(4), p. 567. doi: 10.1002/ieam.5630030416.

Platis, A. *et al.* (2018) 'First in situ evidence of wakes in the far field behind offshore wind farms', *Nature Scientific Reports*, 8. doi: 10.1038/s41598-018-20389-y.

Polagye, B. *et al.* (2008) *Effect of large-scale kinetic power extraction on time-dependent estuaries*, *Proceedings of The Institution of Mechanical Engineers Part A-journal of Power and Energy - PROC INST MECH ENG A-J POWER*. doi: 10.1243/09576509JPE519.

Polagye, B. and Thomson, J. (2013) 'Tidal energy resource characterization: methodology and field study in Admiralty Inlet, Puget Sound, US', *Proceedings of the Institution of Mechanical Engineers, Part A: Journal of Power and Energy*, 227(3), pp. 352–367. doi: 10.1177/0957650912470081.

Pontius Jr, R. G., Thontteh, O. and Chen, H. (2008) 'Components of information for multiple resolution comparison between maps that share a real variable', *Environmental and Ecological Statistics*, 15(2), pp. 111–142. doi: https://doi.org/10.1007/s10651-007-0043-y.

Pugh, D. T. (1996) *Tides, surges and mean sea-level*. John Wiley & Sons Ltd.

Qing, F. and Qian-Lu, X. (2015) 'Velocity and shear stress profiles for tidal effected channels', *Ocean Engineering*, 101, pp. 172–181. doi: 10.1016/j.oceaneng.2015.04.013.

Rahman, A. and Venugopal, V. (2015) 'Inter-Comparison of 3D Tidal Flow Models Applied to Orknet Islands and Pentland Firth', in *Proceedings of the 11th European Wave and Tidal Energy Conference*. Nantes.

Rao, R. S., Vaishnavi, T. and Pais, A. R. (2019) 'PhishDump: A multi-model ensemble based technique for the detection of phishing sites in mobile devices', *Pervasive and Mobile Computing*, 60, p. 101084. doi: https://doi.org/10.1016/j.pmcj.2019.101084.

Rawlinson-smith, R. I. *et al.* (2010) 'The PerAWaT project : Performance Assessment of Wave and Tidal Array Systems', in *3rd International Conference on Ocean Energy*. Bilbao, pp. 1–7.

Rehman, S., Mohandes, M. A. and Alhems, L. M. (2018) 'Wind speed and power characteristics using LiDAR anemometer based measurements', *Sustainable Energy Technologies and Assessments*, 27, pp. 46–62. doi: 10.1016/j.seta.2018.03.009.

Reid, S. (2016) *Nova Innovation secures EC funding for tidal generator*, *The Scotsman*. Available at: https://www.scotsman.com/news/nova-innovation-secures-ec-funding-for-tidal-generator-1-4294962.

reNEWS (2016) *Atlantis to decommission SeaGen*, *reNEWS.biz*. Available at: https://renews.biz/44355/atlantis-to-decommission-seagen/.

reNEWS (2018) *Scots tidal hits milestone*, *reNEWS.biz*. Available at: https://renews.biz/47449/scots-tidal-hits-milestone/.

Riedel, V., Strack, M. and Waldl, H. (2001) 'Robust Approximation of Functional Relationships Between Meterological Data: Alternative Measure-Correlate-Predict Algorithms', in *European Wind Energy Conference*. Copenhagen, Denmark, pp. 806–809.

van Rijn, L. C. (2005) ‘Principles of sedimentation and erosion engineering in rivers, estuaries and coastal seas’, *Aqua Publications*, pp. 1–15.

Rogers, A. L., Rogers, J. W. and Manwell, J. F. (2005a) ‘Comparison of the performance of four measure-correlate-predict algorithms’, *Journal of Wind Engineering and Industrial Aerodynamics*, 93(3), pp. 243–264. doi: 10.1016/j.jweia.2004.12.002.

Rogers, A. L., Rogers, J. W. and Manwell, J. F. (2005b) ‘Uncertainties in Results of Measure-Correlate- Predict Analyses’, in *American Wind Energy Association*. Denver, CO.

Ruhnau, O. *et al.* (2019) ‘Direct or indirect electrification? A review of heat generation and road transport decarbonisation scenarios for Germany 2050’, *Energy*, 166, pp. 989–999. doi: https://doi.org/10.1016/j.energy.2018.10.114.

Rumsey, D. J. (2011) *Statistics for Dummies*. 2nd Editio. Edited by C. Collins et al. Hoboken, NJ: Wiley Publishing Inc.

Russell, F. P. *et al.* (2017) ‘Exploiting the chaotic behaviour of atmospheric models with reconfigurable architectures’, *Computer Physics Communications*, 221, pp. 160–173. doi: https://doi.org/10.1016/j.cpc.2017.08.011.

Saltelli, A. (2002) ‘Sensitivity Analysis for Importance Assessment’, *Society for Risk Analysis*, 22(3).

Saltelli, A. and Annoni, P. (2010) ‘How to avoid a perfunctory sensitivity analysis’, *Environmental Modelling and Software*, 25(12), pp. 1508–1517. doi: 10.1016/j.envsoft.2010.04.012.

Saruwatari, A., Ingram, D. M. and Cradden, L. (2013) ‘Wave–current interaction effects on marine energy converters’, *Ocean Engineering*. Pergamon, 73, pp. 106–118. doi: 10.1016/J.OCEANENG.2013.09.002.

Schureman, P. (1941) *Manual of Harmonic Analysis and Prediction of Tides*. Washington.

Scottish Government (2019) *Saltire Tidal Energy Challenge Fund*. Available at: https://www.gov.scot/news/saltire-tidal-energy-challenge-fund/.

Segura, E. *et al.* (2017) ‘Techno-economic challenges of tidal energy conversion systems: Current status and trends’, *Renewable and Sustainable Energy Reviews*, 77, pp. 536–550. doi: https://doi.org/10.1016/j.rser.2017.04.054.

Serhadlioğlu, S. *et al.* (2013) ‘Tidal stream energy resource assessment of the Anglesey Skerries’, *International Journal of Marine Energy*, 3–4. doi: 10.1016/j.ijome.2013.11.014.

SgurrEnergy and Solórzano, C. (2006) *Effect of Climate Change on UK Wind Speeds*. Glasgow.

Shah, S. (2018) *Improved uncertainty analysis for tidal energy project development*.

Shankleman, J. (2015) *Siemens offloads Marine Current Turbines to Atlantis Resources*, *Business Green*.

Sharp, E. *et al.* (2015) 'Evaluating the accuracy of CFSR reanalysis hourly wind speed forecasts for the UK, using in situ measurements and geographical information', *Renewable Energy*, 77, pp. 527–538. doi: 10.1016/j.renene.2014.12.025.

Shinozuka, M. and Jan, C.-M. (1972) 'Digital simulation of random processes and its applications', *Journal of Sound and Vibration*. Academic Press, 25(1), pp. 111–128. doi: 10.1016/0022-460X(72)90600-1.

SIMEC Atlantis Energy (2019) *Tidal Stream Projects - MeyGen*. Available at: https://simecatlantis.com/projects/meygen/.

Simley, E. and Pao, L. Y. (2012) *LIDAR wind speed measurements of evolving wind fields*, *National Renewable Energy Laboratory*. Boulder, Colorado. doi: 10.2514/6.2012-656.

Smith, K. (2011) 'The Danish wind industry 1980-2010: Lessons for the British marine energy industry', *Underwater Technology*, 30(1), pp. 27–33. doi: 10.3723/ut.30.027.

Song, S. *et al.* (2019) 'The effect of biofouling on the tidal turbine performance'.

Sontek (2001) *SonWave-PRO : Directional Wave Data Collection*, *SonTek Technical Notes*. San Diego.

Soulsby, R. (1997) *Dynamics of Marine Sands: A Manual for Practical Applications*. Thomas Telford.

Soulsby, R. L. *et al.* (1993) 'Wave-current interaction within and outside the bottom boundary layer', *Coastal Engineering*. Elsevier, 21(1–3), pp. 41–69. doi: 10.1016/0378-3839(93)90045-A.

Stock-Williams, C., Parkinson, S. and Gunn, K. (2013) 'An Investigation of Uncertainty in Yield Prediction for Tidal Current Farms', *EWTEC 2013 Proceedings*.

Sufian, S. F., Li, M. and O 'connor, B. A. (2017) '3D Modeling of Impacts from Waves on Tidal Turbine Wake Characteristics and Energy Output', *Renewable Energy*, (17). doi: 10.1016/j.renene.2017.04.030.

Sumer, B. and Fredsoe, J. (2002) *The Mechanics of Scour in the Marine Environment*. doi:

10.1142/4942.

Sutherland, D. R. J., Sellar, B. G. and Bryden, I. (2012) 'The use of Doppler Sensor Arrays to Characterise Turbulence at Tidal Energy Sites', *4th International Conference on Ocean Energy*, (1), pp. 1–6.

Sutherland, G., Foreman, M. and Garrett, C. (2007) 'Tidal current energy assessment for Johnstone Strait, Vancouver Island', *Proceedings of the Institution of Mechanical Engineers, Part A: Journal of Power and Energy*, 221(2), pp. 147–157. doi: 10.1243/09576509JPE338.

Tamura, J. (2012) 'Calculation Method of Losses and Efficiency of Wind Generators', *Wind Energy Conversion Systems*. doi: 10.1007/978-1-4471-2201-2.

Taylor, J. R. (1997) *An Introduction to Error Analysis*. 2nd Editio. Edited by A. McGuire. University Science Books.

Teledyne RD Instruments (2011) *Acoustic doppler current profilers principles of operation: A practical primer*, *RD Instruments*.

Teledyne RD Instruments (2013) 'Workhorse Sentinel Datasheet', pp. 4–5.

Telemac (2007) 'FUDAA - Graphic User Interface for Telemac'.

The World Bank and Climate Investment Funds (2013) *Financing Renewable Energy: Options for Developing Financing Instruments Using Public Funds*.

Thomson, J. *et al.* (2012) 'Measurements of turbulence at two tidal energy sites in puget sound, WA', *IEEE Journal of Oceanic Engineering*, 37(3), pp. 363–374. doi: 10.1109/JOE.2012.2191656.

Thomson, M., Whelan, J. and Gill, L. (2011) 'The Development of a Tool for the Design and Optimisation of Tidal Stream Turbine Arrays', in *European Wave and Tidal Energy Conference*.

Thomson, W. (1881) 'The Tide Guage, tidal harmonic analyser, and tide predicter', *Minutes of the Proceedings of the Institution of Civil Engineers*, 65(1881), pp. 2–25. doi: 10.1680/imotp.1881.22262.

Togneri, M. *et al.* (2017) 'Comparison of ADCP observations and 3D model simulations of turbulence at a tidal energy site', *Renewable Energy*, 114, pp. 273–282. doi: 10.1016/j.renene.2017.03.061.

Touimi, K., Benbouzid, M. and Tavner, P. (2018) 'Tidal stream turbines: With or without a Gearbox?', *Ocean Engineering*, 170, pp. 74–88. doi:

https://doi.org/10.1016/j.oceaneng.2018.10.013.

Tovey, M. (1989) 'Drawing and CAD in industrial design', *Design Studies*. Elsevier, 10(1), pp. 24–39. doi: 10.1016/0142-694X(89)90022-7.

Troup, H. (2016) 'Electricity is on track for decarbonisation, but what about decarbonising heat?', *Renewable Energy Focus*, 17(5), pp. 178–179. doi: https://doi.org/10.1016/j.ref.2016.08.008.

UK Hydrographic Office (2006) *Harmonic Constants Product Specifation*.

UK Hydrographic Office (2018) *Admiralty TotalTide*.

United Nations (2015) 'Paris Agreement'.

Vennell, R. (2011) 'Estimating the power potential of tidal currents and the impact of power extraction on flow speeds', *Renewable Energy*. Pergamon, 36(12), pp. 3558–3565. doi: 10.1016/J.RENENE.2011.05.011.

Vennell, R. (2016) 'An optimal tuning strategy for tidal turbines', *Proceedings of the Royal Society A: Mathematical, Physical and Engineering Science*, (472). doi: 10.1098/rspa.2013.0047.

Vermeulen, B., Sassi, M. G. and Hoitink, A. J. F. (2014) 'Improved flow velocity estimates from moving-boat ADCP measurements', *Water Resources Research*, 50(5), pp. 4186–4196. doi: 10.1002/2013WR015152.

Vögler, A. *et al.* (2017) 'The wave and tidal resource of Scotland', *Renewable Energy*. Pergamon, 114, pp. 3–17. doi: 10.1016/J.RENENE.2017.03.027.

Waldman, S. *et al.* (2017) 'Implementation of tidal turbines in MIKE 3 and Delft3D models of Pentland Firth & Orkney Waters', *Ocean & Coastal Management*, 147, pp. 21–36. doi: 10.1016/j.ocecoaman.2017.04.015.

Walker, J. M. *et al.* (2014) 'Experimental and numerical studies of blade roughness and fouling on marine current turbine performance', *Renewable Energy*. Pergamon, 66, pp. 257–267. doi: 10.1016/j.renene.2013.12.012.

Walker, K. *et al.* (2016) 'An evaluation of the predictive accuracy of wake effects models for offshore wind farms', *Wind Energy*, 19(April 2013), pp. 657–669. doi: 10.1002/we.

Walkington, I. and Burrows, R. (2009) 'Modelling tidal stream power potential', *Applied Ocean Research*. Elsevier Ltd, 31(4), pp. 239–245. doi: 10.1016/j.apor.2009.10.007.

Wanis, P., Symonds, D. and Hull, M. (2015) 'Automating the Quality Screening of Acoustic

Doppler Current Profiler Data', in *2015 IEEE/OES Eleveth Current, Waves and Turbulence Measurement (CWTM)*, pp. 1–5. doi: 10.1109/CWTM.2015.7098145.

Ward, S. L. *et al.* (2015) 'Classifying seabed sediment type using simulated tidal-induced bed shear stress', *Marine Geology*. Elsevier, 367, pp. 94–104. doi: 10.1016/J.MARGEO.2015.05.010.

Warren, I. R. and Bach, H. K. (1992) 'MIKE 21: a modelling system for estuaries, coastal waters and seas', *Environmental Software*. Elsevier, 7(4), pp. 229–240. doi: 10.1016/0266-9838(92)90006-P.

Werapun, W., Tirawanichakul, Y. and Waewsak, J. (2017) 'Wind Shear Coefficients and their Effect on Energy Production', in *Energy Procedia*, pp. 1061–1066. doi: 10.1016/j.egypro.2017.10.111.

Westwood, A. (2008) 'SeaGen installation moves forward', *Renewable Energy Focus*, 9(3), pp. 26–27. doi: https://doi.org/10.1016/S1471-0846(08)70087-8.

Willmott, C. J. and Matsuura, K. (2006) 'On the use of dimensioned measures of error to evaluate the performance of spatial interpolators', *International Journal of Geographical Information Science*, 20(1), pp. 89–102. doi: 10.1080/13658810500286976.

Wilson, P. (2009) *Measurement of the Marine Energy Resource - Practical Solutions for an Expectant Industry*, *International Ocean Systems - Issues Archive*.

Withnall, A. (2015) *Putin's gas threat: What happens if Russia cuts the gas to Europe?*, *Independent*. Available at: https://www.independent.co.uk/news/world/europe/putins-gas-threat-what-happens-if-russia-cuts-the-gas-to-europe-10074294.html.

Wolf, J. and Prandle, D. (1999) 'Some observations of wave–current interaction', *Coastal Engineering*. Elsevier, 37(3–4), pp. 471–485. doi: 10.1016/S0378-3839(99)00039-3.

Wood Plc (2016) *Wind Energy Yield Procedure*.

World Energy Council (2016) *World Energy Resoruces - Marine Energy*.

Yang, Z. *et al.* (2013) 'Modeling In-stream Tidal Energy Extraction and Its Potential Environmental Impacts', in *EWTEC 2013 Proceedings*.

You, Z.-J. (2006) 'Estimation of mean seabed roughness in a tidal channel with an extended log-fit method', *Continental Shelf Research*, 26, pp. 283–294. doi: 10.1016/j.csr.2005.11.009.

Yuan, X.-C. *et al.* (2018) 'China's energy transition strategy at the city level: The role of renewable energy', *Journal of Cleaner Production*, 205, pp. 980–986. doi:

https://doi.org/10.1016/j.jclepro.2018.09.162.

Zervas, C. (1999) *Tidal current analysis procedures and associated computer programs*, *NOAA Technical Memorandum NOS CO-OPS 0021 TIDAL*. Silver Spring, Maryland.

Zhang, J. *et al.* (2017) 'Local blockage effect for wind turbines Assessing blockage of the sensing line in a differential-pressure flow sensor by using the wavelet transform of its output Local blockage effect for wind turbines', *J. Phys.: Conf. Ser*, 625.

Zhu, K. *et al.* (2019) 'Impact of CO2 prices on the design of a highly decarbonised coupled electricity and heating system in Europe', *Applied Energy*, 236, pp. 622–634. doi: https://doi.org/10.1016/j.apenergy.2018.12.016.

Zhu, X. H. *et al.* (2014) 'Tidal and residual currents in the Qiongzhou Strait estimated from shipboard ADCP data using a modified tidal harmonic analysis method', *Journal of Geophysical Research: Oceans*, 119(11), pp. 8039–8060. doi: 10.1002/2014JC009855.

Zio, E. and Pedroni, N. (2013) *Methods for representing uncertainty*. Toulouse, FR.

Zuosheng, Y., Emery, K. O. and Yiu, X. (1989) 'Historical development and use of thousand-year-old tide-prediction tables', *Notes 953 Limnol. Oceanogr*, 34(5), pp. 953–957.

Appendix A: Matlab code to quantify uncertainty in harmonic analysis

```
addpath('Z:/RC/Tidal Resourse Analysis/Matlab/Matlab Original
Files/UTideCurrentVersion');
addpath('Z:/RC/IDCORE- Year 2 & 3/Project Work/Islay Resource/Data
Analysis/Matlab Codes');
addpath('Z:/RC/Tidal Resourse Analysis/Matlab/Matlab Original
Files/compass');
addpath('Z:/RC/Tidal Resourse Analysis/Matlab/Matlab Original Files');

load('IDCore_files_2013.mat', 'velocity_bins')
load('IDCore_files_2013.mat', 'Power_kW')
load('IDCore_files_2013.mat', 'Cp')

% Load the harmonic constituents from ut_solv that you want (coef1)

%% Harmonic Analysis
%This is the U_tide code to execute harmonic analysis

%Syntax for two-dimensional raw input, such as velocities:
%   coef = ut_solv ( t_raw, u_raw, v_raw, lat, cnstit , {options} );
%    [ u_fit, v_fit ] = UR_RECONSTR ( t_fit, coef , {options} );

%  Syntax for one-dimensional raw input, such as sea level:
%   coef = ut_solv ( t_raw, sl_raw, [], lat, cnstit , {options} );
%    [ sl_fit, ~ ] = UT_RECONSTR ( t_fit, coef , {options} );
k=8
M_time = jackknife_matrix(JK_Time,k);
M_u = jackknife_matrix (JK_U,k);
M_v = jackknife_matrix (JK_V,k);

LT_mean=[];
for i=1:k

    HA_coef = ut_solv(M_time(i,:),M_u(i,:),M_v(i,:),55+(50.6172/60),
'auto', 'ols', 'white', 'DiagnPlots', 'NoTrend');

%t_fit2009 =
linspace(datenum(2009,1,1,0,0,0),datenum(2009,12,31,23,59,59),52560)';
%creates the long term period that you want data for

    [u_fit,v_fit] = ut_reconstr (t_fit2009,HA_coef); %reconstructs the
harmonic constituents to fit the long term period (t_fit2009)
 % converts the long term flow velocity into direction and speed
    [LT_direction,LT_speed] = cart2compass(u_fit,v_fit);
    % calculates the mean flow speed for the long term period
    LT_mean(i) = mean(LT_speed);
end
%% Statistical approach to work out power
[direction2009,speed2009] = cart2compass(u_fit2009,v_fit2009);%
converts the long term flow velocity into direction and speed
```

```
[x,y]=hist(speed2009,velocity_bins); % sorts the speeds into velocity
bins
hist(speed2009,velocity_bins); % plots the frequency of the tidal flow
speed
hold on
plot(velocity_bins,Power_kW, 'g');% plots the turbine power curve on
the same graph
x=transpose(x);
Power_output_GWh_year = sum(Power_kW.*x)/1000000


function [chunks] = jackknife_matrix(x, B)
    N = length(x);
    s = ceil(N/B);
    idx_e=0;
    v=[];
    chunks=[];

    for i=1:B
        idx_s=idx_e+1;
        idx_e=idx_s+s-1;
        if idx_e>N
            idx_e=N;
        end
        v = [v [idx_s;idx_e]];
    end

    for i=1:B
        i;
        if i==1
            idx=[v(1,2),v(2,B)];
            chunks(i,:) = x([idx(1):idx(2)]);
        elseif i==B
            idx=[v(1,1),v(2,B-1)];
            tmp=[x([idx(1):idx(2)])];
            chunks(i,:) = tmp(1:size(chunks,2));
        else
            idx=[v(1,1),v(2,i-1),v(1,i+1),v(2,B)];
            chunks(i,:) = x([idx(1):idx(2) idx(3):idx(4)]);
        end
    end
    %chunks=reshape(chunks,[B,s])

    %JK1_results =
ut_solv(JK1_Time,JK1_U_Flow,JK1_V_Flow,55+(50.6172/60), 'auto', 'ols',
'white', 'DiagnPlots', 'NoTrend');
end


%   Load signal (x)
x = Residuals_with_L2;

%   Convert time domain signal (x) into frequency
%   domain signal through fft
X = fft(x);

%   Retrieve the magnitude (real) data from X
X_mag = abs(X);
```

```
%   Retrieve the phase (imaginary) data from X
X_phase = angle(X);

%   Define frequency bins
N = length(x);
Fs = 1/60;
Fbins = ((0:1/N:1-1/N))*Fs;

%   Plot results
helperFFT(Fbins, X_mag, 'Magnitude Response');
%helperFFT(Fbins, X_phase, 'Phase Response');
```

Appendix B: Methodology to set up and run a tidal model in Telemac-2D

Creating the model boundary

1. Open BlueKenue
2. Create an initial closed line (File-New-Closed Line) with any node values and save it.
3. Open up the file (.i2s) in notepad and copy in the nodes (xyz) for the boundary outline and amend the number of nodes in the first line
4. Save the new closed line as (.i2s) then reopen the file in BlueKenue and check that the boundary is what you expect
5. Remember to have the first and last node as the exact same coordinates to ensure they join together

Resample the boundary nodes

6. Select the outline, right-click and select 'resample'
7. Choose how you want to resample the nodes (maximum distance, equal distance, segment count) and the value you want to resample it with
8. To only resample a specific section - select the outline and right-click at the node you want to split the outline and select 'split selected line'. Then resample that line separately
9. To join the lines again – right-click, select cut and then append to the other lines
10. Save the resampled boundary nodes

Create mesh

11. To create the mesh, select File-New-T3 Mesh Generator
12. Drag the resampled outline into the 'outline' tab under 'newT3Mesh'
13. Double-click on 'newT3Mesh' and open the box
14. Make sure the resample outline box is unticked
15. Choose an edge growth ratio or leave it as the default of 1.2

16. Input the default edge length for each element
17. Press run when you are happy with the options
18. Drag new mesh into viewer to check if you are happy with the mesh

Apply bathymetry

19. Open bathymetry file (.xyz) and visualise it by dragging into viewer
20. Click File-New-2D Interpolator
21. Drag bathymetry file into NewInterpolator2D
22. Double-click on NewInterpolator2D and choose method of interpolation
23. Select the mesh file and click Tools-Map Object and select NewInterpolator2D, OK
24. Choose a name for the new attribute (e.g. bathy), then select OK and save the mesh

Preparing the geometry file

25. Select File-New-SELAFIN Object
26. Right-click and add variable
27. Select the mesh file
28. Select OK
29. Save the new Selafin object (.slf) This is now ready for Telemac (1/3)

Preparing the boundary conditions file

30. Select File-New-Boundary Conditions and select the final mesh file
31. Drag the new item into the viewer and the mesh should then be greyed out with a brown line around the boundary (which is a wall by default)
32. Select the boundary you want to change by selecting a node and holding shift and selecting another node
33. Right-click and select Add Boundary Segment
34. Change the boundary by selecting open boundary with the desired attributes from the drop-down menu

35. Do the same for the tracer code
36. The boundary with change colour depending on what option you choose
37. The boundary file is made up of 2 parts
    a. .bc2-required to re-load into Bluekenue and edited
    b. .cli – required for Telemac
38. Save both files This is now ready for Telemac (2/3)

Preparing liquid boundary file

39. Prepare two columns in excel
    a. First column is time step in seconds
    b. Second column is the surface elevation, SL, at the corresponding boundary in metres (i.e. SL(2) for the second boundary)
40. First row is T (for timestamp) and SL(X) for the surface elevation for boundary number, X.
41. Second row is units (i.e. s for seconds, m for meters)
42. Time step must match the timestep in the liquid boundary file
43. The number of time steps is the final time step divided by the time step and should be defined in the steering file (i.e. timestep = 10s, number of timesteps = 100, final timestep = 1000)

Preparing the steering file

44. Open FUDAA to help define the variables in the steering file for Telemac
45. Use a template steering file (.cas file)
46. On the 'Project' tab:
    a. select a geometry file (.slf)
    b. The liquid boundaries file (.f)
    c. The boundary conditions file (.cli)

d. The results file (.slf)

47. Free surface gradient compatibility – values less than 1 suppress spurious oscillations
48. Friction coefficient – define the value linked to the related law
49. Initial conditions – define the initial conditions of the water depth (zero elevation, constant elevation, zero depth, constant depth, or special)
50. Law of bottom friction - (no friction/Haaland's/Chézy/strickler/Manning/Nikuradse)
51. Listing printout period – the number of time steps for the results to be printed
52. Number of time steps – time steps performed when running the code
53. Prescribed elevations – at the inflow boundaries
54. Prescribed flow rates – at the inflow boundaries
55. Prescribed velocities – at the inflow boundaries
56. Time step – defined in seconds
57. Variable for graphic printouts -

U : velocity along x axis (m/s),

V : velocity along y axis (m/s),

C : wave celerity (m/s),

H : water depth (m),

S : free surface elevation (m),

B : bottom elevation (m),

F : Froude number,

Q : scalar flowrate of fluid (m2/s),

T : tracer

K : turbulent kinetic energy in k-epsilon model (J/kg),

E : dissipation of turbulent energy (W/kg),

D : turbulent viscosity of k-epsilon model (m2/s),

I : flowrate along x axis (m2/s),

J : flowrate along y axis (m2/s),

M : scalar velocity (m/s),

X : wind along x axis (m/s)

Y : wind along y axis (m/s),

P : air pressure (Pa),

W : friction coefficient ,

A : drift along x,

G : drift along y,

L : nombre de courant.

58. Save new/amended steering file

Running a Telemac-2D computation

59. Open Telemac-2D command window
60. Cd to move to a new folder
61. Dir to show the directory you are in
62. Cd \ goes back to top
63. Cd.. goes up a level
64. The syntax for the command is

"Telemac2d *name of steering file*.cas"

runcode.py telemac2d –s *name of steering file*.cas

Output and post-processing

65. The results file (.slf) can be imported directly into BlueKenue

66. Once it is imported, drag the output you wish to visualise into a viewer.

67. Data and model results (e.g. timeseries, points in the model) can be extracted from BlueKenue

Appendix C: Example Telemac Steering File

```
/-----------------------------------------------------------------------

/ TELEMAC2D Version v7p1 10-Nov-2018

/ nom inconnu

/-----------------------------------------------------------------------

/-----------------------------------------------------------------------

/ EQUATIONS

/-----------------------------------------------------------------------

LAW OF BOTTOM FRICTION =2


FRICTION COEFFICIENT   =42.23

/-----------------------------------------------------------------------

/ EQUATIONS, BOUNDARY CONDITIONS

/-----------------------------------------------------------------------

PRESCRIBED ELEVATIONS =-2;2

/-----------------------------------------------------------------------

/ INPUT-OUTPUT, FILES

/-----------------------------------------------------------------------

STEERING FILE           ='steering_file_cd_0.025_ct_0.01.cas'

GEOMETRY FILE='../03_Selafin_files/Selafin_file_cd_0.025_ct_0.01.slf'

RESULTS FILE='../05_Results_files/Results_file_cd_0.025_ct_0.01.slf'

BOUNDARY CONDITIONS FILE ='../../boundary_hh.cli'
```

```
/-------------------------------------------------------------------

/ INPUT-OUTPUT, GRAPHICS AND LISTING

/-------------------------------------------------------------------

VARIABLES FOR GRAPHIC PRINTOUTS =B,U,V,H,S,W

/-------------------------------------------------------------------

/ NUMERICAL PARAMETERS

/-------------------------------------------------------------------

TIME STEP                       =20

FREE SURFACE GRADIENT COMPATIBILITY =0.9

NUMBER OF TIME STEPS            =10000

/-------------------------------------------------------------------

/ PHYSICAL CONSTANTS

/-------------------------------------------------------------------

WATER DENSITY =1025
```

Appendix D: MatLab Code to assess uncertainty propagation of input parameter on expected power

```
clc
clear
close all
format compact

addpath('C:\opentelemac-
mascaret\v7p2\05_Roughness_Matrix\Matlab\Matlab');
load('Cd.mat');
load('Ct.mat');
load('Power_Output.mat');
load('Velocity_Output.mat');

%% User defined variables
Output = Power_Output; %Choose either Power (P), velocity (V) or
discharge (Q)
no_of_bins = 100; %Choose the number of bins to split the PDF/CDF into
mu = 0.02; %Choose the mean value of Cd (bed roughness) to use in the
calculations
sigma = 0.01; %Choose the standard deviation of the mean of the Cd (bed
roughness)
Chosen_Ct = 0.4; %Choose the value of localised turbine roughness

%% Interpolating power and velocity outputs
Cd_q = 0.005:0.001:0.055;
Ct_q = 0:0.01:2;
Ct_q = Ct_q';
Pq = interp2(Cd, Ct, Output, Cd_q, Ct_q, 'spline');

%'EdgeColor','none'
%'FaceAlpha',0.5
figure
surf(Cd_q,Ct_q,Pq,'EdgeColor','none');
xlabel('Bed roughness - Cd');
ylabel('Localised turbine roughness - Ct');
zlabel('Expected Power (MW)');
%zlabel('Flow velocity (m/s)');

%figure
%surf(Cd_q,Ct_q,Vq);
%xlabel('Cd value (background roughness)');
%ylabel('Ct value (localised turbine roughness)');
%zlabel('Flow velocity (m/s)');

%% Plotting a normal distribution
x = (mu-4*sigma):(mu/100):(mu+4*sigma);
pdf = normpdf(x,mu,sigma);
%max_pdf=max(pdf);
cdf = normcdf(x,mu,sigma);
```

```
%cdf=cdf*max_pdf;

%% Plotting a normal distribution
%mu = 0;
%sigma = 0.5;
%x = -3:0.1:3;
%pdf = normpdf(x,mu,sigma);
%max_pdf=max(pdf);
%pdf=pdf/max_pdf;
%cdf = normcdf(x,mu,sigma);
%cdf=cdf*max_pdf;
%figure
%plot(x,pdf,'Linewidth',2);
%hold on
%plot(x,cdf,'r','Linewidth',2);
%legend('PDF','CDF');

% Split CDF into bins
no_of_bins_2 = no_of_bins+1;
a = length(x);
x_bins = round(linspace(1,a,no_of_bins_2));
cdf_bins=[];
cdf_mid=[];
for i = 1:no_of_bins_2
    cdf_bins = cdf(x_bins(i));
    pdf_bins = pdf(x_bins(i));
    b(i) = [cdf_bins];
    b2(i) = [pdf_bins];
end
x_bin_val = x(x_bins);

% Finding middle of bins
for j = 2:no_of_bins_2
    x_mid = round(x_bins-(x_bins(2)/2));
    c(j-1) = [x_mid(j)];
    cdf_mid = cdf(x_mid(j));
    pdf_mid = pdf(x_mid(j));
    d(j-1) = [cdf_mid];
    e(j-1) = [pdf_mid];
    Bins(j-1) = [j-1];
end
x_mid_val = x(c);

x_bins_all = round(linspace(1,a,no_of_bins_2*2-1));
x_bins_all_original = x_bins_all;
for i = 1:length(x_bins_all);
    if mod(i,2) == 0;
       x_bins_all(i) = x_bins_all(i)-1;
    end
end

x_values_all = x(x_bins_all);

for k = 1:(no_of_bins_2*2-1)
    cdf_all = cdf(x_bins_all(k));
    pdf_all = pdf(x_bins_all(k));
    f(k) = [cdf_all];
    g(k) = [pdf_all];
end
%for i=1:(no_of_bins*2-1);
```

```
%    neg_1=zeros(size(x_bins));
%end

%% Plotting figures
figure
%yyaxis left
plot(x,pdf,'Linewidth',2);
%yyaxis right
xlabel ('Roughness coefficient (Cd)');
ylabel ('Probability Density Function (PDF)');
%txt = {'Number of bins: ' num2str(no_of_bins) 'mu: ' num2str(mu)
'sigma: ' num2str(sigma) 'Ct Value: ' num2str(Chosen_Ct)};
%text(0.03,50,txt);

figure
plot(x,cdf,'r','Linewidth',2);
%hold on
%plot(x_bin_val,b,'^k','MarkerSize',10);
hold on
plot(x_mid_val,d,'xk','MarkerSize',10);
xlabel ('Roughness coefficient (Cd)');
ylabel ('Cumulative Density Function (CDF)');
%legend('CDF','Middle Bin Value');


%% Finding Power & Velocity
Chosen_Cd = x_values_all;
Power = interp2(Cd,Ct,Output,Chosen_Cd,Chosen_Ct,'spline');
Power_cdf = Power.*f;
Power_pdf = Power.*g;

Velocity = interp2(Cd,Ct,Velocity_Output,Chosen_Cd,Chosen_Ct,'spline');
Velocity_pdf = Velocity.*f;
Velocity_cdf = Velocity.*g;

%Power_all=interp2(Cd,Ct,Power_Output,x,Chosen_Ct,'spline');
%Power_all_pdf=Power_all.*pdf;
%Power_all_cdf=Power_all.*cdf;

%figure
%plot(x,Velocity_all_pdf);

%% Calculating CDF(end)-CDF(beginning) for each bin
H = f(1:2:end);
M = Power(1:2:end);
for i = 1:(length(H)-1);
    Pr(i) = H(i+1)-H(i);
    Delta_P(i) = abs(M(i+1)-M(i));
end
Pr = Pr';
Delta_P = Delta_P';

Power_mid = Power(2:2:end)';
Exp_P = Power_mid.*Pr;
Sum_Exp_P = sum(Exp_P);
Mean = Sum_Exp_P;
Var_P = sum((Exp_P-Sum_Exp_P).^2.*Pr);
Standard_dev = sqrt(Var_P);
Skewness = sum((Exp_P-Sum_Exp_P).^3.*Pr./(Standard_dev^3));
```

```
Kurtosis = sum((Exp_P-Sum_Exp_P).^4.*Pr./(Standard_dev^4));
Prob_P = Pr./Delta_P;
PDF_Power = Prob_P.*Delta_P;
CDF_Power = flipud(cumsum(flipud(PDF_Power)));

%% Results Matrix [Cd Bins, Cd CDF value, Power value at centre of each
bin, Power CDF]
Bins_Results = [x_bin_val; b]';
Mid_Results = [x_values_all;Power;f;Velocity]';
Results = [Pr Exp_P Delta_P Prob_P PDF_Power CDF_Power];
% Results_1 Mean, Variaince, Standard deviation, Skewness, Kurtosis
Results_1 = [Mean Var_P Standard_dev Skewness Kurtosis];
Results_2 = [Bins' x_mid_val' Pr Power_mid];

Ratio = Mean/Standard_dev

% Plot Power PDF and CDF
figure
plot(Power_mid,Prob_P,'Linewidth',2);
xlabel ('Power (MW)');
%xlabel ('Flow Velocity (m/s)');
ylabel ('Probability Density Function (PDF)');
%txt = {'Number of bins: ' num2str(no_of_bins) 'Mean: ' num2str(Mean)
'Variance: ' num2str(Var_P) 'Standard deviation: '
num2str(Standard_dev) 'Skewness: ' num2str(Skewness) 'Kurtosis: '
num2str(Kurtosis)};
%text(6000,0.0005,txt); %Power
%text(1.2,5,txt); %Velocity

figure
plot(Power_mid,CDF_Power,'r','Linewidth',2);
xlabel ('Power (MW)');
%xlabel ('Flow Velocity (m/s)');
ylabel ('Cumulative Density Function (CDF)');

pdf_plot = pdf*15;
power_pdf_plot = Prob_P*7;
b2_plot = b2*15;
```

Appendix E: Telemac model development and methodology

To run a computational model in Telemac a minimum of three files are required: the steering file, the boundary file, and the geometry file. The simplest way to create these inputs is using BlueKenue and FUDAA software before running the computational model in Telemac-2D. There are several other subroutines and additional files which can be used to add detail and complexity to the model depending on the user's requirements. The following sections provide detail of the three main files created for the model computational runs.

Steering file

The steering file is essentially the control panel of the computation. The file contains user-defined inputs to the model and sets the key parameters which will govern how the model is run. The steering file is created using keywords that control various aspects of the computation, such as the time step or the initial conditions within the model. There are over 300 keywords which can be assigned in the steering file. The keywords range from setting the density of the liquid in the model to reading in tide height data. The easiest way to prepare the steering file is through a program called FUDAA, which is a pre-processor graphic user interface (GUI) for Telemac. Although some of the basics required to use the program are discussed here, the user manual (EDF R&D *et al.*, 2014) should be consulted for more detail. This program allows the user to create a steering file in the correct format and change parameters within the file quickly. Telemac-2D will assign default values if a keyword is not defined in the steering file. For this study, the parameters in the steering file are listed in Table 6.2.

Table 6.2: Telemac steering file parameters using FUDAA software

Steering file keywords	Optional/default value	Chosen value
Free surface gradient compatibility	1.0	0.9
Law of bottom friction	0: No Friction 1:Haaland 2: Chézy 3: Strickler 4: Manning 5: Nikuradse grain size	2. Chézy

Steering file keywords	Optional/default value	Chosen value
Friction coefficient	Varies depending on law of bottom friction	42.23
Number of time steps (s)	1	10000
Prescribed model conditions	Elevation (m) Flow rate (m^3/s) Velocity (m/s) Tracer	Elevation (m)
Time step (s)	1	20
Variables for graphic printout	B: bottom elevation U: velocity along x axis V: velocity along y axis H: water depth	B, U, V, H, S, W
Water density (kg/m^3)	1000	1025

The values outlined in Table 6.2 show the parameters chosen in the steering file. Telemac recommends a free surface gradient compatibility value of 0.9 to avoid the use of quasi-bubble triangle discretisation. Values less than 1 suppress spurious oscillations which can result in an increase in computational power and memory (EDF R&D *et al.*, 2014). The bottom friction of the seabed was defined by Chézy roughness values as shown in Equation 6.1. The water density was increased from the default value of $1000kg/m^3$ to $1025kg/m^3$.

Boundary file

The boundary file for the mesh is generated by the pre-processor BlueKenue, enabling the user to modify any of the external node elements. Once the user has selected the nodes, the boundary characteristics are determined by classifying the depth and flow rate conditions for each node as shown in Table 6.3. For each boundary node, Telemac associates a number to the node to classify whether the boundary node is open, closed or open with a prescribed value. For more information, see EDF R&D et al. (2014). For this study, the left boundary was given a prescribed elevation and the flow velocity was free; the right boundary was modified to represent an open ocean, with free depth and velocity. The other boundary nodes are classified as walls and were entirely closed to depth and elevation changes.

Table 6.3: Telemac boundary file coding

	Prescribed open boundary nodes	Closed boundary nodes	Free open boundary nodes
Elevation/depth code	5	2	0
Flow rate code	4	2	0
Colour coding (as shown in Figure 6.1)	Green	Grey	Black

Once the boundary nodes are classified, they are represented by various colour coding in BlueKenue. This file is saved as a '.bc2' file, which can be used to visualise and amend the boundary in BlueKenue. To produce the boundary file in the format for Telemac, the file is saved in '.cli' format.

The aim was to create a tide flowing in a uniform direction from the left-side boundary towards the channel. Therefore, the mesh was rectangular at the left and right boundary, which meant that the initial tidal force at the left boundary entered the model parallel to the channel orientation. The outline of the mesh in the domain is shown in Figure 6.1. The channel was made to be 20 km long and 4 km wide, with curved land forms at the entrance and exit of the channel to replicate the model in Draper's model, shown in Figure 6.2. These dimensions are similar the Sound of Islay site in length (~20 km long), but the width in the model slightly larger than the Sound of Islay width of 1.0 km at its narrowest point. For the purposes of this model, the width was kept uniform along the length of the channel.

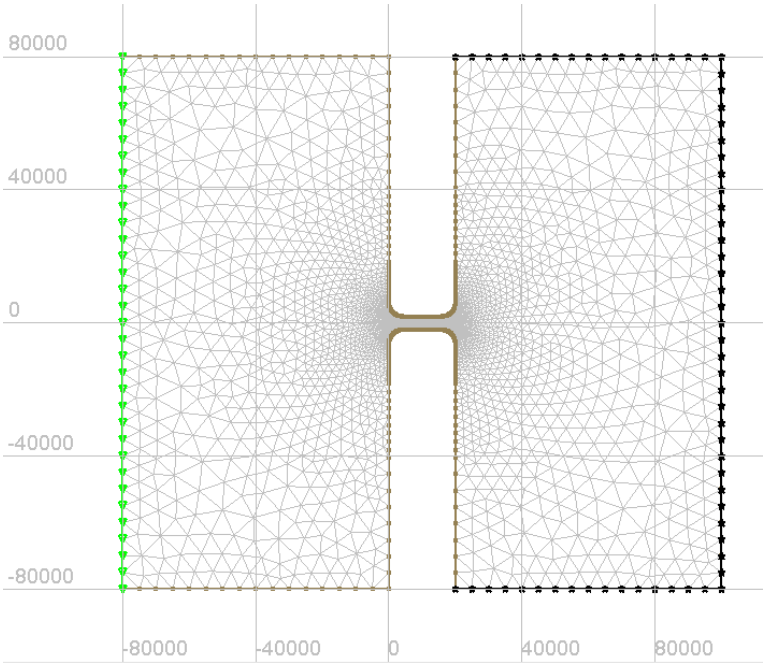

Figure 6.1: Plot of rectangular channel mesh

The mesh to the left and right of the channel was made large enough to represent infinite oceans at each end of the channel. The green boundary to the left is where the tidal variation is initiated for the model, and the black boundary to the right is an open boundary. Each boundary line is dedicated to one point on the mesh boundary and given the same numbering as the points on the lines. Using the BlueKenue software, the boundary and mesh can be created. This process is detailed further in Appendix A:. shows an image of the mesh developed for this study.

Geometry file

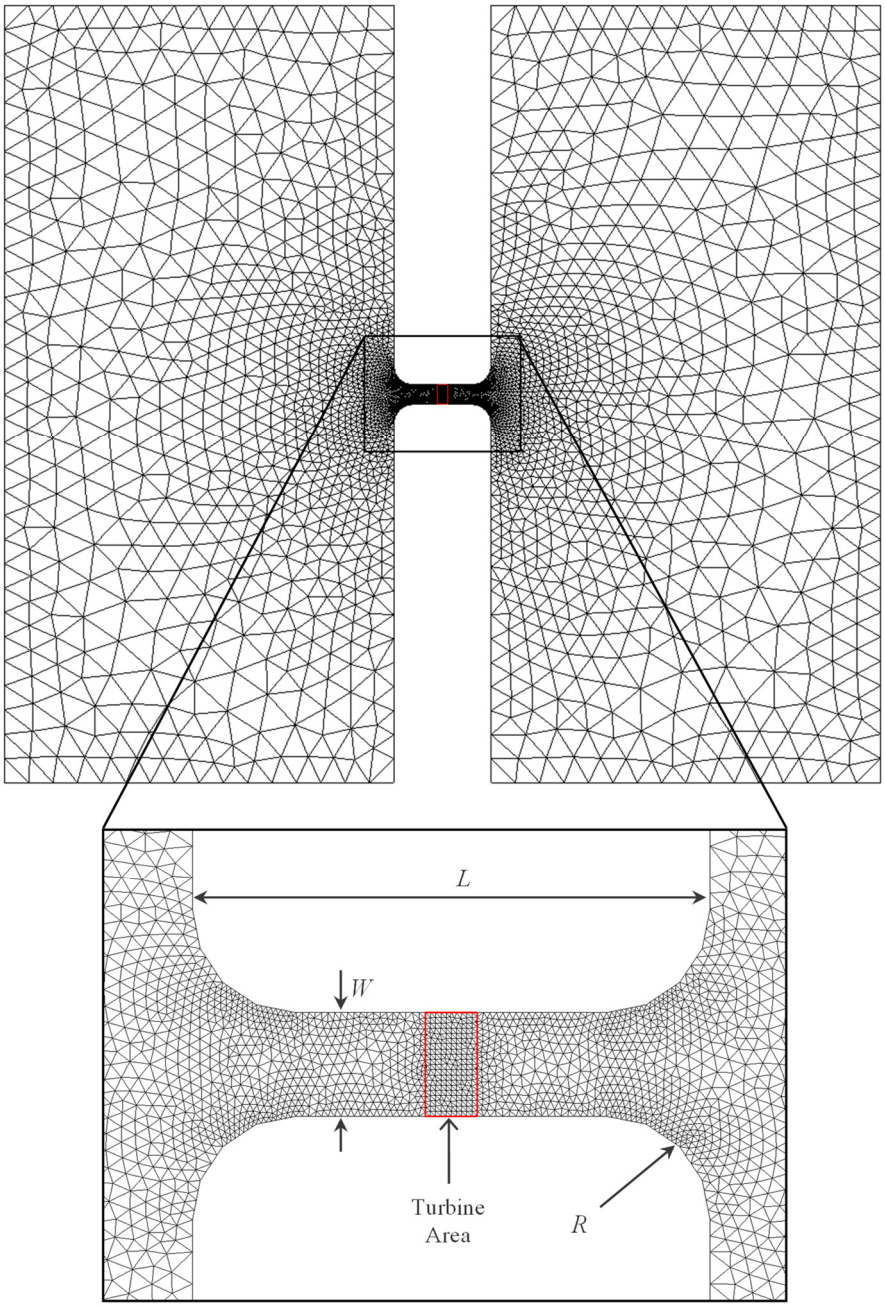

Figure 6.2: Geometry of numerical mesh used to depict a channel between two infinite oceans in Telemac/BlueKenue

The geometry file contains all the information concerning the mesh, comprising the number of mesh points, the number of elements, and the number of nodes per element. This binary file also contains bathymetry information and/or friction coefficient values at each mesh point. The Telemac model developed for this study has 3623 nodes with 6808 elements. The resulting mesh was an unstructured triangular grid with an edge growth ratio of 1.2. This enabled the mesh to be much finer within the area of interest within the channel and coarser towards the left and right

boundary. The red area depicted in Figure 6.3 shows the model mesh with the roughness value attributed to the elements, with the blue area representing the area of enhanced bed roughness.. This area was made to be 2.0 km long and 4.0 km wide, to span the width of the channel. As an approximation, the number of 1.5 MW tidal turbines (with a diameter of 20 m) that could be deployed in this area, equals approximately 560, assuming each neighbouring turbine is a minimum of 4 diameters away in the cross-wise direction and 6 diameters away in the lengthwise directions. This would give an approximate capacity of 840 MW for a tidal farm in this area.

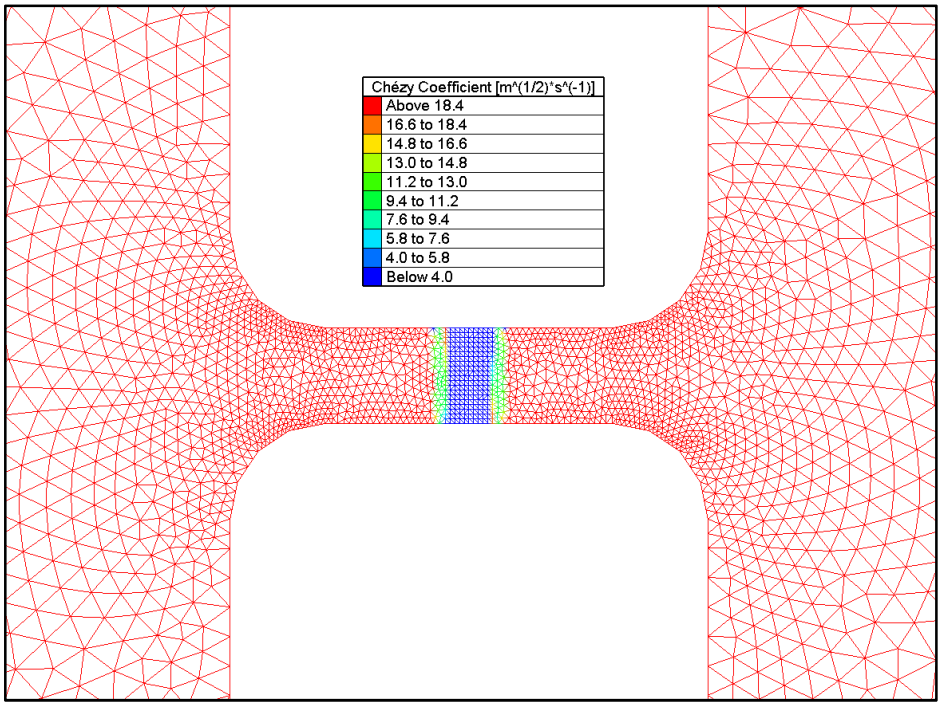

Figure 6.3: Telemac model mesh in BlueKenue, showing example bed friction values representing a tidal fence across the channel. A lower Chézy coefficient value corresponds to a higher bed roughness value.

For this investigation, the influence of bed roughness on power output was investigated. Initially, the C_d, background roughness values, were chosen to lie in the range 0.0055 to 0.055 based on the values in Table 2.6. The values are comparable to the roughness C_d values of 0.013 – 0.052 used in the literature (Coles, Blunden and Bahaj, 2017). This was calculated by rearranging Equation 6.1 to calculate the turbine drag based on Chézy value ranges of 13.4 to 42.2. An area of bed traversing the channel was selected to represent increased turbine roughness. The values selected for turbine roughness, C_T, ranged from 0.005 to 2.0.

Achour (2015) shows that the value of the Chézy coefficient can be determined from Equation 6.1 for a rectangular channel.

$$\text{Chézy} = \sqrt{\frac{g}{C_d}} \tag{6.1}$$

where g is the acceleration force due to gravity and C_d is the natural bed roughness value. The Manning equation can also be used to estimate the average velocity, V, in an open channel as

$$\text{V} = \left(\frac{1}{n}\right) {R_h}^{2/3} S^{1/2} \tag{6.2}$$

where the hydraulic radius, R_h, is defined as A/P_w, A is the cross sectional area of the flow and P_w is the wetted perimeter of the channel. For a rectangular channel, the hydraulic radius can be calculated using the depth, h, and width, w, of the channel as $\frac{hw}{2h+w}$. S is the slope or gradient of the channel and n is the Manning coefficient of roughness which can range from 0.01 $sm^{-\frac{1}{3}}$ for a smooth channel to 0.06 $sm^{-\frac{1}{3}}$ for a channel containing high levels of large sediment, debris or vegetation.